Modification of Biomaterials using Plasma Polymerisation

Juliet Bell

A thesis submitted in fulfilment of the requirements of University of Sheffield for the degree of Doctor of Philosophy

Department of Materials Science and Engineering

December 2013

Acknowledgements

I would like to thank John first and foremost for giving me the opportunity to do a PhD, supporting me through the process, thoroughly checking my thesis (twice) and being such a great, professional supervisor.

Invaluable training in the lab by Katie Smith, Celia Murray-Dunning and Rossukon Kaekhaw was much appreciated, with thorough and patient advice on surface analysis and chemistry provided by Fred Claeyssens and Claire Hurley.

Thank you to Mark Wagner and Claire Johnson, always ready with sound advice and a helping hand.

Celia Murray-Dunning, Katie Smith, Mark Wagner, Robin Delaine-Smith, Priya Viswanathan, Richard Senior, Laura Sidney, Katie van Niekerk, I don't know what I would have done without you!

Thanks of course to all my family, who were always there to hear frustrations and cheer me up, and finally to Russ, who was there through it all and still is. I absolutely couldn't have done this without you.

Publications

- JHA Bell and JW Haycock. *Tissue Eng Part B* 2012 Next Generation Nerve Guides: Materials, Fabrication, Growth Factors, and Cell Delivery 18;**2**:116-128
- JHA Bell and JW Haycock. *Eur Cells Mater* 2012 Investigating the Effect of Plasma Polymers on Neuronal and Glial Cells 23(suppl4):5

Conference Presentations and Awards

- Awarded prize for best talk at the 13th Annual White Rose Work in Progress Meeting of the Biomaterials and Tissue Engineering Group (BITEG) on 20.12.2011: 'Investigating the Effect of Plasma Polymerised Surfaces on Neuronal Cells'
- Talk at the 14th European Conference on Applications of Surface and Interface Analysis on 09.09.2011: 'Investigating the Effect of Plasma Polymerised Surfaces on Neuronal and Schwann Cells'
- Poster 9.P01 at the 3rd World Congress of The Tissue Engineering and Regenerative Medicine International Society (TERMIS) on 08.09.2012: 'Investigating the Effect of Plasma Polymerised Surfaces on Neuronal and Schwann Cells'
- Awarded poster presentation prize at Tissue and Cell Engineering Society (TCES) 2011, for poster entitled 'Investigating the Effect of Plasma Polymerised Surfaces on Neuronal and Schwann Cells'

Contents

Abbreviations

AAc: Acrylic acid

ADSCs: Adipose tissue-derived stem cells

AFM: Atomic force microscopy

B&S: Bottenstein and Sato (medium)

BMSCs: Bone marrow-derived stem cells

BSA: Bovine serum albumin

CMAP: Compound muscle action potential

DAPI: 4',6-diamidino-2-phenylindole

dH$_2$O: Distilled water

DMEM: Dulbecco's modified Eagles medium

DRG: Dorsal root ganglion

ECM: Extracellular matrix

F12 medium: Nutrient F-12 Ham's medium

FCS: Foetal calf serum

FDA: Federal drug agency

FGF: Fibroblast growth factor

FITC: Fluorescein isothiocyanate

FT-IR: Fourier Transform Infrared spectroscopy

GDNF: Glial cell line-derived neurotrophic factor

IgG: Immunoglobulin G

IPA: Isopropanol

MA: Maleic anhydride

MA1: 80 μs on time, 800 μs off time for 20 min with peak power of 5W

MA2: 20 μs on time, 1200 μs off time for 20 min with peak power of 5W

MA3: continuous 1 W power for 20 min

MSC: Mesenchymal stem cells

MBP: Myelin basic protein

MTS: (3-(4,5-dimethylthiazol-2-yl)-5-(3-carboxymethoxyphenyl)-2-(4-sulfophenyl)-2H-tetrazolium)

NF: Neurofilament

NGC: Nerve guide conduit

NGF: Nerve growth factor

NT: Neurotrophin

PBS: Phosphate-buffered saline

PCL: Poly-e-caprolactone

PEG: Poly-ethylene glycol

PGA: Poly-glycolic acid

Phalloidin-TRITC: Phalloidin–Tetramethylrhodamine B isothiocyanate

PHB: Poly-3-hydroxybutyrate

PLA: Poly(lactic acid)

PLGA: Poly(lactic-co-glycolic) acid

PLLA: Poly(L- lactic acid)

PNI: Peripheral nerve injury

RT-PCR: Reverse transcription polymerase chain reaction

S100β: S100 calcium binding protein β

TCPS: Tissue-culture polystyrene

ToF-SIMS: Time of flight-secondary mass spectroscopy

trk: Tyrosine kinase (receptors)

XPS: X-ray photoelectron spectroscopy

Abstract

The peripheral nervous system has a limited ability to repair after injuries (1 mm/day). Current therapies for peripheral nerve injuries include suturing, autografting and nerve guide conduits (NGC). NGC's can be implanted into defects up to 20 mm in length. Possible improvements to the existing designs include material alterations as well as various coatings, fillers and cellular components. Plasma polymerisation is a chemical deposition technique, which can coat any surface with nano to micro-metre layers of desired chemistry.

The aim of the thesis was to investigate the effect of the plasma polymers acrylic acid (AAc) and maleic anhydride on neuronal and Schwann cell metabolic rate and morphology *in vitro*. Evaluation of AAc and maleic anhydride surfaces was assessed using contact angle, X-ray Photoelectric Spectroscopy (XPS) and Time of Flight Secondary Mass Spectrometry (ToF-SIMS).

NG108-15 neuronal cell staining protocols were optimised, then out of three maleic anhydride duty cycles (MA1, 2 and 3), MA1 supported neuronal cells with longer neurites and a higher metabolic rate. Glass and laminin / poly-L-lysine were used throughout as basal and positive controls respectively. Investigations then compared AAc with MA1 coatings under serum and serum free conditions. Whilst there were similar results under serum conditions, NG108-15 neuronal cells on MA1 under serum free conditions had significantly longer neurites compared to glass, also longer than laminin and acrylic acid.

Primary rat Schwann cells were then studied, due to their integral role in peripheral nerve regeneration, on AAc and MA1. It was observed that Schwann cells had a longer, thinner phenotype and a higher total cell count on poly-L-lysine and glass compared to the plasma polymers. Primary rat dorsal root ganglion (DRG) culture was then optimised to look into the effect of both neuronal and glial types, initially using explants. DRG on AAc showed similar neurite outgrowth characteristics to those on glass, whilst DRG on MA 1 had comparatively fewer and shorter neurites. Dissociated DRG culture on MA1 and AAc surfaces were then observed to have longer neurite lengths and a higher percentage of neurons with neurites compared to glass. In conclusion, NG108-15 neuronal cells had longer and more numerous neurites on the plasma polymers compared to glass, which was corroborated using results from dissociated DRG. As the length and number of neurite outgrowths per neuron has been

shown to be indicative of neuronal differentiation[100], plasma polymer coatings may support neuronal differentiation. Conversely, primary rat Schwann cells showed a longer and thinner phenotype on glass compared to the plasma polymers. DRG explants that contain both neuronal and glial cell types extended further on glass compared to the plasma polymers. Using a number of cell types was therefore a very relevant method of evaluating AAc and MA1 for neuronal applications. This work demonstrates the suitability of MA1 and AAc as coatings for nerve guide conduits, and would support further investigations into the effect of plasma polymers on neuronal/glial progenitor cells regarding differentiation and *in vivo* work.

1.1 Introduction

1.1.1 Tissue engineering

The field of tissue engineering and regenerative medicine utilises multidisciplinary knowledge from biology, engineering and materials science in order to replace or repair damaged and diseased tissues[120]. Tissue engineering therapies often use a three-dimensional scaffold, on which cells are then cultured. Scaffolds can be manufactured from natural or synthetic materials, whilst cells are usually from autologous, allogeneic or xenogenic sources. Tissue engineering therapies that have been used clinically include bladders[12], skin grafts[92], vascular grafts[119], airway[127] and cartilage defects[217]. Other relevant developments relating to tissue engineering include high throughput systems for biomaterials testing[94] and the incorporation of stem cells into scaffolds[218]. The advancement of fields such as computational systems biology, bioreactors and 3D imaging techniques is also interlinked and underpins developments in tissue engineering and regenerative medicine.

1.1.2 Peripheral nerve tissue engineering

The peripheral nervous system consists of nerves and associated ganglia that radiate out from the spinal column and brain. It extends the nervous system to the limbs of the body and is divided into the somatic and autonomic systems. Peripheral nerve tissue engineering aims to improve current therapies for peripheral nerve defect injuries by using scaffolds. These scaffolds could be composed of decellularised nerve[106], synthetic[72] or natural[180, 194] materials. Scaffolds may incorporate growth factors[205], hydrogels[132], intra-luminal scaffolds[146], chemotropic gradients[207] or peptides[23] to encourage migration across the defect. Cell types including adipose-derived[68] and bone marrow-derived stem cells[8] have also been harvested and cultured *in vitro,* in order to then be incorporated into a nerve guide and implanted.

1.1.3 Clinical evaluation of peripheral nerve injuries

Peripheral nerve injuries (PNI) among the civilian population commonly result from motor vehicle accidents along with penetrating trauma, falls, and industrial accidents[154, 164]. Over a 16 year study, 73.5% cases of PNI involved upper limb injuries[117]. Ulnar nerve injuries were reported most frequently of the upper limb cases, with the medial, radial and brachial plexus nerves also common injuries. Of the lower limb injuries, peroneal and sciatic nerves were damaged the most. Military PNI

have grown increasingly common due to a higher survival rate. The 'wounded in action' to 'killed in action' ratio has dropped from 3:1 for conflicts such as Vietnam, to 8:1 for recent conflicts[36]. Upper limb injuries are the most prevalent in conflict situations, 37% of which had associated arterial injuries[174]. PNIs were caused primarily by high-energy missiles as well as explosions and gunshot injuries.

Classification of PNI is done using the Seddon[168] or Sunderland[179] index (table 1).

Nerve damage	Sunderland (Degree)	Seddon
No local conduction or wallerian degeneration	I	Neuropraxia
Endoneurium and perineurium intact, axonal damage	II	Axonotmesis
Endoneurium damage	III	
Axonal, endoneurial and perineurial damage. The epineurium remains intact so nerve still in continuity	IV	
Nerve completely transected	V	Neurotmesis

Table 1: Classification of nerve injuries

Neuropraxia, or degree I on the Sunderland scale, describes an intact but non-functional nerve. The Seddon index specifies a partially or completely severed axon as axonotmesis if the connective tissue framework is preserved. The Sunderland index classifies axonotmesis further, specifying endoneurial, perineurial and epineurial damage via degrees II, III and IV respectively. Neurotmesis, or degree V, corresponds to a complete transection of the nerve, where most or all of the connective tissue is damaged. For functional recovery, surgical intervention is required for Sunderland degree III, IV and V. As well as the outcome of surgery, there are additional factors that influence the degree of regeneration and repair[91]. An older patient has less regenerative capacity compared to a younger patient, and the time elapsed between the injury occurring and reparative surgery can influence the response of cells to the treatment. The proximity of the lesion to the distal target is an important parameter, as the nerves will have to regenerate over greater distances if the lesion is more proximal to the distal target. If the soma of a nerve is cut this can also be more damaging to repair compared to the distal end of a nerves neurite being damaged. Associated soft and/or vascular damage can obviously hinder repair of nerve defects, as can the recovery period. Even if the surgery goes well, if the patient does not take care to do the rehabilitative exercises or use it, the recovery can be poor compared to a persistent patient who makes sure to use the damaged limb as much as possible[83].

1.1.4 Pathophysiology of Peripheral Nerve Injuries

The pathophysiology of PNI is more conducive to repair compared to the central nervous system, however it is still limited. If the axon has been damaged, separated ends of the transected nerve will deteriorate and retract, sealing themselves off in the initial phase of Wallerian degeneration[148]. Altered protein metabolism then results in decreased production of neurotransmitters and increased production of specific materials required for regeneration[66]. At the distal end of the stump macrophages are recruited to the site of injury within the first week, playing a part in the phagocytosis and lysis of axonal and myelin debris. The macrophages, along with the degradation products, stimulate Schwann cells to dedifferentiate and shed their myelin sheath. Neuregulin, a growth and maturation factor secreted by axons during development and after injury, has also been found to trigger the dedifferentiation process[216]. Schwann cells then proliferate into the empty connective tissue of the injury site, forming bands of Büngner and laying down a scaffold of basement membrane proteins that include laminin and fibronectin. The proliferation rate of the Schwann cells reaches its peak around day 2-4. Laminin B1 and B2 chains, down regulated after injury, are re-expressed throughout regeneration[65]. Fibronectin and collagen type I, III and IV synthesis is also increased at the injury site[121].

As well as building a scaffold designed to encourage and guide axonal migration, Schwann cells secrete various neurotrophic factors and growth factors. These diffuse through the injury site, exerting a trophic influence on the regenerating axons from the proximal stump[155]. The migration and proliferation of Schwann cells occurs for two weeks and is essential for axonal repair, as inhibition of this results in severe regenerative failure[88] as well as an increase in misdirected axon growth[41]. If regenerating axons manage to bridge the injury gap, a second phase of Schwann cell proliferation is stimulated. Adversely, if innervation across the bands of Büngner does not occur after 100 days, the Schwann cells within the bands will atrophy and die[69].

Axons in the proximal stump of the injury will degenerate back to the first node of Ranvier, which is part of Wallerian degeneration. Hours after the injury has occurred, neuronal sprouts from the proximal stump will start to grow, the number of sprouts in excess of the number of original neurons. Survival signals from target organs encourage axonal sprouts and direct their growth, whilst sprouts that don't receive such encouragement will recede[28]. The tip of the neuronal sprouts, or growth cone, is sensitive to contact guidance and trophic cues. As mentioned before, the scaffold laid

down by Schwann cells stimulates growth cone extension. Adversely, if the growth cones encounter physical barriers such as glial or inflammatory cells whilst trying to cross the injury site, this can result in growth cone collapse[84].

As well as physical guidance cues, chemotropic cues also guide axon growth towards the target organ. Among others, Nerve Growth Factor (NGF) secreted by Schwann cells supports cell survival and axonal elongation[157, 214]. Motor nerve conduction velocities were increased in rats after 6 weeks when NGF was added to a 5 mm sciatic nerve defect[89]. NGF acts primarily through the high affinity tyrosine kinase (trk) A receptors in sensory neurons[103]. Neurotrophin-3 (NT-3) also supports neuronal cell survival as well as their growth, differentiation and formation of neuronal synapses[133]. Glial cell line-derived neurotrophic factor (GDNF) exerts a protective effect on motor neurons[90] as well as improving neurite outgrowth, neuron survival and Schwann cell migration[22], acting through Ret receptors, a subgroup of the tyrosine kinase receptors that can be activated by glial-derived factors. Basic fibroblast growth factor also enhances nerve regeneration following injury to the peripheral nervous system[192].

1.1.5 Current Clinical Treatments

If PNI does not heal, autologous nerve grafts are currently considered the 'gold standard'. However, these have the disadvantage of two surgical sites and donor site morbidity[148]. For cases that require autografting, sensory nerves such as the sural nerve from the leg are primarily used as they are more 'expendable' compared with motor nerves, as well as being relatively easier to harvest, sometimes longer when extracted, and accompanied with lower donor site morbidity[148]. However, it has been found that greater nerve

Figure 1: Illustration of various techniques available to induce nerve repair [154].

regeneration occurs when a motor nerve injury is treated with a motor nerve graft compared with a sensory nerve graft [25]. This suggests that some unsatisfactory clinical outcomes may be due to using a sensory nerve rather than a motor nerve. However donor site morbidity would be expected to increase if motor neurons were harvested instead of sensory neurons. This is because loss of the motor nerve would result in an inability to stimulate the target site, leading to disuse and eventually atrophy. Another surgical procedure called end-to-side coaptation (figure 1) consists of grafting a donor nerve onto the side of an existing nerve, is mostly achieved with the
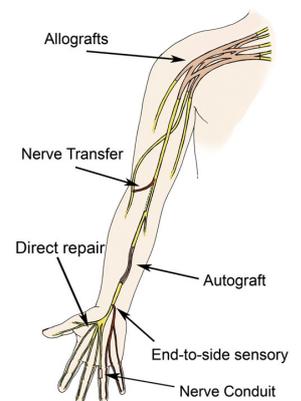
use of a donor nerve and is possible to perform directly. However, this technique has received mixed reviews. It has been suggested that the success of the 'sprouting' and therefore reinnervation could be to do with the topography of the donor nerve, which is not known, and therefore could be leading to unpredictable results[135]. Nerve transfer is another surgical option where a high -level proximal nerve defect will be swopped with a distal nerve in order to convert the injury to a low level distal nerve injury. However, this technique is more complicated for the surgeons compared to autologous grafting, and can result in loss in function of the donor nerve muscle[148].

Nerve allografts can be used instead of autografts when required, for example when the length of the autograft would be shorter than the injuries, or if multiple PNIs have occurred. Advances in the immunosuppressive therapy with medication such as FK506, along with cold storage, has reduced antigenic problems associated with allografts[128]. Whilst FK506 was found to promote neurite outgrowth[126], assessing the therapy using a graft after six weeks showed no significant differences[75]. Although the functional recovery of nerve allografts is comparable to autografts, the use of systemic immunosuppressants and probability of rejection still limit this option. Recently developed decellularised allografts remove the need for immunosuppression or a second surgical site with the associated morbidity. Avance®, a commercial decellularised allogeneic nerve graft, has shown good to excellent results for 10 defects between 5 and 30 mm[105] with no infection or rejection.

Finally, for nerve defects up to 30 mm, nerve guide conduits (NGC) can be used. While the number of commercially available nerve guides is still relatively small, a number of products are FDA approved[109], summarised in table 2. Neuragen® is a type 1 collagen nerve conduit that degrades after 48 months and gives mostly good outcomes for PNIs up to 20 mm[32]. Neurolac®, a transparent poly-DL-lactide (PDLLA) polycaprolactone (PCL) conduit by Polyganics, takes 16 months to degrade and has been shown to heal defects up to 20 mm after 12 months[19]. Neurotube® is a polyglycolic acid (PGA) conduit by Synovis that takes 6 months to degrade[159], whereas NeuroMatrixNeuroFlex® is also manufactured from type 1 collagen by Collagen Matrix Inc and takes 7 months to degrade. Salubridge is made from a polyvinyl alcohol hydrogel, doesn't degrade and is manufactured by Salumedica. AxoGuard™ (Cook Biotech) is a 2-4 cm long conduit made from porcine small intestinal submucosa and RevolNerve® is made from collagen type I and III extracted from porcine skin[6] (which does not have FDA approval at the time of writing).

Commercial name	Company	Material	Company Website
Neuragen®/NeuraWrap™	Integra	Type I collagen	http://www.ilstraining.com
Neurolac®	Polyganics	PDLLA/CL	http://www.polyganics.com
Neurotube®	Synovis	PGA	http://www.synovismicro.com
Neuromatrix/Neuro*flex*™ conduits and NeuroMend™ wrap	Collagen matrix inc	Type I collagen	http://www.collagenmatrix.com
Salubridge™/Salutunnel™	Salumedica	Polyvinyl alcohol hydrogel	http://www.salumedica.com
Surgisis®/Axoguard™	AxoGen Inc	Porcine small intestinal submucosa	http://www.axogeninc.com
Avance®	Axogen Inc	Decellularised nerve	http://www.axogeninc.com
QiGel™	Medovent	Chitosan	www.medovent.com
RevolNerve®	Orthomed	Collagen type I and III from porcine skin	http://www.orthomed.fr/

Table 2 - A summary of commercially available nerve guides and wraps. (apart from Avance®, QiGel™ and RevolNerve®, all other listed nerve devices have been FDA approved).

A recent study[173] compared Neurolac®, NeuraGen® and Neurotube® with a 10mm rat sciatic nerve excision model. Interestingly, there was no difference in recovery between Neurolac® and autograft. Repairs with Neuragen® had lower compound muscle action potentials (CMAP) than Neurolac®, however differences were not significant and the conduit remained structurally stable. Neurotube® demonstrated the poorest outcome, collapsing completely at 12 weeks. A parallel study[187] also found that Neuragen® had a significantly better outcome compared to Neurotube®. In particular, Neurotube® stimulated axonal sprouting that was less organized and sparser compared to Neuragen® or autograft. Another study comparing Avance® conduits with NeuraGen® or autograft[194] found Avance® at six weeks to be superior to NeuraGen® but no difference by 12 weeks.

All currently licensed nerve guide conduits are hollow tubes, whilst the materials used for synthetic guides are not functionalised further to encourage cell migration and proliferation. Nerve guides that incorporate an internal scaffold for cells to migrate across and bioactive cues to encourage proliferation have been demonstrated to improve regeneration distances, which is discussed in the following section.

1.1.6 Advances in materials

There are many factors that need to be considered when designing a nerve guide conduit, such as selection of materials and method of manufacture. If biological components such as cells or growth factors are to be added, the cost and ease of obtaining such cues for a potential commercial product must be evaluated. If there are to be pores within the walls, their sizes must be carefully considered, controllable in manufacture and properly characterised. The potential complications of upscaling to produce nerve guide conduits that include micro- and nano-sized features should be balanced against the benefit of improved regeneration. The conduit should be flexible enough to be sutured into a joint environment, yet stiff enough to withstand collapse. Clinical and experimental data suggest that nerve guides should ideally degrade and be absorbed in 1 to 2 years following implantation. This is of note as non-degradable conduits such as silicone have been associated with chronic inflammation and removal[99].

NGCs can be either natural or synthetic. Natural materials are advantageous as they have cell-binding domains that can encourage cell proliferation and attachment. However, the production of certain natural materials using animal sources carry a minor disease transmission risk (although the majority of natural materials used commercially have regulatory approval) [125]. Their cost can also be substantially higher than some synthetic alternatives. Although they do not have inherent cell attachment sites, synthetic materials can have specifically tailored properties such as stiffness and degradation rate. This control is very desirable, as well as further controlling the manufacturing process to include micro- and nano-sized features.

Type-I collagen has been thoroughly investigated as a suitable material for NGCs, demonstrating comparable regeneration to autografts for up to 20 mm gaps[180, 6, 164, 32] and commercial availability as Neuragen®. Regarding decellularised scaffolds, Zhang et al[218] reported an absence of host rejection after inserting a xenogenic acellular nerve guide into a rat nerve defect for 7 days. Although the results also demonstrated lower CMAP scores with lower myelinated nerve fibre density compared to autograft, the commercial availability of decellularised NGC Avance® shows promise. Although there has been interest in devitalised muscle grafts as a low cost, available alternative to autografts[147, 110], interest seems to have waned in recent years and the method has not been reported clinically, to the author's knowledge. Chitosan conduits were evaluated by Ao et al[8], when a PBS filled NGC was used for a 12mm rat defect for 3 months. Muscle areas, conduction velocity and cross sectional

myelin were half that of autograft controls. However fibrin has shown more promising results[5, 151], as axons managed to cross a 10 mm rat sciatic nerve defect after one month[102]. Silk fibroin has recently gained attention due to favourable degradation properties and low inflammatory response[82, 204, 203, 188, 171, 129, 124]. After a 6 month implantation into rats, electrophysiological, histological and retrograde tracing demonstrated positive results[204]. When compared with collagen guides at 1, 4 and 8 weeks, silk fibroin guides stimulated a similar inflammatory reaction[82]. Although the gastrocnemius muscle weight was 27% lower compared to autograft, greater numbers of proximal and distal connections were present with the silk fibroin conduit. Silk blends have also been investigated. Wang et al[188] compared poly(L-lactic acid-co-ε-caprolactone) (P(LLA-CL)) against a fibroin P(LLA-CL) blend. The fibroin blend gave superior results with electrophysiological, histological and immunohistochemical scores. Other naturally derived blends include gelatin[86], collagen[156, 166] and chitosan[55].
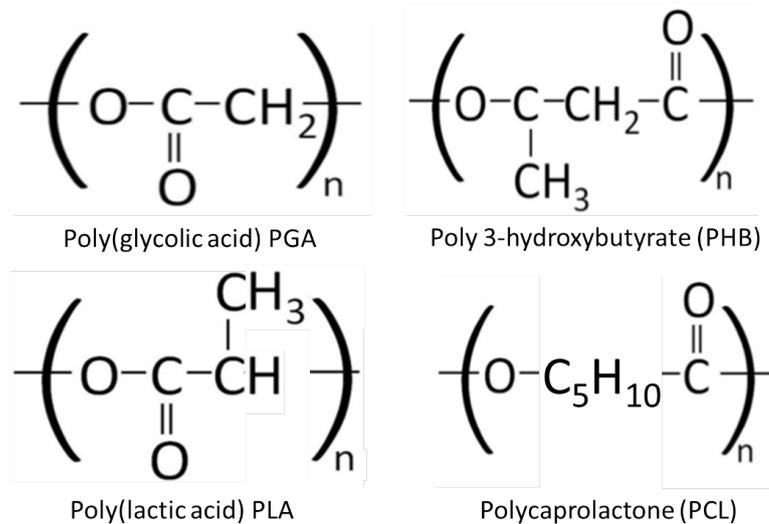
Figure 2: Diagram showing the structure of some synthetic polymers used in nerve guide conduits.

Regarding synthetic materials, the well-researched family of polyesters that include poly(glycolic acid) (PGA), poly(lactic acid) (PLA), polycaprolactone (PCL) and poly(L-lactic acid) (PLLA) are an obvious choice for NGCs (figure 2), a major reason being that various polyesters are already widely used in many FDA approved devices such as sutures, orthopaedic screws and drug delivery systems. A comprehensive study by Weber et al[193] compared PGA conduits against autografts/direct coaptation. PGA implants scored 44% excellent, 30% good and 26% poor results. This was compared to 43% excellent, 43% good and 14% poor for the coaptation/autograft control. Although

results were slightly below the autograft control, use of NGCs wherever possible is more desirable as it eliminates the need for a donor nerve with associated morbidity. In another study using PGA conduits for facial nerve defects, 5 out of 7 reported patients recovered good/very good facial muscle control, whilst 2 reported fair recovery[144]. However, due to a transient pH decline when PGA resorbs, there is a limited amount of PGA that can be used in a conduit before the acidic degradation products start to adversely affect the regeneration process. As PGA conduit Neurotube® was reported to have collapsed after 12 weeks in a rat sciatic nerve model[173], PGA conduits may also be more suitable for injuries associated with areas of low load. A summary of a few studies discussed in this review is given in table 3.

A summary of different approaches for nerve regeneration

Research area	Summary	Key findings	Reference
Material Selection			
Collagen	Digital nerve repair with collagen guides in 12 patients	Good outcomes for defects up to 20 mm	[32]
PCL	Clinical study of neurolac®	34 nerve lesion sites, comparable results to existing treatment	[18]
	Microgrooved ultra-thin PCL and PCL/PLA films tested *in vitro* and *in vivo*	Continuous nerve cable after 2 weeks in 8/9 rats	[178, 177]
PGA	*In vivo* study of neurotube® in rats	Peroneal myelin thickness comparable to autograft	[173]
	Randomised clinical trial with neurotube®	Superior than graft for digital injuries	[193]
PLA/PLLA	Conduit implanted for 8 months in rats	No difference to isograft	[72, 71]
PLGA	Microbraided guide implanted for 1 month in rats	Axons in 9 out of 10 conduits	[21]
PHB	Clinical trial of wrap around implant with tests up to 18 months after surgery	PHB advantageous compared to epineural suturing at 18 months. No adverse effects	[1]
Piezoelectric	PC12 cells subjected to direct and alternating electrical stimulation (ES)	Percentage of neurite bearing cells, number of neurites per cell and neurite length all significantly higher with ES	[161, 139]
Hydrogels	Plain, corrugated and coil reinforced PHEMA-MMA conduits implanted into 10 mm rat defect for 8 and 16 week	Coil reinforced conduits had equivalent results compared to autograft at 16 weeks.	[108]
Silk fibroin (SF)	SF conduits implanted into	Results approach those of autograft	[203]

	10 mm rat defect for 6 months.		
Fibrin glue	Primary Schwann cells, differentiated ADSCs and MSCs seeded fibrin conduits in 1 cm rat defect for 16 weeks	Conduit implanted with ADSCs comparable to autograft	[62]
Acellular nerve Constructs	Monkey MSCs implanted into acellular allografts	Better electrophysiological results with MSCs	[95]
	Early clinical outcomes of decellularised allograft	No inflammation/rejection	[106]

Material Coatings

ECM	Schwann cells cultured on laminin, fibronectin and collagen coated mats	Schwann cell proliferation highest on laminin coated mats	[10]
Synthetic ECM peptides	Electrospun PCL/PEG fibers with linked ECM derived peptide	Higher Schwann cell migration on functionalised fibers	[23]
Plasma polymers	Human neuroblastoma cell line grown on AAc and allylamine surfaces.	Allylamine increased cell adhesion, AAc influenced differentiation marker neurofilament-200	[33]
	Rat Schwann cells grown on AAc coated aligned PLLA microfibres	Increase cell adhesion, alignment and survival versus PLLA alone	[143]

Topographical and chemical cues

Grooves and ridges	DRGs cultured on different grooves	Max alignment with 6 μm deep, 25 μm wide grooves	[26]
	Xenopus spinal and rat hippocampal neurites on various grooves	Xenopus parallel but hippocampal perpendicular to 1 μm deep grooves	[153]
Chemical gradients	PC12 cells on laminin peptide gradients	PC12 cell grow along gradient	[208]
Growth factors	Immobilised vs. conjugated NGF on electrospun scaffolds with rat MSCs.	Higher expression of neuronal markers with conjugated NGF	[44]
Electrospun fibers	19 mm defect with aligned and random polymer fibers	Superior outcome with aligned fibers	[113]
	DRG and Schwann cells on PCL and collagen/PCL electrospun fibers	Higher glial migration on Collagen/PCL	[166]
	3D electrospun structure using 2 pole air gap spinning with 7 weeks *in vivo* rat model	Immunolabelling revealed +ve NF-68, MBP and S100	[96]

	Adult rat hippocampal stem cells on different diameter electrospun fibers	20% increase in neuronal differentiation on 749 nm fibers compared to tissue culture plastic	[48]
Films	Compared 3 and 1 film internal scaffolds	Better functional outcome with 1	[52]
Channels	1, 2, 4 and 7 channel collagen conduits in rats	1 and 4 channel conduits superior	[209, 206]
Addition of Schwann cells			
Autologous Schwann cells	Devitalised muscle tissue seeded with Schwann cells	Higher axon counts and gastrocnemius muscle weight with Schwann cells	[110]
Allogeneic rat Schwann cells	Syngeneic and allogeneic cells seeded in PHB scaffold of sciatic nerve defect for 2, 3 and 6 weeks	Longer regeneration distance with cell seeded guides	[141]
Addition of Stem cells			
BMSCs	BMSCs seeded on acellular allogeneic graft in monkeys for 8 weeks	Higher CMAP scores and nerve fibers compared to grafts without BMSCs	[189]
ADSCs	ADSCs and BMSCs seeded onto fibrin conduit in rat defect for 16 weeks	Higher CMAP scores and axonal diameter compared to BMSCs	[62]

Table 3: Highlighting major strategies to improve nerve regeneration.

Poly(lactic-co-glycolic) acid (PLGA) is another popular choice of research for NGCs as its properties are well characterised and controllable. It is composed of hydrophilic polyglycolide and hydrophobic polylactide, which have a faster degradation rate when co-polymerised due to morphological changes[67]. An 85:15 PLGA foam managed to bridge a 10 mm sciatic nerve defect in rats after 12 weeks successfully[29]. Interestingly, a follow up study showed that subcutaneous implantation of the guides for a week prior to inserting into the nerve defect resulted in significantly more axons after 4 weeks[30]. Micropatterned PLGA guides coated with laminin peptide or collagen type 1 showed greater neurite alignment with 5 μm grooves compared to 10 μm grooves. The laminin coating was also found to be superior to the collagen coating in aligning neuronal outgrowth[211]. However, there was found to be a decrease in neurite number and total neurite length on the PLGA micro structured surfaces compared with the controls. It was suggested that neurites need a physical amount of space to protrude from the soma (cell body), that as the grooves restrict neurite outgrowth, this might

have had an adverse effect on the neurites. Another study adjusted the manufacture of PLGA by using 10:90 microbraided guides to try and overcome the rigidity of the material[20]. Although the average nerve diameter was only ~50% of normal nerve, axons migrated into 9 out of the 10 'conduits' in the guide. The guide degraded after 34 days in PBS however, so the degradation rate of the conduits may be too fast for human nerve defects.

Compared to PLGA, PLLA is stiffer due to a higher degree of crystallinity and takes up to 3 years to degrade[160]. Although the increased stiffness would prevent conduit collapse when implanted, the slow degradation rate could cause problems long term. Evans et al[73] found that after 16 weeks of being implanted in rats, there were twice the number of axons in a 10 mm PLLA guide compared to a PLGA guide. Reasons for the improved results may include the high porosity of the PLLA scaffold, as it was fabricated by a gas foaming/salt leaching technique. An 8 month implantation study in rats[70] showed that 12 mm PLLA conduits resulted in a sciatic functional outcome (SFI index) similar to isografts, proving their potential use in NGCs. The group tried to develop the conduits further by injecting allogeneic Schwann cells into the conduit after *in vivo* implantation[69], but results did not show any significant improvement. To the best of the author's knowledge, no long-term studies have yet been published. Cai etc al[35] studied PLA conduits with PLLA microfilaments embedded and had superior results against PLA conduits or silicone guides. However, an isograft comparison was not used and would have been beneficial for comparison.

Poly 3-hydroxybutyrate (PHB) is a thermoplastic polyhydroxyalkanoate produced by microorganisms such *Bacillus megaterium* and *Ralstonia eutrophus* when under physiological stress. It has been investigated for various medical applications such as sutures and wound dressings due to its excellent biocompatability[39]. It has even been suggested that PHB acts as a 'neural protective' agent, as the percentage of apoptotic cells decreases when exposed to the material compared to tissue culture plastic[200]. The degradation rate of pure PHB is rather slow (18-24 months) compared to other conduit materials. In a study by Freier et al[79] it's molecular weight was found to decrease by only half after a year when in 0.1 M Sørenson buffer at pH 7.4, 37˚C. PHB is also brittle, with low flexibility. However there has been some success in investigating PHB for NGCs. Mosahebi et al[140] filled PHB conduits with an alginate hydrogel, which were injected with syngeneic or allogeneic Schwann cells. Conduits from both types of cells bridged a 10 mm defect after 6 weeks, compared to 9mm

reached by an empty conduit. Young et al[215] also found that empty PHB conduits support peripheral nerve regeneration of up to 4 cm in rabbits after 63 days, bridging a defect site after 42 days. Promisingly, the area of regenerating fibres at 42 days was greater with PHB compared to the autograft. A further study implanted a PHB wrap into six patients, which gave advantageous results compared to epineural suturing at 18 months[1]. However, Kalbermatten et al[102] compared the PHB wrap to a fibrin glue conduit with a rat sciatic nerve model. After a month, Schwann and neuronal cells were located further into the fibrin conduit compared to PHB.

PCL has attractive properties as a biomaterial scaffold for regenerative medicine[198]. Although results with melt-extruded PCL regarding mechanical stiffness and inflexibility leading to detachment from implant site have been published[43], a PDLLA / CL blend is used commercially (Neurolac®). Chung et al[50] conjugated tirofiban and nerve growth factor (NGF) to PCL conduits and implanted them into a 12 mm rat sciatic nerve defect for 8 weeks. Compared to PCL and PCL/NGF, conduits with both tirofiban and NGF demonstrated stronger β-tubulin III and growth-associated protein-43 (GAP-43) labelling, as well as significantly heavier gastrocnemius muscle. Klinkhammer et al[115] developed a non-adherent blend of PCL with NCO-poly(ethylene glycol)-stat-poly(propylene glycol) (PCL / sPEG). After attaching the integrin binding peptide GRGDS, improved Schwann cell migration and improved axonal growth with DRG explants was reported. Other promising polymer blends include PCL / PLA[177] and PCL / PGA[38] conduits. Although PGA, PLA and PCL are clinically approved and safe for use, these materials can be relatively inert regarding neuronal or Schwann cell culture, benefitting from coating or material modifications.

Hydrogels have also been investigated as nerve guide conduits with the reasoning that the high water content mimics the mechanical properties of nerve tissue [98]. Poly(2-hydroxyethyl methacrylate) (PHEMA) was found to be too soft, so it was copolymerised with methyl methacrylate (MMA). After implanting the conduits into a 10 mm rat sciatic nerve gap for 4, 8 and 16 weeks, it was found that the nerve regeneration was comparable to nerve autografts at 4 and 8 weeks. However, at 16 weeks, 60% of the PHEMA-MMA conduits were similar to autografts whilst 40% had inferior outcomes[17]. A follow up paper then reported that 4 out of 14 PHEMA-MMA conduits had collapsed after 16 weeks as well as a number of conduits showing signs of chronic inflammation and calcification[16]. To try and improve the structural integrity of the conduits, Katayama et al[107] then developed plain, corrugated and coil-

reinforced PHEMA-MMA conduits and compared them against autografts after 8 and 16 weeks. The coil reinforced conduits showed better performance in terms of patency as well as nerve regeneration, with statistically similar results to an autograft after 16 weeks.

In efforts to enhance nerve regeneration by introducing electrical conductivity into nerve guide conduits, piezoelectric materials have been studied with varying success. Polyvinylidene fluoride (PVDF) conduits were fabricated and then mechanically stretched to align the dipoles. "Corona poling" by subjecting some of the conduits to an electric field for over 12 hours then caused them to become piezoelectric. The conduits, along with unpoled conduits (unable to conduct electricity) were implanted into a 4 mm sciatic nerve defect in rats for 4 and 12 weeks. The results showed significantly more myelinated axons in the piezoelectric conduits at both time points, and all conduits managed to bridge the defect[3]. This led the authors to suggest that electrical charge generation accelerates early phases of axonal elongation or myelination. Further investigations then progressed to a PVDF and trifluoroethylene (TFE) copolymer, where the piezoelectric conduits showed a significantly greater number of myelinated axons compared to unpoled conduits over 4 weeks in a 10 mm rat sciatic nerve defect model[78].

An electrically conducting polymer of poly(D, l-lactide-co-epsilon-caprolactone) (PDLLA/CL) doped with polypyrrole (PPy) was made using butane sulfonic acid and polystyrenesulfonate[219]. *In vitro* work found significantly more viable cells on the PDLLA/CL doped with PPy using butane sulfonic acid. Nerve measurements increased when exposed to a 10 μA constant current, then further increases were reported when an alternating current was used[139]. After making a conduit with the butane sulfonic acid material, it was implanted into an 8 mm rat sciatic nerve defect for 2 months. The authors reported myelinated axons and Schwann cells similar to native nerve, however they did not have an autograft for comparison. Given that the rats paws remained closed after 2 months from surgery and there was a lack of detail regarding the control conduit, the reported success of this approach required clarification.

Seil et al[169] investigated the nerve regeneration potential of zinc oxide nanoparticles embedded in a polyurethane polymer composite using astrocytes. It was hypothesised that zinc oxide nanoparticles possess increased piezoelectric properties over zinc oxide micron sized particles. Unfortunately the cell density decreased as the

ratio of zinc oxide nanoparticles was increased, demonstrating a deleterious response to the piezoelectric zinc oxide.

A very recent field gaining increased attention is the effect of near infrared laser therapy for stimulating neuronal differentiation and outgrowth[138]. Stimulation of an action potential in neuronal cells using pulsed infrared lasers, rather than the conventional electrical method[15], seems to be a very promising potential therapy. Regarding thermal tissue damage, functional loss was observed for continuous irradiation for 5 hours at 250 Hz, with energies over 25 µJ/pulse. When using a 250 Hz pulsed repetition rate, tissue withstood thermal damage at energies of 98 and 127 µJ/pulse[85]. Corroborating studies reported an increase in neurite outgrowth with near infrared laser irradiation of around 20-30% [170, 51, 199, 34]. Paviolo et al[150] fabricated gold nano rods, which were successfully taken up by NG108-15 neuronal cells. Laser powers of 1.2 – 7.5 W / cm^2 at 780 nm stimulated a neurite length increase of up to 25 µm compared to control (20-30% increase). Given that this effect was also seen when the gold rods were coated with silica, this novel study holds promise for incorporating gold nano particles into nerve guides for laser treatment.

1.1.7 Nerve guide conduit coatings

Selecting an appropriate material that is biocompatible and degrades over a particular time frame can mean compromising cell adhesion and proliferation characteristics. However, synthetic materials can be altered via techniques such as surface coating to make them more amenable to cell attachment, proliferation and migration. Extracellular matrix proteins have been studied extensively for this purpose, due to their documented effects on peripheral nerve regeneration. Laminin is found in the basal lamina, which forms a scaffold on which Schwann cells proliferate/migrate, which then in turn encourage neural cells to cross a defect site. When grown on laminin, Schwann cells increase both the number and outgrowth length of neuronal cells. The effect of laminin to act on neuronal cells through Schwann cells arises through the NF-κB signalling pathway[11]. Laminin was also found to direct the growth of axons directly to within the basal lamina tubes [190]. In implanted grafts obtained from close-cloned Wistar rats in a 1 cm rat sciatic nerve defect, 52% of regenerating axons were found outside the basal lamina scaffold and 48% inside when laminin was blocked. In controls, 92% axons were located within the basal lamina when laminin was not blocked.

In a related study, Armstrong et al[9] found that out of three extracellular matrix (ECM) proteins, laminin promoted Schwann cell proliferation compared to fibronectin, whilst fibronectin caused higher levels of Schwann cell proliferation compared to collagen. Although poly-D-lysine encouraged a higher Schwann cell proliferation than laminin, neurite outgrowth was not significantly different to laminin or fibronectin. Chen et al.[40] combined the three extracellular matrix proteins together in an extracellular gel, which was then loaded into silicone rubber tubes. The filled conduits were associated with 90% nerve regeneration across a 10 mm defect after 6 weeks, compared to 60% regeneration for an empty control conduit. The filled conduits also resulted in a 28% larger cross-sectional area as well as a 28% increase in the number of myelinated axons compared to the empty conduits. However, the control conduits did not contain extracellular matrix gel, so the regeneration success cannot be purely attributed to ECM proteins.

1.1.8 Haptotactic and topographical guidance

Dodla et al[63] investigated whether concentration gradients of laminin and neurotrophic growth factor (NGF) would affect nerve regeneration on isotropic and anisotropic agarose hydrogel scaffolds. Using a 20 mm rat sciatic nerve defect model containing phosphatidyl choline-based lipid microtubules (LMT) containing the active bio molecules for slow release, it was demonstrated that gradients of both laminin and NGF along with anisotropic scaffolds stimulate full nerve regeneration over 4 months, whereas a uniform distribution of laminin and NGF did not. The gradients of NGF and laminin within the anisotropic agarose hydrogel also showed a higher axon density compared to the syngeneic grafts and performed comparably. Interestingly, gradients of laminin and NGF did not stimulate nerve regeneration when on isotropic agarose hydrogel scaffolds, and nerve regeneration was also unsuccessful even on anisotropic gels if either laminin or NGF was present in uniform concentration. Another study[149] also found that laminin worked synergistically with other bioactive molecules such as basic Fibroblast Growth Factor (bFGF). Although immobilised laminin enhanced neurite outgrowth of ex vivo rat dorsal root ganglion (DRG) cells, the outgrowth was significantly enhanced when combined with bFGF.

When coated with laminin and fibronectin, a collagen type 1 nerve guide with collagen bundles had nerve fibers grow into the middle of the 1 cm rat sciatic nerve defect after 30 days, whereas the uncoated control did not[183]. After 60 days, although

both uncoated and coated nerve guides had regenerated across the defect, the uncoated control guide had fewer nerve fibers. The adhesive laminin peptide IKVAV also had an effect on neurite outgrowth. Immobilised gradients of the IKVAV peptide caused neurites of chick embryo DRGs to follow, then turn and migrate along them[2]. The velocity of the neurites slowed when turning along the gradient of IKVAV peptides but then resumed when on a straight course. Interestingly enough, Valentini et al[184] found that when in gel form, the presence of laminin and collagen impeded nerve regeneration across a rat nerve gap.

Intra-luminal scaffolds
- Electrospun fibers
- Films
- Gels
- Channels

Primary support cells
- Autologous, allogeneic and syngeneic Schwann cells

Stem Cells
- Bone marrow-derived stem cells
- Adipose-derived stem cells

Material coatings
- ECM
- Synthetic ECM peptides
- Plasma polymers

Conduit wall material
- PCL
- PGA
- PLA/PLLA
- PLGA
- PHB
- Piezoelectric materials
- Hydrogels
- Silk fibroin
- Acellular nerve
- Fibrin glue
- Chitosan
- Collagen

Topographical and chemical cues
- Grooves and ridges
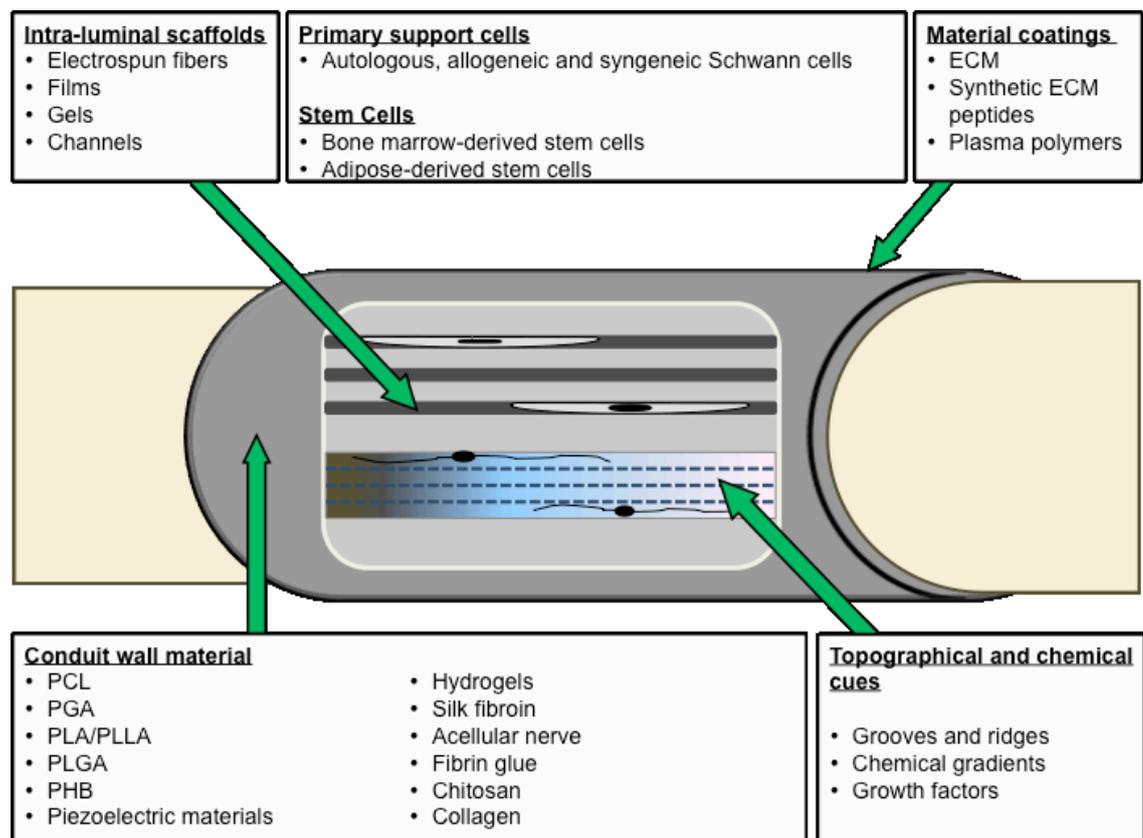- Chemical gradients
- Growth factors

Figure 3: A summary diagram of the various bioengineering approaches used to improve nerve regeneration.

It is now known that various topographies can influence cell differentiation and morphology[45]. Human mesenchymal stem cells cultured on nano-patterned surfaces expressed higher neurofilament light protein and myelin associated protein 2[213]. Britland et al[26] reported that 12 μm wide and 6 μm deep grooves stimulated optimal neurite alignment from DRG explants. When combined with parallel laminin tracks, optimal neurite alignment was then observed with 25 μm wide, 6 μm deep grooves. Perpendicular chemical and topographical cues caused DRGs to mostly follow the chemical cues when adsorbed to grooves with a depth of 500 nm. Supporting the

hypothesis that neurite extension requires a precise physical space, micro-patterned PLGA guides coated with laminin peptides or collagen type-1 showed greater neurite alignment on 5 μm grooves than 10 μm[210]. Similarly, Rajnicek et al[153] found that rat hippocampal neurites orientated perpendicularly to 1 μm wide grooves with depths of 130-1100 nm. This result was then reversed when the grooves were increased to a 4 μm width. NG108-15 neuronal cells and primary Schwann cells showed better alignment on patterns with a small ridge width (5 μm) and bigger groove width (20 μm) when cultured on a rolled micro grooved PCL nerve guides[178]. A similar approach using PCL and PCL/PLA rolled conduits in a 1 cm rat sciatic model for 2 weeks demonstrated nerve cable formation[177].

1.1.9 Addition of growth factors

It is well known that neurotrophic factors also enhance nerve regeneration, and efforts have been made to include them in nerve guide conduits. It was shown that conjugation of growth factors to the scaffold, rather than absorption, results in a greater enhancement of nerve regeneration[44]. After 7 weeks, fibrin cables had formed across a 15 mm rat sciatic nerve defect in 9 out of 10 ethylene vinyl acetate conduits when supplemented with slow release NGF and GDNF[77]. This was compared with no cables when the defect was treated with only the conduit. When added separately, GDNF stimulated a greater number of myelinated axons at the midpoint of the conduit when compared against NGF. A recent study that incorporated GDNF into microspheres within a PCL conduit, observed a significant increase in tissue integration after 6 weeks, when compared to PCL alone[116]. Other work found that a 357 ng/mL/mm gradient of NGF on a PHEMA gel was sufficient to stimulate extension, as well as guide 16±2% PC12 neurites along the gradient[104]. Neurotrophin-3 (NT-3) was investigated as a potential factor to add to nerve guide conduits by impregnating it into fibronectin mats. It was shown that fibronectin bound to and released the neurotrophic factor[175]. Using fibronectin mats as control, the conduit was sutured into a 10 mm rat sciatic nerve gap and then analysed after 5, 10, 15, 30 and 240 days. It was found that NT-3 significantly increased the number of myelinated axons after 8 months and had an optimal dose of 30-500 ng/ml. NT-3 also increased the distance the regenerating axons had penetrated as well as their axonal area after 15 days.

A study that investigated the effects of fibroblast growth factor 1(FGF-1), NT-3 and brain-derived neurotrophic factor (BDNF) found that FGF-1 at 10 μg/ml stimulated

nerve regeneration comparable to the autograft control over a 10 mm rat sciatic nerve defect after 8 weeks. However, FGF-1 was added at 10 μg/ml, whereas the other factors were added at 1 μg/ml. The factors were within a collagen matrix, which was added to the lumen of a PHEMA-MMA guide. Ni et al[145] grafted FGF-1 and chitosan onto gold nanoparticle-containing PLA conduits, which showed superior results to non grafted conduits in a 12 mm rat sciatic defect. Boyd and Gordon[24] investigated the effects of GDNF and BDNF at 0.1 μg and 2 μg/day respectively on chronic and acute axotomy. Although neither factor had an immediate effect, after 28 days of being introduced into the defect site, GDNF significantly increased the number of motor neurons that regenerated their axons. This effect was increased significantly when BDNF was perfused as well. This combination of GDNF and BDNF appears to have a much more stimulatory effect compared to either factor added in isolation. Whilst there is agreement that growth factors can significantly increase the speed of nerve regeneration, the cost of including such components into scaffolds can limit their use commercially.

1.2.0 Intraluminal Guidance

Electrospun micro- and nanofibres have attractive physical properties as intra-luminal scaffolds, and can be fabricated from a wide range of biocompatible materials[113]. Aligned fibres were shown to be more effective at guiding neuronal and Schwann cells compared to non-aligned[44, 191, 156, 118, 113, 42, 201, 188, 129, 96, 86]. Cho et al[44] demonstrated higher expression of nestin, β-tubulin III and MAP-2 on NGF-conjugated aligned PCL nanofibres versus non-aligned fibres, using rat mesenchymal stem cells. Regardless of whether the directional guidance is from channels, fibers or grooves, neuronal cells seem to be optimally guided with widths in the range of 5-20 μm and 10-20 μm in diameter. Whilst numerous studies agree that aligned nanofibers can also stimulate positive guidance[97, 86, 37], Schwann and neuronal cells tend to spread across nanofibers as a mat (reviewed in detail by Cunha et al[57]) rather than being restricted to a single cell / micro-fibre interaction. Please see figure 4 for micrographs.

It was reported[166] that DRGs extended faster on PCL aligned nanofibres (559 ± 300nm and 541 ± 164nm) compared to PCL containing collagen, but then had improved axonal guidance on PCL/collagen. Myelin P0 was found to be upregulated in human Schwann cells when cultured on aligned PCL, which was not observed on

random fibers[42]. Jha et al[96] described a novel 2-pole air gap electrospinnng method. The method was used to fabricate a 10 mm nerve guide, consisting of aligned fibres varying from 200 nm to 1.5-1.8 μm. After implantation into a rat sciatic model for 7 weeks, the defect was bridged with Schwann, neuronal and blood vessel formation. In contrast to fibres, a stainless steel wire template method for forming collagen multi-channels[206] was developed, which supported DRG explant outgrowth. Interestingly, collagen conduits containing multiple channels (4 or 7) had better physical properties compared to a single channel. Regarding the size of channels, Krych et al[118] found more regenerating axons in 450 μm channels instead of 650 μm channels when implanted into a rat spinal cord defect. Regarding intraluminal films, Clements et al[52] reported positive results using 1 intra-luminal film of poly-(acrylonitrile-co-methylacrylate) contained in a polysulfone conduit. In contrast, 3 films resulted in misaligned collagen bands and poor morphological organisation.
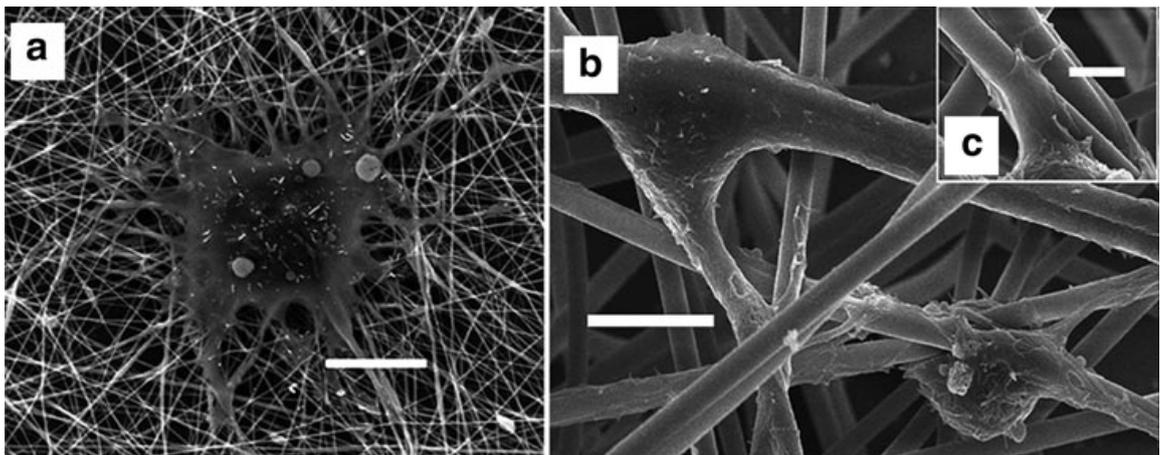

Figure 4: Scanning electron micrographs of rat neural stem progenitor cells cultured on (a) 283 nm and (b, c) 1452 nm fibres. Different morphologies were exhibited dependent on the fibre thickness. Scale bars are 10 μm for (b) and (c), 2 μm for (a). Modified and reproduced with permission[48].

Recent studies to bridge the gap between *in vitro* and *in vivo* includes work by Murray-Dunning et al[142], who described a closed-loop perfused bioreactor to introduce and culture cells on various nerve scaffolds. Conduits up to 8cm in length and 1.2mm internal diameter were studied, which were then filled with aligned intra-luminal PLLA microfibers. Surface modification of fibres by AAc plasma polymerisation demonstrated enhanced Schwann cell survival. A similar investigation introduced Schwann cells to a rotating wall bioreactor. Authors found that proliferation

was higher on spiral shaped scaffolds compared to porous, tubular or cylindrical shaped conduits[185].

1.2.1 Incorporation of cellular components into nerve guide conduits

Another strategy of improving nerve guide conduits is to inject cells into the scaffold, with recent efforts focused on Schwann cells due to their essential role in the formation of a basement scaffold for the growth of neuronal cells[81]. Another reason for the addition of Schwann cells was researched by Schlosshauer et al[165], who found that axons grow / extend 8 times faster than Schwann cells can migrate, when on poly-D-lysine or laminin. As the axons only grow across a defect when in intimate contact with Schwann cells, Schwann cell migration can be a limiting factor. If Schwann cells could be injected into a guide when implanted, their presence would potentially speed up axon growth dramatically. It was found that primary Schwann cells seeded on ECM (fibronectin, collagen and laminin) coated inserts above NG108-15 neuronal cells enhanced the number of neurites as well as the overall percentage of neuronal cells that had neurites[9]. When in direct contact with Schwann cells, neurites from the NG108-15 neuronal cells were longer compared to diffusible factors from Schwann cells alone. The presence of matrix proteins is reported to directly activate the neurotrophic properties of Schwann cells, but also the physical effects of Schwann cells (most likely via matrix protein formation) for neuronal cell differentiation. This gives further evidence for the use of Schwann cells in nerve guides.

Bryan et al[29] investigated the effect of adding autologous Schwann cells and glial growth factor (GGF) to a PLGA conduit in a 10 mm rat sciatic nerve defect. GGF stimulated an increase in axon number and a significant increase in the number of blood vessels. Adversely, the presence of exogenously added autologous Schwann cells caused a decrease in total axon count, as well as significantly lowering the number of myelinated axons compared to the saline filled controls. The negative results of the Schwann cells also extended to GGF by negating its positive effects when added in combination. The results did not correlate with numerous other studies, which demonstrated that the addition of autologous Schwann cells was significantly beneficial to nerve regeneration. The authors suggested that the small gap of 10 mm might have only stimulated a limited amount of growth factors to be released into the microenvironment. The added Schwann cells may have competed for and diluted the growth factors, reducing effect of growth factors overall. Another postulation was that

the available GGF receptors in the axonal membranes were saturated, and this had a knock on effect on the Schwann cells.

Allogeneic Schwann cells have also been investigated, as the cells would potentially be ready for injecting into a defect site immediately. The nerve regeneration benefits may also outweigh any immune response if mild enough. Mosahebi et al[140] added allogeneic and syngeneic Schwann cells into an alginate hydrogel and then into a PHB conduit, which was then sutured into a 10 mm rat sciatic nerve defect. 3 weeks after the guides were implanted there was a significant increase in regeneration distance in defects containing both types of Schwann cells compared to guides without. Allogeneic cells equalled syngeneic cells in the regeneration distance crossed. As well as showing similar results to the syngeneic Schwann cells, it was reported that the allogeneic cells did not induce any deleterious immune response. This could be very clinically promising due to the potential availability of allogeneic Schwann cells from cadavers. However, other studies have not had such agreeable results. Evans et al[69] injected $1x10^4$ and $1x10^6$ allogeneic Schwann cells into a collagen matrix, then implanted the matrix into a PLLA nerve guide. The guide was inserted into a 12 mm rat sciatic nerve defect and evaluated at 2 and 4 months. Unfortunately there were no positive significant differences between the cell injected and empty guide as well as an inferior performance compared to the reversed isograft. Further investigations may be warranted to ascertain the apparent differences recorded with allogeneic Schwann cells.

A drawback for translating promising *in vitro* results into clinical solutions is the very limited availability of autologous Schwann cells. One approach to circumnavigate the problem is to use stem cells from another location. The stem cells could be differentiated towards a Schwann cell lineage, which would be especially advantageous if the stem cells were accessible and available in higher numbers. Mesenchymal stem / stromal cells (MSCs) (first identified in 1966[80]) show promising properties, such as hypo-immunogenicity [4, 158, 61] and a 'homing' mechanism towards injury sites [158]. The International Society for Cellular Therapy (ISCT) suggests three identifying characteristic of MSCs[64]: 1) plastic adherence under standard conditions; 2) $\geq$ 95% population positive for CD105, CD73 and CD90 and 3) negative ($\leq$ 2%) for CD45, CD34, CD14 / CD11b, CD79 / CD19 and human leukocyte antigen class II. MSCs can be differentiated into glial-like cells and aid neuronal survival[110, 60, 152, 167, 136, 181, 13, 197, 202, 27], as the expression on neuronal and glial proteins is present in naïve MSC, then increases during differentiation[182]. Mahay et al[130] found that

differentiated MSCs (dMSCs) produced NGF and BDNF, increased motor recovery, and myelinated mouse sciatic axon number, when delivered in collagen tubes. Similarly, decellularised allografts that contained autologous BMSCs showed improved electrophysiology after 8 weeks[189] and 6 months[95] implantation into Rhesus monkeys. BMSC-derived Schwann cells[8] were also reported to perform as well as autologous Schwann cells when implanted with chitosan conduits, with a higher number of myelinated axons and comparable muscle fiber histology. A recent study combined autografting with differentiated Schwann-like BMSC, which was then contained within a PGA nerve guide[56]. Whilst the differentiated BMSCs showed superior results, nondifferentiated BMSCs also stimulated better regeneration compared to controls.

Adipose tissue derived stem cells (ADSCs) have some significant advantages over BMSCs[114, 196], including a higher stem cell number recovered and less invasive isolation procedure[123, 46]. It is also worth noting that 1 out of 25,000 - 100,000 bone-marrow cells are stem-like, compared to 2% from adipose tissue[176]. Di Summa et al[62] compared differentiated rat ADSCs to MSCs, using a fibrin conduit and sciatic nerve defect. After 16 weeks, the ADSC conduit showed a superior motor regeneration and evoked a higher potential at gastrocnemius muscle. Recently, Kaewkhaw et al[101] studied the effects of anatomical origin regarding ADSCs for differentiation to Schwann cells. There were revealing differences between kidney, subcutaneous, and epididymis fat sources, together with supporting evidence for subcutaneous ADSC differentiation to Schwann cells and function.

Another study injected autologous, non differentiated human ADSCs into a RGD peptide coated PCL nerve guide to investigate whether the nerve environment would stimulate neural differentiation[163]. The guides were implanted into a 6 mm sciatic nerve defect in athymic rats with evaluation of the guides after 12 weeks. Any early regeneration improvements were not apparent by week 12 and lipid droplets were found in the ADSC guide. It indicated that the stem cells had differentiated into fat cells, even though the physical and biochemical environment had changed. Although the study was relevant for addressing whether ADSCs need to be predifferentiated before implantation into a guide, the lack of immune response could have been a factor as to why the stem cells did not differentiate towards a neuronal lineage.

Alternative stem cell types have been investigated as potential sources for Schwann cells. Stem cells that reside in the hair follicle bulge have shown promising

results as a Schwann cell source[7] as studies have found that they test negative for keratinocyte marker 15 and express nestin, a protein marker for neural stem cells.

Although it has been shown that the addition of exogenously added glial cells can significantly improve nerve regeneration, there are many detrimental practical considerations. Getting approval for a product that uses autologous, allogeneic or xenogeneic cells is complicated, time consuming and costly. Funding for such bespoke treatment can difficult, and without it, clinical trials cannot go ahead. Even if patient trials are successful, economic studies may show that it is not economically viable, especially if one considers the cost of implanting a nerve guide conduit with dADSCs. The conduit, as well as the extraction, purification and differentiation of cells and two surgical procedures must be taken into account. Laboratory start-up costs and trained technicians to prepare the samples mean that unless there is high enough demand, the treatment may not be commercially viable. In addition to cost, the practical considerations of implanting a cellular scaffold within a restricted time frame after the initial surgery could also cause limitations. For example, Myskin™, an autologous epidermal substitute used to treat burns and chronic ulcers produced originally by company CellTran Ltd, involves a 2 week period to expand the samples and a 2-3 day window to implant. A 10 year audit[92] found that 53.2% of the cell sheets prepared had to be discarded due to restricted time frame of patient availability. Compared against autografts which use the patient's own nerve and need only one surgical procedure, operations such as Myskin™ can be comparatively complicated.

A lesson learnt from commercially available nerve guide conduits is that they do not use biologics and are off the shelf products. If these products can be improved, the complications involved with including Schwann cells or expensive neurotrophic factor treatment might be avoided. It could be both clinically and economically more viable to develop an off the shelf product that can be implanted immediately into the patient. There are already a number of materials available that have the right mechanical and degradation characteristics; however their cell adhesion, migration and proliferation properties could be improved. As discussed previously, there has been some promising research into coating conduits in order to improve them. This project has therefore looked into the effect of AAc and maleic anhydride plasma polymerised coatings on the metabolic rate and morphology of neuronal and Schwann cells.

1.2.2 Plasma polymerisation

Plasma polymerisation is a cheap, quick and relatively easy method of coating any substrate with ~10+ nm functionalised layer. Plasma polymerisation in this thesis used organic species and was usually performed under a rough vacuum, but can also be performed on an industrial scale at atmospheric pressure[172]. Radio frequency (RF) energy ionises the monomer into positively and negatively charged species[212]. A partially ionised gas is formed, in which will be ions, electrons, neutral and excited species and photons. The plasma causes the positively charged species to coat all surfaces in contact with the plasma. In order to retain functionality and have a well-adhered coating, the flow rate must be balanced against the amount of RF energy put into the system. If the flow rate is too low compared to the RF input, the monomer will fragment to a comparatively greater extent and functionality will be lost. A very high RF energy/molecule ratio with organic species will result in an oil-like layer, as it will mostly be composed of carbon. If the flow rate is too high compared to the RF input, the monomer will not be ionised enough. Although there would be a high retention of functionality, the coating will be loosely adhered and may come off. If the flow rate and RF input are matched correctly, a well-adhered layer will result with functional groups retained.

Plasma polymers have desirable features that lend their use in biomedical and material coating applications. Termed as Chemical Vapour Deposition (CVD) when used at higher powers for engineering-based applications, uses of CVD include refractory ceramic materials used for hard coatings, protection against corrosion, optoelectronics and energy conversion devices, along with semiconductors, dielectrics and metallic films for microelectronics[47]. Within the biomedical industry, the company CellTran™ developed Myskin™, which used plasma polymerised silicone substrates as cell carriers. The acrylic acid-coated silicone substrates were used as cell culture platforms to expand autologous keratinocytes, which were released after a given period of time. The sheets of keratinocytes were then used to heal chronic ulcers and burn injuries[87, 92]. Celltran™ also investigated the effect of controlling the spatial distribution and growth of vascular smooth muscle cells, porcine mesenchymal stem cells and human skeletal muscle cells adhesion using octadiene and acrylic acid[76]. Cerebellar neurons and growth plate chondrocytes have also been investigated for potential applications in controlling cellular distribution and growth, using plasma polymerisation[31]. The company Plasso Ltd also utilised plasma polymerisation of acrylic acid in order to develop biologically relevant coatings for *in vitro* applications

[14]. Whilst the company was bought out, the plasma polymerisation technique was used to bind heparin onto cell culture plates[131].

1.2.3 Acrylic acid and maleic anhydride plasma polymers

There is substantial research on AAc surfaces, which include clinical use in CellTran and Myskin™, which indicate that the density of carboxyl groups on the plasma polymerised surfaces has an effect on cell adhesion and differentiation. Detomaso et al[59] cultured hTERT-BJ1 fibroblasts onto AAc coated surfaces of polystyrene and compared them against uncoated surfaces. There was a significant difference between the two surfaces, AAc supported a higher number of adhered cells and higher percentage of area covered by cells. Morphologically, the cells had a flatter phenotype, with multiple fillipodia on the AAc coated surface, which had an average carboxyl group density of 2.3×10^{-9} mol/cm^2. The coating conditions were 100W continuous plasma deposition, which resulted in high fragmentation of the monomer. AFM analysis showed a substantially altered topology of the plasma treated surfaces compared to uncoated surfaces.

Another study evaluated the effect of carboxyl group gradients on C17.2 neuronal cells[122]. UV grafting was used to attach the –COOH gradient, with argon post plasma treatment to create a more 'uniform' cell distribution when seeding. Interestingly, up to 3.7 times more cells developed neurites when moving down the gradient of acid group, rather than at higher densities of acid group. When migrating down the gradients, the neuronal cells also demonstrated longer neurites, and more cells were observed on the surfaces with the low density of –COOH groups than high. This shows that although an acidic surface can be beneficial, a low density of acid groups may be preferential. Mesenchymal stem cell adhesion was also evaluated on plasma polymerised AAc sililcon elastomer surfaces along with 10% DMEM and serum free conditions, with TCPS as a control[53]. Cell counts after 3 hours of seeding cells in 10% DMEM onto the AAc coated surfaces showed a large increase from 30 to 70 per field of view compared to TCPS. However this difference diminished after 24 hours, which also occurred under serum free conditions. After 10 days there weren't any significant differences between the surfaces in either medium. However, a 4-fold increase in cell number was found when cultured in serum free conditions compared to serum conditions when on TCPS.

Co-cultures of melanocytes and keratinocytes were investigated on plasma polymerised AAc and allylamine surfaces[74] as well by Eves etc al, along with different medium compositions. Whilst both cell types attached and proliferated on the two plasma treated surfaces, any differences between the AAc and allylamine surfaces seemed to be dependent on the medium used. Morphology differences were reported regarding melanocytes. On 100% AAc surfaces the melanocytes had smaller cytoplasmic bodies and spindly, longer processes. On the allylamine surfaces the cells had 'fatter' bodies with shorter processes. As certain morphological characteristics can indicate differentiation, this may suggest that AAc had a more dramatic effect on the differentiation of cells compared to allylamine.

The effect that cell culture medium can have in altering cellular response to different plasma polymerised surfaces has also been reported by Buttiglione et al[33]. Although changes in cell culture medium seemed to have a dominant effect on cell adhesion of human neuroblastoma SH-SY5Y cells, the plasma modified surfaces (AAc and allylamine at 50W and 100W) then enhanced the cAMP-dependent (medium component) differentiation of cells. Regarding acrylic acid, there was a larger area covered by cells with the higher-powered regime of 100W, again indicating that a lower distribution of acid groups had a positive effect on cell proliferation. 100W power would have resulted in a higher degree of monomer fragmentation and an increase in the hydrocarbon ratio, reducing the percentage of carboxylic acid groups on the surface compared to 50W power. It was suggested that the response of cells to the more hydrocarbon-based surface could have been due to electrostatic interactions between the negatively charged acid groups and negatively charged cell membrane. When there is a low density of –COOH groups, the increased hydrophilicity imparted onto the surface is amenable to cell attachment, whilst the electrostatic repulsions between the surface and membrane are not strong enough to repel attachment. However at high densities of acid groups this electrostatic repulsion becomes stronger, leading to a detrimental effect on cell attachment. If serum is present, this repulsion will be mitigated. This can be contrasted to allylamine, which is positively charged and showed superior cell adhesion. The results from Buttiglione also corroborated with Eves et al. in terms of differentiation. AAc coatings at both powers sustained neuronal differentiation even in 10% DMEM as shown by positive neurofilament marker 200 staining, whilst the allylamine surfaces did not. Overall, low densities of plasma polymerised AAc appeared

to have a positive effect on cell adhesion and proliferation as well as neuronal differentiation.

Thin surface layers such as plasma-polymerised coatings can have an effect on protein adsorption. The finding that initially adsorbed proteins can be displaced by other proteins that have a higher affinity with the surface was first described by Vroman et al[186]. When a surface is exposed to a solution containing various proteins such as bovine serum albumin (BSA), smaller and more mobile proteins that reach the surface initially will bind electrostatically. As more proteins reach the surface, the surface chemistry will dictate which proteins have the greater affinity. For example, vitronectin frequently has a greater surface affinity compared to fibronectin due to the ability of vitronectin to adsorb competitively over adhesion-inhibiting proteins[195]. The composition and conformation of proteins on a surface will therefore adjust over 24 hours due to the replacement, rearrangement and conformational changes of initially absorbed proteins such as albumin, in order to facilitate further protein attachment and make way for proteins with higher surface affinity[93]. The presence, composition and conformation of serum proteins has been shown to have a dramatic effect on the adhesion, proliferation and differentiation of various cell types[111, 112, 54, 58, 134].

Plasma polymerised maleic anhydride surfaces with cell culture investigations have not previously been reported on to the author's knowledge. However, there have been reports into different duty cycles of maleic anhydride and the effect on the anhydride functionality retention. The first group to publish results on the plasma polymerisation of maleic anhydride was Ryan et al[162]. By using X-ray photoelectron spectroscopy (XPS) and transmission infrared spectroscopy, they found that a fixed duty cycle of 20 μs on and 1200 μs off with a peak power of 5W produced a significant enhancement of the –C(O)=O anhydride group at the expense of the hydrocarbon and –C=O/O-C-O environments, with a parallel increase in the oxygen and carbon ratio. It was found that anhydride functionality was favoured with lower powers as well as shorter on-times and longer off-times in the duty cycle. Chu et al[49] investigated the hydrolysis and swelling behaviour of plasma polymerised maleic anhydride films using optical waveguide spectroscopy. As the humidity increased, so too did the thickness and refractive index of the 500-700 nm film, indicating water penetration and uptake. The increased thickness of the film with the addition of water was, and has been since, attributed to the swelling of the polymer networks and reaction of the anhydride groups, leading to carboxylic acid groups. Chu et al also found that the thickness and refractive

index of the films increased with an increase in pH and ionic strength. It was suggested that the increased thickness at high pH was because the –COOH groups dissociated and the negative charge repulsion led to a small increase in the thickness. In a high ionic strength solution, it was postulated that an increase in Na^+ ions associating with the –COO^- groups would also cause a small increase in film thickness.

The most recent study on plasma polymerised maleic anhydride was by Mishra et al[137], who analysed fresh and reacted surfaces of maleic anhydride with XPS, fourier transform infrared spectroscopy and time of flight static secondary ion mass spectrometry (ToF-SIMS). In agreement with previous studies, the highest anhydride retention was found on the microsecond pulsing regimes, with longer off-times and a lower peak power. In investigating hydrolysis of the films it was found that under conditions of deionised water and hydrochloric acid (pH 2, ~0.3 mM) at 90˚C, it took up to 4 hours to open the anhydride ring, when the film had been coated with a 80 μs on time, 800 μs off time and peak power of 10W. ATR-FTIR analysis did not find any carboxylic acid groups in the lower peak power cycles, suggesting that a nominal power of 1W or lower is insufficient to open the maleic anhydride ring, which leads to a higher retention of anhydride groups.

1.2.4 Aims and Objectives

The aim of this work was to investigate the effect of plasma polymerised surfaces on the metabolic rate and morphological characteristics of neuronal cells, Schwann cells, explanted and dissociated primary rat dorsal root ganglion (DRG). This extends previous work reporting that neuronal and Schwann cell proliferation and neurite extension is enhanced on particular plasma polymerised surfaces[143]:

1. Investigation of acrylic acid (AAc) and maleic anhydride (MA) plasma polymerised surfaces. Characterisation was performed using contact angle, x-ray photoelectron spectroscopy and time-of-flight secondary mass spectroscopy.

2. Investigate conditions of NG108-15 neuronal cell line for plasma polymer work. This included the optimisation of culture conditions and determining which labelling agents should be used for optimal assessment of neurite outgrowth.

3. Culturing NG108-15 neuronal cells on AAc and MA plasma polymers. Assessment of morphology using the following neuronal measurements: Percentage of neurons with neurites, maximum neurite length per neuron and number of neurites per neuron, plus metabolic rate assays.

4. Investigate primary rat Schwann cell culture in response to AAc and MA plasma polymers as Schwann cells play a key role in nerve regeneration. As previous work has already optimised Schwann cell culture conditions[100], established conditions will be used.

5. Investigate and optimise plasma polymer surfaces with primary rat DRG explant cultures in order to investigate primary neuronal cell culture with plasma polymers. As the NG108-15 neuronal cell line was immortal, investigations with mortal primary neuronal cell cultures could be more indicative of primary human neuronal cell response.

6. Investigate the effect of AAc and MA plasma polymers with dissociated primary rat DRG cultures, as dissociated DRG tend to have less contaminating fibroblasts. As dissociated DRG have multiple cell types contained within each DRG, co-immunostaining protocols will be developed. Again, neuronal measurements will be taken in order to quantitatively evaluate surfaces. As DRG cultures can yield varying numbers of cells, which are generally metabolically quite senescent, MTS metabolic rate assays would be inappropriate with DRG cultures.

1.2.5 References

1. Åberg, M., C. Ljungberg, E. Edin, et al., Clinical evaluation of a resorbable wrap-around implant as an alternative to nerve repair: A prospective, assessor-blinded, randomised clinical study of sensory, motor and functional recovery after peripheral nerve repair. Journal of Plastic, Reconstructive & Aesthetic Surgery, 2009. **62**(11): p. 1503-1509.

2. Adams, D.N., E.Y.C. Kao, C.L. Hypolite, et al., Growth cones turn and migrate up an immobilized gradient of the laminin IKVAV peptide. Journal of Neurobiology, 2005. **62**(1): p. 134-147.

3. Aebischer, P., R.F. Valentini, P. Dario, et al., Piezoelectric guidance channels enhance regeneration in the mouse sciatic nerve after axotomy. Brain Research, 1987. **436**(1): p. 165-168.

4. Aggarwal, S. and M.F. Pittenger, Human mesenchymal stem cells modulate allogeneic immune cell responses. Blood, 2005. **105**(4): p. 1815-1822.

5. Ahmed, T.A.E., E.V. Dare, and M. Hincke, Fibrin: A versatile scaffold for tissue engineering applications. Tissue Engineering Part B-Reviews, 2008. **14**(2): p. 199-215.

6. Alluin, O., C. Wittmann, T. Marqueste, et al., Functional recovery after peripheral nerve injury and implantation of a collagen guide. Biomaterials, 2009. **30**(3): p. 363-373.

7. Amoh, Y., L. Li, R. Campillo, et al., Implanted hair follicle stem cells form Schwann cells that support repair of severed peripheral nerves. Proceedings of the National Academy of Sciences of the United States of America, 2005. **102**(49): p. 17734-17738.

8. Ao, Q., C.K. Fung, A.Y. Tsui, et al., The regeneration of transected sciatic nerves of adult rats using chitosan nerve conduits seeded with bone marrow stromal cell-derived Schwann cells. Biomaterials, 2011. **32**(3): p. 787-796.

9. Armstrong, S.J., M. Wiberg, G. Terenghi, et al., ECM Molecules Mediate Both Schwann Cell Proliferation and Activation to Enhance Neurite Outgrowth. Tissue Engineering, 2007. **13**(12): p. 2863-2870.

10. Armstrong, S.J., M. Wiberg, G. Terenghi, et al., ECM molecules mediate both Schwann cell proliferation and activation to enhance neurite outgrowth. Tissue Engineering, 2007. **13**(12): p. 2863-2870.

11. Armstrong, S.J., M. Wiberg, G. Terenghi, et al., Laminin activates NF-[kappa]B in Schwann cells to enhance neurite outgrowth. Neuroscience Letters, 2008. **439**(1): p. 42-46.

12. Atala, A., S.B. Bauer, S. Soker, et al., Tissue-engineered autologous bladders for patients needing cystoplasty. Lancet, 2006. **367**(9518): p. 1241-1246.

13. Barry, F.P. and J.M. Murphy, Mesenchymal stem cells: clinical applications and biological characterization. The International Journal of Biochemistry & Cell Biology, 2004. **36**(4): p. 568-584.

14. Barton, D., A.G. Shard, R.D. Short, et al., The effect of positive ion energy on plasma polymerization: A comparison between acrylic and propionic acids. Journal of Physical Chemistry B, 2005. **109**(8): p. 3207-3211.

15. Bec, J.M., E.S. Albert, I. Marc, et al., Characteristics of laser stimulation by near infrared pulses of retinal and vestibular primary neurons. Lasers in Surgery and Medicine, 2012. **44**(9): p. 736-745.

16. Belkas, J.S., C.A. Munro, M.S. Shoichet, et al., Long-term in vivo biomechanical properties and biocompatibility of poly(2-hydroxyethyl

methacrylate-co-methyl methacrylate) nerve conduits. Biomaterials, 2005. **26**(14): p. 1741-1749.

17. Belkas, J.S., C.A. Munro, M.S. Shoichet, et al., Peripheral nerve regeneration through a synthetic hydrogel nerve tube. Restorative Neurology and Neuroscience, 2005. **23**(1): p. 19-29.

18. Bertleff, M.J., M.F. Meek, and J.P. Nicolai, A prospective clinical evaluation of biodegradable neurolac nerve guides for sensory nerve repair in the hand. The Journal of Hand Surgery, 2005. **30**(3): p. 513-518.

19. Bertleff, M.J.O.E., M.F. Meek, and J.-P.A. Nicolai, A Prospective Clinical Evaluation of Biodegradable Neurolac Nerve Guides for Sensory Nerve Repair in the Hand. The Journal of Hand Surgery, 2005. **30**(3): p. 513-518.

20. Bini, T.B., S. Gao, X. Xu, et al., Peripheral nerve regeneration by microbraided poly(L-lactide-co-glycolide) biodegradable polymer fibers. Journal of Biomedical Materials Research Part A, 2004. **68A**(2): p. 286-295.

21. Bini, T.B., S.J. Gao, X.Y. Xu, et al., Peripheral nerve regeneration by microbraided poly(L-lactide-co-glycolide) biodegradable polymer fibers. Journal of Biomedical Materials Research Part A, 2004. **68A**(2): p. 286-295.

22. Blesch, A. and M.H. Tuszynski, Cellular GDNF delivery promotes growth of motor and dorsal column sensory axons after partial and complete spinal cord transections and induces remyelination. The Journal of Comparative Neurology, 2003. **467**(3): p. 403-417.

23. Bockelmann, J., K. Klinkhammer, A. von Holst, et al., Functionalization of electrospun poly(epsilon-caprolactone) fibers with the extracellular matrix-derived peptide GRGDS improves guidance of schwann cell migration and axonal growth. Tissue engineering. Part A, 2011. **17**(3-4): p. 475-486.

24. Boyd, J.G. and T. Gordon, Glial cell line-derived neurotrophic factor and brain-derived neurotrophic factor sustain the axonal regeneration of chronically axotomized motoneurons in vivo. Experimental Neurology, 2003. **183**(2): p. 610-619.

25. Brenner, M.J., J.R. Hess, T.M. Myckatyn, et al., Repair of Motor Nerve Gaps With Sensory Nerve Inhibits Regeneration in Rats. The Laryngoscope, 2006. **116**(9): p. 1685-1692.

26. Britland, S., C. Perridge, M. Denyer, et al., Morphogenetic guidance cues can interact synergistically and hierarchically in steering nerve cell growt. Experimental Biology Online, 1996. **1**(2).

27. Brohlin, M., D. Mahay, L.N. Novikov, et al., Characterisation of human mesenchymal stem cells following differentiation into Schwann cell-like cells. Neuroscience Research, 2009. **64**(1): p. 41-49.

28. Brushart, T., Motor axons preferentially reinnervate motor pathways. J. Neurosci., 1993. **13**(6): p. 2730-2738.

29. Bryan, D.J., A.H. Holway, K.-K. Wang, et al., Influence of Glial Growth Factor and Schwann Cells in a Bioresorbable Guidance Channel on Peripheral Nerve Regeneration. Tissue Engineering, 2000. **6**(2): p. 129-138.

30. Bryan, D.J., J.B. Tang, A.H. Holway, et al., Enhanced Peripheral Nerve Regeneration Elicited by Cell-Mediated Events Delivered via a Bioresorbable PLGA Guide. J reconstr Microsurg, 2003. **19**(02): p. 125-134.

31. Bullett, N.A., D.P. Bullett, F.E. Truica-Marasescu, et al., Polymer surface micropatterning by plasma and VUV-photochemical modification for controlled cell culture. Applied Surface Science, 2004. **235**(4): p. 395-405.

32. Bushnell, B.D., A.D. McWilliams, G.B. Whitener, et al., Early Clinical Experience With Collagen Nerve Tubes in Digital Nerve Repair. The Journal of Hand Surgery, 2008. **33**(7): p. 1081-1087.

33. Buttiglione, M., F. Vitiello, E. Sardella, et al., Behaviour of SH-SY5Y neuroblastoma cell line grown in different media and on different chemically modified substrates. Biomaterials, 2007. **28**(19): p. 2932-2945.

34. Byrnes, K.R., R.W. Waynant, I.K. Ilev, et al., Light promotes regeneration and functional recovery and alters the immune response after spinal cord injury. Lasers in Surgery and Medicine, 2005. **36**(3): p. 171-185.

35. Cai, J., X. Peng, K.D. Nelson, et al., Permeable guidance channels containing microfilament scaffolds enhance axon growth and maturation. Journal of Biomedical Materials Research Part A, 2005. **75A**(2): p. 374-386.

36. Campbell, W.W., Evaluation and management of peripheral nerve injury. Clinical Neurophysiology, 2008. **119**(9): p. 1951-1965.

37. Cao, H., T. Liu, and S.Y. Chew, The application of nanofibrous scaffolds in neural tissue engineering. Advanced Drug Delivery Reviews, 2009. **61**(12): p. 1055-1064.

38. Chan-Park, M.B., A.P. Zhu, J.Y. Shen, et al., Novel Photopolymerizable Biodegradable Triblock Polymers for Tissue Engineering Scaffolds: Synthesis and Characterization. Macromolecular Bioscience, 2004. **4**(7): p. 665-673.

39. Chen, G.-Q. and Q. Wu, The application of polyhydroxyalkanoates as tissue engineering materials. Biomaterials, 2005. **26**(33): p. 6565-6578.

40. Chen, Y.-S., C.-L. Hsieh, C.-C. Tsai, et al., Peripheral nerve regeneration using silicone rubber chambers filled with collagen, laminin and fibronectin. Biomaterials, 2000. **21**(15): p. 1541-1547.

41. Chen, Y.Y., D. McDonald, C. Cheng, et al., Axon and Schwann Cell Partnership During Nerve Regrowth. Journal of Neuropathology & Experimental Neurology, 2005. **64**(7): p. 613-622.

42. Chew, S.Y., R. Mi, A. Hoke, et al., The effect of the alignment of electrospun fibrous scaffolds on Schwann cell maturation. Biomaterials, 2008. **29**(6): p. 653-661.

43. Chiono, V., G. Vozzi, F. Vozzi, et al., Melt-extruded guides for peripheral nerve regeneration. Part I: Poly(epsilon-caprolactone). Biomedical Microdevices, 2009. **11**(5): p. 1037-1050.

44. Cho, Y.I., J.S. Choi, S.Y. Jeong, et al., Nerve growth factor (NGF)-conjugated electrospun nanostructures with topographical cues for neuronal differentiation of mesenchymal stem cells. Acta Biomaterialia, 2010. **6**(12): p. 4725-4733.

45. Choi, C.K., M.T. Breckenridge, and C.S. Chen, Engineered materials and the cellular microenvironment: a strengthening interface between cell biology and bioengineering. Trends in Cell Biology, 2010. **20**(12): p. 705-714.

46. Choi, J.H., J.M. Gimble, K. Lee, et al., Adipose Tissue Engineering for Soft Tissue Regeneration. Tissue Engineering Part B: Reviews, 2010. **16**(4): p. 413-426.

47. Choy, K.L., Chemical vapour deposition of coatings. Progress in Materials Science, 2003. **48**(2): p. 57-170.

48. Christopherson, G.T., H. Song, and H.Q. Mao, The influence of fiber diameter of electrospun substrates on neural stem cell differentiation and proliferation. Biomaterials, 2009. **30**(4): p. 556-564.

49. Chu, L.-Q., R. Förch, and W. Knoll, Pulsed Plasma Polymerized Maleic Anhydride Films in Humid Air and in Aqueous Solutions Studied with Optical Waveguide Spectroscopy. Langmuir, 2006. **22**(6): p. 2822-2826.

50.   Chung, T.W., M.C. Yang, C.C. Tseng, et al., Promoting regeneration of peripheral nerves in-vivo using new PCL-NGF/Tirofiban nerve conduits. Biomaterials, 2011. **32**(3): p. 734-743.

51.   Ciofani, G., S. Danti, D. D'Alessandro, et al., Enhancement of neurite outgrowth in neuronal-like cells following boron nitride nanotube-mediated stimulation. ACS nano, 2010. **4**(10): p. 6267-6277.

52.   Clements, I.P., Y.-t. Kim, A.W. English, et al., Thin-film enhanced nerve guidance channels for peripheral nerve repair. Biomaterials, 2009. **30**(23-24): p. 3834-3846.

53.   Colley, H.E., G. Mishra, A.M. Scutt, et al., Plasma Polymer Coatings to Support Mesenchymal Stem Cell Adhesion, Growth and Differentiation on Variable Stiffness Silicone Elastomers. Plasma Processes and Polymers, 2009. **6**(12): p. 831-839.

54.   Collier, T.O., C.R. Jenney, K.M. DeFife, et al., Protein adsorption on chemically modified surfaces. Biomedical sciences instrumentation, 1997. **33**: p. 178-183.

55.   Cooper, A., N. Bhattarai, and M. Zhang, Fabrication and cellular compatibility of aligned chitosan–PCL fibers for nerve tissue regeneration. Carbohydrate Polymers, 2011. **85**(1): p. 149-156.

56.   Costaa, H.J.Z.R., R.F. Bentoa, R. Salomonea, et al., Mesenchymal bone marrow stem cells within polyglycolic acid tube observed in vivo after six weeks enhance facial nerve regeneration. Brain Research, 2013. (1510): p. 10-21.

57.   Cunha, C., S. Panseri, and S. Antonini, Emerging nanotechnology approaches in tissue engineering for peripheral nerve regeneration. Nanomedicine : nanotechnology, biology, and medicine, 2011. **7**(1): p. 50-59.

58.   Curtis, A. and C. Wilkinson, Topographical control of cells. Biomaterials, 1997. **18**(24): p. 1573-1583.

59.   Detomaso, L., R. Gristina, G.S. Senesi, et al., Stable plasma-deposited acrylic acid surfaces for cell culture applications. Biomaterials, 2005. **26**(18): p. 3831-3841.

60.   Dezawa, M., I. Takahashi, M. Esaki, et al., Sciatic nerve regeneration in rats induced by transplantation of in vitro differentiated bone-marrow stromal cells. European Journal of Neuroscience, 2001. **14**(11): p. 1771-1776.

61.   Di Nicola, M., Human bone marrow stromal cells suppress T-lymphocyte proliferation induced by cellular or nonspecific mitogenic stimuli. Blood, 2002. **99**(10): p. 3838-3843.

62.   di Summa, P.G., D.F. Kalbermatten, E. Pralong, et al., Long-term in vivo regeneration of peripheral nerves through bioengineered nerve grafts. Neuroscience, 2011. **181**: p. 278-291.

63.   Dodla, M.C. and R.V. Bellamkonda, Differences between the effect of anisotropic and isotropic laminin and nerve growth factor presenting scaffolds on nerve regeneration across long peripheral nerve gaps. Biomaterials, 2008. **29**(1): p. 33-46.

64.   Dominici, M., K. Le Blanc, I. Mueller, et al., Minimal criteria for defining multipotent mesenchymal stromal cells. The International Society for Cellular Therapy position statement. Cytotherapy, 2006. **8**(4): p. 315-317.

65.   Doyu M, S.G., Ken E, Kimata K, Shinomura T, Yamada Y, Mitsuma T, Takahashi A., Laminin A, B1, and B2 chain gene expression in transected and regenerating nerves: regulation by axonal signals. J Neurochem, 1993. **60**(2): p. 543-551.

66.   Ducker, T.B., L.G. Kempe, and G.J. Hayes, The Metabolic Background for Peripheral Nerve Surgery. Journal of Neurosurgery, 1969. **30**(3part1): p. 270-280.

67.   Engelberg, I. and J. Kohn, Physico-mechanical properties of degradable polymers used in medical applications: A comparative study. Biomaterials, 1991. **12**(3): p. 292-304.

68.   Erba, P., C. Mantovani, D.F. Kalbermatten, et al., Regeneration potential and survival of transplanted undifferentiated adipose tissue-derived stem cells in peripheral nerve conduits. Journal of Plastic, Reconstructive & Aesthetic Surgery, 2010. **63**(12): p. e811-e817.

69.   Evans, G.R.D., K. Brandt, S. Katz, et al., Bioactive poly(-lactic acid) conduits seeded with Schwann cells for peripheral nerve regeneration. Biomaterials, 2002. **23**(3): p. 841-848.

70.   Evans, G.R.D., K. Brandt, A.D. Niederbichler, et al., Clinical long-term in vivo evaluation of poly(L-lactic acid) porous conduits for peripheral nerve regeneration. Journal of Biomaterials Science, Polymer Edition, 2000. **11**: p. 869-878.

71.   Evans, G.R.D., K. Brandt, A.D. Niederbichler, et al., Clinical long-term in vivo evaluation of poly(L-lactic acid) porous conduits for peripheral nerve regeneration. Journal of Biomaterials Science-Polymer Edition, 2000. **11**(8): p. 869-878.

72.   Evans, G.R.D., K. Brandt, M.S. Widmer, et al., In vivo evaluation of poly(L-lactic acid) porous conduits for peripheral nerve regeneration. Biomaterials, 1999. **20**(12): p. 1109-1115.

73.   Evans, G.R.D., K. Brandt, M.S. Widmer, et al., In vivo evaluation of poly(-lactic acid) porous conduits for peripheral nerve regeneration. Biomaterials, 1999. **20**(12): p. 1109-1115.

74.   Eves, P.C., A.J. Beck, A.G. Shard, et al., A chemically defined surface for the co-culture of melanocytes and keratinocytes. Biomaterials, 2005. **26**(34): p. 7068-7081.

75.   Fansa, H., G. Keilhoff, S. Altmann, et al., The effect of the immunosuppressant FK 506 on peripheral nerve regeneration following nerve grafting. Journal of Hand Surgery-British and European Volume, 1999. **24B**(1): p. 38-42.

76.   Filova, E., N.A. Bullett, L. Bacakova, et al., Regionally-Selective Cell Colonization of Micropatterned Surfaces Prepared by Plasma Polymerization of Acrylic Acid and 1,7-Octadiene. Physiological Research, 2009. **58**(5): p. 669-684.

77.   Fine, E.G., I. Decosterd, M. Papaloïzos, et al., GDNF and NGF released by synthetic guidance channels support sciatic nerve regeneration across a long gap. European Journal of Neuroscience, 2002. **15**(4): p. 589-601.

78.   Fine, E.G., R.F. Valentini, R. Bellamkonda, et al., Improved nerve regeneration through piezoelectric vinylidenefluoride-trifluoroethylene copolymer guidance channels. Biomaterials, 1991. **12**(8): p. 775-780.

79.   Freier, T., C. Kunze, C. Nischan, et al., In vitro and in vivo degradation studies for development of a biodegradable patch based on poly(3-hydroxybutyrate). Biomaterials, 2002. **23**(13): p. 2649-2657.

80.   Friedenstein, A.J., S. Piatetzky, II, and K.V. Petrakova, Osteogenesis in transplants of bone marrow cells. Journal of embryology and experimental morphology, 1966. **16**(3): p. 381-390.

81.   Frostick, S.P., Q. Yin, and G.J. Kemp, Schwann cells, neurotrophic factors, and peripheral nerve regeneration. Microsurgery, 1998 **18**(7): p. 397-405.

82. Ghaznavi, A.M., L.E. Kokai, M.L. Lovett, et al., Silk Fibroin Conduits A Cellular and Functional Assessment of Peripheral Nerve Repair. Annals of Plastic Surgery, 2011. **66**(3): p. 273-279.

83. Gilbert, A., G. Pivato, and T. Kheiralla, Long-term results of primary repair of brachial plexus lesions in children. Microsurgery, 2006. **26**(4): p. 334-342.

84. Gopalakrishnan, S.M., N. Teusch, C. Imhof, et al., Role of Rho kinase pathway in chondroitin sulfate proteoglycan-mediated inhibition of neurite outgrowth in PC12 cells. Journal of Neuroscience Research, 2008. **86**(10): p. 2214-2226.

85. Goyal, V., S. Rajguru, A.I. Matic, et al., Acute Damage Threshold for Infrared Neural Stimulation of the Cochlea: Functional and Histological Evaluation. Anatomical Record-Advances in Integrative Anatomy and Evolutionary Biology, 2012. **295**(11): p. 1987-1999.

86. Gupta, D., J. Venugopal, M.P. Prabhakaran, et al., Aligned and random nanofibrous substrate for the in vitro culture of Schwann cells for neural tissue engineering. Acta Biomaterialia, 2009. **5**(7): p. 2560-2569.

87. Haddow, D.B., D.A. Steele, R.D. Short, et al., Plasma-polymerized surfaces for culture of human keratinocytes and transfer of cells to an in vitro wound-bed model. Journal of Biomedical Materials Research Part A, 2003. **64A**(1): p. 80-87.

88. Hall, S.M., Regeneration in cellular and acellular autografts in the peripheral nervous system. Neuropathology and Applied Neurobiology, 1986. **12**(1): p. 27-46.

89. He, C. and Z. Chen, Enhancement of motor nerve regeneration by nerve growth factor. Microsurgery, 1992. **13**(3): p. 151-154.

90. Henderson, C., H. Phillips, R. Pollock, et al., GDNF: a potent survival factor for motoneurons present in peripheral nerve and muscle. Science, 1994. **266**(5187): p. 1062-1064.

91. Hentz VR and N. A., The results of microneurosurgical reconstruction in complete brachial plexus palsy. Assessing outcome and predicting results. Orthop Clin North Am., 1988 **19**(1): p. 107-114.

92. Hernon, C.A., R.A. Dawson, E. Freedlander, et al., Clinical experience using cultured epithelial autografts leads to an alternative methodology for transferring skin cells from the laboratory to the patient. Regenerative Medicine, 2006. **1**(6): p. 809-821.

93. Holmberg, M., K.B. Stibius, N.B. Larsen, et al., Competitive protein adsorption to polymer surfaces from human serum. Journal of Materials Science-Materials in Medicine, 2008. **19**(5): p. 2179-2185.

94. Hook, A.L., D.G. Anderson, R. Langer, et al., High throughput methods applied in biomaterial development and discovery. Biomaterials, 2010. **31**(2): p. 187-198.

95. Hu, J., Q.T. Zhu, X.L. Liu, et al., Repair of extended peripheral nerve lesions in rhesus monkeys using acellular allogenic nerve grafts implanted with autologous mesenchymal stem cells. Experimental Neurology, 2007. **204**(2): p. 658-666.

96. Jha, B.S., R.J. Colello, J.R. Bowman, et al., Two pole air gap electrospinning: Fabrication of highly aligned, three-dimensional scaffolds for nerve reconstruction. Acta Biomaterialia, 2011. **7**(1): p. 203-215.

97. Jiang, H., Y. Hu, Y. Li, et al., A facile technique to prepare biodegradable coaxial electrospun nanofibers for controlled release of bioactive agents. Journal of Controlled Release, 2005. **108**(2-3): p. 237-243.

98.   Jiang, X., S.H. Lim, H.Q. Mao, et al., Current applications and future perspectives of artificial nerve conduits. Experimental Neurology, 2010. **223**(1): p. 86-101.

99.   Johnson, E.O. and P.N. Soucacos, Nerve repair: experimental and clinical evaluation of biodegradable artificial nerve guides. Injury, 2008. **39 Suppl 3**: p. S30-36.

100. Kaekhaw, R., Primary Schwann and adipose-derived stem cells for peripheral nerve repair. Edition ed. Series Primary Schwann and adipose-derived stem cells for peripheral nerve repair, ed. Series Editor. Vol. Volume. 2011, Sheffield: Publisher. 150.

101. Kaewkhaw, R., A.M. Scutt, and J.W. Haycock, Anatomical site influences the differentiation of adipose-derived stem cells for Schwann-cell phenotype and function. Glia, 2011. **59**(5): p. 734-749.

102. Kalbermatten, D.F., J. Pettersson, P.J. Kingham, et al., New fibrin conduit for peripheral nerve repair. J Reconstr Microsurg, 2009. **25**(1): p. 27-33.

103. Kaplan, D., B. Hempstead, D. Martin-Zanca, et al., The trk proto-oncogene product: a signal transducing receptor for nerve growth factor. Science, 1991. **252**(5005): p. 554-558.

104. Kapur, T.A. and M.S. Shoichet, Immobilized concentration gradients of nerve growth factor guide neurite outgrowth. Journal of Biomedical Materials Research Part A, 2004. **68A**(2): p. 235-243.

105. Karabekmez, F., A. Duymaz, and S. Moran, Early Clinical Outcomes with the Use of Decellularized Nerve Allograft for Repair of Sensory Defects Within the Hand. Hand, 2009. **4**(3): p. 245-249.

106. Karabekmez, F.E., A. Duymaz, and S.L. Moran, Early clinical outcomes with the use of decellularized nerve allograft for repair of sensory defects within the hand. Hand, 2009. **4**(3): p. 245-249.

107. Katayama, Y., R. Montenegro, T. Freier, et al., Coil-reinforced hydrogel tubes promote nerve regeneration equivalent to that of nerve autografts. Biomaterials, 2006. **27**(3): p. 505-518.

108. Katayama, Y., R. Montenegro, T. Freier, et al., Coil-reinforced hydrogel tubes promote nerve regeneration equivalent to that of nerve autografts. Biomaterials, 2006. **27**(3): p. 505-518.

109. Kehoe, S., X.F. Zhang, and D. Boyd, FDA approved guidance conduits and wraps for peripheral nerve injury: a review of materials and efficacy. Injury, 2012. **43**(5): p. 553-572.

110. Keilhoff, G., A. Goihl, F. Stang, et al., Peripheral nerve tissue engineering: Autologous Schwann cells vs. transdifferentiated mesenchymal stem cells. Tissue Engineering, 2006. **12**(6): p. 1451-1465.

111. Keselowsky, B.G., D.M. Collard, and A.J. Garcia, Integrin binding specificity regulates biomaterial surface chemistry effects on cell differentiation. Proceedings of the National Academy of Sciences of the United States of America, 2005. **102**(17): p. 5953-5957.

112. Khan, S. and G. Newaz, A comprehensive review of surface modification for neural cell adhesion and patterning. Journal of biomedical materials research. Part A, 2010. **93**(3): p. 1209-1224.

113. Kim, Y.T., V.K. Haftel, S. Kumar, et al., The role of aligned polymer fiber-based constructs in the bridging of long peripheral nerve gaps. Biomaterials, 2008. **29**(21): p. 3117-3127.

114. Kingham, P.J., D.F. Kalbermatten, D. Mahay, et al., Adipose-derived stem cells differentiate into a Schwann cell phenotype and promote neurite outgrowth in vitro. Experimental Neurology, 2007. **207**(2): p. 267-274.

115. Klinkhammer, K., J. Bockelmann, C. Simitzis, et al., Functionalization of electrospun fibers of poly(ε-caprolactone) with star shaped NCO-poly(ethylene glycol)-stat-poly(propylene glycol) for neuronal cell guidance. Journal of Materials Science: Materials in Medicine, 2010. **21**(9): p. 2637-2651.

116. Kokai, L.E., A.M. Ghaznavi, and K.G. Marra, Incorporation of double-walled microspheres into polymer nerve guides for the sustained delivery of glial cell line-derived neurotrophic factor. Biomaterials, 2010. **31**(8): p. 2313-2322.

117. Kouyoumdjian, J.A., Peripheral nerve injuries: a retrospective survey of 456 cases. Muscle & Nerve, 2006. **34**(6): p. 785-788.

118. Krych, A.J., G.E. Rooney, B. Chen, et al., Relationship between scaffold channel diameter and number of regenerating axons in the transected rat spinal cord. Acta Biomaterialia, 2009. **5**(7): p. 2551-2559.

119. L'Heureux, N., N. Dusserre, A. Marini, et al., Technology insight: the evolution of tissue-engineered vascular grafts--from research to clinical practice. Nature clinical practice. Cardiovascular medicine, 2007. **4**(7): p. 389-395.

120. Langer, R. and J.P. Vacanti, Tissue engineering. Science, 1993. **260**(5110): p. 920-926.

121. Lefcort, F., K. Venstrom, J.A. McDonald, et al., Regulation of the expression of fibronectin and its receptor, a5b1, during developing and regeneration of peripheral nerve. Development, 1992. **116**: p. 767-782.

122. Li, B., Y. Ma, S. Wang, et al., Influence of carboxyl group density on neuron cell attachment and differentiation behavior: Gradient-guided neurite outgrowth. Biomaterials, 2005. **26**(24): p. 4956-4963.

123. Lin, C.S., Z.C. Xin, C.H. Deng, et al., Defining adipose tissue-derived stem cells in tissue and in culture. Histology and histopathology, 2010. **25**(6): p. 807-815.

124. Lu, Q., Y. Huang, M. Li, et al., Silk fibroin electrogelation mechanisms. Acta Biomaterialia, 2011. **7**(6): p. 2394-2400.

125. Lynn, A.K., I.V. Yannas, and W. Bonfield, Antigenicity and immunogenicity of collagen. Journal of Biomedical Materials Research, 2004. **71B**(2): p. 343-354.

126. Lyons, W.E., E.B. George, T.M. Dawson, et al., Immunosuppressant Fk506 Promotes Neurite Outgrowth in Cultures of Pc12 Cells and Sensory Ganglia. Proceedings of the National Academy of Sciences of the United States of America, 1994. **91**(8): p. 3191-3195.

127. Macchiarini, P., P. Jungebluth, T. Go, et al., Clinical transplantation of a tissue-engineered airway. Lancet, 2008. **372**(9655): p. 2023-2030.

128. Mackinnon, S.E., V.B. Doolabh, C.B. Novak, et al., Clinical Outcome following Nerve Allograft Transplantation. Plastic and Reconstructive Surgery, 2001. **107**(6): p. 1419-1429.

129. Madduri, S., M. Papaloïzos, and B. Gander, Trophically and topographically functionalized silk fibroin nerve conduits for guided peripheral nerve regeneration. Biomaterials, 2010. **31**(8): p. 2323-2334.

130. Mahay, D., G. Terenghi, and S.G. Shawcross, Schwann cell mediated trophic effects by differentiated mesenchymal stem cells. Experimental Cell Research, 2008. **314**(14): p. 2692-2701.

131. Mahoney, D.J., J.D. Whittle, C.M. Milner, et al., A method for the non-covalent immobilization of heparin to surfaces. Analytical Biochemistry, 2004. **330**(1): p. 123-129.

132. Mahoney, M.J. and K.S. Anseth, Three-dimensional growth and function of neural tissue in degradable polyethylene glycol hydrogels. Biomaterials, 2006. **27**(10): p. 2265-2274.

133. Maisonpierre, P., L. Belluscio, S. Squinto, et al., Neurotrophin-3: a neurotrophic factor related to NGF and BDNF. Science, 1990. **247**(4949): p. 1446-1451.

134. McFarland, C.D., C.H. Thomas, C. DeFilippis, et al., Protein Adsorption and Cell Attachment to Patterned Surfaces. Journal of Biomedical Material Research A, 2000. **49**: p. 200-210.

135. Millesi, H. and S. Tsolakidis, End-to-side coaptation: An important tool in peripheral nerve surgery. European Surgery, 2005. **37**(4): p. 228-233.

136. Mimura, T., M. Dezawa, H. Kanno, et al., Peripheral nerve regeneration by transplantation of bone marrow stromal cell-derived Schwann cells in adult rats. Journal of Neurosurgery, 2004. **101**(5): p. 806-812.

137. Mishra, G. and S.L. McArthur, Plasma Polymerization of Maleic Anhydride: Just What Are the Right Deposition Conditions? Langmuir, 2010. **26**(12): p. 9645-9658.

138. Mittnacht, U., H. Hartmann, S. Hein, et al., Chitosan/siRNA Nanoparticles Biofunctionalize Nerve Implants and Enable Neurite Outgrowth. Nano letters, 2010. **10**(10): p. 3933-3939.

139. Moroder, P., M.B. Runge, H. Wang, et al., Material properties and electrical stimulation regimens of polycaprolactone fumarate-polypyrrole scaffolds as potential conductive nerve conduits. Acta Biomaterialia, 2011. **7**(3): p. 944-953.

140. Mosahebi, A., P. Fuller, M. Wiberg, et al., Effect of Allogeneic Schwann Cell Transplantation on Peripheral Nerve Regeneration. Experimental Neurology, 2002. **173**(2): p. 213-223.

141. Mosahebi, A., P. Fuller, M. Wiberg, et al., Effect of allogeneic Schwann cell transplantation on peripheral nerve regeneration. Experimental Neurology, 2002. **173**(2): p. 213-223.

142. Murray-Dunning, C., Electrospun aligned biodegradable microfibers and plasma polymerization techniques to improve peripheral nerve repair. 2010, Sheffield: 200 pages.

143. Murray-Dunning, C., S.L. McArthur, T. Sun, et al., Three-dimensional alignment of schwann cells using hydrolysable microfiber scaffolds: strategies for peripheral nerve repair. Methods in Molecular Biology, 2011. **695**: p. 155-166.

144. Navissano, M., F. Malan, R. Carnino, et al., Neurotube® for facial nerve repair. Microsurgery, 2005. **25**(4): p. 268-271.

145. Ni, H.C., Z.Y. Lin, S.H. Hsu, et al., The use of air plasma in surface modification of peripheral nerve conduits. Acta Biomaterialia, 2010. **6**(6): p. 2066-2076.

146. Novikov, L.N., L.N. Novikova, A. Mosahebi, et al., A novel biodegradable implant for neuronal rescue and regeneration after spinal cord injury. Biomaterials, 2002. **23**(16): p. 3369-3376.

147. Oliveira, E.F., N. Mazzer, C.H. Barbieri, et al., The use of a muscle graft to repair a segmentary nerve defect - An experimental study using the sciatic nerve of rats as model. Journal of Neuroscience Methods, 2004. **133**(1-2): p. 19-26.

148. Pabari, A., S.Y. Yang, A.M. Seifalian, et al., Modern surgical management of peripheral nerve gap. Journal of Plastic, Reconstructive & Aesthetic Surgery, 2010. **63**(12): p. 1941-1948.

149. Patel, S., K. Kurpinski, R. Quigley, et al., Bioactive Nanofibers:‰ Synergistic Effects of Nanotopography and Chemical Signaling on Cell Guidance. Nano Letters, 2007. **7**(7): p. 2122-2128.

150. Paviolo, C., J.W. Haycock, J. Yong, et al., Laser exposure of gold nanorods can increase neuronal cell outgrowth. Biotechnology and Bioengineering, 2013.

151. Pettersson, J., A. McGrath, D.F. Kalbermatten, et al., Muscle recovery after repair of short and long peripheral nerve gaps using fibrin conduits. Neuroscience Letters, 2011. **500**(1): p. 41-46.

152. Prabhakaran, M.P., J.R. Venugopal, and S. Ramakrishna, Mesenchymal stem cell differentiation to neuronal cells on electrospun nanofibrous substrates for nerve tissue engineering. Biomaterials, 2009. **30**(28): p. 4996-5003.

153. Rajnicek, A.M., S. Britland, and C.D. McCaig, Contact guidance of CNS neurites on grooved quartz: influence of groove dimensions, neuronal age and cell type. Journal of cell science, 1997. **110**: p. 2905-2913.

154. Ray, W. and S. Mackinnon, Management of nerve gaps: Autografts, allografts, nerve transfers, and end-to-side neurorrhaphy. Experimental Neurology, 2010. **223**(1): p. 77-85.

155. Reynolds, M.L. and C.J. Woolf, Reciprocal Schwann cell-axon interactions. Current Opinion in Neurobiology, 1993. **3**(5): p. 683-693.

156. Ribeiro-Resende, V.T., B. Koenig, S. Nichterwitz, et al., Strategies for inducing the formation of bands of Bungner in peripheral nerve regeneration. Biomaterials, 2009. **30**(29): p. 5251-5259.

157. Rich, K.M., J.R. Luszczynski, P.A. Osborne, et al., Nerve growth factor protects adult sensory neurons from cell death and atrophy caused by nerve injury. Journal of Neurocytology, 1987. **16**(2): p. 261-268.

158. Rombouts, W.J.C. and R.E. Ploemacher, Primary murine MSC show highly efficient homing to the bone marrow but lose homing ability following culture. Leukemia, 2003. **17**(1): p. 160-170.

159. Rosson, G.D., E.H. Williams, and A.L. Dellon, Motor nerve regeneration across a conduit. Microsurgery, 2009. **29**(2): p. 107-114.

160. Rozema FR, de Bruijn WC, Bos RRM, et al., eds. Late tissue response to bone plates and screws of poly(L-lactide) used for fracture fixation of the zygomatic bone., ed. W.R. Doherty PJ, Williams DF,. Vol. 10.

161. Runge, M.B., M. Dadsetan, J. Baltrusaitis, et al., The development of electrically conductive polycaprolactone fumarate-polypyrrole composite materials for nerve regeneration. Biomaterials, 2010. **31**(23): p. 5916-5926.

162. Ryan, M.E., A.M. Hynes, and J.P.S. Badyal, Pulsed plasma polymerization of maleic anhydride. Chemistry of Materials, 1996. **8**(1): p. 37-42.

163. Santiago, L.Y., J. Clavijo-Alvarez, C. Brayfield, et al., Delivery of Adipose-Derived Precursor Cells for Peripheral Nerve Repair. Cell Transplantation, 2009. **18**: p. 145-158.

164. Schlosshauer, B., L. Dreesmann, H.-E. Schaller, et al., Synthetic Nerve Guide Implants in Humans: A Comprehensive Survey. Neurosurgery, 2006. **59**(4): p. 740-748.

165. Schlosshauer, B., E. Müller, B. Schröder, et al., Rat Schwann cells in bioresorbable nerve guides to promote and accelerate axonal regeneration. Brain Research, 2003. **963**(1-2): p. 321-326.

166. Schnell, E., K. Klinkhammer, S. Balzer, et al., Guidance of glial cell migration and axonal growth on electrospun nanofibers of poly-epsilon-caprolactone and a collagen/poly-epsilon-caprolactone blend. Biomaterials, 2007. **28**(19): p. 3012-3025.

167. Scuteri, A., A. Cassetti, and G. Tredici, Adult mesenchymal stem cells rescue dorsal root ganglia neurons from dying. Brain Research, 2006. **1116**(1): p. 75-81.

168. Seddon, H.J., Three Types of Nerve Injury. Brain Research, 1943 **66**: p. 237-288.

169. Seil, J.T. and T.J. Webster, Decreased astroglial cell adhesion and proliferation on zinc oxide nanoparticle polyurethane composites. Int J Nanomedicine, 2008. **3**(4): p. 523-531.

170. Shen, C.C., Y.C. Yang, and B.S. Liu, Large-area irradiated low-level laser effect in a biodegradable nerve guide conduit on neural regeneration of peripheral nerve injury in rats. Injury-International Journal of the Care of the Injured, 2011. **42**(8): p. 803-813.

171. Shen, Y., Y. Qian, H. Zhang, et al., Guidance of Olfactory Ensheathing Cell Growth and Migration on Electrospun Silk Fibroin Scaffolds. Cell Transplantation, 2010. **19**(2): p. 147-157.

172. Shenton, M.J. and G.C. Stevens, Surface modification of polymer surfaces: atmospheric plasma versus vacuum plasma treatments. Journal of Physics D-Applied Physics, 2001. **34**(18): p. 2761-2768.

173. Shin, R.H., P.F. Friedrich, B.A. Crum, et al., Treatment of a segmental nerve defect in the rat with use of bioabsorbable synthetic nerve conduits: a comparison of commercially available conduits. The Journal of bone and joint surgery. American volume, 2009. **91**(9): p. 2194-2204.

174. Stanec, S., I. Tonkovic, Z. Stanec, et al., Treatment of upper limb nerve war injuries associated with vascular trauma. Injury, 1997. **28**(7): p. 463-468.

175. Sterne, G.D., R.A. Brown, C.J. Green, et al., Neurotrophin-3 Delivered Locally via Fibronectin Mats Enhances Peripheral Nerve Regeneration. European Journal of Neuroscience, 1997. **9**(7): p. 1388-1396.

176. Strem, B.M., K.C. Hicok, M. Zhu, et al., Multipotential differentiation of adipose tissue-derived stem cells. The Keio journal of medicine, 2005. **54**(3): p. 132-141.

177. Sun, M., P.J. Kingham, A.J. Reid, et al., In vitro and in vivo testing of novel ultrathin PCL and PCL/PLA blend films as peripheral nerve conduit. Journal of Biomedical Materials Research Part A, 2009. **9999A**: p. NA-NA.

178. Sun, M.Z., M. McGowan, P.J. Kingham, et al., Novel thin-walled nerve conduit with microgrooved surface patterns for enhanced peripheral nerve repair. Journal of Materials Science-Materials in Medicine, 2010. **21**(10): p. 2765-2774.

179. Sunderland, S.S., The anatomy and physiology of nerve injury. Muscle & Nerve, 1990. **13**(9): p. 771-784.

180. Taras, J.S., S.M. Jacoby, and C.J. Lincoski, Reconstruction of digital nerves with collagen conduits. The Journal of Hand Surgery, 2011. **36**(9): p. 1441-1446.

181. Tohill, M., C. Mantovani, M. Wiberg, et al., Rat bone marrow mesenchymal stem cells express glial markers and stimulate nerve regeneration. Neuroscience Letters, 2004. **362**(3): p. 200-203.

182. Tondreau, T., L. Lagneaux, M. Dejeneffe, et al., Bone marrow-derived mesenchymal stem cells already express specific neural proteins before any differentiation. Differentiation, 2004. **72**(7): p. 319-326.

183. Tong, X.-j., K.-I. Hirai, H. Shimada, et al., Sciatic nerve regeneration navigated by laminin-fibronectin double coated biodegradable collagen grafts in rats. Brain Research, 1994. **663**(1): p. 155-162.

184.   Valentini, R.F., P. Aebischer, S.R. Winn, et al., Collagen- and laminin-containing gels impede peripheral nerve regeneration through semipermeable nerve guidance channels. Experimental Neurology, 1987. **98**(2): p. 350-356.

185.   Valmikinathan, C.M., J. Hoffman, and X. Yu, Impact of Scaffold Micro and Macro Architecture on Schwann Cell Proliferation under Dynamic Conditions in a Rotating Wall Vessel Bioreactor. Materials science & engineering. C, Materials for biological applications, 2011. **31**(1): p. 22-29.

186.   Vroman, L., Effect of adsorbed proteins on the wettability of hydrophilic and hydrophobic solids. Nature, 1962. **196**: p. 476-477.

187.   Waitayawinyu, T., D.M. Parisi, B. Miller, et al., A comparison of polyglycolic acid versus type 1 collagen bioabsorbable nerve conduits in a rat model: an alternative to autografting. The Journal of Hand Surgery, 2007. **32**(10): p. 1521-1529.

188.   Wang, C.-Y., K.-H. Zhang, C.-Y. Fan, et al., Aligned natural–synthetic polyblend nanofibers for peripheral nerve regeneration. Acta Biomaterialia, 2011. **7**(2): p. 634-643.

189.   Wang, D., X.-L. Liu, J.-K. Zhu, et al., Bridging small-gap peripheral nerve defects using acellular nerve allograft implanted with autologous bone marrow stromal cells in primates. Brain Research, 2008. **1188**: p. 44-53.

190.   Wang, G.-Y., K.-I. Hirai, and H. Shimada, The role of laminin, a component of Schwann cell basal lamina, in rat sciatic nerve regeneration within antiserum-treated nerve grafts. Brain Research, 1992. **570**(1-2): p. 116-125.

191.   Wang, H.B., M.E. Mullins, J.M. Cregg, et al., Varying the diameter of aligned electrospun fibers alters neurite outgrowth and Schwann cell migration. Acta Biomaterialia, 2010. **6**(8): p. 2970-2978.

192.   Wang, S., Q. Cai, J. Hou, et al., Acceleration effect of basic fibroblast growth factor on the regeneration of peripheral nerve through a 15-mm gap. Journal of Biomedical Materials Research Part A, 2003. **66A**(3): p. 522-531.

193.   Weber, R.A., W.C. Breidenbach, R.E. Brown, et al., A Randomized Prospective Study of Polyglycolic Acid Conduits for Digital Nerve Reconstruction in Humans. Plastic and Reconstructive Surgery, 2000. **106**(5): p. 1036-1045.

194.   Whitlock, E.L., S.H. Tuffaha, J.P. Luciano, et al., Processed allografts and type I collagen conduits for repair of peripheral nerve gaps. Muscle & Nerve, 2009. **39**(6): p. 787-799.

195.   Wilson, C.J., R.E. Clegg, D.I. Leavesley, et al., Mediation of biomaterial-cell interactions by adsorbed proteins: a review. Tissue Engineering, 2005. **11**(1-2): p. 1-18.

196.   Witkowska-Zimny, M. and K. Walenko, Stem cells from adipose tissue. Cellular & Molecular Biology Letters, 2011. **16**(2): p. 236-257.

197.   Woodbury, D., E.J. Schwarz, D.J. Prockop, et al., Adult rat and human bone marrow stromal cells differentiate into neurons. Journal of Neuroscience Research, 2000. **61**(4): p. 364-370.

198.   Woodruff, M.A. and D.W. Hutmacher, The return of a forgotten polymer—Polycaprolactone in the 21st century. Progress in Polymer Science, 2010. **35**(10): p. 1217-1256.

199.   Wu, X., A.E. Dmitriev, M.J. Cardoso, et al., 810 nm Wavelength light: an effective therapy for transected or contused rat spinal cord. Lasers in Surgery and Medicine, 2009. **41**(1): p. 36-41.

200.   Xiao, X.-Q., Y. Zhao, and G.-Q. Chen, The effect of 3-hydroxybutyrate and its derivatives on the growth of glial cells. Biomaterials, 2007. **28**(25): p. 3608-3616.

201. Yang, F., R. Murugan, S. Wang, et al., Electrospinning of nano/micro scale poly(l-lactic acid) aligned fibers and their potential in neural tissue engineering. Biomaterials, 2005. **26**(15): p. 2603-2610.

202. Yang, J., Q. Lou, R. Huang, et al., Dorsal root ganglion neurons induce transdifferentiation of mesenchymal stem cells along a Schwann cell lineage. Neuroscience Letters, 2008. **445**(3): p. 246-251.

203. Yang, Y., X. Chen, F. Ding, et al., Biocompatibility evaluation of silk fibroin with peripheral nerve tissues and cells in vitro. Biomaterials, 2007. **28**(9): p. 1643-1652.

204. Yang, Y., F. Ding, J. Wu, et al., Development and evaluation of silk fibroin-based nerve grafts used for peripheral nerve regeneration. Biomaterials, 2007. **28**(36): p. 5526-5535.

205. Yang, Y., W. Zhao, J. He, et al., Nerve conduits based on immobilization of nerve growth factor onto modified chitosan by using genipin as a crosslinking agent. European Journal of Pharmaceutics and Biopharmaceutics, 2011. **79**(3): p. 519-525.

206. Yao, L., K.L. Billiar, A.J. Windebank, et al., Multichanneled Collagen Conduits for Peripheral Nerve Regeneration: Design, Fabrication, and Characterization. Tissue Engineering Part C: Methods, 2010. **16**(6): p. 1585-1596.

207. Yao, L., G. Damodaran, N. Nikolskaya, et al., The effect of laminin peptide gradient in enzymatically cross-linked collagen scaffolds on neurite growth. Journal of Biomedical Materials Research Part A, 2009. **9999A**: p. NA-NA.

208. Yao, L., G. Damodaran, N. Nikolskaya, et al., The effect of laminin peptide gradient in enzymatically cross-linked collagen scaffolds on neurite growth. Journal of Biomedical Materials Research Part A, 2010. **92A**(2): p. 484-492.

209. Yao, L., G.C. de Ruiter, H. Wang, et al., Controlling dispersion of axonal regeneration using a multichannel collagen nerve conduit. Biomaterials, 2010. **31**(22): p. 5789-5797.

210. Yao, L., S. Wang, W. Cui, et al., Effect of functionalized micropatterned PLGA on guided neurite growth. Acta Biomaterialia, 2009. **5**(2): p. 580-588.

211. Yao, L., S. Wang, W. Cui, et al., Effect of functionalized micropatterned PLGA on guided neurite growth. Acta Biomaterialia, 2009. **5**(2): p. 580-588.

212. Yasuda, H., L. Ledernez, F. Olcaytug, et al., Electron dynamics of low-pressure deposition plasma. Pure and Applied Chemistry, 2008. **80**(9): p. 1883-1892.

213. Yim, E.K., S.W. Pang, and K.W. Leong, Synthetic nanostructures inducing differentiation of human mesenchymal stem cells into neuronal lineage. Experimental Cell Research, 2007. **313**(9): p. 1820-1829.

214. Yip, H., K. Rich, P. Lampe, et al., The effects of nerve growth factor and its antiserum on the postnatal development and survival after injury of sensory neurons in rat dorsal root ganglia. J. Neurosci., 1984. **4**(12): p. 2986-2992.

215. Young, R.C., G. Terenghi, and M. Wiberg, Poly-3-hydroxybutyrate (PHB): a resorbable conduit for long-gap repair in peripheral nerves. British Journal of Plastic Surgery, 2002. **55**(3): p. 235-240.

216. Zanazzi, G., S. Einheber, R. Westreich, et al., Glial Growth Factor/Neuregulin Inhibits Schwann Cell Myelination and Induces Demyelination. J Cell Biol., 2001 **152**(6): p. 1289-1300.

217. Zaslav, K., B. Cole, R. Brewster, et al., A prospective study of autologous chondrocyte implantation in patients with failed prior treatment for articular cartilage defect of the knee: results of the Study of the Treatment of Articular Repair (STAR) clinical trial. The American journal of sports medicine, 2009. **37**(1): p. 42-55.

218. Zhang, Y., H. Luo, Z. Zhang, et al., A nerve graft constructed with xenogeneic acellular nerve matrix and autologous adipose-derived mesenchymal stem cells. Biomaterials, 2010. **31**(20): p. 5312-5324.
219. Zhang, Z., M. Rouabhia, Z. Wang, et al., Electrically Conductive Biodegradable Polymer Composite for Nerve Regeneration: Electricity-Stimulated Neurite Outgrowth and Axon Regeneration. Artificial Organs, 2007. **31**(1): p. 13-22.

2.1 Plasma Polymers: Fabrication and Evaluation

2.1.1 Introduction to plasma polymerisation technique and analysis methods

Along with the composition of the bulk material, there are other important characteristics that dictate the response of an implant once within a biological system. Mechanical stiffness, surface energy, roughness, spatial and topological organization are important factors that affect the adherence and immunoreactivity of the biological system[3-5, 9, 20, 22]. Various coating techniques have been used to modulate the biological properties of a bulk material. From self assembled monolayers which control the ability of fibroblasts to attach[17], to peptide-modified surfaces with defined spacing in order to maximise integrin attachment[26], many methods have been employed to control or maximise cell attachment and proliferation.

Plasma polymerisation (also termed chemical vapour deposition, CVD) is a versatile technique, which could theoretically coat any desired surface with a nano to micrometre thin pinhole-free layer. As the process used in this chapter is within conditions of a vacuum, the material has to be dry and withstand the conditions of a rough vacuum without collapsing. However, advances in room pressure plasma polymerisation techniques mean that plasma polymerisation can be scaled up and performed at ambient temperatures and pressures[22, 27, 29, 31]. The technique does not affect the bulk material, but sterilises the surface during the coating step. Chemical functionality differences were therefore investigated between the plasma polymers and uncoated glass, whilst topography was also studied.

Regarding the plasma polymerisation technique, a balance of power and flow rate had to be achieved in order to achieve a functionalised and adherent layer. If the RF energy used was too small, the energy imparted to the monomer species would not have been enough to create an adherent layer. The ions would not have had enough energy to graft onto the surfaces firmly, resulting in a loosely adherent, powdery coating [38]. If the RF energy was too high, the ions would have been highly fragmented before the grafting occurred. This would have resulted in a loss of functionality and an increase in hydrocarbons, which would have caused an oily coating. As it is very important to retain the functionality of the monomer species during plasma polymerisation, the flow rate (F) of the monomer was calculated in order to optimise the plasma polymerisation process:

$$F=\Delta(pf\text{-}pi)$$

Δ is a constant, which is dependent on the dimensions of each reactor. Once the reactor has been pumped down to base pressure and the monomer let into the system and allowed to equilibrate at the desired pressure, a 30 second pressure measurement can be done to deduce the flow rate. Pi is the initial pressure of the monomer flow rate at equilibrium. Pf is the pressure once the reactor has been shut off from the vacuum pump for 30 secs, but the monomer inlet is still open. The pressure difference is a measure of how much monomer is drawn through in 30 secs, which when multiplied by the reactor constant gives a flow rate. This can then be used to optimise flow rate conditions and then reproduce them.

Regarding the choice of plasma polymer to use, maleic anhydride was initially chosen due to intriguing preliminary cell culture work done within the research group. Processing parameters have been investigated by a number of research groups in order to optimise the relative percentage of anhydride groups by changing the duty cycles, power etc [2, 12, 18, 24, 30]. Acrylic acid was also then used as comparative plasma polymerised surface. It has been investigated extensively with various cell types[1, 13], with promising results when used as a culture substrate for neuronal cell lines and Schwann cells[19].

Regarding the optimisation of the functional groups by altering the processing parameters of the plasma polymerised surfaces, optimisation of both the acrylic acid and maleic anhydride coating conditions have been performed previously [18, 21, 28]. Investigations into acrylic acid have shown that good retention of the acid groups occurs with duty cycles around 10-20W continuous power, for around 20 min [8, 19, 21]. Maleic anhydride is a more reactive monomer, and requires less power in order to fragment. In order to retain the functional anhydride group on the plasma polymerised surface, pulsed plasmas are used with an overall power of around 1W [18]. There is also a general consensus that the pulses should be maintained at around 20-80 μs on-time, then 800-1200 μs off time[24, 28, 30]. However, as there has been no previously published manuscripts regarding maleic anhydride and cell culture, different conditions were initially used to investigate which coatings would promote NG108-15 neuronal cell adhesion, proliferation and neuritogenesis. As work has previously been done on acrylic acid and NG108-15 neuronal cells[19], the same condition was used and characterised. A disadvantage of plasma polymerisation process is that the coatings are affected by the reactor dimensions, due to the diffusion characteristics of the monomer inlet flow [15, 38]. However, previous work on the plasma reactors used for this thesis optimised both coating conditions [4, 18].

XPS was used to determine the percentage of different chemical environments present within the initial 10 nm of a surface. XPS is widely used in the development and modification of materials for medical applications [9, 32, 40] and can be used to study the effect of varying functional groups on cell response. Monochromated x-rays irradiate the surface, which cause photoelectrons to be emitted. Different functional groups on a surface will interact with electrons in a specific way, so too the energy levels of the electrons change discretely upon interaction with different binding environments. This change can be detected, quantified and related back to the chemical environment on the surface that caused the shift in electron 'binding energy'. As a carbon singly bonded with another carbon always gives a binding energy of 284.6 eV, this value can be used to calibrate the other measurements. Other chemical environments can then be deduced from the characteristic binding energy shift. An electron energy analyser separates the photoelectrons according to binding energy, from which the elemental identity and chemical state can be identified. The intensity of each peak also gives the relative percentage of each chemical species on the surface. This is a very useful technique, as acrylic acid coated slides often show a large percentage of carbon, oxygen and carboxylic acid groups compared to glass.

Regarding maleic anhydride, the binding energies of carboxylic acid and anhydride groups are so similar that they cannot be distinguished with XPS. Because of this, although the acrylic acid will be characterised using XPS and contact angle, another technique such as Fourier Transform Infrared spectroscopy (FT-IR) or ToF-SIMS should be utilised to separate and identify the acid and anhydride groups present in maleic anhydride coatings. FT-IR measures the frequency of infra-red radiation required to excite vibrations in molecular bonds, and can be carried out under ambient conditions [28]. Whilst the technique is capable of differentiating between anhydride and acid groups, its depth of penetration of up to a micron can cause problems when resolving the surface analytical zone.

As the maleic anhydride surfaces were known to be thinner than 10 nm through XPS work, ToF-SIMS was used to verify that anhydride groups were present on plasma polymerised maleic anhydride, rather than carboxylic acid groups. ToF-SIMS, although not as widely used as XPS in the field of biomaterial characterisation, is increasingly being used as a tool in high-throughput industrial evaluation of materials and their modification[10]. ToF-SIMS is used to deduce the molecular mass of chemical species on the topmost 1-2 atomic layers of a surface. ToF-SIMS uses a primary ion beam to ablate and ionise material. The chemical species are then accelerated through a mass

spectrometer, which separates the species according to their molecular weight, using the equation:

$$ke = 1/2mv^2$$

Where ke = kinetic energy, m = mass and v = velocity. As the secondary ion beam is very focused and rasters across the surface, secondary ions that hit the detector can be linked back to their position on the surface. As a mass spectrum is acquired per pixel, this can be used to make an 'ion' micrograph, which shows the distribution of detected chemical species across an area, usually of around 100 μm^2. Therefore, ToF-SIMS is a very useful technique as a chemical map can be built of the surface, showing which species of a given molecular mass are in which location. Whilst spectra can also be acquired through different depths by shallow sputter depth profiling, this technique was not utilised for this chapter.

Atomic force microscopy (AFM) is a widely used technique for thin surfaces, and provides very detailed topographical information[5, 34]. A cantilever with an atomically sharp tip moves over the surface, which interacts with the surface by becoming attracted or repulsed by the surface chemistry. A laser monitors and records the movement of the cantilever, so that a high-resolution micrograph of the surface can be built up. The cantilever can be used for contact or non-contact applications, and functional groups can be attached to the tip.

2.1.2 Materials and methods

Glass slide preparation

13 mm^2 glass slides (VWR international) free from contamination were rinsed in isopropanol (IPA), before being left to dry in a fume cupboard. Slides were then either coated with plasma polymerised species or analysed fresh as uncoated glass control samples.

Silicon wafer preparation

Silicon wafers were cut with a diamond tipped pen, then individually placed in a stream of air to remove any silicon dust or particles. Wafers were sonicated for 15 min in isopropyl alcohol (IPA), after which the IPA was replaced and the process repeated a minimum of 5 times. Wafers were then stored in fresh IPA and blown dry with high purity N_2 gas when required for use.

Plasma polymerisation process

A reactor of defined dimensions was used, with the monomer inlet attached at one end of the vacuum line. On the opposite side of the reactor there was a vacuum gauge and valve attached, which maintained the vessel under vacuum when not in use. After the valve, a cold trap was inserted, which consisted of a cylindrical vessel filled with liquid nitrogen. The cold trap lowered the temperature to around -196°C, which froze the monomer to the sides of the trap and reduced contamination of the vacuum pump. It also compressed any gaseous volume that entered the cold trap, which increased the efficiency of the vacuum pump by up to 6 times[37]. The cold trap was attached to the vacuum pump, which produces a rough vacuum.

Once the vacuum pump was on and both the vacuum line and monomer inlet opened up, the vacuum pump drew the liquid monomer through the reactor. Coils around the reactor emitted tuneable RF energy into the body of the reactor, which was then transmitted to the monomer species being drawn through. The RF energy ionised a fraction of the monomer, splitting it into positively charged ions and electrons. These separated components were of different densities, so the lighter electrons became 'hotter' compared to the protons. A non-uniform temperature across the various charged species resulted in a non-equilibrium or non-thermal plasma, in which only 1% of the monomer species may have been ionised. Comparatively, the definition of thermal / equilibrium plasmas is where all the ionised species are at the same temperature (i.e. solar plasma). Depending on the RF intensity, there will be a given energy density per

molecule. The desired RF intensity for this work would have resulted in a partially fragmented monomer, where the functionality of the molecule (ie. the acid or anhydride group) was maintained within the positively charged, heavier ion. The positive ions were eventually grafted onto all surfaces within the reactor, coating the surfaces with the desired functionality. As the electrons were 'hotter', they travelled faster and collided with the reactor walls more frequently compared to the ions, resulting in a negatively charged surface. This charge mismatch developed into a Debye sheath, where there could have been multiple layers of positively and neutrally charged ions that attempted to neutralise the negatively charged surface[23]. The minimum size of plasma reactors was therefore restricted by the presence of the plasma sheath.

Plasma polymerisation of maleic anhydride

A proprietary system was used for coating the samples, which were placed in a 15.2 L stainless steel T-piece reaction chamber[25]. Pressure was measured using a home built probe and vacuum gauge (BOC Edwards), whilst temperature was controlled at 33°C using a furnace power supply (Eurotherm 91e). Radio frequency power generator output (13.56 MHz Coaxial Power Supplies Ltd., UK) was connected to the chamber through a manually tunable impedance matching unit (coaxial Power Systems, UK) to a single powered electrode. A BOC Edwards single-stage rotary pump (RV8) was used to create a low vacuum, with a liquid nitrogen cold trap between the chamber throttle valve and pump to prevent corrosion, freeze the monomer and lower the vacuum further.

Glass slides or silicon wafers were specifically placed in the centre of the reactor on a sample stage, as previous preliminary work demonstrated slight fluctuations in the surface composition at different positions within both the glass cylindrical and metal T-piece reactors. The system was pumped to a base pressure of 1×10^{-3} mbar or below. Freshly crushed briquettes of maleic anhydride (MA) (Sigma) were used to coat the glass samples, the monomer flow rates controlled by a speedivalve. Pressure changes were measured by isolating the reactor from the vacuum for 30 seconds. It has previously been shown that monomer residence time within the reactor can affect the coating efficacy[13], therefore the flow rate was monitored for both MA and acrylic acid coatings. Using a method described by Yasuda[37], the pressure change was converted to monomer flow rate (cm^3 min^{-1}) at standard temperature and pressure, which was 2.7 $cm^3 min^{-1}$ and used for all experiments. In order to pulse the plasma, a TGP 10 MHz pulse generator (Thurlby Thandar Instruments, UK) was connected to a

TDS3014 oscilloscope (Tektronix) and the radio frequency unit. A capacitive probe, the tip of which was in the glow discharge region, was attached to the oscilloscope in order to detect the plasma characteristics. This allowed comparison with the triggered pulse generated from the pulse generator, as mismatches between the ON-time of the plasma compared to the trigger can occur due to stray capacitance and inductance. The peak power (P_p) was set at 5W for pulsed conditions (10W incident, 5W reflected) and 1W for continuous plasma polymerisation, both conditions were carried out for 20 minutes. The first coating condition, MA 1, had an on time of 80 μs and an off time of 800 μs. The second coating condition, MA 2, had an on time of 20 μs and off time of 1200 μs, whereas the third condition, MA 3, was 1W continuous polymerisation. In comparisons against acrylic acid, the first condition (MA 1, 80 μs on and 800 μs off) was used. After the radiofrequency was turned off, monomer was allowed to flow over the samples for 5 minutes to react with any ionised species then was stored in a vacuum desiccator for up to a week before use.

Plasma polymerisation of acrylic acid

A home built system was used, using a glass chamber with two stainless steel metal flanges and an external copper coil electrode. A vacuum gauge (BOC Edwards) measured pressure fluctuations, whilst a radiofrequency generator (13.56 MHz Coaxial Power Supplies Ltd., UK) sustained the plasma via a manually tunable impedance matching unit (Coaxial Power Supplies Ltd., UK). A BOC Edwards dual-stage rotary pump (E2M5, Edwards) was used to obtain a base pressure of at least 3×10^{-3} mbar or below before acrylic acid (AAc) monomer was let in via a needle valve, having been freeze-thawed previously to remove any gases. Pressure changes were read by isolating the reactor from the vacuum pump for 30 sec intervals. Pressure conversion was again performed using conditions described by Yasuda[37] to monomer flow rate ($cm^3 \ min^{-1}$), which corresponded to $\sim 2.9 \times 10^{-2}$ mbar. Peak power was set at a continuous 15W with 0 reflected and maintained for 10 minutes to coat the glass surfaces. After the RF power was switched off monomer was allowed to flow over the sample for 5 minutes to react with any ionised species still on the surface, then stored in a vacuum desiccator for up to 2 weeks before use.

X-ray photoelectron spectroscopy

As it was not possible to coat the samples and conduct XPS analysis in the same day, coated silicon wafers were left under 0 bar vacuum overnight and XPS was performed the next morning using an Axis Ultra DLD spectrometer (Kratos analytical, UK). A monochromated Al K_α source was used under a pressure of at least 2×10^{-8} mbar at a power of 150W. Results were converted to a VAMAS format and calibrated using CasaXPS software. 160 eV pass energy with 1 eV step size was used to obtain a survey spectra, whilst 20 eV and a step width of 0.1 eV was used to derive the C1s high resolution scan. Analysis was performed at least N=2.

Time of flight secondary ion mass spectrometry

Secondary-ion mass spectrometric analysis was carried out with an IoN-ToF V instrument (IoN-ToF, Münster, Germany), with a Bismuth cluster liquid metal primary ion source. As negative ion spectra have previously been found to be more useful for MA analysis[18], negative ion spectra were acquired using a high current bunched mode approach, (50 KeV Bi_3^{2+}). Images were acquired by rastering the stage under the pulsed primary ion beam (300x300 μm^2 and primary ion beam current of 0.1 pA). The primary ion dose was maintained at less than 10^{12} ions/cm^2 to keep the static SIMS condition. Analysis on each sample was performed N=2, results shown were normalised to total counts.

Atomic Force Microscopy

Tapping mode atomic force microscopy (AFM) was performed in air using a Veeco Dimension 3100 NIIIa, with an ActivResonance controller (Infitesima). A fresh TESPA cantilever tip (Bruker) was used for all samples. The spring constant was 42 N / m, with a resonance frequency of 320 KHz. The root mean square of the measured roughness (R_q) was used to quantify the surface topography.

Contact Angle

Contact angle is a simple but powerful tool for studying the surface energy of a given surface that was used in order to elucidate the relative wettability/hydrophobicity of the surfaces studied. This technique was used to analyse any similarities or clear differences between contact angle and *in vitro* response. When a liquid droplet rests on a surface, there are three tension forces that maintain its shape (Figure 2.0):

1. *Between the interface of the liquid and vapor phases (Υ^{LV})*

2. *The interface of the solid and the liquid (Υ^{SL})*

3. *The interface between the solid and vapour interface (Υ^{SV})[41].*

Through measurement of the contact angle θ between Υ^{SL} and Υ^{LV}, the free energy of the solid surface Υ^{SV} can be found. This has been shown to be very important with regards to cell attachment, proliferation and migration[33]. Generally, contact angles of >90° have been found to be detrimental to surface attachment and neuronal cells will actively migrate away from a hydrophobic surface[39], whilst contact angles below 90° are more amenable to cell attachment. After coating glass slides, samples were placed in a vacuum desiccator overnight, then contact angle was read the next day. 2 x 4 μl distilled water was placed on each of the 3 coated glass slides per run by a Hamilton syringe and one reading was taken per droplet immediately using a goniometer (Ramé Hart instruments, USA).

Young's Equation

$$\gamma^{sv} = \gamma^{sl} + \gamma^{lv}\cos\theta$$

VAPOR

LIQUID

SOLID

γ^{lv}

γ^{sl} θ γ^{sv}

θ is the contact angle

γ^{sl} is the solid/liquid interfacial free energy

γ^{sv} is the solid surface free energy

γ^{lv} is the liquid surface free energy

ramé-hart instrument co.
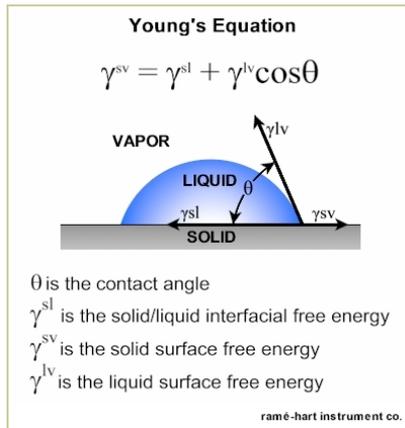
Figure 2.0: A diagram showing the mechanisms by which Young's equation is derived.

2.1.3 Results: Effect of plasma polymerisation on topography using atomic force microscopy

In order to characterise the plasma-polymerised surfaces, contact angle, XPS, ToF-SIMS and atomic force microscopy (AFM) techniques were used. As the chemical characteristics of the glass surfaces were modified, AFM was used to assess whether the physical topography had been altered. Previous work has shown that the physical topography can significantly affect the adhesion, differentiation capabilities and proliferation of cell types[14, 36], it was important to verify the surface characteristics of the plasma polymerised surfaces.

Silicon

Acrylic acid

Maleic anhydride 1

Maleic anhydride 3
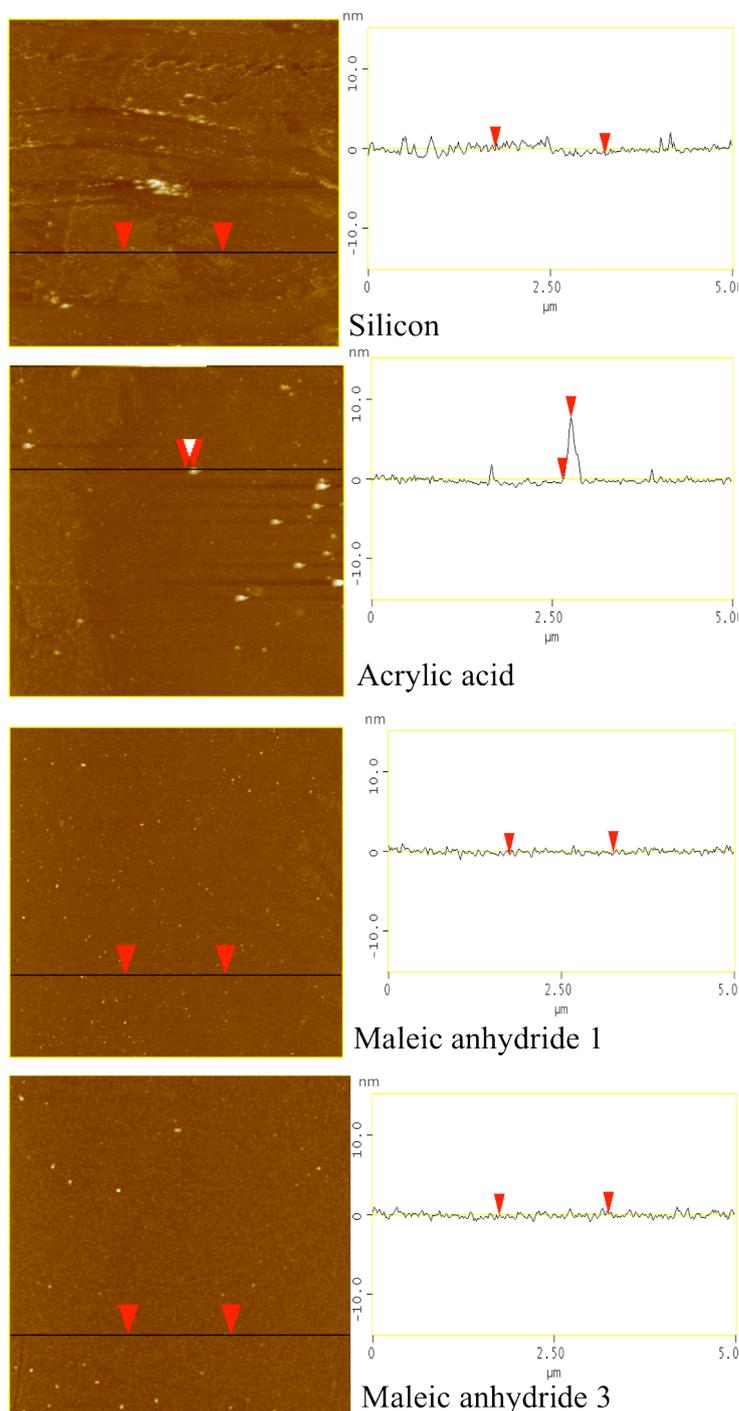
Figure 2.1: Tapping AFM micrographs of plasma polymerised coatings on cleaned silicon wafers. MA 1: Pulsed on-time of 80 μs and an off-time of 800 μs, with 5W peak power. MA 3: continuous 1W power for 20 min. Practical complications meant that MA 2 was not analysed. All surfaces were coated for 20 min. N=2.

Silicon was used as the base substrate for AFM as it is nearly atomically flat and chemically inert. Cleaned silicon wafers were either dried with high purity N_2 gas then analysed, or dried and coated using plasma polymerisation. Results demonstrated that AAc, MA 1 and MA 3 topographies were largely unaffected by the plasma polymerisation coating regime.

There were some nanometre features on the silicon wafers. The root mean square of roughness measurements (R_q) was 0.620 nm, which could be from slight residue due to evaporation of IPA. There were features on AAc with a height of around 10 nm, with an R_q of 2.783 nm. MA 1 demonstrated a flatter surface than silicon with an R_q of 0.276 nm, whilst due to gravitational complications MA 2 was not analysed. MA 3 demonstrated a very smooth surface with an R_q of 0.346, smoother compared to uncoated silicon.

2.1.4 Results: surface characterisation of fresh maleic anhydride and acrylic acid using X-ray photoelectron spectroscopy

Silicon wafers were used for XPS analysis as glass is not suitable, due to charging effects. Silicon wafers were cut with a diamond tipped pen, then individually placed in a stream of air to remove any silicon dust or particles. Wafers were sonicated for 15 min in isopropyl alcohol (IPA), after which the IPA was replaced and the process repeated a minimum of 5 times. Wafers were then stored in fresh IPA and blown dry with high purity N_2 gas when required for use.

Condition	Wide Scan				High Resolution C 1s (%)				
	%Si	%C	%O	O/C	C-C	C-(O)=O	C-C-(O)=O	C-O	C=O/O-C-O
AAc: 15W continuous, 20 min	0.6	75.0	23.3	0.31	45.0	9.2	18.8	17.5	9.6
MA 1: 80 µs on, 800 µs off, 5W.	17.2	55.9	24.6	0.44	43.0	16.2	26.4	10.1	4.3
MA 2: 20 µs on, 1200 µs off, 5W.	25.5	43.8	30	0.68	37.8	21.5	27.9	7.4	5.5
MA 3: 1W continuous	48.0	26.8	23.5	0.88	56.2	5.3	13.1	16.6	8.7

Table 2: XPS elemental composition as detected by the wide scan and C1s narrow scan for acrylic acid and various maleic anhydride plasma polymerised coatings on silicon wafers. Samples were then stored in a vacuum dessicator before analysis. Data shows the average of duplicate samples.

Wafers were coated using plasma polymerisation with AAc and various conditions of MA, then left in a vacuum desiccator over night. Samples were then immediately taken to the XPS and analysed. As hydrolysis of the MA can occur under atmospheric conditions, care was always taken to minimise air exposure between the coating and analysis steps. Three different conditions were devised for MA deposition, followed by chemical and biological evaluation. The conditions consisted of MA 1 = 80 μs on, 800 μs off, MA 2 = 20 μs on-time, 1200 μs off-time, both with a peak power of
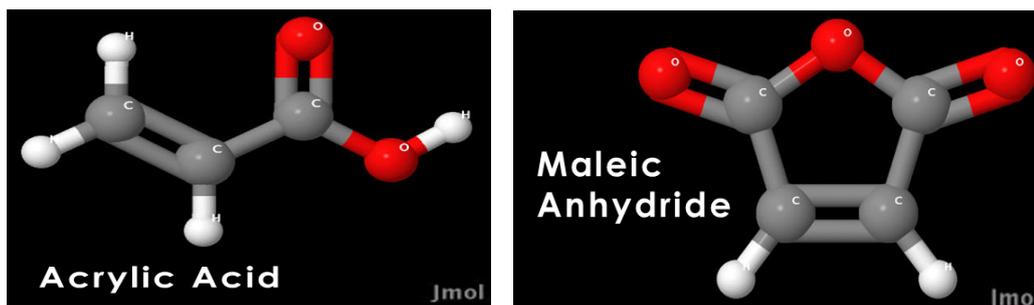
Figure 2.2: Illustration of the acrylic acid and maleic anhydride monomers from http://jmol.sourceforge.net

5W for 20 min. MA3 regime was 1W continuous power for 20 min. As AAc has previously been optimised with neuronal cells by Murray Dunning et al[19], the same condition was used and characterised. The chemical environments and elemental atomic compositions are shown in table 1. Whilst the table shows the averages of N=3, the figures illustrating the wide and narrow scans illustrate a representative analysis.

CASA XPS software was used to fit five components to the spectra using established binding energy shifts of particular carbon environments, which were; C-C (285.0 eV), C-C(O)=O (285.7 eV), C-O (286.7 eV), C=O/O-C-O (287.9 eV) and C(O)=O (289.0 eV). The XPS demonstrated that all the surfaces were rich in carbon and oxygen species; therefore the coating step was successful in coating the slides. There was a slightly higher ratio of oxygen to carbon for the MA 1 samples (0.44) compared to acrylic acid (0.31). As it can be seen from the monomer diagrams in figure 2.3, a higher ratio of oxygen to carbon would be expected on MA plasma polymers compared to AAc. The oxygen to carbon ratio then increases from 0.44 regarding MA 1 to 0.68 for MA 2, then 0.88 for MA 3. As there is a shorter pulsed on time of 20 μs used for MA 2, it was expected that more anhydride functionalities would be retained, therefore leading to higher fraction of oxygen groups to carbon in the wide scan. This enhanced retention was also demonstrated by the increased C(O)=O peak on the narrow scans for MA 2 compared to MA 1.
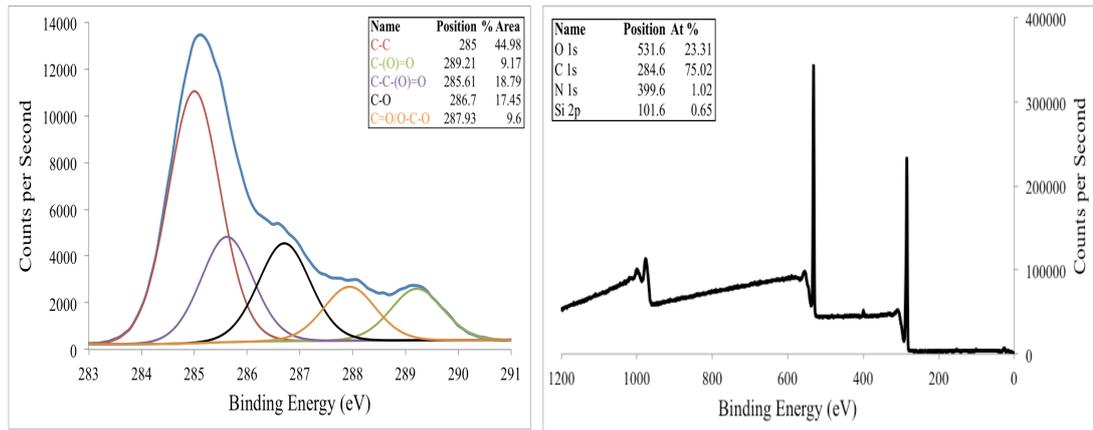
Figure 2.3: X-ray spectroscopy graphs, showing the wide and narrow scans of acrylic acid (AAc). AAc had continuous 15W power for 20 min. Samples were then stored in a vacuum dessicator before analysis. N=2.

The condition for MA3 was 1W continuous, the highest power used for MA plasma polymerisation in this work. It would have been expected for the oxygen to carbon ratio drop, as increased power would lead to reduced functional groups and therefore a less prominent presence of oxygen. Interestingly, the carbon percentage decreases by more than half for the MA 3 condition compared to MA 1, whereas the oxygen percentage stays very similar to MA 1. Because of this, the oxygen to carbon ratio for MA 3 is 0.88, compared to 0.44 ratio found with MA 1.

Regarding the retention of functional groups, AAc had a C-(O)=O peak of 9.2% and C-C-(O)=O peak of 18.8%. It is therefore clear that the plasma polymerisation protocol of AAc retained acid functionality, similar to previous studies[21]. Looking at the functional groups of MA 1, the anhydride / acid component was 16.2%, whilst the C-C-(O)=O component was 26.4%. Although the C-(O)=O component would be
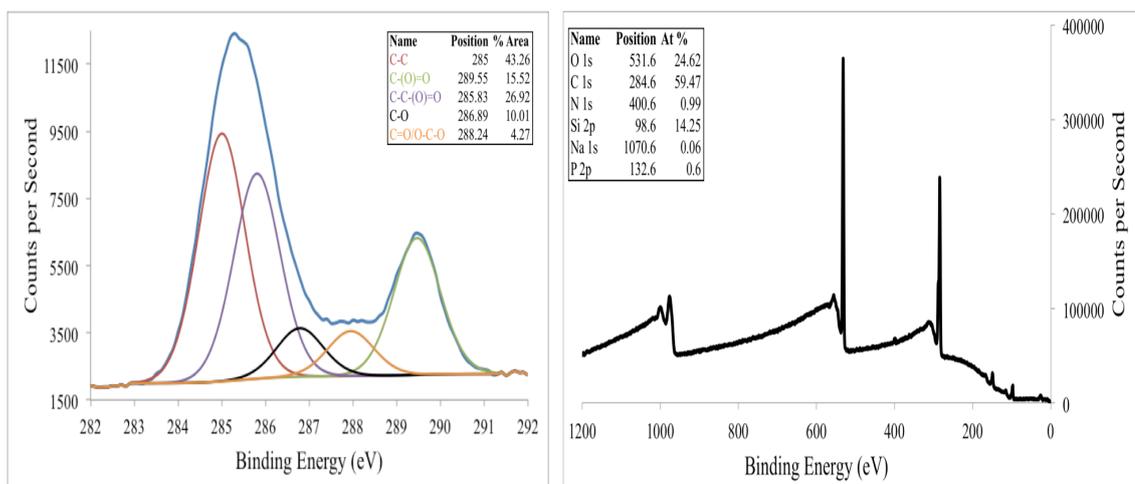
Figure 2.4: X-ray spectroscopy graphs, showing the wide and narrow scans of maleic anhydride (MA) 1. MA 1 coating condition had a pulsed on-time of 80 μs and an off-time of 800 μs, with 5W peak power. Samples were then stored in a vacuum dessicator before analysis (N=3).

indicative of the anhydride group component, due to similarities in the binding shift

position with esters and acids it cannot be determined explicitly from XPS data alone. This again shows that the plasma polymerisation was successful in coating the glass slides with functional groups, the percentages of which are very similar to published work [18]. There is then an increase in the anhydride / acid component for MA 2 component to 21.54%. The percentage area of the C-C-(O)=O component also increased to 27.88% compared to MA 1.
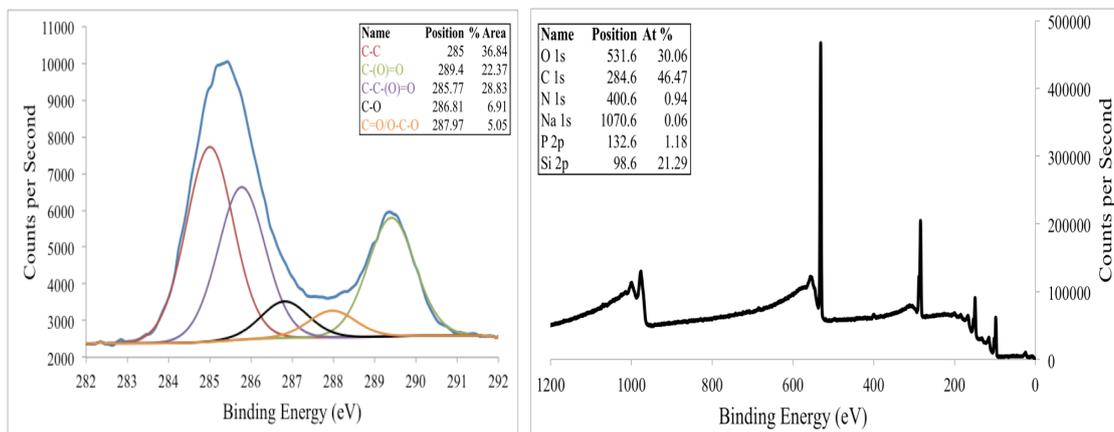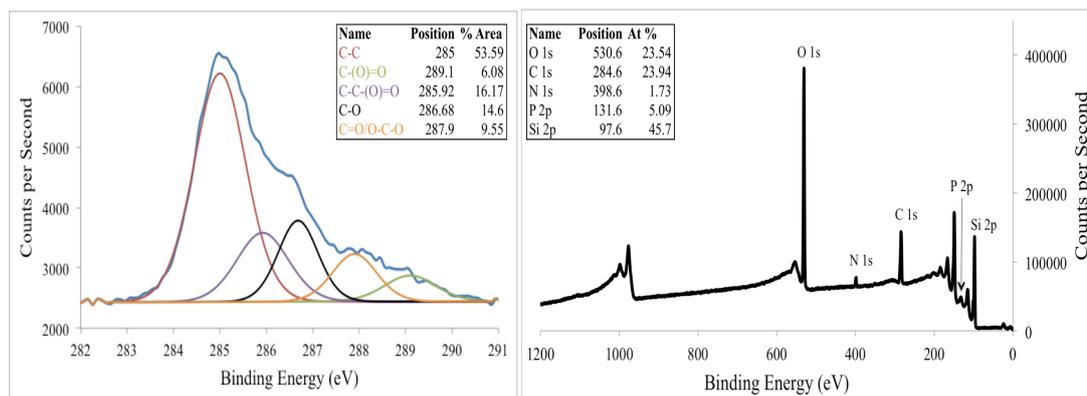

Figure 2.5: X-ray spectroscopy graphs, showing the wide and narrow scans of maleic anhydride (MA) 2. MA 2 coating condition had a pulsed on time of 20 μs and an off-time of 1200 μs, with 5W peak power. Samples were then stored in a vacuum dessicator before analysis. N=2.

As the pulsed on time used for MA 2 was the lowest, it was expected that the retained functionality would be the highest for this regime, as demonstrated in other publications [30]. The lowest retained functionality is shown on MA 3. The C=(O)=O component drops to 5.3%, whilst the C-C-(O)=O functionality is 13.4%. This was again expected, as previous publications demonstrate that a higher continuous power results in a lower percentage of anhydride groups [24, 28, 30].

Other differences between MA 3 and MA 1 & 2 include a marked increase in C-C environment, an increase in the C-O environment and a slight increase in the C=O/O-C-O environment. The increase in the carbon environment regarding MA 3 could have been due to the coating condition. The pulsed regime for MA 1 and 2 was a low power one which has long off time periods, which resulted in higher anhydride functionality. This is shown by the four-fold increase in anhydride groups for MA 1 and 2.

The average silicon environmental percentages were 17%, 25% and 48% for the MA 1, 2 and 3 coatings respectively. Although the accuracy of XPS is ±10%, the averages were from two samples and the silicon environments for the MA coatings were all above 10%.

As MA 2 has the lowest total power, it was expected that the silicon percentage would be higher than MA 1 and MA 3. A 14% silicon environment demonstrated for

MA 1 could have been due to the low power of the regime. 46% silicon peak on the wide scan of MA 3 was very high. Although the exact coating thickness could not be verified as angle-resolved XPS was not used, 46% of silicon demonstrates that the surface coating of MA 3 was probably thinner than MA 1 or 2. Since a higher power usually results in a greater proportion of the species in the chamber becoming ionised and grafting to the surface, it was contradictory to previous publications that the highest powered MA regime had the highest XPS wide scan atomic percentage of silicon. As AAc had a silicon atomic percentage of 0.65%, it could be surmised that the coating was around 10 nm, having used a continuous power of 15W. Presumably, a higher fraction of monomer would have been ionised and fragmented compared to the MA conditions, resulting in to a thicker functionalised adhered layer. As AAc monomer is not as reactive as MA, the power could be increased without sacrificing the functionality.

Figure 2.6: X-ray Spectroscopy graphs, showing the wide and narrow scans of maleic anhydride (MA) 3. MA 3 coating condition had a continuous power of 1W. Samples were then stored in a vacuum dessicator before analysis. N=2

2.1.5 Surface characterisation of fresh maleic anhydride conditions using time of flight-secondary mass spectrometry.

As mentioned previously, carboxyl and anhydride binding energies are very similar when submitted to XPS analysis. Because of this, ToF-SIMS was also used to analyse fresh MA in order to verify the presence of anhydride groups. As only carboxyl groups would be present on AAc plasma polymerised surfaces, ToF-SIMS was not required to additionally characterise AAc. Cleaned silicon wafers were coated with MA, then stored in a vacuum desiccator overnight.

The molecular mass of the negatively charged monomer was 97, which is shown as a prominent peak for MA 1, 2 and 3 (Figure 2.7). The coatings were therefore successful in retaining the anhydride groups during the plasma polymerisation process. This shows that the conditions used were appropriate, otherwise the coating would have

either fragmented the anhydride groups or the groups would not have attached. Whilst the coatings for MA 2 and 3 demonstrated a high silicon percentage using XPS, it can be demonstrated with ToF-SIMS that the C(O)=O components of the XPS results contain anhydride functionalities. As there was no signal at the molecular mass of 28 for MA 1, 2 or 3, there was no silicon environment present on the top 2-3 atomic layers of the coating. Significant peaks of C_xH_y corroborate with the XPS results in that there were hydrocarbon functionalities as well as oxygen containing ones.
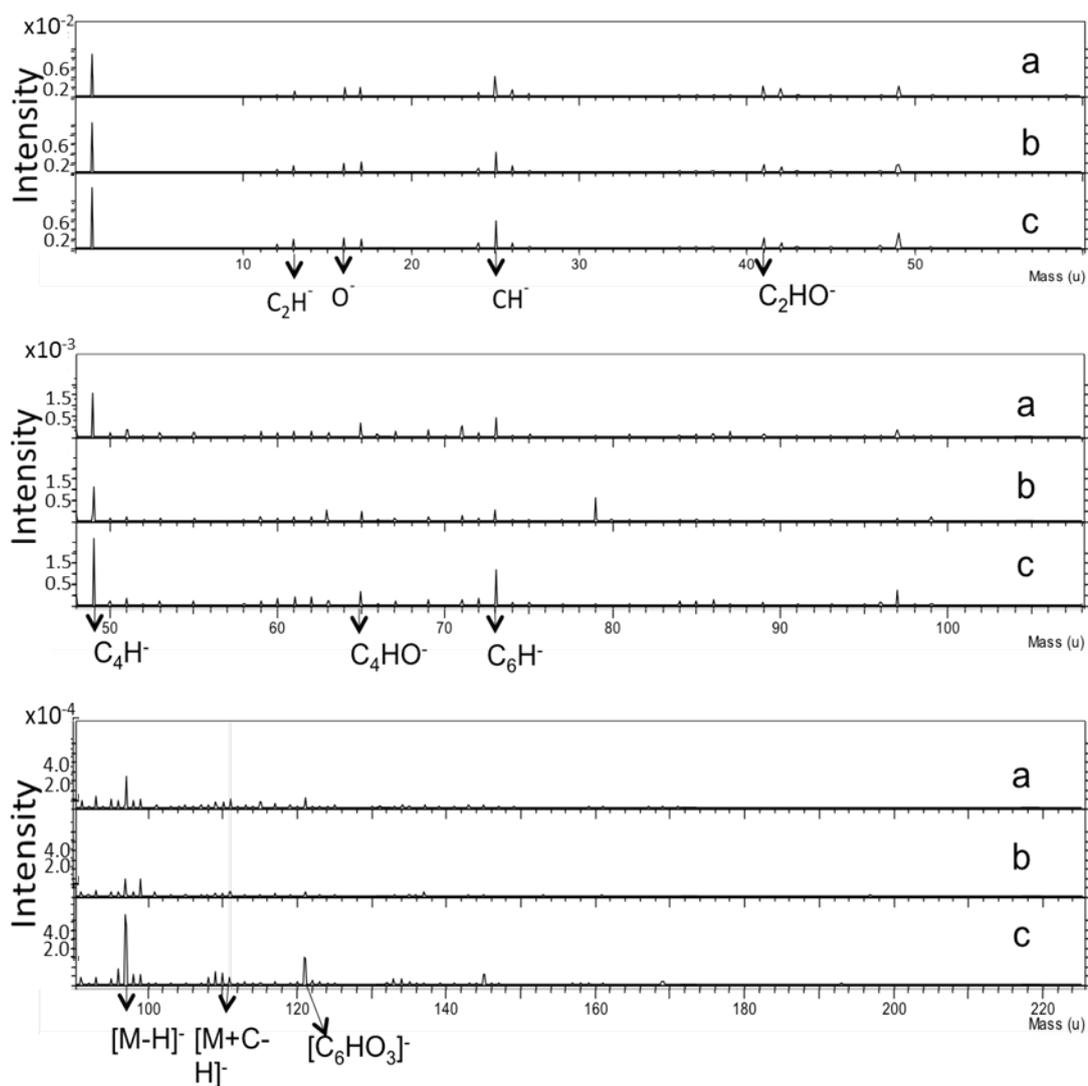
Figure 2.7: Negative ion ToF-SIMS mass spectrum of the three maleic anhydride conditions; a) MA 1, pulsed on-time of 80 μs and an off-time of 800 μs, with 5W peak power, b) MA 2, pulsed on-time of 20 μs and an off-time of 1200 μs, with 5W peak power and c) MA 3, continuous 1W power. All surfaces were coated for 20 min. n=3.

Although similar results were shown between MA 1, 2 and 3 regarding species of molecular mass below 73, C_4H^- and C_6H^- were present in higher amounts on MA 3. Presumably, the higher power condition resulted in a higher degree of fragmentation, which resulted in higher counts of lower molecular weight species. Significant peaks after 99 MW demonstrate that the anhydride monomer polymerised with carbon

containing molecules during the pulsed on time, resulting in species with the molecular weights of 110, 121 and 145.
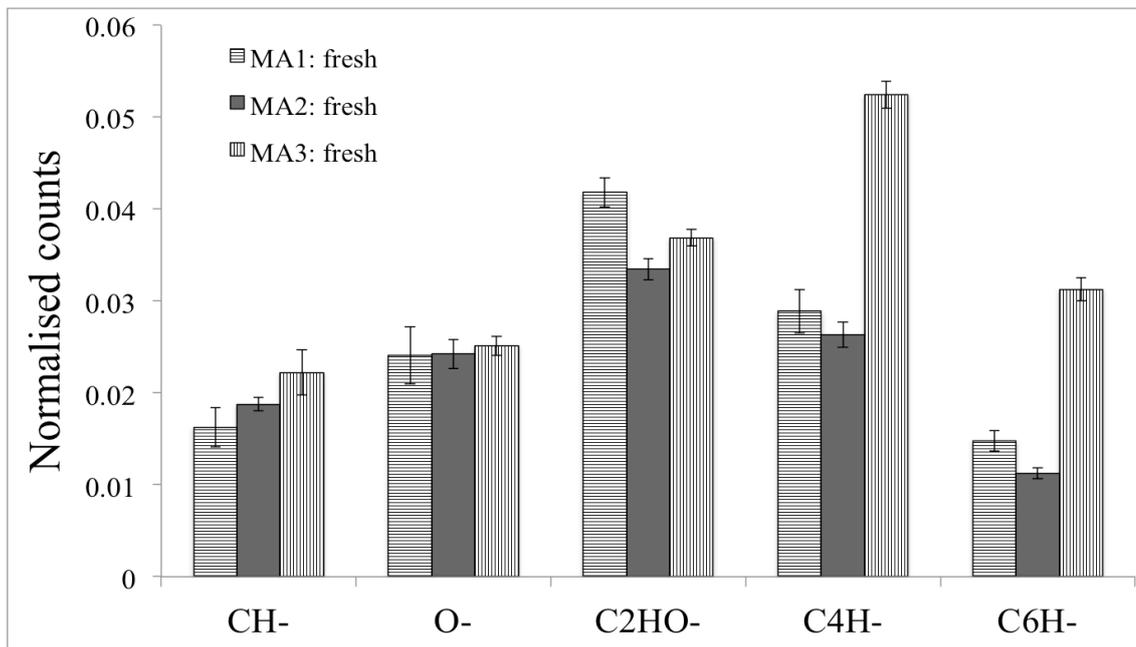
Figure 2.8: Negative ion ToF-SIMS smaller mass fragments from the three maleic anhydride conditions; a) MA 1, pulsed on time of 80 μs and an off-time of 800 μs, with 5W peak power, b) MA 2, pulsed on time of 20 μs and an off time of 1200 μs, with 5W peak power and c) MA 3, continuous 1W power. All surfaces were coated for 20 min. N=2.
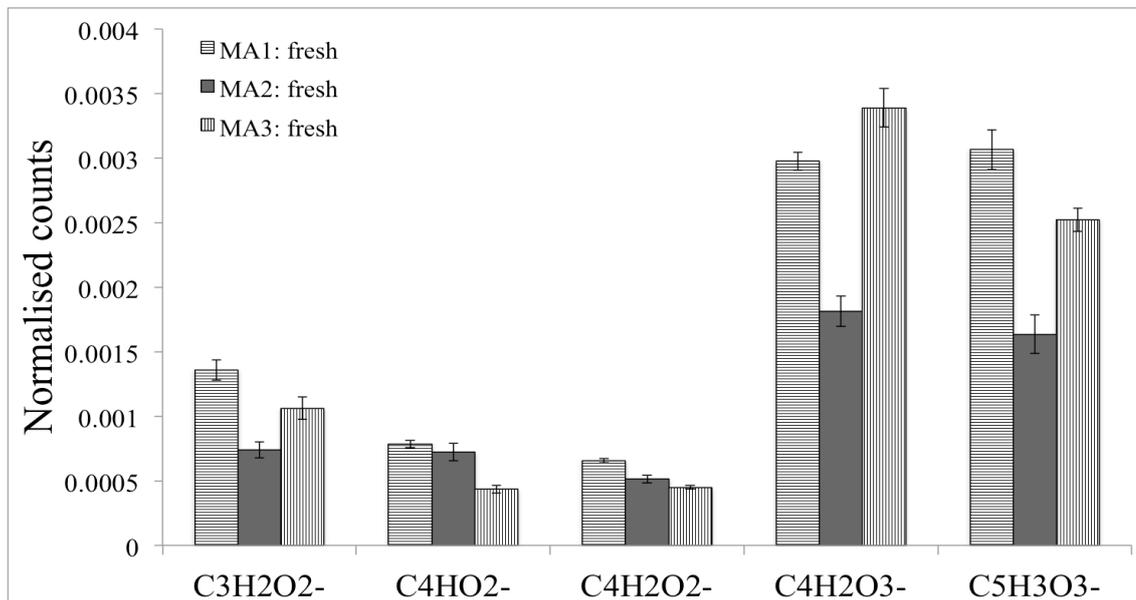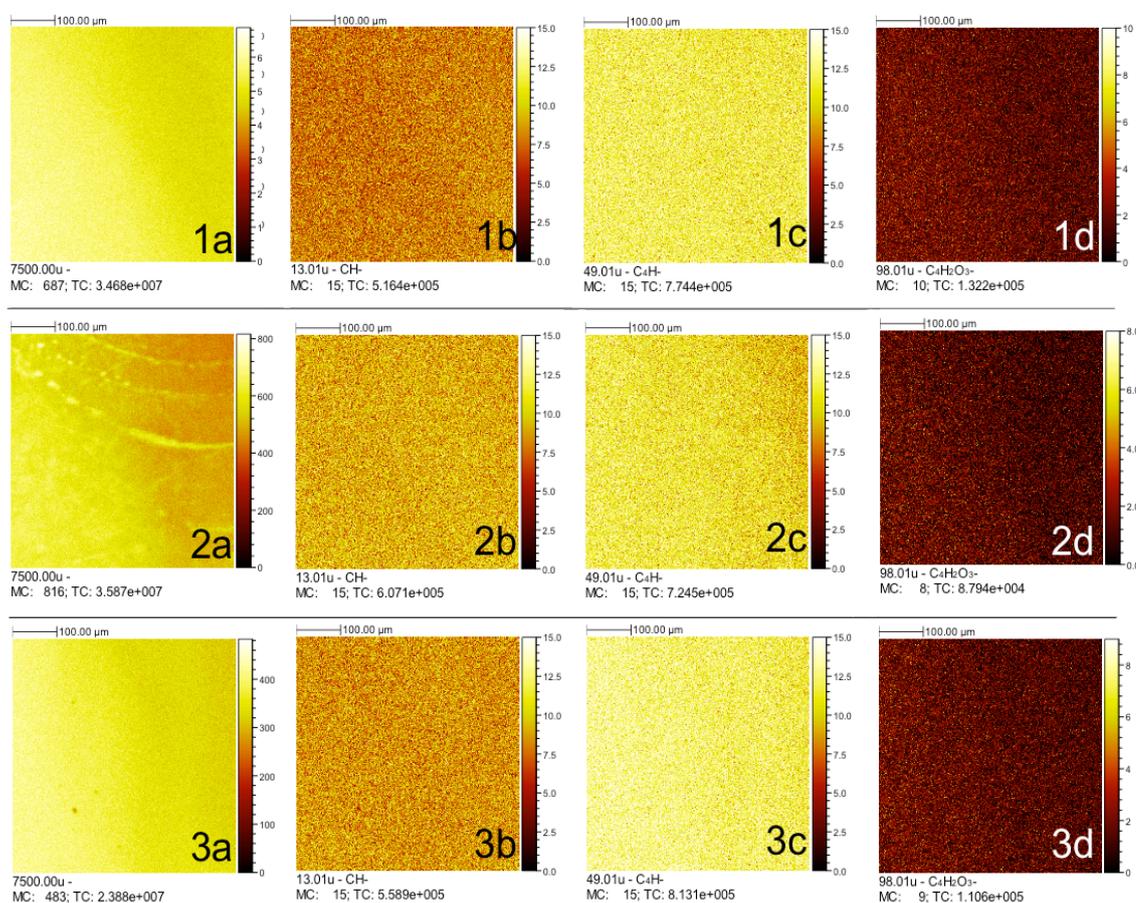

Figure 2.9: Negative ion ToF-SIMS larger fragments from the three maleic anhydride conditions; a) MA 1, pulsed on time of 80 μs and an off time of 800 μs, with 5W peak power, b) MA 2, pulsed on time of 20 μs and an off time of 1200 μs, with 5W peak power and c) MA 3, continuous 1W power. All surfaces were coated for 20 min. N=2.

Regarding the larger fragments detected with ToF-SIMS in figure 2.9, MA 1 and 3 show higher counts of the ionised MA monomer mass compared to MA 2. There were also higher counts of molecular mass 111 for MA 1 and 3. Whilst there is a much wider

possible range of structures at higher molecular masses, mass 111 could refer to $C_5H_3O_3^-$. Overall, a lower count of structures with a higher molecular mass from MA 2 was demonstrated. This result was expected as MA 2 condition had the lowest power, leading to a lower fraction of polymerised species. Figure 2.10 demonstrates that MA 1 and 3 had even surfaces without pinholes or patches, which demonstrated the efficacy of the coating process and the absence of defects. There was also an even distribution of selected ions, which included low and high molecular masses. The total ion image for MA 2 showed uneven coverage, with lines where certain molecular masses were present at higher densities. As the uneven coverage was not seen in the images of selected ions, the uneven coverage was from unknown species. Therefore, whilst it was shown that the MA mass had an even distribution, the same cannot be reported for all species.

Figure 2.10: Negative ion ToF-SIMS mass spectra of the three maleic anhydride conditions; 1) MA 1, pulsed on time of 80 μs and an off-time of 800 μs, with 5W peak power, 2) MA 2, pulsed on time of 20 μs and an off time of 1200 μs, with 5W peak power and 3) MA 3, continuous 1W power for 20 min. All surfaces were coated for 20 min. a) Total ion count, b) CH⁻ distribution, c) C_4H^- distribution and d) Negatively charged maleic anhydride monomer distribution. N=2.

2.1.6 Results: Atmospheric ageing study of acrylic acid and maleic anhydride conditions using sessile-drop contact angle

In order to ascertain if the hydrophilicity of the exposed glass surface was modified during the plasma polymerisation coating, contact angle measurements were taken fresh. An ageing study was also carried out for up to 3 weeks in order to verify whether the gradual hydrolysis of MA surfaces affected the contact angle. Preliminary studies (not shown) compared the contact angle from milli-Q water with dH_2O. Results demonstrated no difference in contact angle between the two types of water, so dH_2O was used because of low cost and high availability. The contact angle for glass shows an interesting progression. The fresh contact angle was 48.9°, more hydrophilic than expected. It dipped initially after 24 hours but then gradually increased to 54.8° over 3 weeks. The glass slides were rinsed in methanol, volatile enough to evaporate off without leaving any residue. It is likely that hydrocarbons contained in the laboratory's atmosphere coated the glass slide progressively over the time points, resulting in the rising contact angle measurements due to slightly increased hydrophobicity, as postulated by Englander et al[7]. As the 24-hour time point had a comparatively high standard error mean, the angle of 47° may not be reliable.
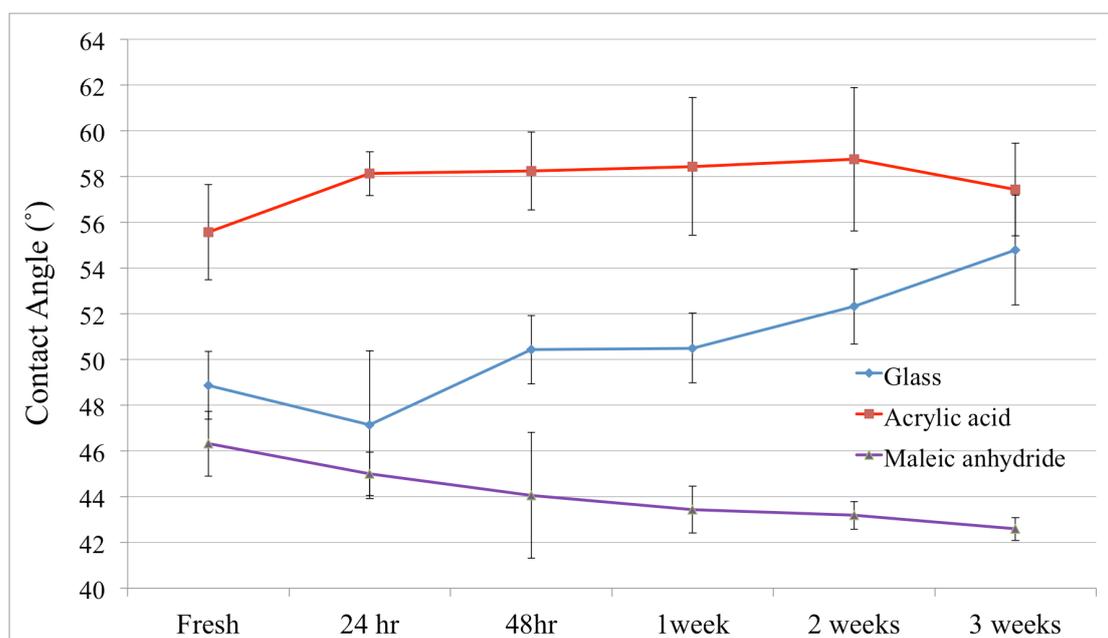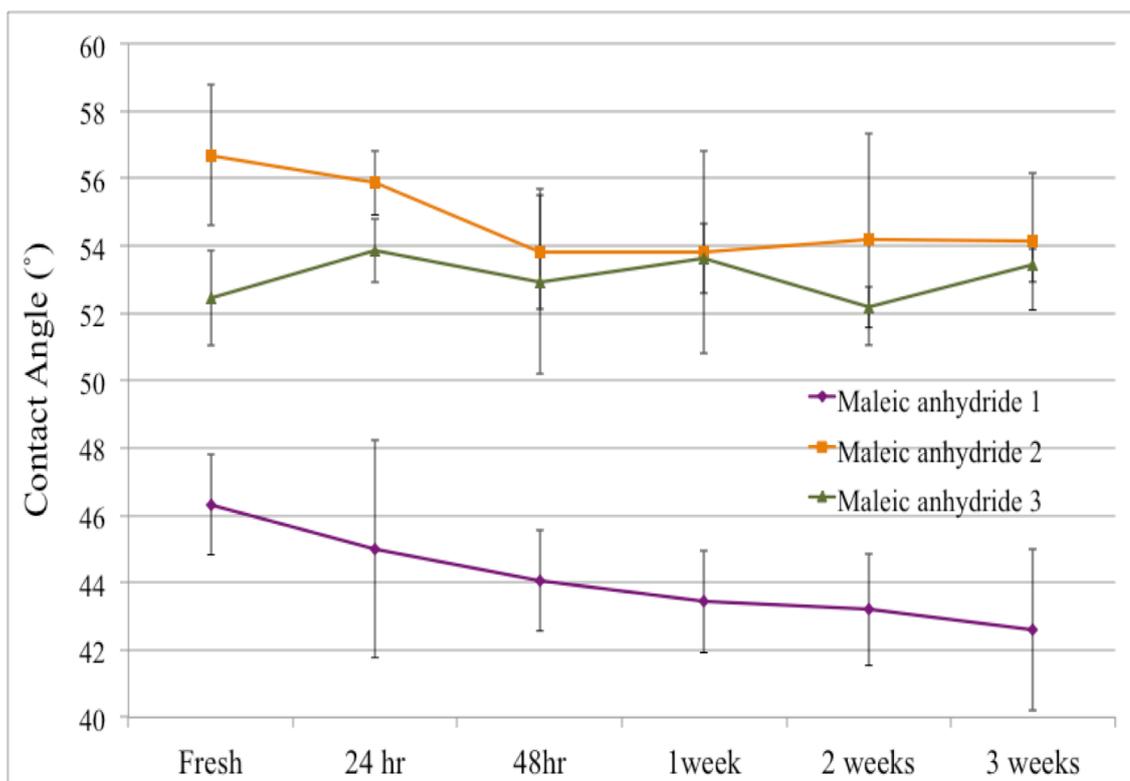

Figure 2.11: Comparison of ageing contact angles of modified surfaces after various time points. 13 mm^2 glass slides were cleaned in methanol, left to dry, then either plasma treated (AAc and MA1) or used as control. Samples were kept in a vacuum desiccator overnight, before being analysed using contact angle. Slides were then stored in a cool, dark environment through the duration of the ageing experiment. Data points show mean ± SEM (N=2).

AAc was observed to have a average fresh contact angle of 55.6°, similar to previously published values [1, 4]. The average contact angle plateaus at 58° for the remaining time points. The plateau was expected, as the carboxylic acid groups will not hydrolyse in the presence of air. It has previously been reported that the AAc plasma

polymer can be stable under atmospheric conditions without any difference in carbon or oxygen content for up to 400 days, as determined by XPS[35]. The contact angle corroborates the findings, however there is a slight decrease at week 3 to 57.4°. As any variances of the contact angle are within 2°, these changes were not significant.

It is well documented that maleic anhydride hydrolyses under atmospheric conditions, whereby the anhydride groups are converted into carboxylic acid groups [2, 6]. A lower contact angle compared to AAc was expected as the anhydride group has two acid groups per monomer, compared to one acid group per monomer of AAc. The gradual and smooth decrease in contact angle from 46.3° to 42.6° demonstrated the hydrolysis of MA1 and increase in more hydrophilic oxygen groups.

Figure 2.12: Comparison of ageing contact angles of modified surfaces after various time points. 13 mm^2 glass slides were cleaned in methanol, left to dry, then plasma treated. Samples were kept in a vacuum desiccator overnight, before being analysed using contact angle. Slides were then stored in a cool, dark environment through the duration of the ageing experiment. Data points show mean ± SEM (N=2).

MA 2 and 3 surfaces have a higher contact angle compared to MA 1 (Figure 2.12). MA 2 had a fresh contact angle of 56.7°, which then decreased to 54° after 48 hr. This agreed with MA 1 regarding the hydrolysis of the anhydride groups, resulting in a lower contact angle. MA 3 contact angle ranged from 52.2° to 53.9° over the course of 3 weeks. As the presence of anhydride functionality on MA 3 was demonstrated with XPS and ToF-SIMS, it was unexpected that the contact angle would increase slightly after 3 weeks, from 52.4° to 53.4°.

2.1.7 Results: stability of maleic anhydride 1 under various storage conditions

It is known that AAc is stable for up to 400 days, when analysed by XPS[35]. For this reason, further stability studies were not conducted for AAc. However, biological studies later in this report indicated that MA 1 was a preferential surface for NG108-15 neuronal cells. As in-depth biological studies were completed using MA 1, further surface characterisation was also performed with this condition. The stability of the MA 1 coating under varying storage conditions was assessed, relevant to potential clinical usage. Common storage methods for medical devices include being packed under atmospheric conditions, being vacuum packed and under N_2 gas.

Surface	Wide Scan			High Resolution C 1s (%)				
	%C	%O	O/C	C-C	C-C-(O)=O	C-O	C=O/O-C-O	C-(O)=O
MA, fresh	72 ±2	26 ±2	0.37	44 ±3	22 ±1	10 ±4	7 ±1	16 ±3
MA, 2 weeks vacuum	72 ±0.5	26 ±0.2	0.36	45 ±1	22 ±0.6	9 ±0.9	8 ±0.4	16 ±0.5
MA, 2 weeks N_2 gas	71 ±0.4	27 ±0.4	0.38	44 ±0.5	22 ±0.3	8 ±0.9	8 ±0.4	18 ±0.4
MA, 2 weeks atmosphere	71 ±0.4	27 ±0.3	0.38	44 ±1	22 ±0.6	8 ±0.7	8 ±0.8	17 ±0.3
MA, 1 month vacuum	72 ±0.2	25 ±0.2	0.35	45 ±0.2	23 ±0.1	10 ±0.4	8 ±0.1	15 ±0.4

Table 2.2: XPS elemental composition as detected by the wide scan and C1s narrow scan for maleic anhydride plasma polymerised coatings on silicon wafers. Samples were aged under the specified conditions then analysed. Results show average ±standard deviation, n=3.

XPS and ToF-SIMS were used to analyse the effect of storing MA under varying conditions, for varying time points. All storage methods were kept in the dark; atmospheric samples were kept in a tissue-culture plate with a loose lid, not sealed. Vacuum storage refers to storage under rough vacuum (~1 x 10^{-3} mbar). Samples were stored under nitrogen gas by placing into a sample holder, then pouring nitrogen gas from a vessel of liquid nitrogen. The lid was then sealed with Parafilm. The XPS results in table 2.2 illustrate some small variances between fresh and stored MA. Carbon accounts for 72% of detected species, whilst oxygen is present at around 26%. After two weeks storage in N_2 gas, the oxygen percentage increased from 26.42% to 27.41%. This increase was also seen for MA stored under atmospheric conditions, rising to 27.25%. Although comparisons from differences of ~2% are limited as XPS has an accuracy of 10%, this rise may indicate the hydrolysis of anhydride groups leading to incorporation of oxygen. It was not practically feasible to coat the surfaces all at once, so surfaces were prepared a month before, 2 weeks before and the night before XPS analysis. This may have resulted in the small differences seen by XPS. Regarding the components from the narrow C1s scan, C-C and C-C-(O)=O environments remained
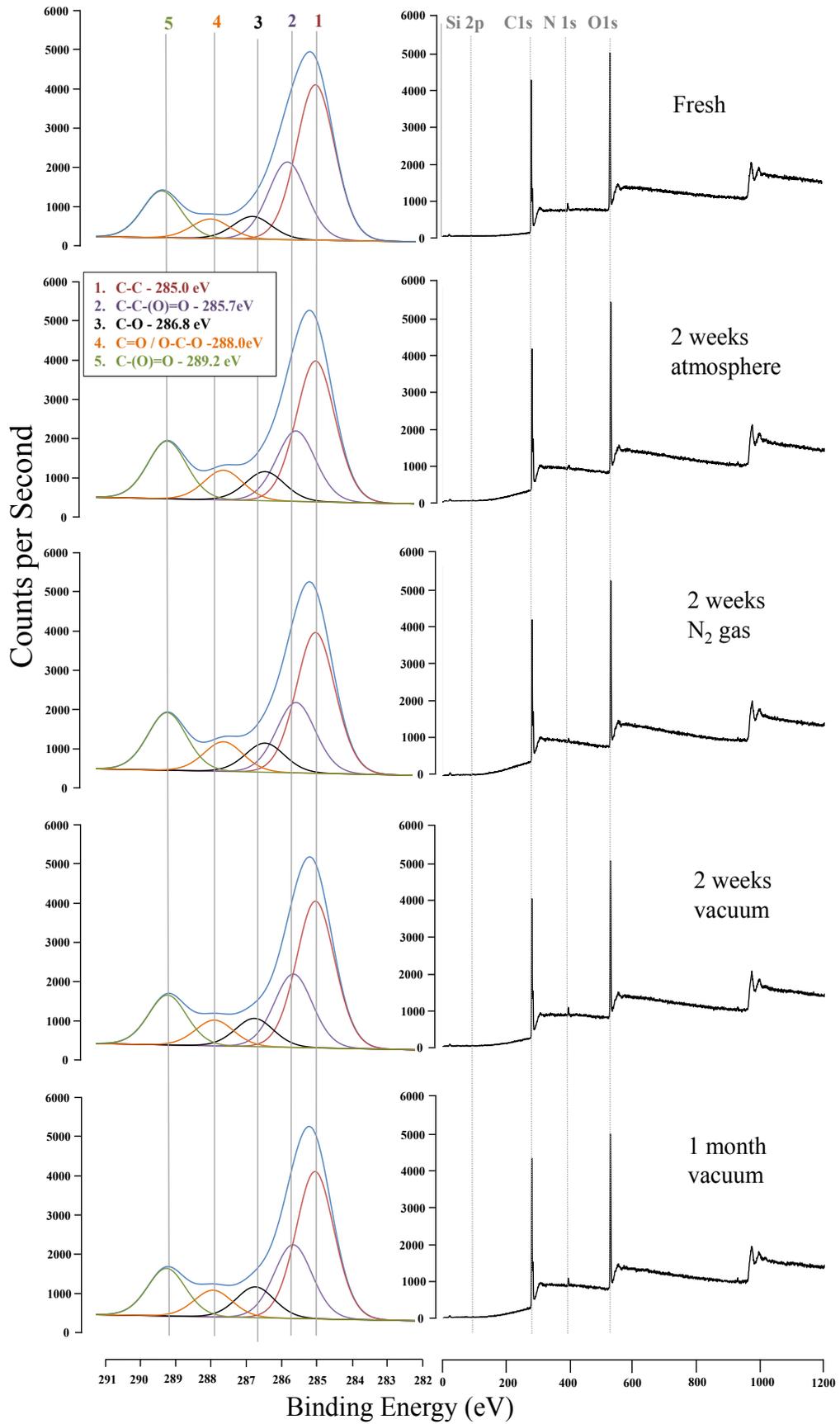
Figure 2.13: The narrow (left) and wide (right) XPS scans for maleic anhydride 1 under various storage conditions as indicated. N=2.

very similar for all conditions. The C-O component dropped from 9.94% for fresh MA down to 7.5% and 8.43% for N_2 gas and atmospheric storage respectively. This was expected, as leakage of N_2 gas before sealing the samples in Parafilm was a possibility. The C=O / O-C-O component slightly increased with all types of storage, from 7.5% to 8.15%. The anhydride component C-(O)=O decreased slightly with vacuum storage, from 16.07% fresh to 15.89% at 2 weeks, then 14.51% at 4 weeks vacuum storage. The anhydride component increased by 1% with N_2 gas and atmospheric storage to 17.87% and 17.26%, respectively. Examining the wide scans from figure 2.13, all samples had a small nitrogen content of up to 1.5%. The nitrogen content for N_2 gas stored MA dropped by 0.5% compared to fresh. Silicon content detected for fresh MA was 0.29%, whereas previous analysis comparing the maleic anhydride regimes had a silicon content of 14%. As this study used different XPS equipment, a different power and set up used may be a possible reason for the difference. Additionally, the XPS technique has an accuracy of 10%. However, it highlights the possibility of variance with regards to the coating depth, as the analyses were conducted over a period of 3 years. There was no difference in detected silicon content of MA stored for 2 weeks under vacuum, under N_2 gas or under atmospheric conditions. The silicon content for MA stored for 1 month under vacuum increased slightly to 0.54%. No contaminating species (calcium, fluorine) were detected on the wide scans of the fresh or stored conditions.

The main hydrolysis action of an anhydride to an acid would only be detected with XPS as a slight increase in oxygen. It cannot distinguish between anhydride and carboxylic acid groups. ToF-SIMS was therefore also used to analyse molecular masses present at different time points. From the ToF-SIMS spectra shown in figure 2.14, the quantified distribution of selected fragments from various storage conditions were shown in figure 2.15. The possible composition and arrangement of molecular masses have been derived, using knowledge of the chemical species on the surface (i.e. oxygen, carbon and hydrogen). The listed species are the most probable, given the monomer used and plasma polymerisation process. For purposes of analysis, certain anticipated masses were chosen beforehand, in order to produce images of ion distribution and spectral area analysis. These masses (with postulated structures in brackets) were: 13 (CH^-), 16 (O^-), 41 (C_2HO^-), 49 (C_4H^-), 73 (C_6H^-), 70 ($C_3H_2O_2^-$), 81 ($C_4HO_2^-$), 82 ($C_4H_2O_2^-$), 98 ($C_4H_2O_3^-$) and 111 ($C_5H_3O_3^-$). Other molecular masses that were present with a significant number of normalised counts included 17 (CH_4), 26 ($C_2H_2^-$), 42 ($C_2H_2O^-$), 49 (C_4H^-) and 71 ($C_4H_7O^-$).

Selected species of smaller fragments including CH^-, O^-, C_2HO^-, C_4H^- and C_6H^- were present in quantities over x10 more abundant than some larger fragments. C_2HO^- was the most abundant species for all conditions.
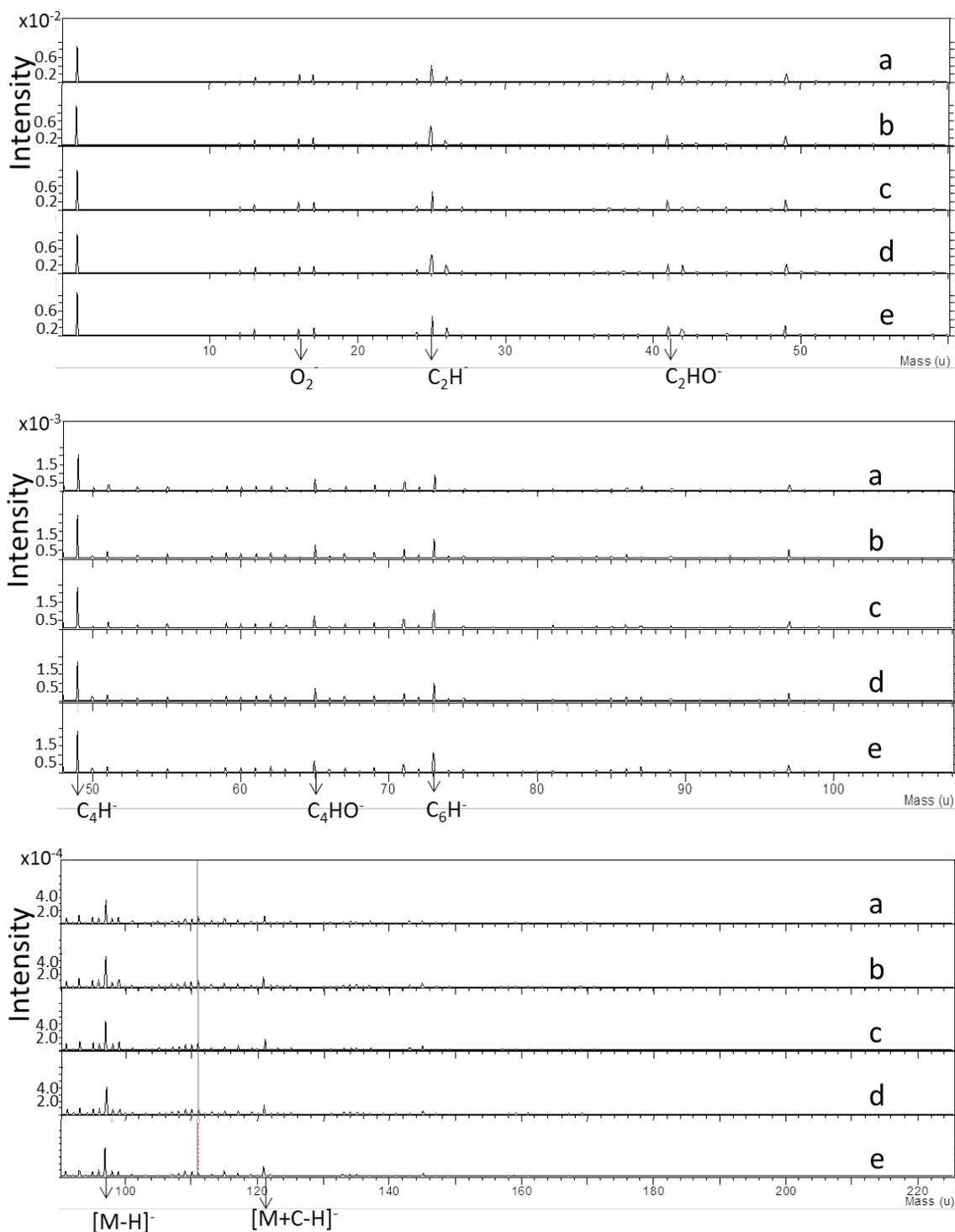

Figure 2.14: ToF-SIMS spectra of maleic anhydride 1, after storage under varying conditions; a) fresh, b) 2 weeks atmospheric, c) 2 weeks N_2 gas, d) 2 weeks vacuum and e) 4 weeks vacuum. Significant negative ion fragments are indicated below, where M = monomer mass. N=2.

Fresh MA had a slightly lower abundance of C_4H^- and C_6H^- species compared to all other storage conditions at 0.029 and 0.015 respectively, compared to ~0.036 and ~0.19

for storage conditions. Storing MA under N_2 gas and atmospheric conditions also led to a slight increase of C_2HO^-, 0.048 and 0.047 respectively, compared to 0.042 for fresh.
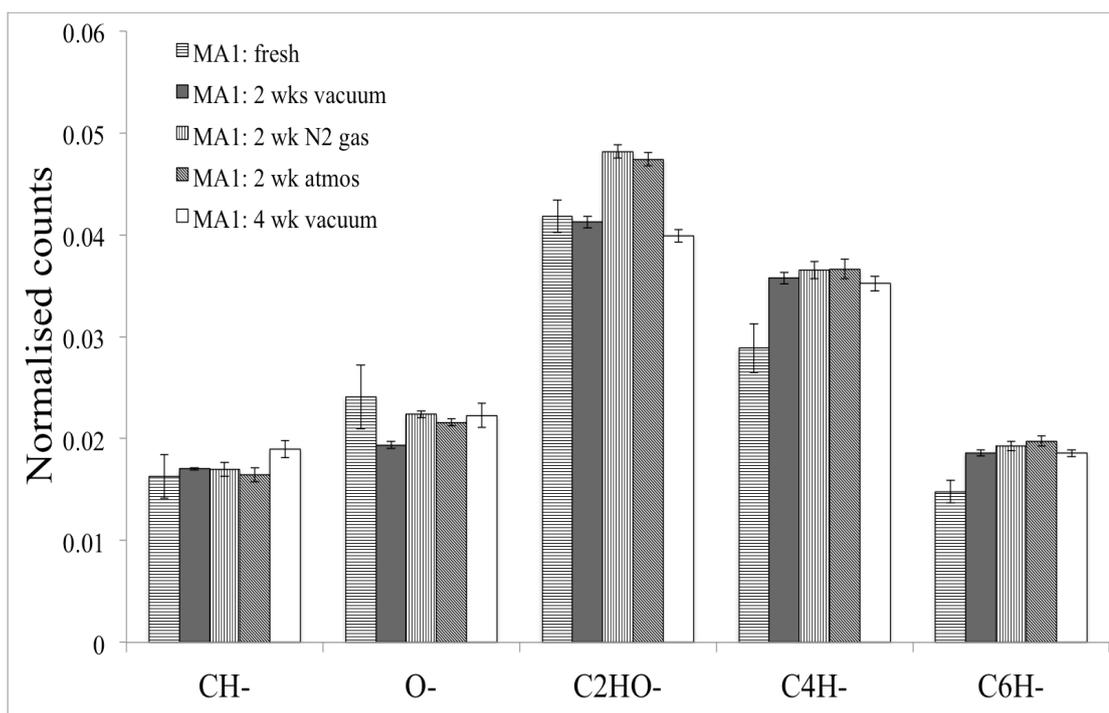
Figure 2.15: Negative ion ToF-SIMS smaller fragments from maleic anhydride 1, after storage under varying conditions. Area normalised to total counts, n=4.
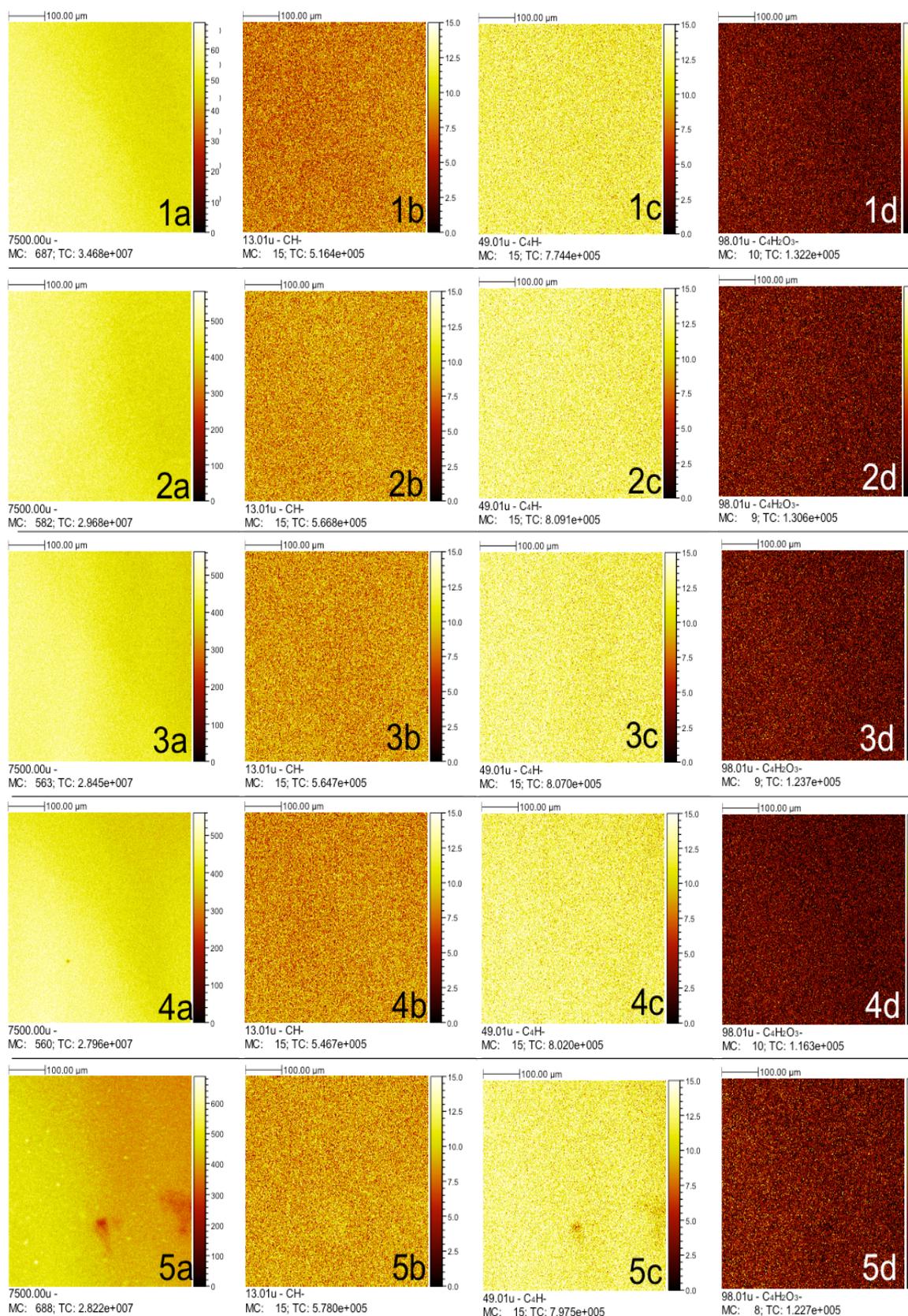
Larger selected fragments of $C_3H_2O_2^-$, $C_4HO_2^-$, $C_4H_2O_2^-$, $C_4H_2O_3^-$ and $C_5H_3O_3^-$ had varying distribution depending on storage method.
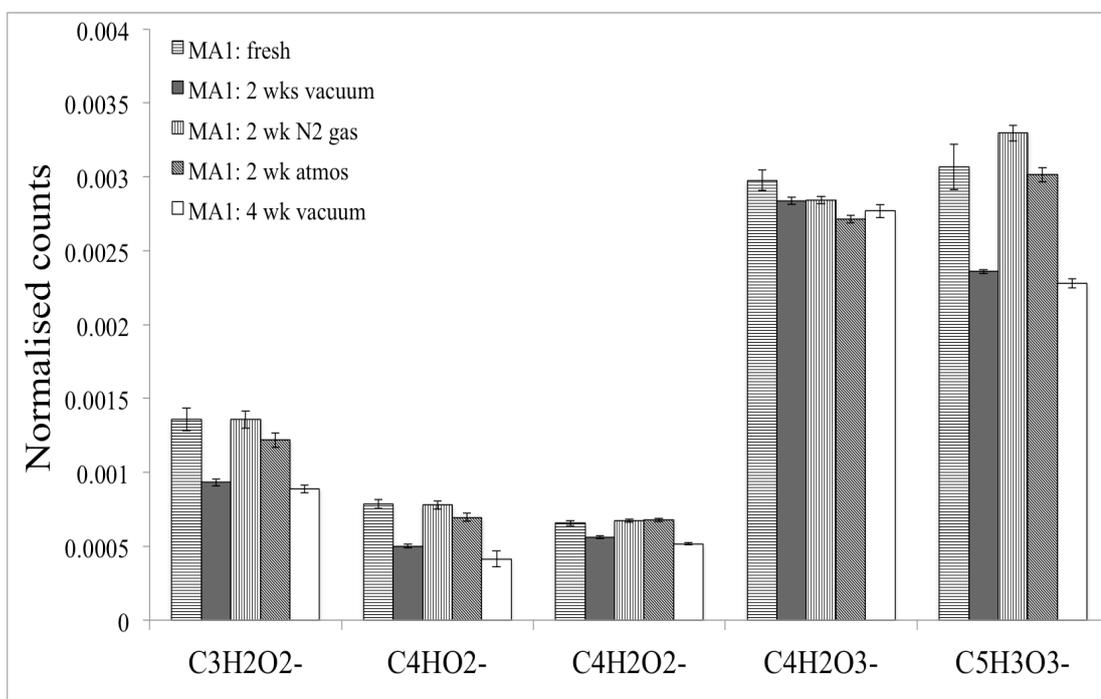
Figure 2.16: Negative ion ToF-SIMS larger fragments from maleic anhydride 1, after storage under varying conditions. Area normalised to total counts, n=4.

Figure 2.17: Negative ion ToF-SIMS mass distribution images of the maleic anhydride 1 condition, after storage under varying conditions; 1) fresh, 2) 2 weeks vacuum, 3) 2 weeks N_2 gas, 4) 2 weeks atmosphere and 5) 4 weeks vacuum. a) total ion count, b) CH$^-$ distribution, c) C_4H^- distribution and d) negatively charged maleic anhydride monomer distribution. N=2.

The 2 and 4 week vacuum method showed a slightly lower abundance of all molecular masses ≥ 70 compared to fresh maleic anhydride. The $C_3H_2O_2^-$ fragment abundance was 9.3×10^{-4} for 2 week vacuum, 8.9×10^{-4} for 4 week vacuum, then $1.4x \times 10^{-3}$ 0.0014 for fresh MA. The abundance of $C_4HO_2^-$ was 0.0008 for fresh MA, compared to 5.0×10^{-4} and 4.0×10^{-4} for 2 and 4-week vacuum respectively. Regarding the abundance of the intact MA monomer, all storage conditions demonstrated lower counts compared to fresh MA. However, whilst the vacuum and N_2 gas storage methods dropped only to 2.8×10^{-3} from 3.0×10^{-3} from fresh, atmospheric storage dropped to 2.7×10^{-3}.

This was interesting, as water in the atmosphere may have reacted with the anhydride groups. It was interesting that the monomer group would hydrolyse after 2 weeks under atmospheric conditions to a structure that contained two carboxylic acid groups, with a molecular mass of 115. Although a peak at 115 is present, the area does not change significantly between 2 weeks storage under atmosphere compared to fresh. As water immersion studies have also been reported in the next section, it will be interesting to compare results.

Regarding $C_5H_3O_3^-$, fresh MA had 3×10^{-3} normalised counts whilst 2 and 4 week vacuum counts dropped to 2.4×10^{-3} and 2.3×10^{-3} respectively. As well as spectra of molecular masses detected using ToF-SIMS, the positions of selected species can also be mapped onto a ToF-SIMS image to demonstrate distribution. Whilst the selected ions from the fresh and 2 week storage methods of MA1 showed an even distribution, this was not so for 4 week vacuum storage. There was an area of depletion regarding certain species, which included molecular mass 49 (Postulated structure C_4H^-), 16 (O^-), 41 (C_2HO^-) and 73 (C_6H^-).

2.1.8 Results: stability of maleic anhydride 1 under dH$_2$O

As biological characterisation involved the immersion of the given surface in aqueous medium for varying amounts of time, further characterisation of MA was carried out using distilled water as a model. Fresh MA coated silicon wafers were immersed in distilled water for 20 minutes, 4 days and 14 days. Excess water was then wicked off and the slides dried at 50°C for 1 hour then stored under vacuum overnight before fresh XPS and ToF-SIMS analysis.

Surface	Wide Scan			High Resolution C 1s (%)				
	%C	%O	O/C	C-C	C-C-(O)=O	C-O	C=O/O-C-O	C-(O)=O
MA, fresh	72 ±2	26 ±2	0.37	44 ±3	22 ±1	10 ±4	7 ±1	16 ±3
MA, 20 min dH$_2$O	71 ±0.6	28 ±0.3	0.39	44 ±0.3	22 ±0.1	9 ±0.4	8 ±0.2	18 ±0.2
MA, 4 days dH$_2$O	71 ±0.5	28 ±0.4	0.39	44 ±0.7	22 ±0.4	10 ±0.8	9 ±0.7	16 ±1
MA, 2 weeks dH$_2$O	71 ±0.4	27 ±0.2	0.38	44 ±0.1	22 ±0.1	10 ±0.6	8 ±0.4	16 ±0.1

Table 2.3: XPS elemental composition as detected by the wide scan and C1s narrow scan for maleic anhydride plasma polymerised coatings on silicon wafers. Samples were immersed in dH$_2$O for the specified time, then analysed. Standard deviation in parenthesis, n=2.

From the results shown in table 2.3, there are no significant differences between conditions regarding the carbon and oxygen ratio. Whilst the most dramatic carbon decrease is 72.16% to 70.94% after 4 days in dH_2O, the standard deviation for carbon in MA fresh is 1.81. Because of this, the difference is not notable. Again, any differences between MA coatings that have been dipped in water regarding total oxygen percentage are obscured by the standard deviation of 1.52 for fresh MA.
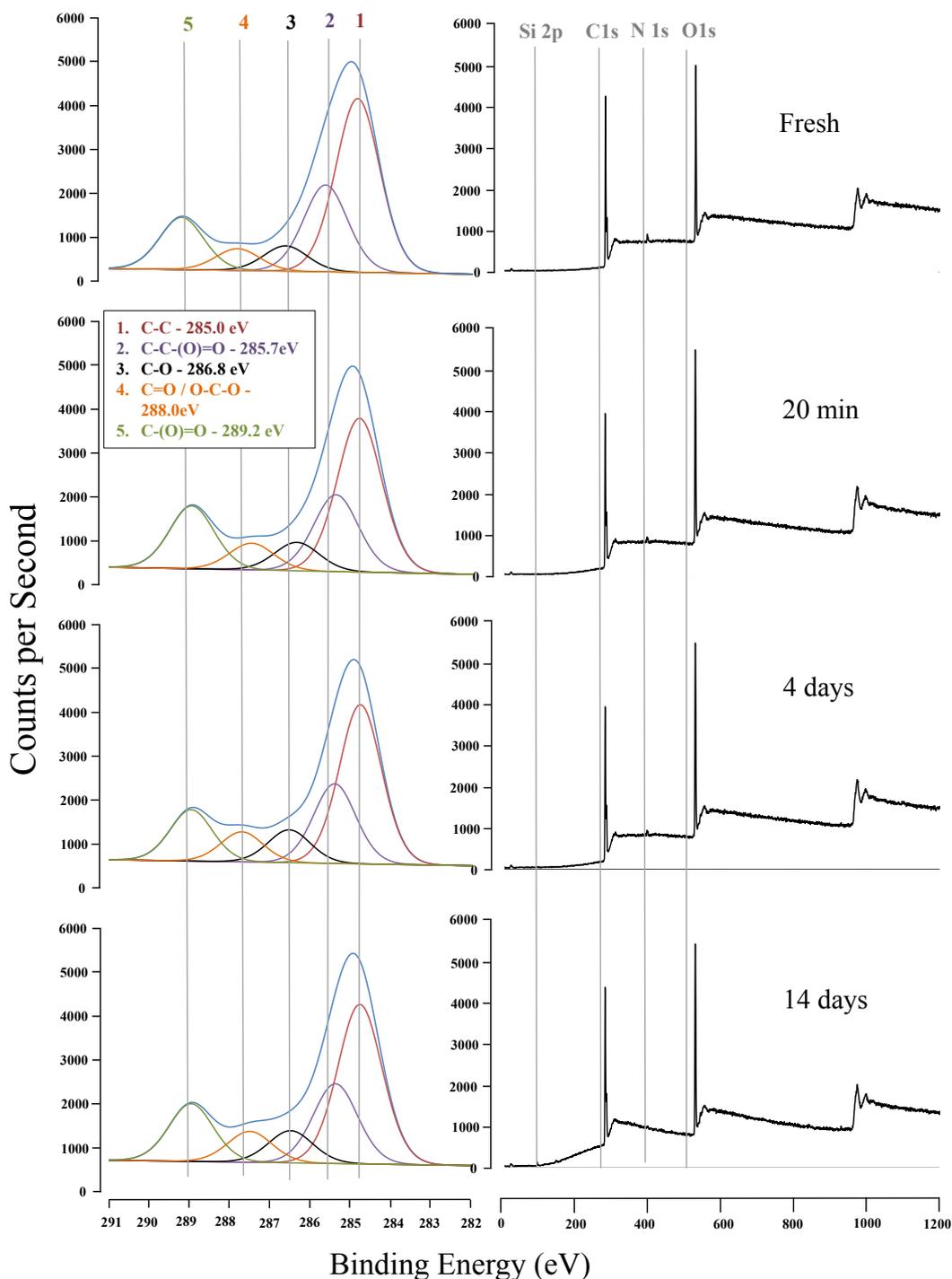

Figure 2.18: The narrow (Left) and wide (Right) XPS scans for maleic anhydride 1 immersed in distilled water for various time points as indicated. N=2.

Inspection of the C1s narrow scan components show that the water immersed environments again show no difference compared to fresh MA. There was very little difference in the C-C environment across the water ageing conditions. As the standard deviation for fresh MA was 2.6, the decrease to 43.99% from 44.35% can be disregarded. For all carbon components, MA immersed for 20 min dH$_2$O showed the most difference in environments compared to fresh apart from the C=O / O-C-O environment. The C-C-(O)=O environment demonstrated no difference between fresh and water immersed MA coated wafers, whilst the C-O environment decreases from 9.94% to 8.62%. As the standard deviation for fresh MA was 3.7, any difference was again masked by the deviation. The only difference of the C=O/O-C-O environment was between fresh (7.48%) and 4 days water aged (8.50%). As the difference was 0.02 over the standard deviation of 1.0, this was again a slight difference. Finally, any differences between conditions with the anhydride / acid component C-(O)=O were again within the range of standard deviation. The anhydride / acid component percentage increased from 16.07 to 17.82 after 20 min in dH$_2$O, then decreased to 15.56 after 4 days. The anhydride component was reported as 15.89% after 2 weeks immersed in distilled water. These results were intriguing, as water is known to react with any anhydride groups present[6]. It was interesting that the percentage of the C-(O)=O component would increase due to hydrolysis of each anhydride group to two acid groups, which did not occur with any significance. Further investigations with ToF-SIMS were then performed to analyse any molecular mass differences between surfaces that had been aged with distilled water. Again, selected molecular masses (with postulated structures in brackets) shown in figure 2.19: 13 (CH$^-$), 16 (O$^-$), 41 (C$_2$HO$^-$), 49 (C$_4$H$^-$), 73 (C$_6$H$^-$), 70 (C$_3$H$_2$O$_2^-$), 81 (C$_4$HO$_2^-$), 82 (C$_4$H$_2$O$_2^-$), 97 (C$_4$HO$_3^-$) and 111 (C$_5$H$_3$O$_3^-$). Other molecular masses present included 17 (CH$_4$), 26 (C$_2$H$_2^-$), 42 (C$_2$H$_2$O$^-$), 49 (C$_4$H$^-$), 51 (C$_4$H$_3$), 71 (C$_4$H$_7$O$^-$), 97 (C$_4$HO$_3^-$), 109 (C$_5$HO$_3^-$), 110 (C$_5$H$_2$O$_3^-$), 111 (C$_5$H$_3$O$_3^-$), 115 (C$_4$H$_3$O$_4^-$), and 121 (C$_5$HO$_3^-$).

Examination of the smaller structures shown in figure 2.20, the normalised count of CH$^-$ increased with time immersed in water, from 0.16 fresh to 0.022 after 2 weeks in distilled water. The levels of oxygen species remained very similar throughout the 2-week period, whilst C$_2$HO$^-$ levels increased from 0.042 to 0.046 after 20 min in water. Counts then dropped slightly to 0.045 after 2 weeks in water. Interestingly, the structure C$_4$H$^-$ increased in abundance from 0.029 fresh, to 0.034 after 20 min dH$_2$O. Counts then increased further to 0.038 after 2 days, then dropped again to 0.034 after 2 weeks in

dH_2O. This pattern was repeated for the C_6H^- structure, which increased from 0.015 fresh to 0.02 after 4 days, and then slightly dropping down to 0.018 after 2 weeks.
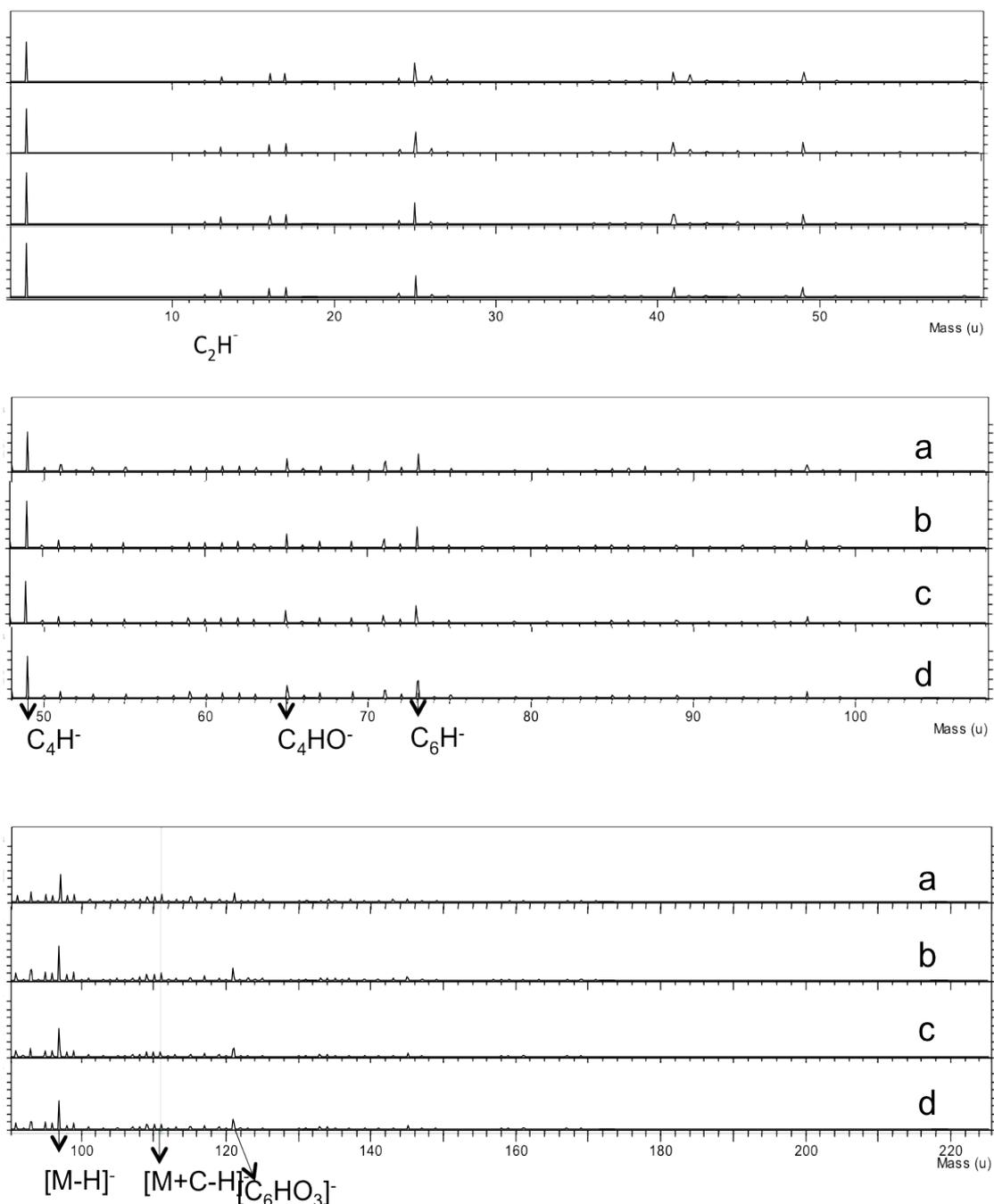

Figure 2.19: ToF-SIMS spectra of maleic anhydride 1 condition, after immersion in distilled water for various time points; a) Fresh, b) 20 min, c) 4 days and d) 2 weeks. Significant negative ion fragments indicated, where M = monomer mass. n=4.

Reporting on possible structures with larger molecular masses shown in figure 2.21, there was a trend of decreasing abundance of certain species with longer periods of immersion in distilled water. The normalised counts of $C_3H_2O_2^-$ lowered from 1.4×10^{-3} fresh, to 9.0×10^{-4} for 4 days and 2 weeks dH_2O immersion. This was repeated for $C_4HO_2^-$; 8.0×10^{-4} for fresh MA, then depleting in abundance to 5.0×10^{-4} after 2

weeks in distilled water. $C_4H_2O_2^-$ was less affected, dropping to only 6.0×10^{-4} after storage in distilled water for 2 weeks, from 6.6×10^{-4} fresh.
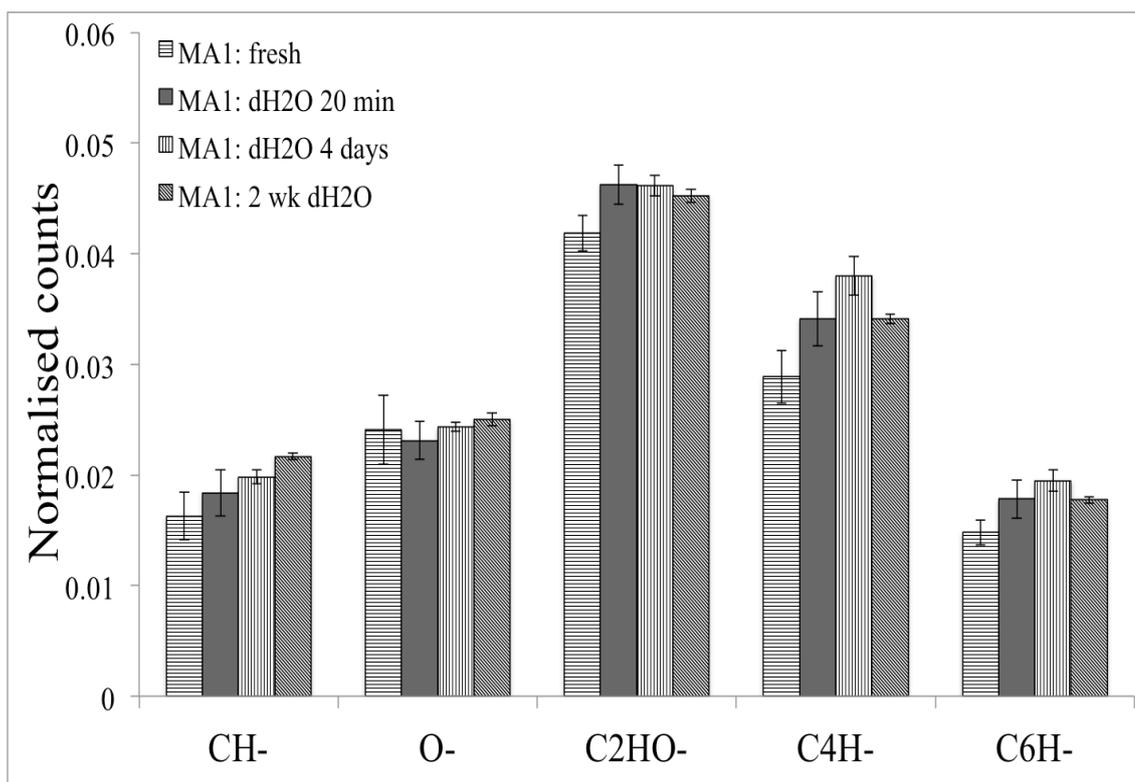
Figure 2.20: Smaller fragments from the negative ToF-SIMS spectra of maleic anhydride 1, after immersion in distilled water for various time points. Areas shown were normalised to total counts, n=4.
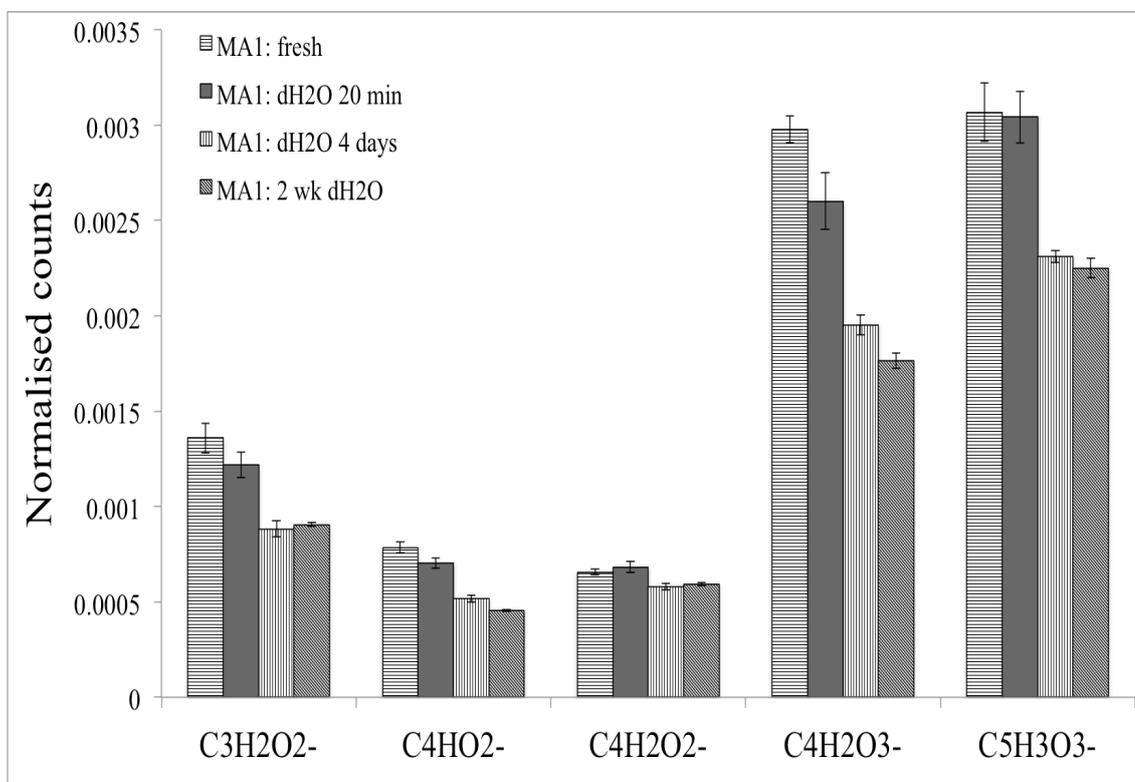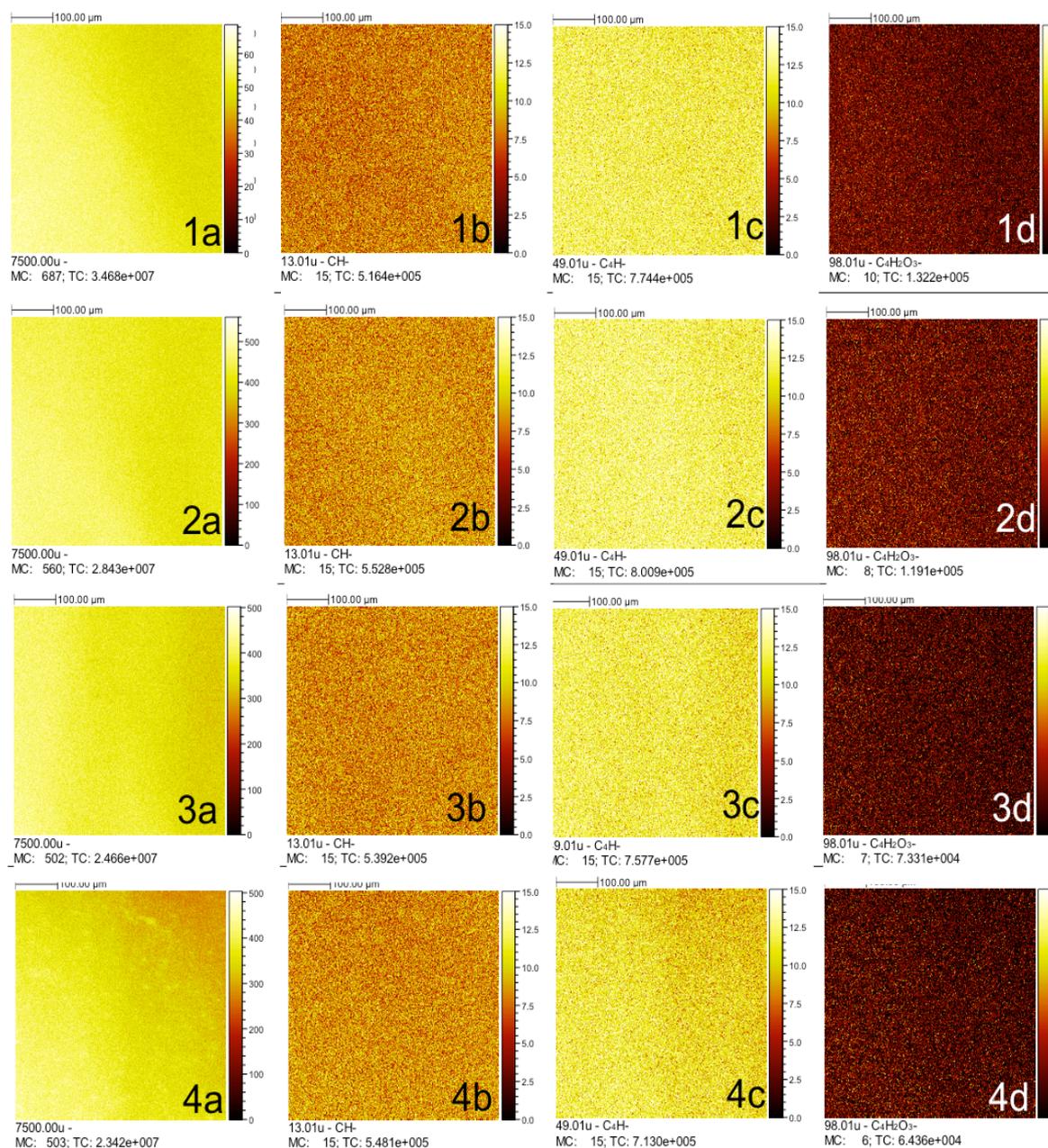

Figure 2.21: Larger fragments from the negative ToF-SIMS spectra of maleic anhydride 1, after immersion in distilled water for various time points. Areas shown were normalised to total counts, n=4.

Figure 2.22: Negative ion ToF-SIMS mass distribution images of the maleic anhydride 1 condition, after immersion in distilled water for various time points; 1) Fresh, 2) 20 min, 3) 4 days and 4) 2 weeks. a) Total ion count, b) CH⁻ distribution, c) C_4H^- distribution and d) Negatively charged maleic anhydride monomer distribution. N=2.

Considering the monomer structure $C_4HO_3^-$, its relative abundance compared to other larger structures was high, with normalised counts at 3.0×10^{-3} for fresh MA. The abundance then decreased sharply, to 2.6×10^{-3} after 20 min, 2.0×10^{-3} after 4 days, then 1.8×10^{-3} after 2 weeks. This could have occurred due to rapid hydrolysis of the anhydride group by dH_2O.

However, the decrease in anhydride groups would be expected to correlate with an increase in the structure $C_4H_3O_4^-$, molecular mass 115. This did not occur; instead the normalised counts of molecular mass 115 decreased over the duration of water

immersion (Figure 2.19). The trend of decreasing abundance of larger structures continues with $C_5H_3O_3^-$, counts decreasing from 3.0×10^{-3} fresh, to 2.3×10^{-3} after both 4 days and 2 weeks of water immersion that could have been due to water penetration into the polymer network leading to further hydrolysis of larger molecules.

Looking at the ToF-SIMS molecular mass images of ion distribution, it can be seen that there was an even distribution of all ions for fresh, 20 min and 4 day time points. It can be seen from figure 2.22 that there was an uneven distribution of certain ions after 2 weeks of MA immersion in dH_2O. As the uneven distribution was not seen on any images of selected ions, the distribution was caused by unknown ions. This could have been from the effects of prolonged immersion in water, due to the swelling, expansion[6], then the possible breakdown of certain discrete areas within the polymer network after 2 weeks.

2.1.9 Discussion

Investigations were carried out to ascertain the surface characteristics and composition of plasma polymerised surfaces. AAc and MA plasma polymer coatings were produced, by controlling the flow rate of monomer and total power over a given time frame. Surfaces were then analysed using contact angle, AFM, XPS and ToF-SIMS techniques. Tapping-mode AFM demonstrated that there was no significant difference in topology between the uncoated silicon and plasma-polymerised surfaces. The root mean square of roughness (R_q) is a function that takes the square of the AFM measurements. Whilst studies generally report rougher surfaces with AFM after plasma polymerisation of AAc[34], coating conditions, feed blends and reactor dimensions affect coating characteristics. The only other study that analysed acrylic acid surfaces with AFM used an argon / acrylic acid blend as feed and pulsed the coating[5]. Another study reported an R_q of 0.19 nm for a coating that had similar coating parameters to MA 1 (R_q 0.276 nm)[30]. Conversely, Hu et al[11] found an increase of roughness values using AFM; a difference in R_q from 0.66 nm uncoated PET, to 5.8 nm with MA, using a duty cycle of 1 ms on, 100 ms off and 100W power. The roughness then increased with the power used, for up to 99 nm for 5W continuous. As the R_q of MA 1 and 3 was lower than silicon, the low power used did not increase the surface roughness.

For all plasma polymerised coatings analysed by XPS, the C1s envelopes were fitted with 5 components which corresponded to C-C (285.0 eV), C-C(O)=O (285.8 eV), C-O (286.7 eV), C=O/O-C-O (287.9 eV) and C(O)=O (289.5 eV). The C-C environment was the prominent component of the C1s peak, with varying percentages of acid groups and oxygen containing functionalities. Regarding the XPS for AAc, the surface was rich with carbon and oxygen species. The average silicon environment of 0.65% from the wide scans demonstrated that the coating covered the silicon surface successfully and evenly. From the wide scan of AAc, it can also be seen that there was no contamination from dirt between coating and analysis. Although there was a 1% nitrogen peak, this occurred in all the wide scans of plasma-polymerised surfaces. The nitrogen presence could be from residual molecules trapped in the coating during plasma polymerisation, which would not have been not completely excluded, as a rough vacuum was used. Regarding the oxygen and carbon components, C-C(O)=O was the most prominent at 18.8%. Alongside the C-(O)=O component of 9.2%, it demonstrated that the carboxylic functionality remained intact after the coating step. The relative percentages of acid groups to hydrocarbon groups corroborates well with existing work

[5, 13, 21, 35], and show explicitly that the plasma polymerisation step was successful. Although the XPS was useful for demonstrating the retention of carbon and oxygen species on the coated surfaces, the relatively low accuracy of 10% means that the exact quantities of anhydride or acid groups could not be ascertained. Chemical derivatisation using trifluoroethylamine in methanol may have been a more accurate method of determining the anhydride groups present on MA 1, 2 and 3 and may have provided a more informative result for future biological characterisation work. Chemical derivatisation techniques such as use of diazomethane could have also been used with acrylic acid surfaces to determine the number of carboxylic acid groups.

Regarding fresh MA 1 (80 µs on, 800 µs off), the binding energy peak C(O)=O that would contain the anhydride functionality was 16.2%. This was slightly lower compared to Mishra et al[18], who reported 24.7% anhydride component with 10W power. It may be that the 5W duty power, combined with pulsed conditions, was too low to ionise enough monomeric species for optimal attachment. Whilst the C(O)=O peak of MA 2 was higher at 21.5% due to the shorter on-times[24], it was much more reduced for the MA 3 condition of 1W continuous (5.3%). This was an interesting result, as it has been shown[24] that the greatest retention of anhydride groups occurs with low power and pulsed duty cycles with short on-times and long off-times. Schiller's work demonstrated a C-(O)=O environment of 13.8% for a duty cycle of 1 ms on, 40 ms off with 100W peak power[28]. Although the power was much greater, the pulsed times were also correspondingly larger. Schiller's work also corroborates the findings of this chapter, as the retention of functional groups was lower than MA 1 or 2, but higher than MA 3. The highest retention of the C(O)=O components was shown in Siffer et al[30], who achieves a C(O)=O component of 32% when combining 5W peak power with a 25 µs on-time and 1200 µs off-time. The work was very similar to MA 2, which also had a high anhydride component.

The aim of using pulsed conditions is to ionise the monomer and open up the anhydride ring during the on-time (if the power is high enough). The off-time of the cycle then allows the reactive monomer to attach onto the surface without further fragmentation, resulting in a higher proportion of the anhydride group to be preserved. Comparatively, with continuous power, there was a higher fragmentation rate of the reactive anhydride group and therefore lower retention of functionality. Correspondingly, there was a much larger percentage of carbon on MA 3 compared to MA 1 or 2. The higher degree of fragmentation that leads to an increase in lower weight hydrocarbon species has been reported previously[18]. It can therefore be shown that

with decreasing power and pulsed conditions, a higher retention of anhydride groups within the polymer film occurred and an accompanying decrease in cross linking throughout the polymer network. This corroborates with published work on plasma polymerised MA coatings [18, 24, 28, 30].

Regarding the thickness of the samples, XPS showed that MA 3 had the highest percentage of silicon of 45%. The silicon environment for MA 2 was 21.3%, and 5.3% for MA 1. This difference in thickness between MA 1 and 2 could have been due to the shorter pulsed on-times for MA 2 and therefore shorter ionisation times, which led to a thinner coating. Angle-resolved XPS or ellipsometry would have been useful to exactly determine the thickness of the samples, however due to time and practical constraints this wasn't possible. However, as MA 3 had the continuous condition of 1W, the high silicon environment somewhat conflicts with the higher powered regime used, which would have led to the ionisation of a greater proportion of the gaseous species. TOF-SIMS results demonstrated almost twice the relative amounts of C_4H^- and C_6H^- species on MA 3 compared to MA 1 or 2, which may have altered the molecular interactions within the plasma species and therefore affected the coating thickness. The next step would be to use the characterised surfaces to investigate the relationship between varying plasma polymerised coating conditions and neurite outgrowth and extension.

ToF-SIMS results of the MA 1, 2 and 3 conditions were valuable and agreed with the overall XPS data, demonstrating explicitly that the anhydride functionality remained intact during the plasma polymerisation process. These results were corroborated by previous studies[18], which also proved retained anhydride functionalities at low pulsed power cycles with either FTIR or ToF-SIMS[24, 28, 30]. There was enhanced retention of some hydrocarbon structures and masses over 97 found in the MA 3 coating compared to MA 2, whilst MA 1 also demonstrated higher counts of heavier molecular mass species.

Interestingly, there was a lower count of MA monomer on MA 2 compared to MA 1 and 3. As MA 2 had the lowest power, it could have led to a smaller fraction of the ionised monomer. However, the XPS C1s narrow scan analysis shows the highest anhydride / acid component for MA 2. There is a peak that is only present in MA 2 at molecular mass 79, which could correspond to $C_5OH_3^-$. However, that would not be detected as the anhydride / acid component with XPS. Smaller fragments that would have been detected by XPS as the C-(O)=O anhydride component were all present in lower quantities compared to MA 1 and 3. Therefore, it is not clear where the high abundance of anhydride / acid functionality from XPS component analysis arose from.

The coating for MA 1 and 3 was shown to be pin hole free and evenly distributed, which was very beneficial to know as investigations progressed towards biological characterisation. MA 2 had some uneven distribution of unknown ions, which could be due to the low power duty cycle.

In order to characterise the plasma-polymerised coatings with regards to hydrophobicity for cell culture comparisons, contact angle measurements were performed. A contact angle of 48.5˚ for AAc was compared to similar work of Colley et al[4] and Buttiglione et al[1], who report 43˚±3˚ and 55±2˚, respectively. This is because the monomer flow rate Colley et al. used was higher, leading to lower energy per monomer imparted and therefore a higher retention of functional groups. This would result in more acidic groups on the surface and a more hydrophilic coating, leading to a lower contact angle compared to the conditions used in this chapter for AAc. Meanwhile, Buttiglione et al. used a minimum power of 50W, which is much higher. The increased energy per monomer would have resulted in higher fragmentation and a higher proportion of carbon bonds, giving a more hydrophobic contact angle.

The fresh contact angle of 46.3° for maleic anhydride could have been due to the high proportion of anhydride groups, that may have increased the hydrophilicity of the surfaces. It was difficult to compare contact angles of maleic anhydride, as the only other published work is by Schiller et al[28], who reported a contact angle of 57˚ with 10 μl milli-Q water and 31˚ after 24hr hydrolysis with the water. However, the coating conditions were 100W for 4 minutes, with 1 ms on and 40 ms off; a much higher power. The study was therefore in agreement with results found, as a higher duty cycle could have resulted in a more hydrophobic coating and a higher contact angle. As the contact angle decreases with immersion in water[28], this also concurs with contact angle results found with this study. Whilst the surfaces were not immersed in water during the contact angle study, storage under atmospheric conditions would have exposed the surfaces to vaporised water. Contact angle performed with MA 2 also agrees with Schiller et al[28] in that the surface becomes more hydrophilic after 24hrs when exposed to atmospheric water vapour. MA 3 contradicted existing studies[28], as the contact angle remained very similar throughout the ageing experiment. As it was shown with ToF-SIMS measurements that the maleic anhydride monomer was present in MA 3, it is puzzling why atmospheric hydrolysis of anhydride groups did not lead to a lower contact angle. Fresh MA 3 had the lowest fraction of anhydride / acid groups as demonstrated by XPS which would agree with the stable contact angle values when exposed to atmospheric conditions over time, so the ToF-SIMS may show the presence

of a molecular mass of 98 that is not maleic anhydride. As the experiment was performed in January during cold temperatures, atmospheric humidity would have contained enough water vapour to hydrolyse anhydride groups.

Results in chapter 3 demonstrate that MA 1 is the optimal coating condition for neurite outgrowth of NG108-15 neuronal cells. Because of this, further surface analysis work was conducted to characterise MA 1 herein with regards to storage and water immersion. In apprehension of the use of MA 1 clinically, the coatings were stored for 2 weeks under rough vacuum, N_2 gas and atmosphere. Samples were also analysed after 1-month storage under rough vacuum. XPS results demonstrated no difference between fresh and stored MA 1 with regards to carbon and oxygen content. Analysis of the C1s narrow scan component also showed very small differences, which were negligible due to the larger standard deviation of fresh MA 1.

ToF-SIMS analysis then enabled further insight into the effect of storing MA 1 under certain conditions. Storing MA 1 samples in vacuum for 2 and 4 weeks, N_2 gas and atmospheric environment led to a slight enhancement of lower weight hydrocarbon species compared to fresh MA 1. Results from 2 week and 4 week vacuum storage then demonstrated a slightly lower retention of molecular mass species that corresponded to species $C_3H_2O_2^-$, $C_4HO_2^-$, $C_4H_2O_2^-$ and $C_4H_2O_3^-$. There was a dramatic decrease in the species $C_5H_3O_3^-$ after 2 and 4 weeks vacuum storage. Interestingly, N_2 gas and atmospheric storage had similar normalised counts of the larger molecular weight species to fresh MA 1. Previous publications report the maleic anhydride molecular mass to be significantly lowered after 2 weeks exposure at atmospheric conditions due to hydrolysis[6]. Although there could be another structure present that has the molecular mass of maleic anhydride but a different composition, it is also likely that the MA 1 monomer remained.

The ion images provided by ToF-SIMS mapping show even distribution of species for all storage and fresh conditions, apart from 4 weeks vacuum storage. It was possible that the coating was uneven when prepared, however evidence shown from MA 1 fresh contradicts such assertions. Chu et al[2] reports on the gradual destruction of the MA 1 polymer network by hydrolysis. However, as fresh desiccant was also used with the vacuum storage, this is unlikely.

Due to biological characterisation in chapters 3, 4 and 5, further studies with MA 1 looked into the effect of immersion into dH_2O for varying amounts of time. dH_2O was used to model medium components used in biological experiments. As it has been found that the presence of anhydride groups is directly related to the irreversible binding

of bovine serum albumin (BSA)[16], this was a relevant study. However, small differences demonstrated by XPS studies were again obscured by the standard deviation for fresh MA 1. The C(O)=O component from the C1s narrow scan increased from 16.06% fresh to 17.82% after 20 min dH_2O, however there was also a standard deviation of 2.6.

ToF-SIMS was then used in order to have a detailed look at the species left on the surface after hydrolysis. As chemical species on the surface after 4 days could have potentially stimulated or maintained neurite outgrowth, it was important to characterise the ageing process thoroughly. An increase in lower molecular weight hydrocarbons was found after 20 min, 4 days and 2 weeks dH_2O hydrolysis compared to fresh MA 1. The normalised counts of larger molecular weight species with oxygen functionalities dropped off gradually through all the time points, as hydrolysis occurred.

Interestingly, the assertion by Chu et al[2] that hydrolysis of maleic anhydride occurs after 24 hour immersion in water may not be entirely accurate. The molecular mass corresponding to the MA monomer was detected by ToF-SIMS after 2 weeks immersion in distilled water. These could be erroneous structures that have the same molecular mass as MA, but not the same structure and chemical constituents. Otherwise, it could be postulated that intact, unreacted MA was trapped in the polymeric network. Schiller postulated that MA films formed at low power lead to hydrolysis of a few main chain bonds and partial dissolution of the surface layer, behaviour similar to a polyelectrolyte[28]. A partial dissolution of the surface layer may result in the MA monomer remaining in the base layer of the coating. As silicon was detected in negligible amounts using XPS analysis for the storage and water immersion investigations, the depth of the coating would be around 10 nm.

2.2.1 Conclusions

- The plasma polymerisation process was shown to be successful through AFM, contact angle, XPS and ToF-SIMS analysis

- AFM characterisation demonstrated small differences in the coated and uncoated silicon wafers, indicating that the topology was not significantly altered. There was also a significant enough difference between the contact angle of the uncoated and coated surfaces to show that the hydrophobicity and wettability of the coated glass surfaces had been modified

- XPS analysis probed further into the surface characteristics of the plasma polymerised surfaces. XPS spectra for AAc demonstrated a well-covered surface, rich in carbon and oxygen species. There was good retention of functional groups, which corroborated with previous work. It was found that the greatest apparent retention of functional groups regarding maleic anhydride was the MA 2, which had a condition of 20 µs on-time, 1200 µs off-time and 5W peak power.

- ToF-SIMS was then performed, which indicated that MA 1 and 3 conditions led to the greater retention of the starting monomer compared to MA 2

- As the XPS and ToF-SIMS results did not fully agree, it was not possible to extract quantitative conclusions from the data regarding the relative amount of anhydride groups on fresh MA surfaces respectively. Chemical derivatisation techniques would have therefore been beneficial

- Further characterisation work into the effects of storage on MA 1 demonstrated slightly reduced retention of the maleic anhydride structure when stored for 2 and 4 weeks under vacuum, N_2 gas, and atmospheric conditions

- A dramatic drop off in the MA 1 monomer was demonstrated after 4 days and 2 weeks immersion in dH_2O

2.2.2 References

1. Buttiglione, M., F. Vitiello, E. Sardella, et al., Behaviour of SH-SY5Y neuroblastoma cell line grown in different media and on different chemically modified substrates. Biomaterials, 2007. **28**(19): p. 2932-2945.
2. Chu, L.Q., R. Forch, and W. Knoll, Pulsed plasma polymerized maleic anhydride films in humid air and in aqueous solutions studied with optical waveguide spectroscopy. Langmuir, 2006. **22**(6): p. 2822-2826.
3. Clements, I.P., Y.-t. Kim, A.W. English, et al., Thin-film enhanced nerve guidance channels for peripheral nerve repair. Biomaterials, 2009. **30**(23-24): p. 3834-3846.
4. Colley, H.E., G. Mishra, A.M. Scutt, et al., Plasma Polymer Coatings to Support Mesenchymal Stem Cell Adhesion, Growth and Differentiation on Variable Stiffness Silicone Elastomers. Plasma Processes and Polymers, 2009. **6**(12): p. 831-839.
5. Detomaso, L., R. Gristina, G.S. Senesi, et al., Stable plasma-deposited acrylic acid surfaces for cell culture applications. Biomaterials, 2005. **26**(18): p. 3831-3841.
6. Drews, J., H. Launay, C.M. Hansen, et al., Hydrolysis and stability of thin pulsed plasma polymerised maleic anhydride coatings. Applied Surface Science, 2008. **254**(15): p. 4720-4725.
7. Englander, T., D. Wiegel, L. Naji, et al., Dehydration of glass surfaces studied by contact angle measurements. Journal of Colloid and Interface Science, 1996. **179**(2): p. 635-636.
8. Eves, P.C., A.J. Beck, A.G. Shard, et al., A chemically defined surface for the co-culture of melanocytes and keratinocytes. Biomaterials, 2005. **26**(34): p. 7068-7081.
9. Harsch, A., J. Calderon, R.B. Timmons, et al., Pulsed plasma deposition of allylamine on polysiloxane: a stable surface for neuronal cell adhesion. Journal of Neuroscience Methods, 2000. **98**(2): p. 135-144.
10. Hook, A.L., D.G. Anderson, R. Langer, et al., High throughput methods applied in biomaterial development and discovery. Biomaterials, 2010. **31**(2): p. 187-198.
11. Hu, J., C. Yin, H.Q. Mao, et al., Functionalization of Poly(ethylene terephthalate) Film by Pulsed Plasma Deposition of Maleic Anhydride. Advanced Functional Materials, 2003. **13**: p. 692.
12. Jenkins, A.T.A., J. Hu, Y.Z. Wang, et al., Pulsed plasma deposited maleic anhydride thin films as supports for lipid bilayers. Langmuir, 2000. **16**(16): p. 6381-6384.
13. Kelly, J.M., R.D. Short, and M.R. Alexander, Experimental evidence of a relationship between monomer plasma residence time and carboxyl group retention in acrylic acid plasma polymers. Polymer, 2003. **44**(11): p. 3173-3176.
14. Khung, Y.L., G. Barritt, and N.H. Voelcker, Using continuous porous silicon gradients to study the influence of surface topography on the behaviour of neuroblastoma cells. Experimental Cell Research, 2008. **314**(4): p. 789-800.
15. Kobayashi, H., A.T. Bell, and M. Shen, Effects of Monomer Flow-Rate, Flow Configuration, and Reactor Geometry on Rate of Plasma Polymerization. Journal of Macromolecular Science-Chemistry, 1976. **A 10**(3): p. 491-500.
16. Liu, S., M.M.L.M. Vareiro, S. Fraser, et al., Control of attachment of bovine serum albumin to pulse plasma-polymerized maleic anhydride by variation of pulse conditions. Langmuir, 2005. **21**(19): p. 8572-8575.

17.   Michel, R., J.W. Lussi, G. Csucs, et al., Selective molecular assembly patterning: A new approach to micro- and nanochemical patterning of surfaces for biological applications. Langmuir, 2002. **18**(8): p. 3281-3287.

18.   Mishra, G. and S.L. McArthur, Plasma polymerization of maleic anhydride: just what are the right deposition conditions? Langmuir : the ACS journal of surfaces and colloids, 2010. **26**(12): p. 9645-9658.

19.   Murray-Dunning, C., Electrospun aligned biodegradable microfibers and plasma polymerization techniques to improve peripheral nerve repair. 2010, Sheffield: 200 pages.

20.   Ni, H.C., Z.Y. Lin, S.H. Hsu, et al., The use of air plasma in surface modification of peripheral nerve conduits. Acta Biomaterialia, 2010. **6**(6): p. 2066-2076.

21.   OToole, L., A.J. Beck, and R.D. Short, Characterization of plasma polymers of acrylic acid and propanoic acid. Macromolecules, 1996. **29**(15): p. 5172-5177.

22.   Park, G.Y., S.J. Park, M.Y. Choi, et al., Atmospheric-pressure plasma sources for biomedical applications. Plasma Sources Science & Technology, 2012. **21**(4).

23.   Riemann, K.U., Kinetic-Theory of the Plasma Sheath Transition in a Weakly Ionized Plasma. Physics of Fluids, 1981. **24**(12): p. 2163-2172.

24.   Ryan, M.E., A.M. Hynes, and J.P.S. Badyal, Pulsed plasma polymerization of maleic anhydride. Chemistry of Materials, 1996. **8**(1): p. 37-42.

25.   Salim, M., G. Mishra, G.J.S. Fowler, et al., Non-fouling microfluidic chip produced by radio frequency tetraglyme plasma deposition. Lab Chip, 2007. **7**(4): p. 523 - 525.

26.   Santiago, L.Y., R.W. Nowak, J.P. Rubin, et al., Peptide-surface modification of poly(caprolactone) with laminin-derived sequences for adipose-derived stem cell applications. Biomaterials, 2006. **27**(15): p. 2962-2969.

27.   Sardella, E., P. Favia, R. Gristina, et al., Plasma-Aided Micro- and Nanopatterning Processes for Biomedical Applications. Plasma Processes and Polymers, 2006. **3**(6-7): p. 456-469.

28.   Schiller, S., J. Hu, A.T.A. Jenkins, et al., Chemical structure and properties of plasma-polymerized maleic anhydride films. Chemistry of Materials, 2002. **14**(1): p. 235-242.

29.   Shenton, M.J. and G.C. Stevens, Surface modification of polymer surfaces: atmospheric plasma versus vacuum plasma treatments. Journal of Physics D-Applied Physics, 2001. **34**(18): p. 2761-2768.

30.   Siffer, F., A. Ponche, P. Fioux, et al., A chemometric investigation of the effect of the process parameters during maleic anhydride pulsed plasma polymerization. Analytica Chimica Acta, 2005. **539**(1-2): p. 289-299.

31.   Spatenka, P., H.J. Endres, J. Krumeich, et al., Process control of plasma polymerization in a large industrial reactor. Surface & Coatings Technology, 1999. **116**: p. 1228-1232.

32.   Todd, S.J., D.J. Scurr, J.E. Gough, et al., Enzyme-activated RGD ligands on functionalized poly(ethylene glycol) monolayers: surface analysis and cellular response. Langmuir : the ACS journal of surfaces and colloids, 2009. **25**(13): p. 7533-7539.

33.   Vanwachem, P.B., A.H. Hogt, T. Beugeling, et al., Adhesion of Cultured Human-Endothelial Cells onto Methacrylate Polymers with Varying Surface Wettability and Charge. Biomaterials, 1987. **8**(5): p. 323-328.

34.   Walther, F., W.M. Heckl, and R.W. Stark, Evaluation of nanoscale roughness measurements on a plasma treated SU-8 polymer surface by atomic force microscopy. Applied Surface Science, 2008. **254**(22): p. 7290-7295.

35.   Whittle, J.D., R.D. Short, C.W.I. Douglas, et al., Differences in the aging of allyl alcohol, acrylic acid, allylamine, and octa-1,7-diene plasma polymers as studied by X-ray photoelectron spectroscopy. Chemistry of Materials, 2000. **12**(9): p. 2664-2671.

36.   Yang, J., F.R.A.J. Rose, N. Gadegaard, et al., A High-Throughput Assay of Cell-Surface Interactions using Topographical and Chemical Gradients. Advanced Materials, 2009. **21**(3): p. 300-304.

37.   Yasuda, H., Plasma Polymerization1985, Orlando, Florida: Academic Press, Inc.

38.   Yasuda, H., L. Ledernez, F. Olcaytug, et al., Electron dynamics of low-pressure deposition plasma. Pure and Applied Chemistry, 2008. **80**(9): p. 1883-1892.

39.   Zelzer, M., M.R. Alexander, and N.A. Russell, Hippocampal cell response to substrates with surface chemistry gradients. Acta Biomaterialia, 2011. **7**(12): p. 4120-4130.

40.   Zhang, Y.Z., X. Wang, Y. Feng, et al., Coaxial electrospinning of (fluorescein isothiocyanate-conjugated bovine serum albumin)-encapsulated poly(epsilon-caprolactone) nanofibers for sustained release. Biomacromolecules, 2006. **7**(4): p. 1049-1057.

41.   Zisman, W.A., Relation of the Equilibrium Contact Angle to Liquid and Solid Constitution. 1964. **43**: p. 1-51.

3.1 Biological Evaluation of Plasma Polymers Using NG108-15 Neuronal Cells

3.1.1 NG108-15 neuronal cell culture

There has recently been a lot of interest in the area of nerve regeneration, and the improvement of clinically available nerve guides[4]. Whilst nerve guides have advantages over autografts such as donor site morbidity and therefore reduced risk of infection, they are currently only effective for defects around 20 mm. There have been various strategies to improve nerve guides, from changing the material of the guide, to adding extra Schwann cells to the defect site upon implantation. Methods of *in vitro* analysis regarding neuronal cells include proliferation[11] and metabolic assays[15], immunohistochemistry (IHC) labelling for neuronal markers such as neurofilament 200, and area of cell coverage[5].

A cost effective and rapid method to evaluate the effectiveness of a given treatment with regards to potential neuronal differentiation *in vitro* is to quantitatively evaluate neurite outgrowth. Measuring neurite length, number of neurites and percentage of neurons with neurites, has been shown to be a good indicator of neuronal differentiation when combined with analyses such as flow cytometry, Western blotting and reverse transcription polymerase chain reaction (RT-PCR)[14]. However, it can be time consuming to quantify a large enough sample of neurons for the neurite outgrowth to be significant compared to other treatments.

There are also inherently high variances in neuronal measurements, as a neuron will be constantly extending and retracting neurites when probing or moving across a surface. Because of this, the sample number usually has to be of at least 100 cells per condition. This chapter describes the initial investigation of a high throughput method to accurately measure neuronal cells, which was accurate and easy to use. A high throughput epifluorescence microscope was utilised (Axon / Molecular Devices ImageXpress). Using the ImageXpress analysis software, over 2000 cells could then be identified, quantified, and the data exported into an Excel worksheet. The software has the capability to measure; 1) Maximum neurite length, 2) Number of neurites per neuron and 3) Percentage of neurons with neurites - the three common measurements that can indicate neuronal differentiation.

The initial experiment assessed which immunolabelling detection method was more suitable for analysis - β-tubulin III or F-actin (Figure 2). Using the ImageXpress

analysis software, differences between neuronal cells labelled for β-tubulin III versus F-actin were analysed, with regards to neuronal measurements. The NG108-15 neuronal cell line was chosen for experimentation, as they are well characterised[25, 31] and have been documented in many publications[17, 2]. It has been shown numerous times that results obtained with NG108-15 neuronal cells can be indicative of primary neuronal cell response under defined conditions[3].
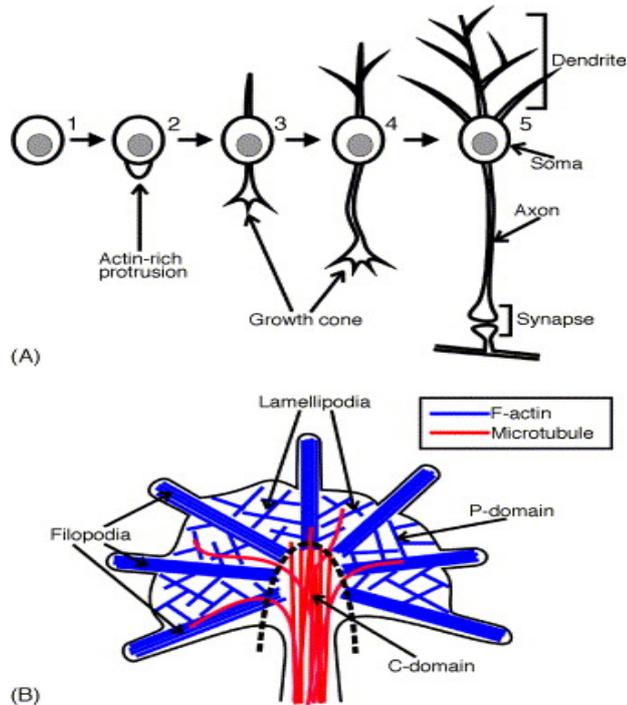

Figure 3.0: (A) Morphological changes throughout neuronal differentiation, where neuritogenesis (2) occurs at thin, actin-rich peripheral protrusions surrounding the soma. Neurite outgrowth, pathfinding, and targeting (3 and 4) are then driven by the growth cone. After reaching the correct target, the growth cone stops extending and forms a synapse with the post-synaptic cell (5). (B) Cytoskeletal structure of the leading edge of the growth cone. The structure can be divided into two cytoplasmic domains: the central domain (C-domain) contains microtubules, whilst the peripheral domain (P-domain) contains F-actin. The P-domain is composed of filopodia (bundles of longer F-actin) and lamellipodia (randomly oriented networks of shorter F-actin between the filopodia). Reproduced with permission[30].

After investigating the most accurate method of neurite outgrowth identification, investigation then moved onto the application of plasma polymerisation on neuronal cell biology. Using uncoated glass slides and laminin coated glass slides as controls, NG108-15 neuronal cells were cultured on acrylic acid (AAc) and maleic anhydride (MA), and conditions optimised. As the MA plasma polymer has not previously been investigated regarding neuronal cell culture extensively[22], results will be novel. The AAc plasma polymer was also chosen, as there are a number of published studies that demonstrate its efficacy of improving cell adhesion, migration and proliferation[6, 9, 8]. The experimental aim was to compare MA versus the control materials of glass and laminin as well as acrylic acid, to which published studies can be compared. Once optimal conditions were ascertained, such as serum containing versus non-serum containing medium, neuronal measurements were collected and analysed. Using MTS metabolic assays and neuronal measurements from immunolabelling, the neuronal cells were assessed to determine whether neuronal growth and neurite extension was maintained on laminin, glass and the plasma polymers. .

3.1.2 Materials and Methods

NG108-15 neuronal cell culture

A mouse neuroblastoma and rat glioma hybrid NG108-15 cell line (ECACC) was chosen for experimentation as it has been well characterised and displays a neuronal-like phenotype[31]. Cells were maintained in DMEM (Biosera) with 10% FCS, 100 U ml^{-1} penicillin / 100 μg ml^{-1} streptomycin and 2 mM glutamine (Sigma). Cells were seeded at 5×10^3 cells/well in a 24 well plate, and used between passages 11-21. Substrates used included MA 1 (on time of 80 μs and an off time of 800 μs, 5W peak power for 20 min), MA 2 (on time of 20 μs and off time of 1200 μs, 5W peak power for 20 min), MA 3 (1W continuous for 20 min) and AAc (15W continuous for 10 minutes). The cells were cultured for 72 hours on the substrates, and kept in culture medium for the first 48 hours. For the last 24 hours the medium was changed to 1:1 DMEM:Hams F12 (Biosera), with 1% (v/v) N$_2$ supplement (GIBCO, BRL, UK), 100 U/ml penicillin and 100 μg/ml streptomycin and 2 mM glutamine (Sigma). N$_2$ supplement contains 5 mg/l recombinant insulin, 10 mg/l human transferrin, 5.2 μg/l sodium selenite, 1.6 mg/l putrescine and 6.3 μg/l progesterone. As this protocol had been used previously [100], it was used in this study to compare neurite outgrowth of neurons on glass, laminin and the plasma polymers. Further studies then used serum free media to determine the effect of serum/non-serum conditions on the ability of neuronal cells to support and extend neurites on plasma polymerised surfaces.

NG108-15 neuronal cell culture under serum free conditions for plasma polymer investigation

NG108-15 neuronal cells were maintained in DMEM (Biosera) with 10% FCS, 100 U/ml penicillin and 100 μg/ml streptomycin and 2 mM glutamine (Sigma) and used between passages 11 and 21. Cells were seeded at 1×10^4 cells/well on each substrate in a 24 well plate. Substrates used included MA 1 (on-time of 80 μs and an off-time of 800 μs, 5W peak power for 20 minutes) and AAc (15W continuous power for 10 minutes). Cells were cultured on surfaces for 4 days under serum free conditions, DMEM (Biosera) with 100 U/ml penicillin and 100 μg/ml streptomycin and 2 mM glutamine (Sigma). As NG108-15 adhesion is low in serum free conditions, medium changes were warmed to 37°C before being conducted. PBS was also warmed to 37°C before being used to wash cells prior to fixation.

Immunocytochemistry for β-tubulin III labelling

NG108-15 neuronal cells were rinsed in warmed PBS, then fixed in 3.7% (v/v) formalin for 20 min. Cells were permeabilised with 1% (v/v) Triton X-100 for 5 min at 4°C, then carefully rinsed with PBS x3 for 10 min. Samples were blocked with 3% BSA (w/v) in PBS for 60 min then rinsed with PBS. A monoclonal IgG mouse species anti-β-tubulin III antibody (1:2000; Promega) in 1% BSA (w/v) was added and samples stored at 4°C overnight, and then rinsed with 3 x 5 min PBS. Texas-red conjugated secondary antibody (horse anti-mouse IgG, 1:100; Vector labs, UK) in 1% BSA (w/v) was added for 1 hour at room temperature, before 3x10 min wash. For the serum free experiments, NG108-15 neuronal cells were also stained with 300nM / 1:500 (w/v) 4',6-diamidino-2-phenylindole (DAPI) that labels the nuclei of fixed cells for 15 mins, then washed 3 x 3 min with PBS.

Immunocytochemistry for F-actin labelling

NG108-15 neuronal cells washed 3x5 min with PBS at 37°C were fixed for 20 min with 3.7% (v/v) formalin in PBS (37°C). After rinsing with PBS, 0.5 ml 1% Triton X-100 (v/v) in PBS was added for 5 min at 4°C to permeabilise the cells. After 3x5 min gentle PBS washes, 0.5 ml phalloidin–tetramethyl rhodamine isothiocyanate (TRITC) (1:5000, Sigma) was added to the cells for 30 min, then 3x5 min PBS washes were performed again.

Image Analysis

Fluorescently labelled samples were imaged using an epifluorescence microscope (ImageXpress, Molecular Devices, USA) at x20 magnification. Micrographs of the indirectly labelled Texas Red conjugated anti-β-tubulin III antigen were taken using λex = 595 nm / λem = 615 nm. Directly labelled F-actin (with phalloidin-TRITC) were visualised using λex = 557 nm / λem = 576 nm. Nuclei directly labelled with DAPI were imaged using λex = 350 nm / λem = 470 nm. 20 micrographs of each condition were taken and analysed for 3 different parameters using an existing script of the ImageXpress analysis software, which had been optimised previously[15]. By ensuring that there were labelled cells visible in every micrograph taken, this method enabled around 2000 cells to be measured per condition.
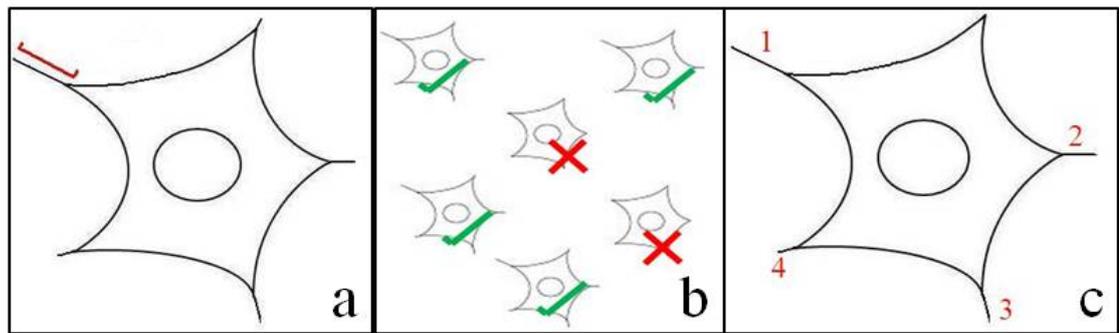
Figure 3.1: Diagram illustrating a) Maximum neurite length b) Percentage of neuronal cells with neurites and c) Number of neurites per neuron.

The reasoning behind the analysis of such a high number of cells was the high inherent variation of dynamic neurite outgrowths. The following three parameters for neuronal cells were measured (Figure 3.1): 1) Percentage of neurons with neurites, 2) The number of neurites per neuron and 3) Maximum neurite length per neuron. The last two conditions were restricted to cells that had neurites.

Statistical Analysis

Statistical analysis was performed using SigmaStat. Each experiment was carried out in triplicate, then repeated three times (N=3). Results show the mean ± SEM. Due to the inherently high variance of neuronal measurements, significant results were determined by performing t-tests for comparisons using the averages and standard deviation of the three repeats for β-tubulin III and F-actin results. One-way analysis of variance (ANOVA) statistical test was performed for experiments that had more than two conditions, again using the averages and standard deviation of the three repeats. If the differences in mean values among treatment groups were greater than would be expected by chance, Holm-Sidak post-hoc analysis versus the control group (glass) was used to determine if results were significant.

3.1.3: Results: β-tubulin III versus F-actin labelling of NG108-15 neuronal cells

Neuronal measurements of NG108-15 neuronal cells labelled with β-tubulin III and F-actin
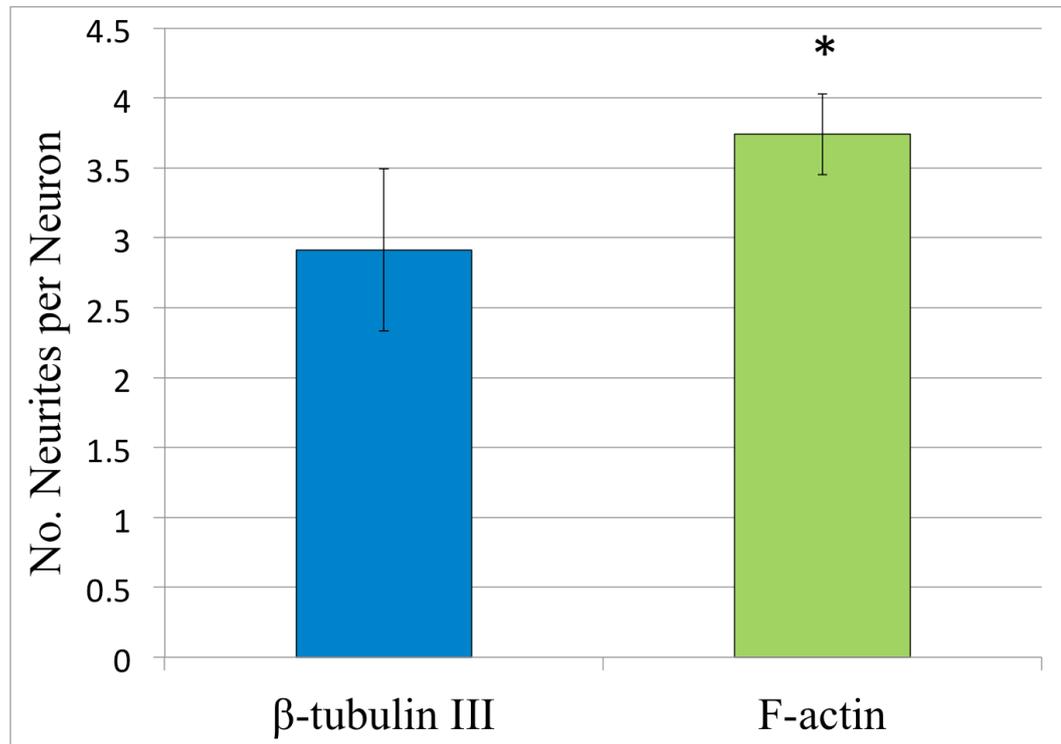
Figure 3.2: Comparison of F-actin and β-tubulin III labels on the effect of neurite outgrowth. 5 x 10^3 NG108-15 neuronal cells were seeded onto TCPS and cultured in serum conditions for 72 hours, then transferred to serum free conditions with supplements for 24 hours. Cells were fixed and labelled with β-tubulin III or F-actin, then analysed using ImageXpress analysis software for number of neurites each neuron sprouted. Data points show mean ± SEM (N=3); *p<0.05 compared to β-tubulin III (N=3).

Results from the neuronal quantification confirmed that the image analysis software was accurate at determining neuronal measurement as each outline was checked, then any erroneous results discarded. Results were not modified before exporting, only discarded if the outline was not accurate. Regarding neuronal measurements, whilst β-tubulin III labelled 2.9 neurites per neuron, F-actin labelling identified an average of 3.74 neurites. This was an interesting result, as F-actin labels all actin-based protrusions from the cell, including lamellipodia and fillipodia. As β-tubulin III will only label regions where polymerised tubulin is present, it would label fewer neurites per neuron compared to F-actin, due to the location of the tubulin filaments compared to F-actin[19]. There are potential discrepancies within the experiment, as the labelling procedures required a different number of washes. As β-tubulin III immunolabelled cells were washed more times compared to the F-actin labelled NG108-15 neuronal cells, the cellular attachment may have been adversely affected. This may lead to erroneous results from the β-tubulin III labelled cells, however this effect should be small due to the presence of serum

proteins. It has been shown that the presence of serum increases the attachment of NG108-15 neuronal cells[7]. Because of the stronger attachment of NG108-15 cells, fewer cells would have been washed off during the immunohistochemical procedure.
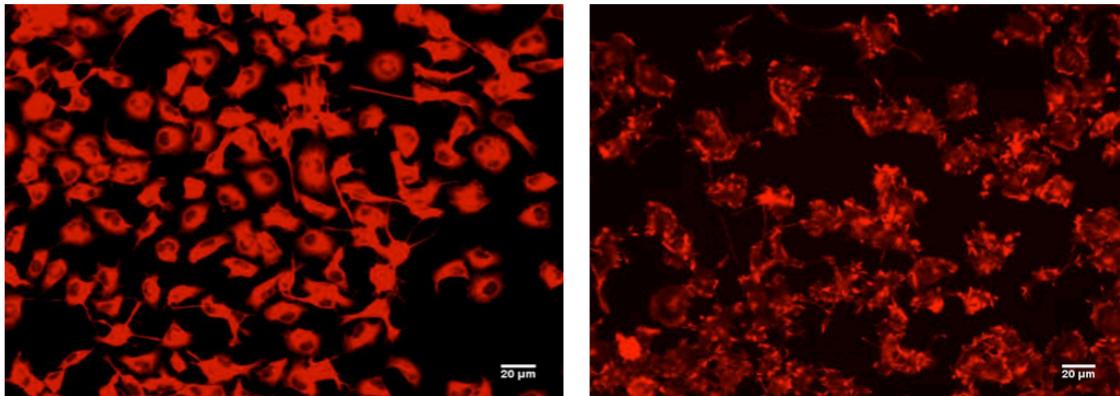

Figure 3.3: Micrographs of NG108-15 neuronal cells labelled with β-tubulin III (left) and F-actin (right). With the F-actin label, the ImageXpress analysis software could not outline the majority of cells when clustered as the cell borders were not as clearly defined as when labelling with β-tubulin III.

By monitoring the fixed cells under a light microscope during most of the labelling process, it would have been noted if there were a significant difference in cell numbers after certain washing stages. Careful washing also minimised cellular sloughing. This is a potential discrepancy for all neuronal measurement comparisons between β-tubulin III and F-actin, which could not be avoided.
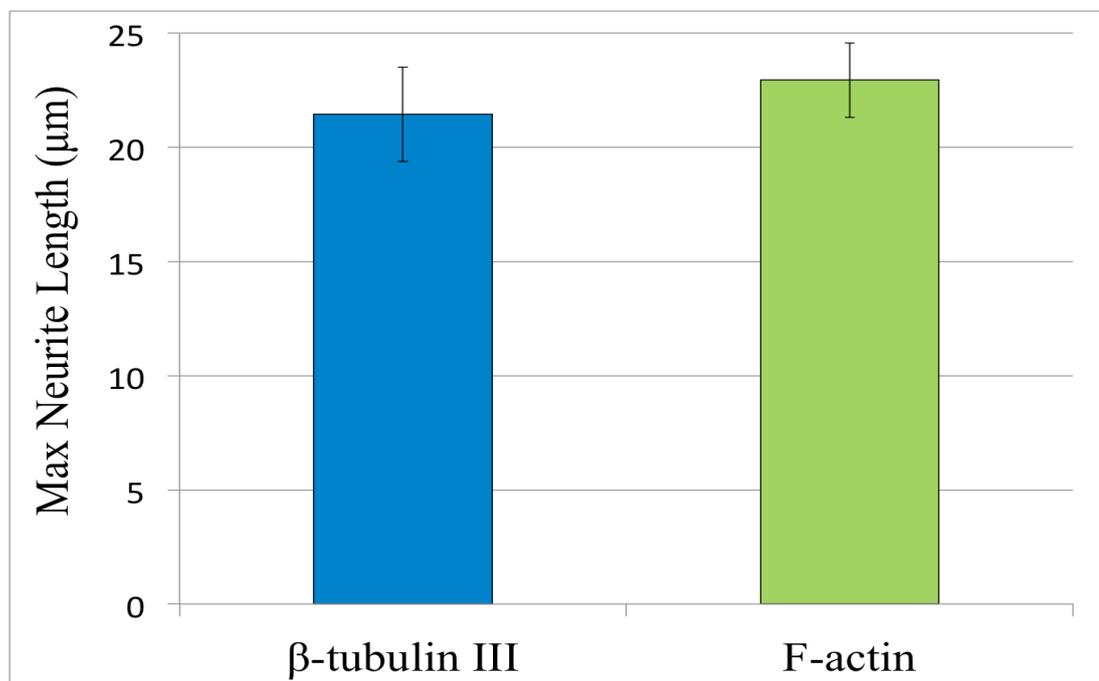
Figure 3.4: Comparison of F-actin and β-tubulin III labels on the effect of maximum neurite length. 5 x 10^3 NG108-15 neuronal cells were seeded onto TCPS and cultured in serum conditions for 72 hours, then transferred to serum free conditions with supplements for 24 hours. Cells were fixed and labelled with β-tubulin III or F-actin then analysed using ImageXpress analysis software for length of the longest neurite per neuron. Data points show mean ± SEM (N=3).

The micrographs shown in figure 3.3 corroborate the statistical findings. Although the cell borders are clear when labelled with β-tubulin III, cells labelled with F-actin demonstrate a higher number of neurites. Whilst there were low numbers of cells seeded at the beginning of the experiment so that cell clumping would be minimised, colonies of cells were still distinguishable when labelled with β-tubulin III. Colonies of cells labelled with F-actin were often not distinguished with the ImageXpress software. The shape of each NG108-15 neuronal cell was more angular when labelled with F-actin, with multiple protrusions from each cell. These multiple protrusions usually merged with any adjacent NG108-15 neuronal cell, which caused the ImageXpress analysis software to outline multiple NG108-15 cells as a single cell. These inaccurate outlines were then discarded. As there were also intensity differences of the fluorescence signal across each cell when labelled with F-actin and Phalloidin TRITC(See figure 3.3), this also hindered the ability of the analysis software to outline individual cells accurately.
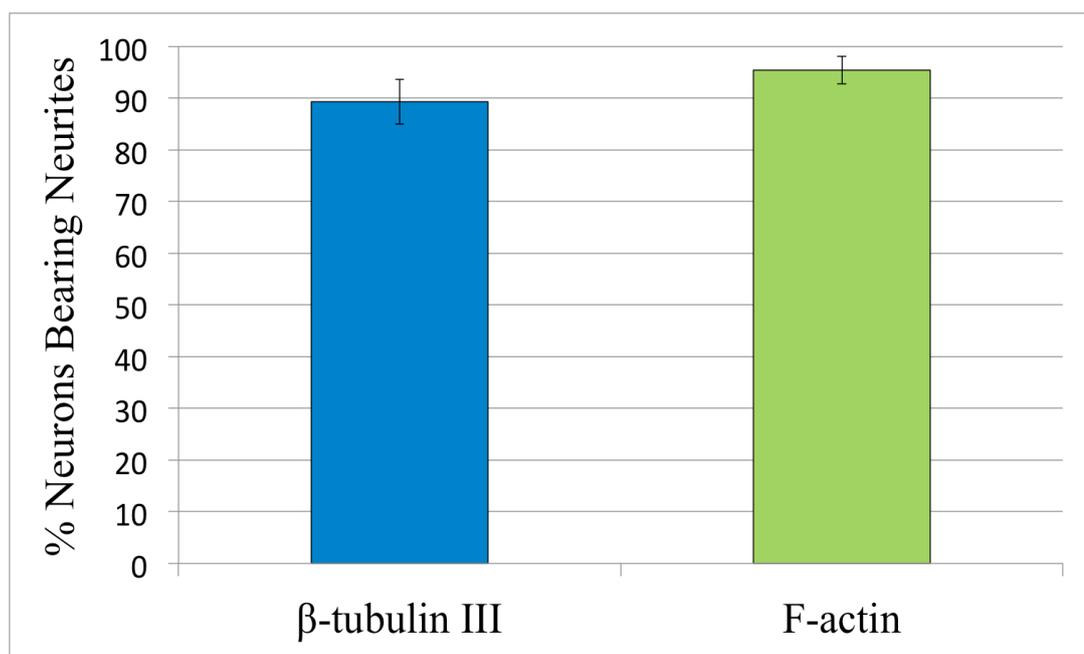
Figure 3.5: Comparison of F-actin and β-tubulin III labels on the percentage of neurons with sprouting neurites. 5 x 10^3 NG108-15 neuronal cells were seeded onto TCPS and cultured in serum conditions for 72 hours, then transferred to serum free conditions with supplements for 24 hours. Cells were fixed and labelled with β-tubulin III or F-actin. Data points show mean ± SEM (N=3).

Measurements of the maximum neurite length of each neuron using β-tubulin III gave shorter values of 21.44 μm compared to 22.94 μm with the F-actin label. As actin filaments extend to the edges of each cell in fillipodia[26], this agrees with existing published work. The results from figure 3.5 also corroborate with existing literature. The F-actin labelling highlighted 95.4% of the neurons with neurites, whilst 89.28%

neurons labelled with β-tubulin III had neurites. Again, as F-actin highlights all leading edges and protrusions of the cytoplasm, it can be postulated that more 'neurites' would have been detected[12].

It was observed, however, that while F-actin labelled all protrusions, β-tubulin III only labelled more established neurites, which were therefore mature enough to be pathfinding to other neurons. The ImageXpress software also detected far fewer neuronal cells when labelled with F-actin compared to β-tubulin III, which was a disadvantage. This was mainly due to the differences in fluorescence intensity across each cell, and the inability for the ImageXpress software to define the edges each cell when labelled with F-actin. Additionally, if investigations moved onto mixed cell cultures containing neuronal and non-neuronal cells, β-tubulin III labelling could also be used in order to distinguish between neuronal and glial cell types. Thus, from the results gathered, it was determined that β-tubulin III was the most appropriate label.

3.1.4 Results: NG108-15 neuronal cells on plasma polymers

NG108-15 neuronal cells on maleic anhydride surfaces coated with different conditions
Whilst acrylic acid has previously been investigated and has demonstrated positive results with neuronal cell types[23, 6] there is no published work of plasma polymerised maleic anhydride (MA) as a substrate for cell culture previously. In order to optimise the conditions of MA for NG108-15 neuronal cells, biological investigation into plasma polymerised surfaces were started by culturing NG108-15 neuronal cells on different conditions of MA. Cleaned glass slides were plasma polymerised for 20 minutes using different conditions; MA 1(80 μs on, 800 μs off), MA 2 (20 μs on, 1200 μs off) and MA 3 (1W continuous).

NG108-15 neuronal cells were cultured on the coated slides for 72 hours under serum conditions, then for a further 24 hours with serum free medium and N2 supplement. Serum conditions were used for 72 hours following an approach described by Buttuglione et al[6], who found that NG108-15 neuronal cells when cultured under serum containing medium on acrylic acid plasma polymerised surfaces increased levels of Neurofilament 200 (which plays an active part in neuronal differentiation). However, it has also been established that serum free medium with N2 supplement can act as a differentiation stimulus for NG108-15 neuronal cells[18]. Serum free medium was therefore used for the last 24 hours alongside N2 supplement. Controls of TCPS, glass and laminin were also used. β tubulin III labelling of the NG108-15 neuronal cells was then analysed using ImageXpress analysis software, which compared the effect of the

surfaces on maximum neurite length, percentage of cells with neurites and number of neurites per cell. MTS metabolic rate assays were also used to check that the NG108-15 neuronal cells were metabolically active throughout the experiment, and to assess which conditions stimulated the highest metabolic rate. Immuno-micrographs were also used to ascertain the phenotype of NG108-15 neuronal cells.
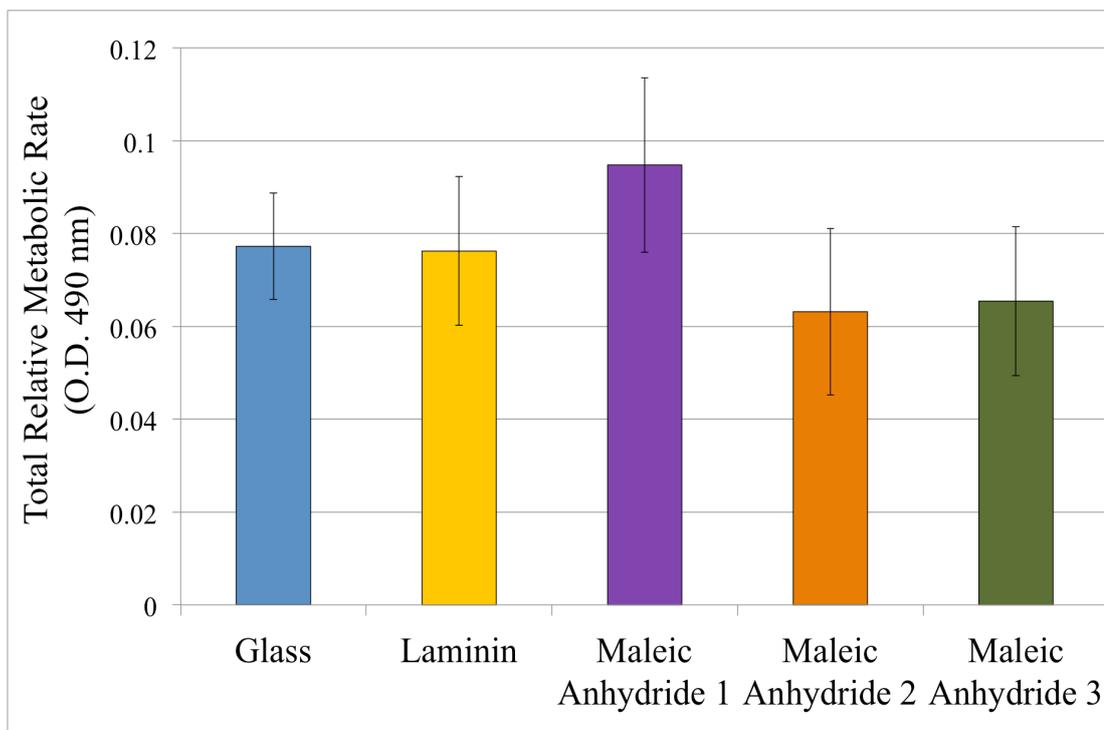

Figure 3.6: Comparison of different surfaces on the cell relative metabolic rate of NG108-15 neuronal cells. Maleic anhydride (MA) conditions: MA 1 = 80 μs on, 800 μs off, 5W power. MA 2 = 20 μs on, 1200 μs off, 5W power. MA 3 = 1W cont. 5 x 10^3 NG108-15 neuronal cells were seeded onto 13 mm^2 coated and uncoated glass slides then cultured for 72 hours. Cells were immersed in MTS solution for 2 hr, then colour change was read. Tissue culture plastic has been omitted due to the difference in area and therefore number of cells. Data points show mean ± SEM (N=3).

Results from the metabolic rate assay (Figure 3.6) with different conditions of maleic anhydride demonstrated that NG108-15 neuronal cells on MA 1 demonstrated the highest reading of 0.095. Neuronal cells on glass and laminin showed very similar relative metabolic rates of 0.077 and 0.076 respectively, whilst the MTS metabolic rate assay demonstrated that neuronal cells on MA 2 and MA 3 had lowest relative metabolic rate of 0.063 and 0.065 respectively. Neuronal cells on MA 3 also had the highest relative amount of anhydride groups as shown by ToF-SIMS. Whilst MA1 had similar levels of the monomer maleic anhydride, MA2 had lower levels of the retained monomer. It therefore does not seem that there is a correlation between anhydride density and metabolic rate of NG108-15 neuronal cells. An increase in anhydride groups would have led to a decrease in the local pH environment, which may have resulted in
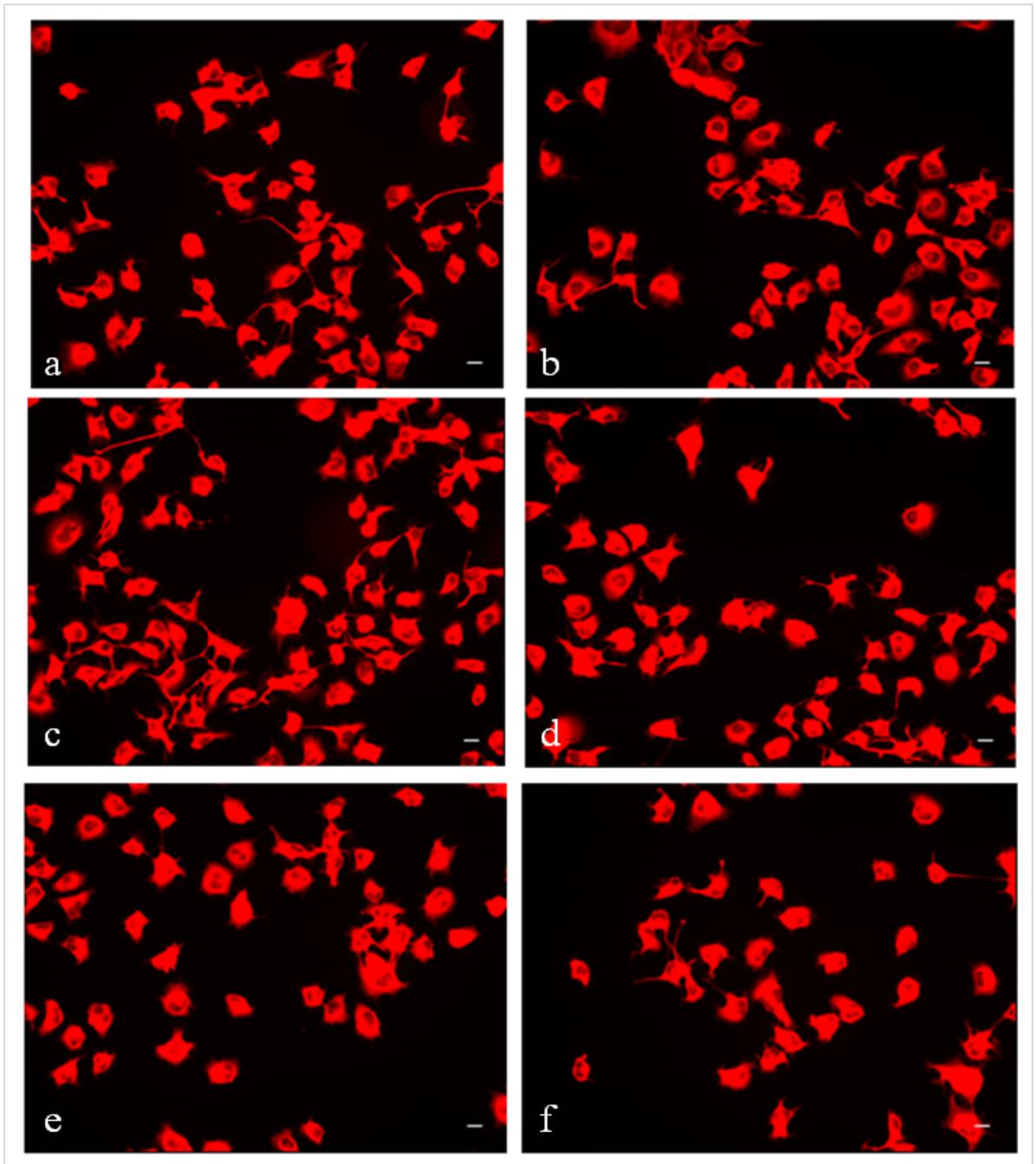
Figure 3.7: Micrographs of β-tubulin III labelled NG108-15 neuronal cells, which were then outlined by the ImageXpress software to obtain neuronal measurements. a) TCPS b) Glass c) Laminin d) Maleic anhydride 1 (80 μs on, 800 μs off, 5W power.) e) Maleic anhydride 2 (20 μs on, 1200 μs off, 5W power.) f) Maleic anhydride 3 (1W continuous power). Scale bar shows 20 μm.

an increase of cellular stress in the NG108-15 neuronal cells. This would have then given a misleadingly higher metabolic rate reading, as high stress levels result in a higher rate of metabolic activity[24]. However, as it has been established that bovine serum albumin (BSA) covalently binds with anhydride groups through a reaction of the amine groups on lysine residues[21], the hydrolysis of the anhydride groups leading to a lowered pH may not have occurred substantially.

The micrographs shown in figure 3.7 agree with the quantitative results, that there were neurons with more neurites on TCPS, laminin and MA 1 compared to other

surfaces. There are also more NG108-15 neuronal cells on laminin and fewer on MA 2 and MA 3, which agree with the metabolic rate results. The micrographs show strong and well defined microfilament labelling, indicating good adhesion to the surfaces. The micrographs indicate that the cells weren't stressed, as the morphological characteristics show a good neuronal phenotype with neurite projections. A live/dead assay with propidium iodide and SYTO 9 or analysis into the levels of NF-κB between surfaces would have been advantageous to determine the percentages of cells alive/dead and relative stress of the cells, however time constraints restricted this.

There was little difference between the percentages of neurons with neurites (figure 3.8) apart from neuronal cells cultured on MA 3, which had the lowest percentage of neurons with neurites (86.7%). However, it also had the highest standard errors. As there were values close to being outliers, the results should be interpreted with caution. ImageXpress analysis software showed that 96.8% neurons on maleic anhydride 1 had one or more neurites, whilst the percentage of neuronal cells with neurites on laminin, TCPS and glass was 96.3%, 96.4%, and 95.8% respectively. Immunolabelling highlighted 93.9% neurons with neurites on MA 2, lower than all other samples apart from MA 3.
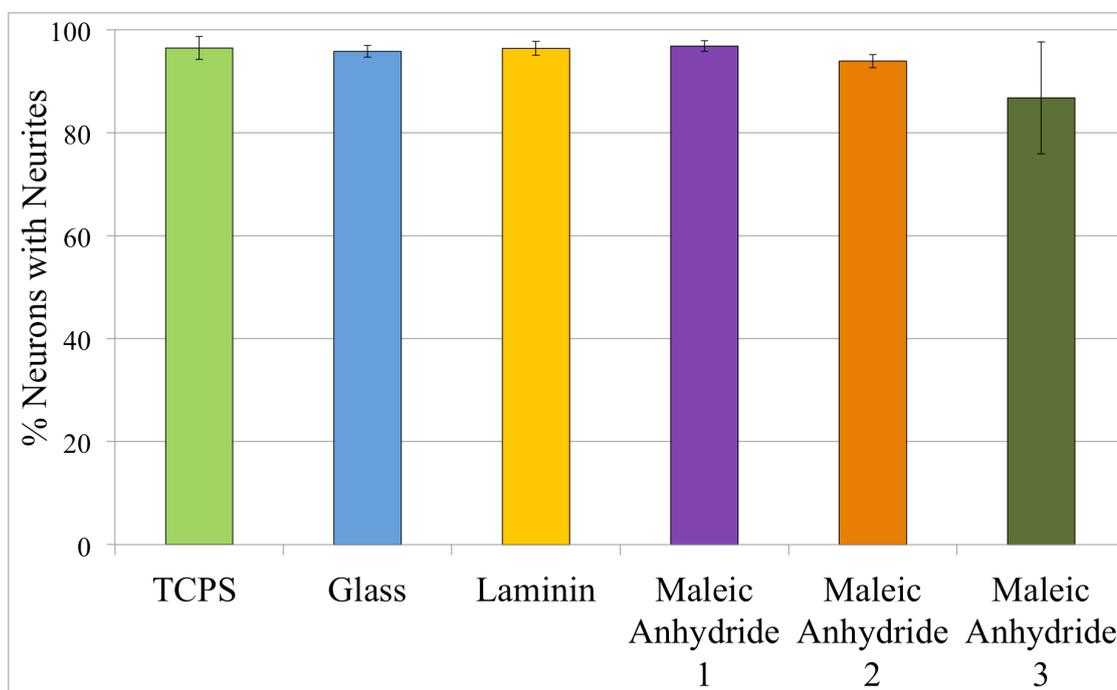

Figure 3.8: Comparison of percentage of neurons that had neurites, TCPS = tissue cultured polystyrene. Maleic anhydride (MA) conditions: MA 1 = 80 μs on, 800 μs off, 5W power. MA 2 = 20 μs on, 1200 μs off, 5W power. MA 3 = 1W cont. 5 x 10^3 NG108-15 neuronal cells were seeded onto coated/uncoated 13mm^2 glass slides and cultured for 72 hours. Cells were fixed and labelled with β-tubulin III and analysed using ImageXpress analysis software for whether or not each neuron had a neurite. Data points show mean ± SEM (N=3).

As there is no existing literature on metabolic rate measurements on maleic anhydride it is not possible to compare and contrast results form published work. However, the metabolic rate and percentage of neurons with neurites show that MA 1 supported more cells, as well as more neurons with neurites.

Regarding the number of neurites each neuronal cell had, MA 1 supported neuronal cells with the highest average number of neurites (3.9). This was significantly higher than neuronal cells on glass, which had an average of 3.5. MA 3 and TCPS also supported significantly higher numbers of neurites per neuron, 3.8 and 3.9 respectively. There was an average of 3.6 neurites per neuron on the laminin surface, whilst neuronal cells on glass and MA 2 had an average of 3.5 and 3.5 neurites respectively. It has been previously shown that laminin stimulates neurite outgrowth and an increase in neurite length through the heparin binding domain[10]. It is therefore intriguing that laminin would stimulate fewer neurites per neuron compared to TCPS and maleic anhydride.
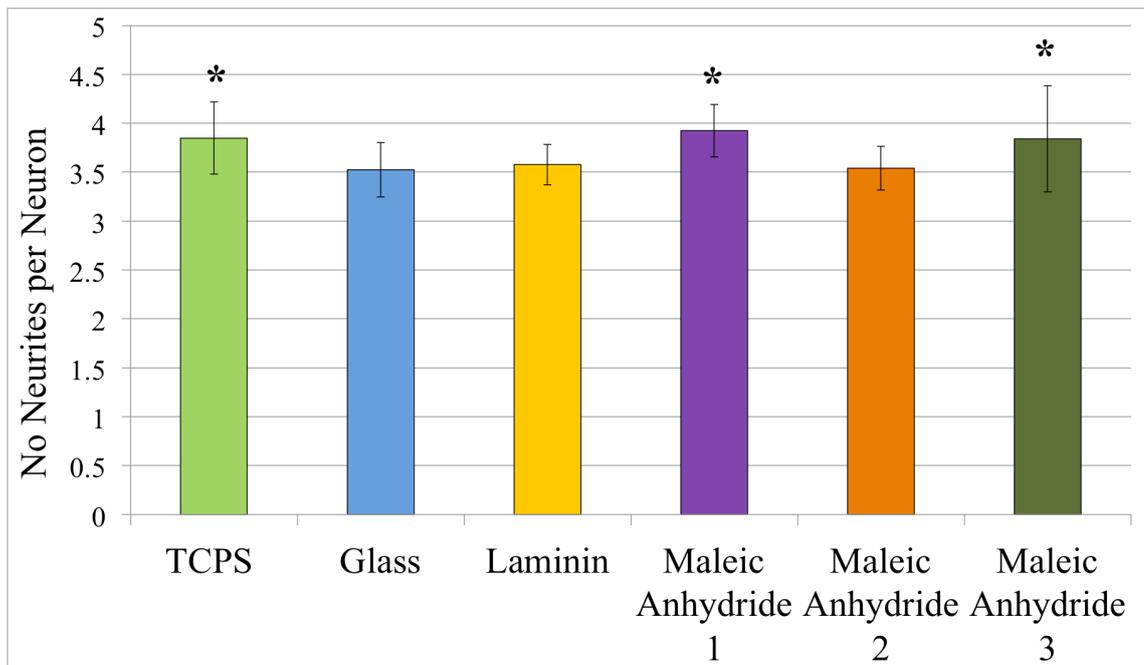

Figure 3.9: Comparison of different surfaces on the number of neurites per neuron. a) TCPS b) Glass c) Laminin d) Maleic anhydride 1 (80 μs on, 800 μs off, 5W power.) e) Maleic anhydride 2 (20 μs on, 1200 μs off, 5W power.) f) Maleic anhydride 3 (1W continuous power). 5 x 10^3 NG108-15 neuronal cells were seeded onto coated/uncoated 13mm^2 glass slides and cultured for 72 hours. Cells were fixed and labelled with β-tubulin III and analysed using ImageXpress analysis software for the length of the longest neurite per neuron. Data points show mean ± SEM (N=3); *p<0.001 compared to glass control.

Laminin supported neurons with the longest neurite length of 29.55 μm, which was in agreement with Edgar et al[10]. The average maximum neurite length of neuronal cells was 27.4 μm on MA 3, and 27.1 μm on MA 1. MA 2 also supported very similar maximum neurite lengths of 26.9 μm, whilst neurons on TPCS demonstrated an average 25.2 μm maximum neurite length and neuronal cells on glass 23.0 μm. This

corresponds well with previous published results, that laminin stimulates significantly longer neurite lengths compared to glass. Whilst there are no previous results to compare the maleic anhydride conditions to, these results are not entirely different from those shown in figures 3.7 and 3.9.

Overall, MA 1 demonstrated very promising results across all the neuronal measurements and metabolic rate assays, even compared to laminin. The higher values compared to laminin in the relative metabolic rate assay showed a surface that promoted cell adhesion and proliferation, as well as neurite outgrowth and extension. These results were then confirmed by the micrographs in figure 3.7. MA 2 did not seem to be a surface that warranted further investigation. Although neuronal cells on MA3 showed comparatively low results in metabolic rate assays, there were good results regarding the number of neurites per neuron and maximum neurite length on MA 3.
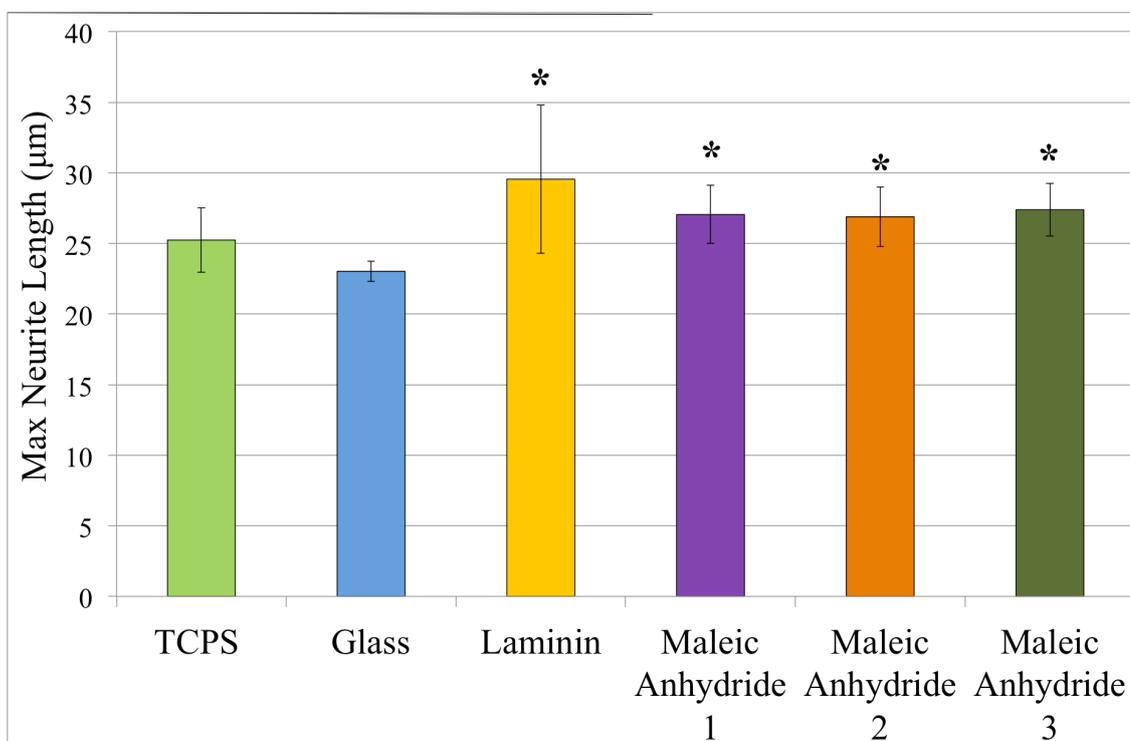

Figure 3.10: Comparison of different surfaces on the maximum neurite length, a) TCPS b) Glass c) Laminin d) Maleic anhydride 1 (80 μs on, 800 μs off, 5W power.) e) Maleic anhydride 2 (20 μs on, 1200 μs off, 5W power.) f) Maleic anhydride 3 (1W continuous power). 5×10^3 NG108-15 neuronal cells were seeded onto coated/uncoated 13mm^2 glass slides and cultured for 72 hours. Cells were fixed and labelled with β-tubulin III and analysed using ImageXpress analysis software for the length of the longest neurite per neuron. Data points show mean ± SEM (N=3); *p<0.001 compared to glass control.

NG108-15 neuronal cells grown on acrylic acid and maleic anhydride surfaces

After optimising conditions for maleic anhydride deposition and NG108-15 neuronal cell culture, MA 1 was then compared against plasma-polymerised acrylic acid (AAc), of which there has been previously published work[6, 9]. NG108-15 neuronal cells were

cultured on glass, laminin, AAc and maleic anhydride surfaces for 72 hours in serum containing medium, then for another 24 hours in supplemented serum free medium. MTS metabolic rate assay was then utilised, as well as immunolabelling for β tubulin III. The morphology of neuronal cells was quantified using ImageXpress image analysis software, which outlined the cells and ranked them in terms of maximum neurite length, number of neurites per neuron and percentage of neurons with neurites. Although TCPS could be analysed for neuronal measurements, the difference in surface area between the TCPS well and 13 mm^2 glass slides meant that comparisons with TCPS and the other surfaces using MTS metabolic rate assay could not be performed.
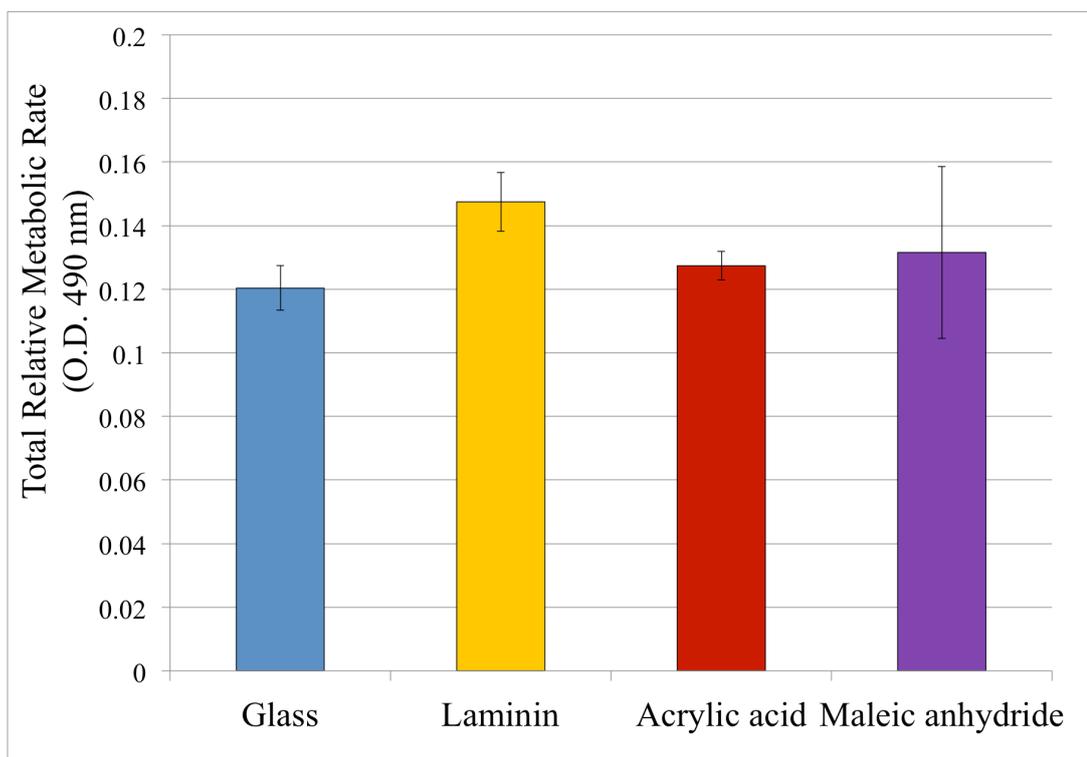

Figure 3.11: Comparison of different surfaces on the cell metabolic rate of NG108-15 neuronal cells. 5 x 10^3 NG108-15 neuronal cells were seeded onto 13 mm^2 coated and uncoated glass slides then cultured in serum conditions for 72 hours, then transferred to serum free conditions with supplements for 24 hours. Cells were immersed in MTS solution for 2 hours, then the colour change was read. Tissue culture plastic was omitted due to the difference in area and therefore number of cells. Data points show mean ± SEM (N=3).

There were no significant differences between the surfaces in the MTS metabolic rate assay, although neuronal cells on laminin showed the highest reading of 0.148 optical density/absorbance. Laminin is found in the extracellular matrix of cells as well as in the bands of Büngner, and has been shown to enhance neurite outgrowth and Schwann or neuronal cell proliferation[3]. The NG108-15 neuronal cells on the AAc and MA 1 surfaces had very similar metabolic rates of 0.127 and 0.13 respectively, whilst neuronal cells on the glass surface resulted in the lowest metabolic rate of 0.12.

As glass had no functional groups that could interact with cellular integrins compared to AAc and maleic anhydride, this may have been a negative characteristic with regards to protein orientation and attachment that may have led to reduced cell adhesion.
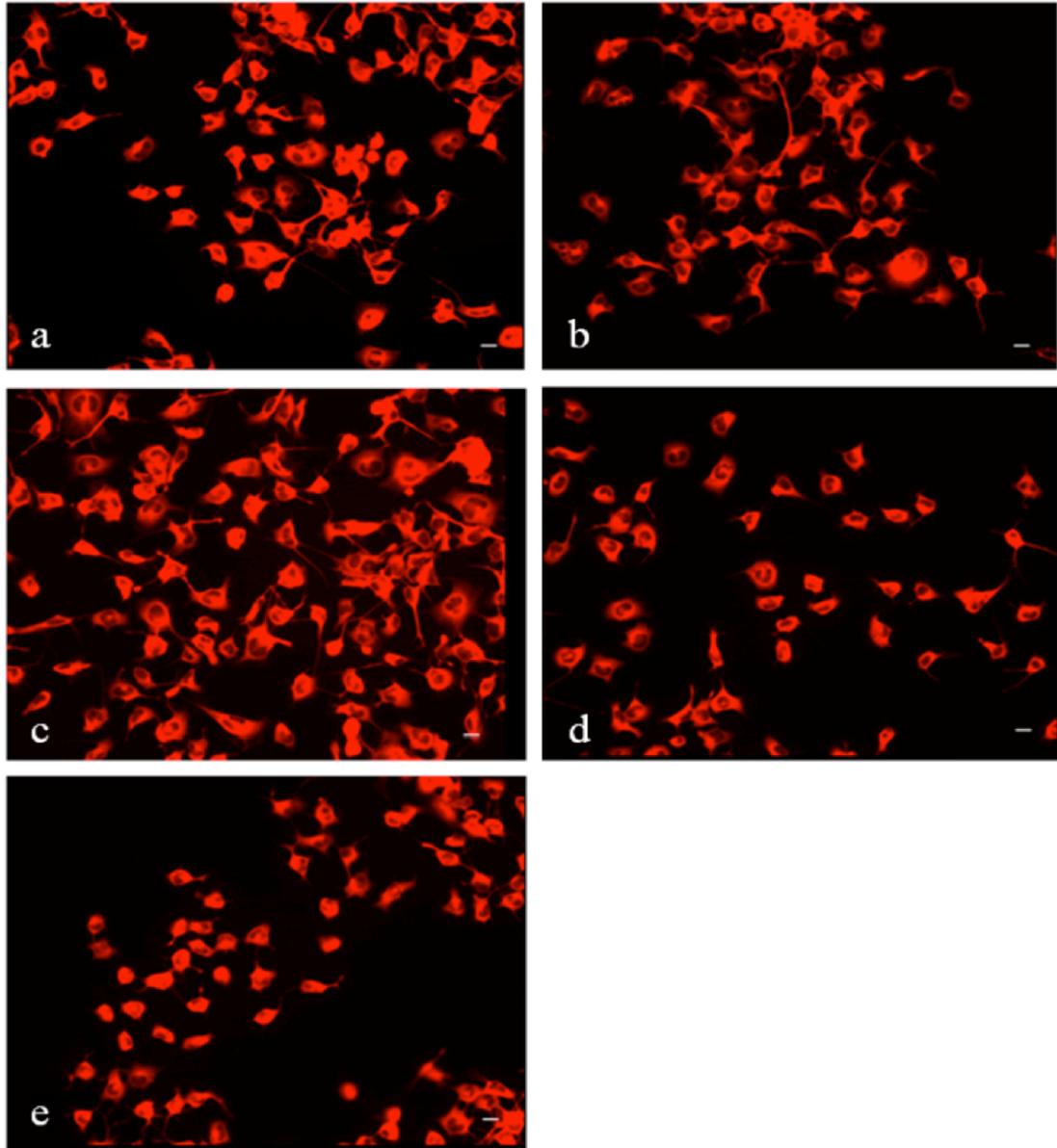

Figure 3.12: Micrographs of β-tubulin III labelled NG108-15 neuronal cells, cultured in serum conditions for 72 hours then in supplemented serum free conditions for a further 24 hours. a) TCPS b) Glass c) Laminin d) AAc and d) Maleic anhydride. Scale bar shows 20 μm.

The micrographs in figure 3.12 show strong labelling of β-tubulin III, whilst the cellular phenotype demonstrated neurite outgrowth and good adhesion to the surfaces. The higher number of cells on laminin agrees with the metabolic rate readings from figure 3.6. Overall, the micrographs show established NG108-15 neuronal cells whose phenotypes are comparable to micrographs from the ECACC website, from where the cells were purchased[1] and other studies [22].

Similar results were observed between groups on the percentage of neurons that had one or more neurites. Neuronal cells on TCPS had the highest percentage of cells with neurites at 94.7%. As TCPS is plasma treated polystyrene, it is more hydrophilic compared to glass and therefore would be expected to result in more neurons with
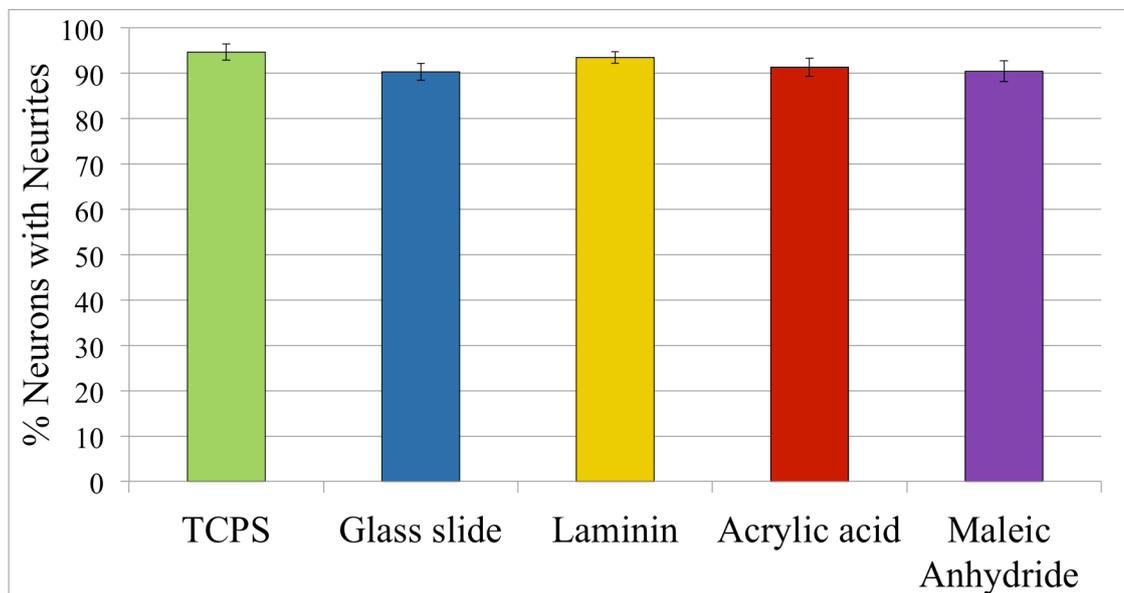

Figure 3.13: Comparison of percentage of neurons that had neurites. 5 x 10^3 NG108-15 neuronal cells were seeded onto coated/uncoated 13mm^2 glass slides, cultured in serum conditions for 72 hours, then transferred to serum free conditions with supplements for 24 hours. TCPS = tissue cultured polystyrene. Cells were fixed and labelled with β-tubulin III. Data points show mean±SEM between experiments.

neurites. Laminin coating resulted in 93.5% neurons with neurites, whilst 91.4% neurons on AAc sprouted neurites. NG108-15 neuronal cells on glass and MA 1 had very similar results of 90.3% and 90.5% with neurites respectively.

Regarding number of neurites per neuron, neuronal cells on TCPS showed the highest number again, at 3.25. NG108-15 neuronal cells on laminin again had the second highest result, with an average of 2.93 neurites per neuron. There were 2.91 neurites per neuron on AAc, whilst MA 1 and glass both supported 2.85 neurites per neuron. Again, as MA 1 coated the glass with a hydrophilic surface as shown by the contact angle results compared to the native surface of glass, it was interesting to observe such similar results.

Regarding the mean data for maximum neurite length, NG108-15 neuronal cells on AAc had the longest neurites (26.6 μm), significantly longer than the neurites formed on glass (24.25 μm). The maximum neurite length of NG108-15 neuronal cells on laminin and TCPS were also significantly longer than glass, at 25.81 μm and 25.99 μm respectively. MA 1 supported NG108-15 neuronal cells that had a maximum neurite length of 24.84 μm.

It could be that soluble factors contained in the medium had a dominant effect on the neuronal cells over the surface, as proposed by Buttiglione. The medium consisted of 10% DMEM for the first 48 hours, followed by differentiation medium that contained DMEM and Hams F12 in a 1:1 ratio and N_2 supplement. The effect of the N_2 supplement in addition to the adsorption of proteins from FCS in the first 48 hours could have caused certain adhesion proteins such as vitronectin to assume a particular conformation on AAc. As maleic anhydride has not been previously investigated for biological purposes, it is possible that maleic anhydride may have a different effect on neuronal measurements under different culture conditions, such as serum free.
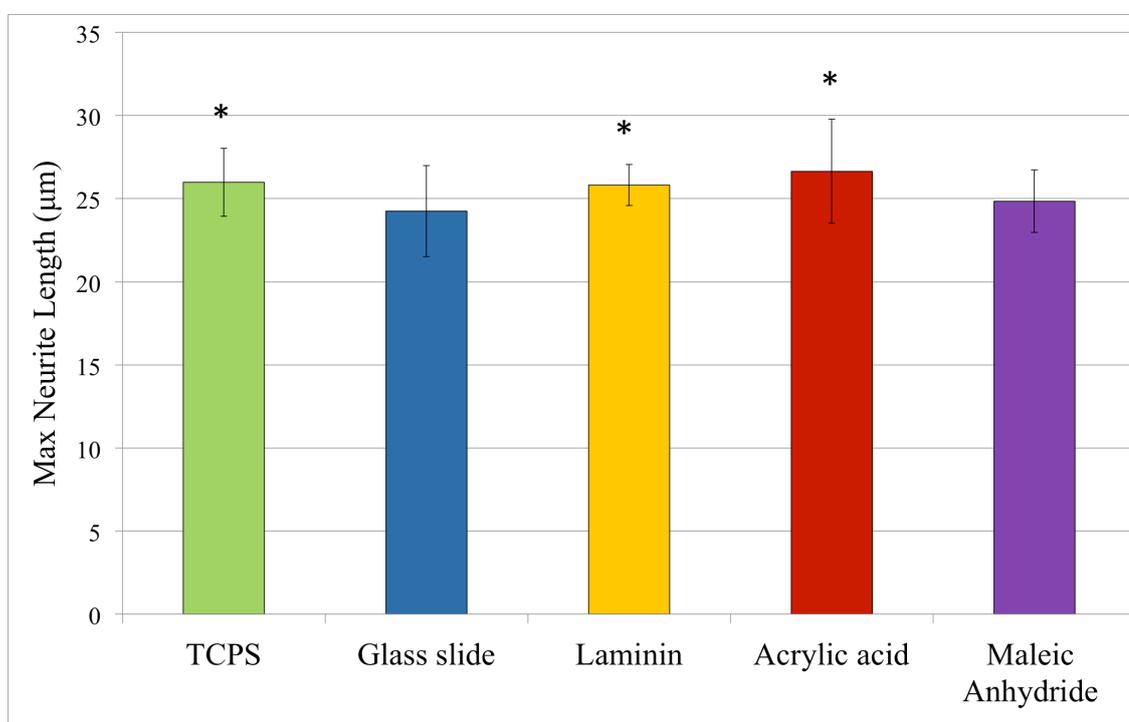

Figure 3.14: Comparison of different surfaces on the average maximum neurite length. 5 x 10^3 NG108-15 neuronal cells were seeded onto coated/uncoated 13mm^2 glass slides, cultured in serum conditions for 72 hours, then transferred to serum free conditions with supplements for 24 hours. Cells were fixed and labelled with β-tubulin III and analysed using ImageXpress analysis software. Data points show mean ± SEM (N=3); *p<0.001 compared to glass control.
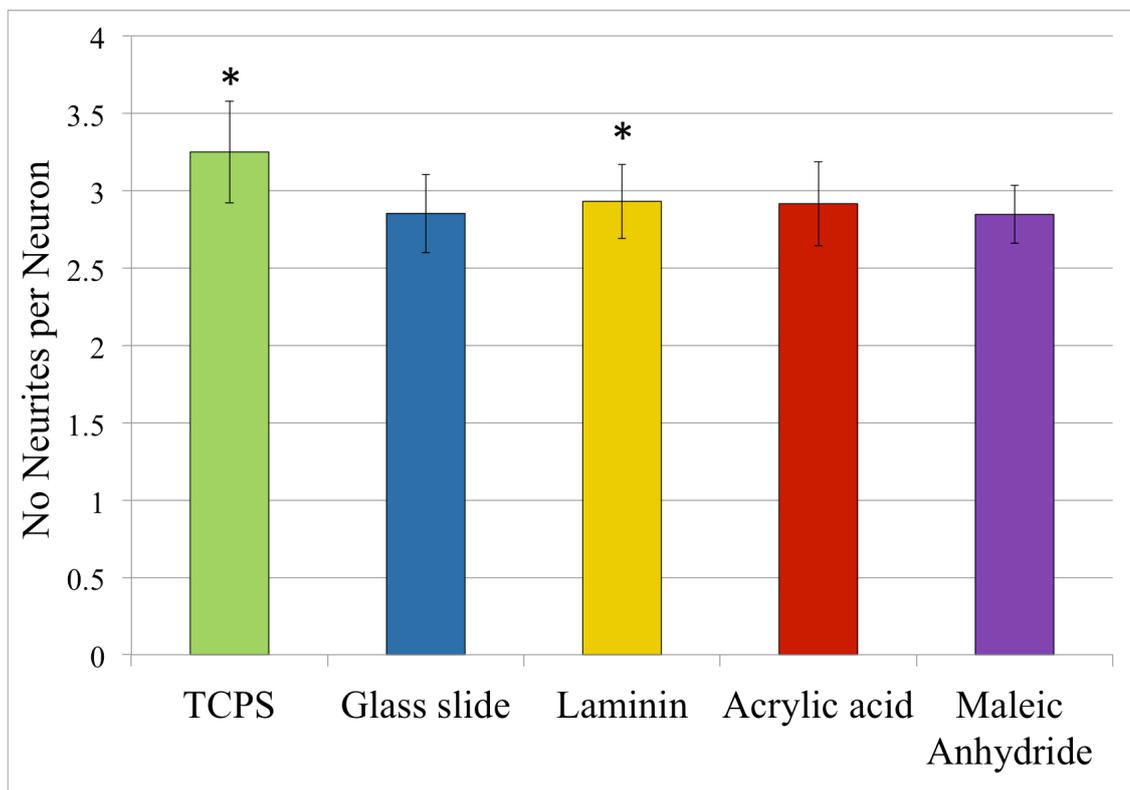
Figure 3.15: Comparison of different surfaces on the number of neurites per neuron. 5 x 10³ NG108-15 neuronal cells were seeded onto coated/uncoated 13mm² glass slides, cultured in serum conditions for 72 hours, then transferred to serum free conditions with supplements for 24 hours. Cells were fixed and labelled with β-tubulin III and analysed using ImageXpress analysis software. Data points show mean ± SEM (N=3); *p<0.001 compared to glass control.

NG108-15 neuronal cells on acrylic acid and maleic anhydride 1 surfaces in the absence of serum

Whilst the results obtained with the plasma polymers under serum containing conditions were comparable to laminin, the results compared to glass were not very dissimilar either. It was considered that the foetal calf serum proteins might have assumed similar conformations on the plasma polymerised and glass surfaces. The main components of serum are lipids and proteins, most of which are albumin and globulins. It has been reported that the amine groups on lysine residues in BSA covalently bind with anhydride groups[21], which may have affected the adhesion and proliferation of NG108-15 neuronal cells. In order to characterise MA 1 further, it was decided to repeat the experiment under serum free conditions. The comparison would be useful to discover if the serum proteins were having a significant effect on the plasma polymerised surfaces. The results showed that the presence of serum proteins indeed had an effect on the plasma polymerised surfaces. It has been shown previously that serum free medium can be used as a differentiation stimulus, along with supplements such as N2[31]. 1 x 10⁴ NG108-15 neuronal cells were cultured on TCPS, glass, laminin, AAc and MA 1 for 4 days in serum free medium. After the culture, cells were

fixed and labelled with β-tubulin III and DAPI, then micrographs quantified using the ImageXpress analysis software. MTS assays were also used to characterise the relative metabolic rate of NG108-15 neuronal cells on the different surfaces, and compare with the phenotypic data retrieved from the immunolabelled cells. For these experiments, random fields of view were taken so that total cell number could be quantified using DAPI nuclear stain and β-tubulin III identification.
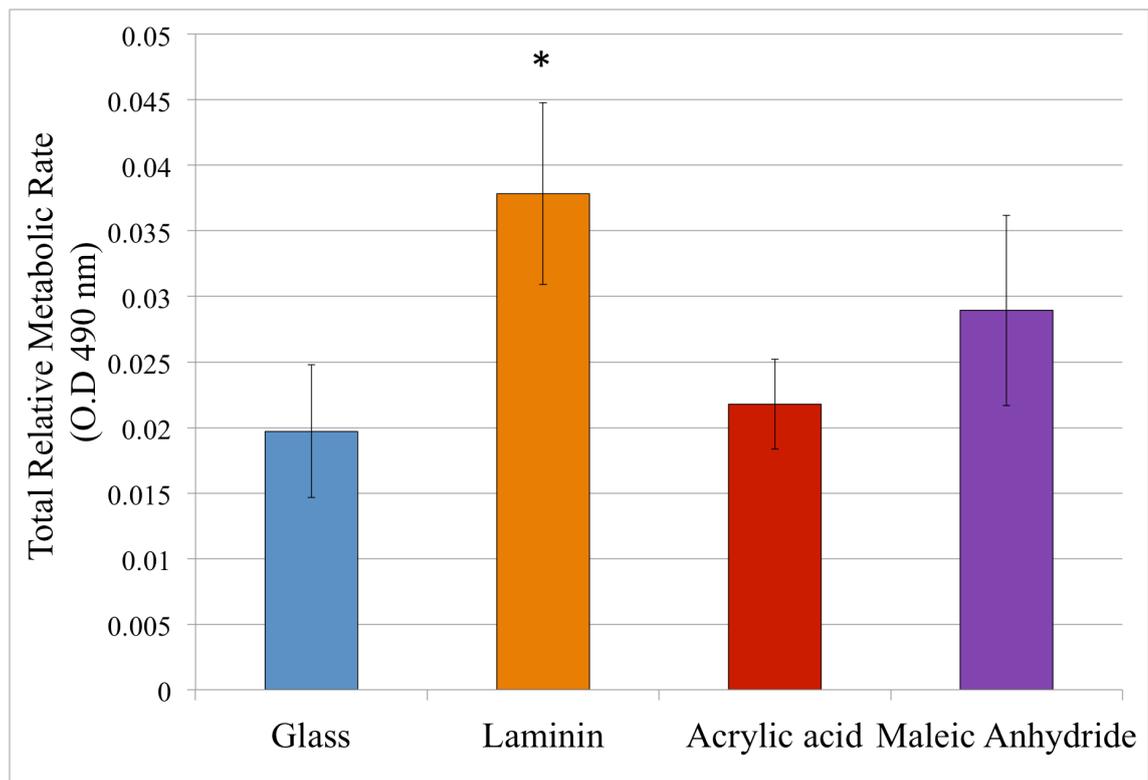

Figure 3.16: Comparison of different surfaces on the metabolic rate of NG108-15 neuronal cells. 1 x 10^4 NG108-15 neuronal cells were seeded onto coated/uncoated 13mm^2 glass slides, then cultured in serum free conditions for 96 hours. Cells were fixed and labelled with β-tubulin III and analysed using ImageXpress analysis software. Data points show mean ± SEM (N=3); *p<0.05 compared to glass control.

The metabolic rate results demonstrated that laminin supported NG108-15 neuronal cells with the highest metabolic rate at 0.038, significantly higher compared to neuronal cells on glass. Although the metabolic rate values of the NG108-15 in serum free conditions were quite low, the averages from N=3 were in good agreement. This indicated that the differences in metabolic rate were due to the surfaces, rather than errors of the MTS metabolic rate assay method or plate reader-reading values. The higher metabolic rate results from cells on laminin were in agreement with previous studies[3] as the positive control within the group, as was the lowest metabolic rate value of 0.02 from the base control glass. NG108-15 neuronal cells on AAc surfaces demonstrated a metabolic rate of 0.022, whilst the metabolic rate result from NG108-15

cells on MA 1 was 0.029. This result from neuronal cells on MA 1 further corroborates previous results from the experiment that contained serum and different maleic anhydride conditions (Figure 3.6).
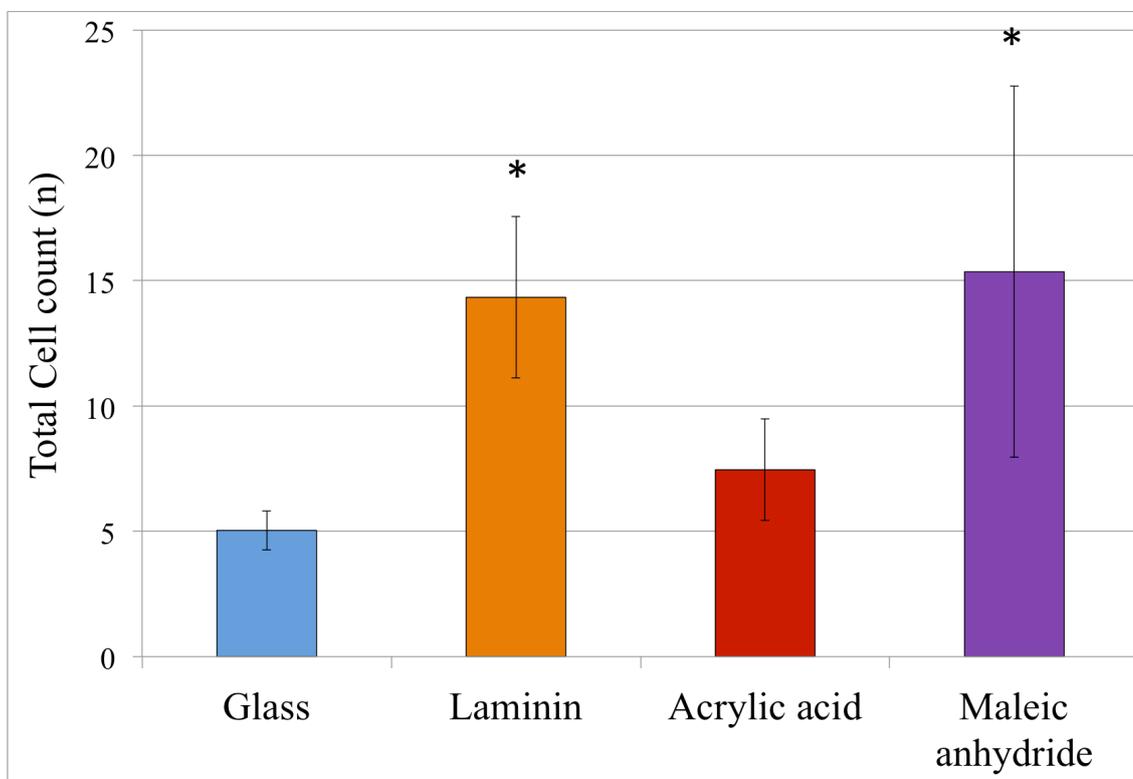

Figure 3.17: Comparison of different surfaces on the average cell count per field of view of NG108-15 neuronal cells. 1 x 10^4 NG108-15 neuronal cells were seeded onto coated/uncoated 13mm^2 glass slides, then cultured in serum free conditions for 96 hours. Cells were fixed and labelled with β-tubulin III and DAPI, then cells co-labelled with DAPI and β-tubulin III were counted. Image J program was used for data analysis. Data points show mean ± SEM (N=3); *p<0.001 compared to glass control.

The results from the total cell count again agree with the MTS metabolic rate assay (Figure 3.17), in that glass supports fewer cells compared to the plasma polymers or laminin. This has been shown repeatedly through metabolic rate and total cell counts, and in two different types of medium. MA 1 supported on average 15.4 cells / field of view, whilst laminin supported very similar numbers of cells, 14.3. Both were significantly higher compared to glass. There were an average of 7.45 cells / field of view on AAc, whilst the uncoated glass control only had 5 cells / field of view.

Looking at the results from maximum neurite length (figure 3.18), the results are very different compared to serum containing conditions (figure 3.9), which was reported by Buttiglione et al.[6] The neuronal cells responded to the MA 1 substrate, demonstrating significantly longer neurites compared to glass with an average maximum neurite length of 69 μm. The maximum neurite length of cells on maleic anhydride was 21 μm longer than glass, on which cells had maximum neurite length of

48.44 μm. NG108-15 neuronal cells on laminin also had longer maximum neurite lengths compared to those on glass, at 49.95 μm. The maximum neurite length of neuronal cells on AAc plasma polymerised surface was 43.7 μm, shorter than both glass and laminin. NG108-15 neuronal cells on TCPS had a maximum neurite length of 39.88 μm, the shortest neurites. This is a very different result compared to the serum conditions, where the neuronal cells on TCPS had significantly longer neurite lengths compared to glass.
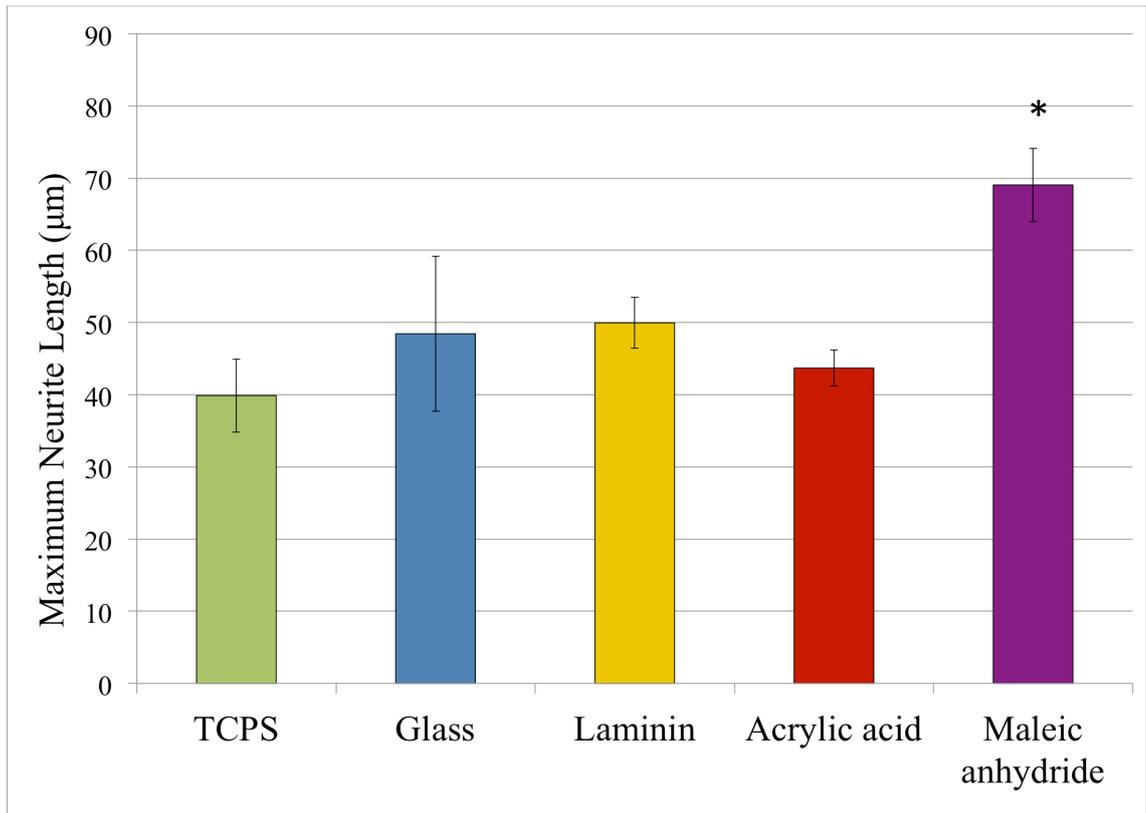

Figure 3.18: Comparison of different surfaces on the maximum neurite length. 1 x 10^4 NG108-15 neuronal cells were seeded onto coated/uncoated 13mm^2 glass slides, then cultured in serum free conditions for 96 hours. Cells were fixed and labelled with β-tubulin III and analysed using ImageXpress analysis software. Data points show mean ± SEM (N=3); *$p<0.05$ compared to glass control.

The micrographs from figure 3.19 showed that the neuronal cells had clearly established β-tubulin III formation, with clear neurites that indicate good attachment. Therefore, it is less likely that the metabolic rate results would have been affected by cellular stress. However, the neuronal cells on glass did not form many neurites, and there are few cells. On laminin the neuronal cells were well adhered and had multiple neurites per neuron, which was documented in other published reports[3]. There were fewer neuronal cells on AAc compared to laminin, with only one neurite visible on the selected micrograph. However, there were many neuronal cells on MA 1, most of which had long neurites. As a general observation, it was found that the neuronal cells tended

to form close colonies on MA 1. In contrast, on the other surfaces it was observed that neuronal cells were in both close and sparse proximity from each other.
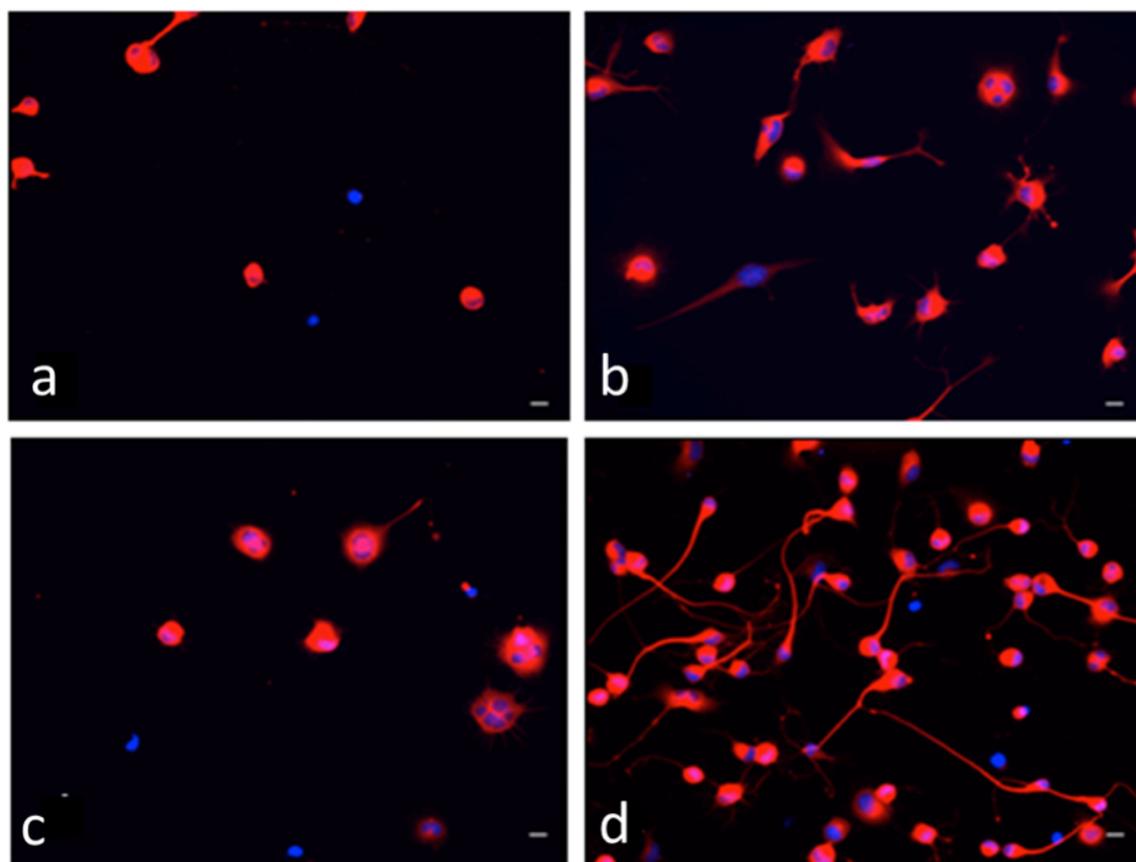

Figure 3.19: Micrographs of β-tubulin III and DAPI labelled NG108-15 neuronal cells, cultured in serum free conditions for 96 hours. a) Glass, b) Laminin, c) AAc, and d) Maleic anhydride. Scale bar shows 20 μm.

Results from figure 3.20 show the percentage of neurons with neurites on different surfaces. As expected, neuronal cells on glass had the lowest population of neurons with neurites, 77%. Neuronal cells on plasma polymerised AAc and MA 1, TCPS and laminin surfaces all demonstrated a similar percentage of neurons. Neuronal cells on laminin had the most neurons with neurites (94%), which agrees with previously published data[6]. 90.5% neuronal cells on TCPS had neurites, whilst neuronal cells on AAc 92.86% and MA 1 90.8%. This was expected, as glass did not have functional groups that could interact with serum proteins compared to the other surfaces and therefore was less amenable to cell attachment and neurite spreading. The results indicate the suitability of plasma polymers for supporting neuronal adhesion and differentiation. Again, there was an enhanced difference between glass and the coated surfaces under serum free conditions compared to the results that contained serum (Figure 3.8).
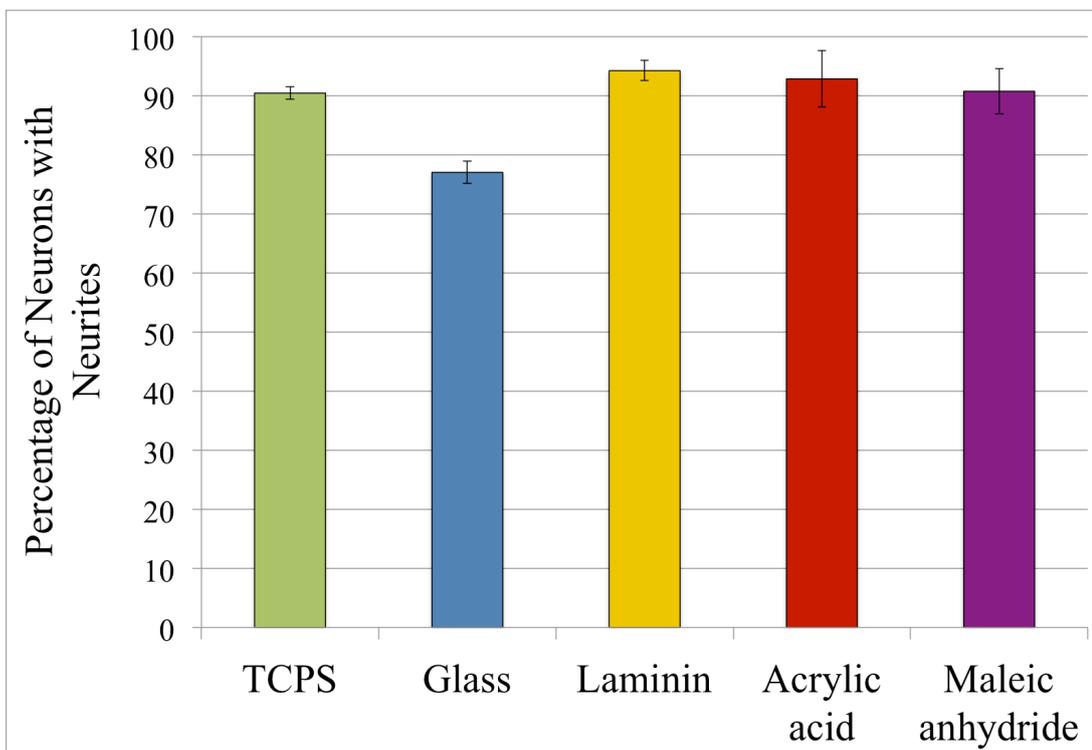
Figure 3.20: Comparison of different surfaces on the percentage of neurons with neurites. 1 x 10^4 NG108-15 neuronal cells were seeded onto coated/uncoated 13mm^2 glass slides, then cultured in serum free conditions for 96 hours. Cells were fixed and labelled with β-tubulin III and analysed using ImageXpress analysis software. Data points show mean ± SEM (N=3).

Results from figure 3.21 show the number of neurites per neuronal cell on different surfaces, with similar trends to the metabolic rate and total cell count measurements (Figures 3.17 and 3.18). There were fewer neurites per neuron on glass and AAc surfaces, both with an average of 3.04. The remaining surfaces had similar results. Neuronal cells on TCPS had 3.9 neurites per neuron, laminin 3.95, and MA 1 3.94, all significantly higher compared to glass. It was expected that glass would support lower numbers of neurites per neuron due to its lack of carbon and oxygen-containing functional groups, however it was unexpected that AAc should support the same number. As AAc is charged and hydrophilic, it would have been expected to support similar numbers of neurites compared to maleic anhydride. Again, there were marked differences between the neuronal characteristics on glass and the other surfaces when under serum free conditions compared to serum containing. These results support the theory that serum proteins adopt particular conformations on the plasma-polymerised surfaces and modulate the adhesion of neuronal cells.
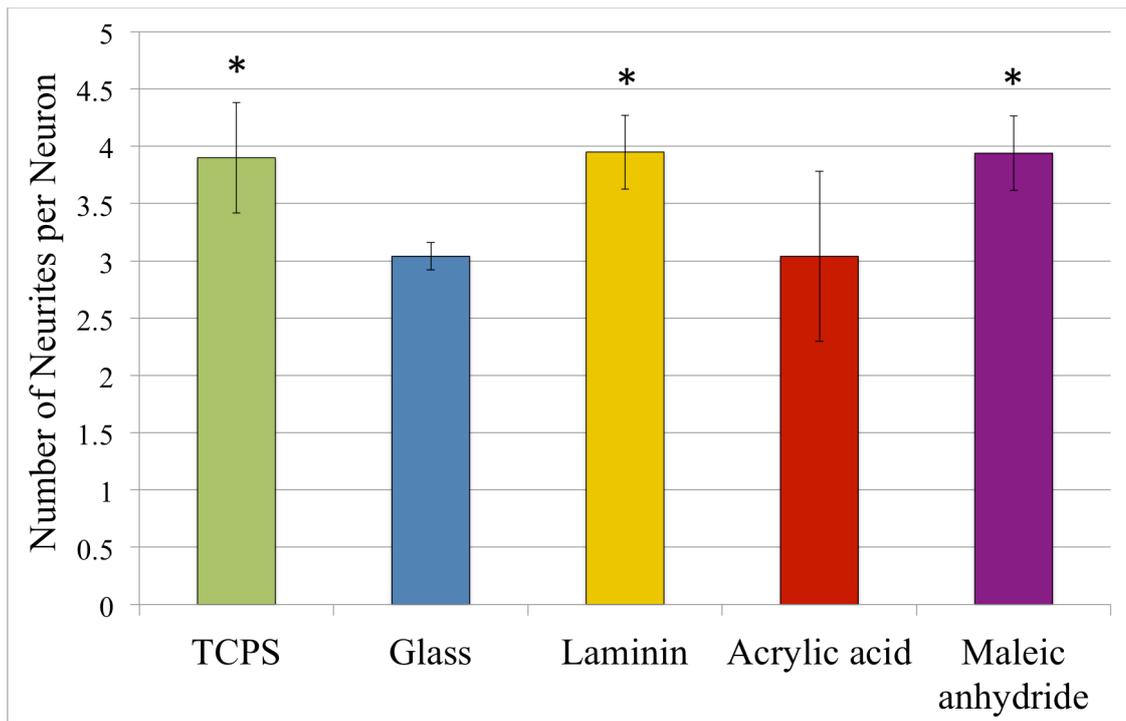
Figure 3.21: Comparison of different surfaces on the number of neurites per neuron. 1 x 10^4 NG108-15 neuronal cells were seeded onto coated/uncoated 13mm^2 glass slides, then cultured in serum free conditions for 96 hours. Cells were fixed and labelled with β-tubulin III and analysed using ImageXpress analysis software. Data points show mean ± SEM (N=3).

3.1.5 Discussion

Overall, results have shown the potential of plasma polymerised surfaces as coatings for neuronal cell culture and the modulatory effect serum proteins had on adhesion, proliferation and neuritogenesis. A serum-containing media environment was used in initial experiments to optimise the detection method for neuronal measurements and to determine which maleic anhydride coating condition was optimal for neuronal cell attachment, proliferation and neuritogenesis and to compare the plasma polymerised surfaces AAc and MA 1. The experiment comparing AAc to MA 1 was then repeated under serum-free media conditions in order to evaluate the effect of serum on NG108-15 neuronal cells and plasma polymerised surfaces.

ImageXpress analysis software proved to be a high throughput, cost efficient and robust method of quantifying neuronal phenotypic measurements. Over 2000 cells were outlined, quantified and processed via an Excel worksheet within a shorter time period compared to manually, which demonstrated the capability of the system. Computer programming experience was not required to develop the script, as there were already a significant number of analysis scripts within the ImageXpress software. The existing scripts were adjusted and developed to the required specifications by a non-specialist.

Neuronal measurements indicated that measuring F-actin filament organisation highlighted significantly more neurites per neuron compared to β-tubulin III, 3.74 compared to 2.91. Although there does not seem to be any published work comparing the two different approaches to measuring neuronal differentiation, reasons for the results could be the location of the actin filaments that F-actin highlights compared to the microtubules. Actin filaments have an essential role in the movement of the cell and are located throughout the cell, including the cell surface and edges[26]. Actin filaments repeatedly form through polymerisation, then retract by depolymerisation, which only become stable when bound to actin-binding capping proteins. At the tip of a growth cone, there is the central domain (C domain), which consists of both actin and microtubule filaments. Fanning out from the C domain, lamellipodia and fillipodia probe the surface. These structures in the P domain are composed of actin filaments rather than microtubule filaments[29]. The actin protrusions probe the surface for chemical functionalities, hydrophilic characteristics and physical topologies. If these protrusions extend from the cell sufficiently, they may be mistaken for neurites once fixed and labelled by F-actin. This could be why the F-actin label revealed more neurites per neuron compared to β-tubulin III. β-tubulin III attaches to the β subunit in microtubules, which are involved in transport within the cell. Although the tubulin

filaments extend to the edges of the cell, the filaments are not stabilised with a capping protein within lamellipodia or filipodia. The F-actin label could therefore give misleading results where a protrusion is identified as a neurite. β-tubulin III may a more appropriate method in this regard as it is less likely to be present in a transient protrusion, but would identify a more permanent, neurite-like extension[12].

The above explanation also gives a reason as to why F-actin labels longer neurites compared to β-tubulin III; 22.94 μm versus 21.44 μm respectively. As F-actin is at the very tip of any protrusion and growth cone it will highlight the leading edge, whereas β-tubulin III is not present at the very end of the moving tip[27]. Discussing the percentage of neurons bearing neurites, it can be postulated that identifying F-actin highlights more protrusions that could be mistaken for neurites, therefore resulting in a higher population of neurons with 'neurites' compared to β-tubulin III.

Another point of discussion is the ability of the ImageXpress software to outline different numbers of cells, depending on the label used. Far fewer cells were measured with F-actin, as the software could not readily determine the cellular leading edges that are composed of actin proteins, and would therefore count colonies of cells as one neuron. As illustrated in figure 3.3, β-tubulin III immunolabelling shows distinct borders of cell within a sub confluent colony, whereas the same cells cannot be as clearly defined when using F-actin. Because of the clarity with which the ImageXpress software could identify each neuronal cell as a 'blob' with 'sproutings' extending out from it, this allowed the analysis software to identify more than double the number of β-tubulin III labelled neuronal cells compared to F-actin.

Investigations then moved onto NG108-15 neuronal cells cultured on plasma polymers, with laminin as a positive control and glass as the basal. As maleic anhydride has not been studied with any cell type previously, studies started with different conditions of maleic anhydride. As seen from the ToF-SIMS results of the first chapter, MA3 had the highest retention of anhydride groups, whilst MA1 had slightly lower retention and MA2 had the lowest percentage of anhydride groups. The metabolic rate results demonstrated that NG108-15 neuronal cells on MA1 demonstrated the highest metabolic rate, whilst neuronal cells on glass and laminin had similar metabolic rates. As laminin was used as a positive control and glass as the basal, a similar result between neuronal cells on the two surfaces was unexpected. However, a relatively high standard error could explain the lack of differences. Whilst the standard error for the relative metabolic rate experiment is higher than the neuronal measurements, the relative metabolic rates for NG108-15 neuronal cells on MA 2 and 3 are clearly lower than all

other surfaces. This is supported by the micrographs, which also show fewer cells on MA 2 and 3.

Reports demonstrate that BSA covalently binds to anhydride groups when in aqueous medium through the amine groups on lysine residues[21]. This reduced mobility would have resulted from, and then further influenced the mobility, of other proteins through the 'Vroman effect'. The 'Vroman effect' is exhibited when serum adsorption by proteins occurs on a surface. Small, highly motile proteins adsorb to the surface initially, which then eventually get replaced by larger proteins that have a higher affinity. It has been shown previously that although albumin reaches and adsorbs to a hydrophilic surface quicker than larger proteins, larger proteins such as fibrinogen then replace albumin preferentially. This results in a gradual drop in albumin adsorption within twenty-four hours[13]. As BSA is covalently bound to the MA surface, rearrangement and conformational changes by the protein cannot occur to optimise protein coverage. Presumably, this would lead to a decrease in the levels of larger proteins, thus affecting cellular adhesion and proliferation. As MA 1 and 2 had similar retention of anhydride / acid groups as demonstrated by the XPS, similar results with neuronal cells was again expected. Therefore, uneven distribution of ions on the surface of MA 2 as demonstrated by the ToF-SIMS ion image mapping may account for these differences, whilst MA 1 and 3 both demonstrated a smooth and even distribution of ions.

Regarding the percentage of NG108-15 neurons with neurites, cells on TCPS, glass, laminin and maleic anhydride 1 show little differences with small standard error, with averages close to 96%. Neuronal cells on MA 2 had slightly fewer neurite projections at 93.9%, whilst there were 86.7% neurons with neurites on MA 3 and the highest standard error. This agrees with the relative metabolic rate measurements regarding maleic anhydride conditions, in that maleic anhydride 1 seems to be a superior surface with regards to supporting NG108-15 neuronal cells and neuritogenesis compared to the other conditions.

The results regarding the number of neurites per neuron were different compared to the metabolic rate assays and seemed to correlate with the relative amount of intact maleic anhydride monomer on the surfaces as determined by ToF-SIMS, as cells on MA 3 gave similar results to MA 1. Both results were significantly higher compared to neuronal cells on glass. Neuronal cells on glass and laminin showed similar results regarding neurites per neuron, which contradicts existing studies[22]. Maleic anhydride 2 supported fewer neurites per neuron compared to the other conditions, which do agree

with the other neuronal measurements and the retention of anhydride functionality by ToF-SIMS. TCPS also supported significantly more neurites per neuron compared to glass, which was expected. Regarding the maximum neurite length, all three maleic anhydride conditions gave very similar values, all of which were significant compared to glass. Laminin supported longer maximum neurite lengths compared to glass, which was more expected. TCPS supported fewer neurites per neuron compared to the maleic anhydride conditions, however the difference was minor.

Overall, neuronal cells on the MA1 condition showed the highest metabolic rate, number of neurites per neuron and a percentage of neurons with neurites compared to the other conditions. Due to the results, MA1 was then taken forward for further experiments. As there is no literature to compare against, MA1 was then compared against AAc with regards to neuronal cell attachment, proliferation and neurite extension. AAc has been shown to be a positive substrate for multiple cell types, including neuronal and Schwann cells[6, 9, 8, 22]. It was thought that AAc would be a useful comparison in order to see if there were any differences in cellular response between the plasma polymers. As most biological studies have compared a single plasma polymer against substrates such as laminin, these following experiments are again novel.

The experiment comparing neuronal cells on TCPS, glass, laminin, AAc and maleic anhydride with serum showed clear results regarding the cell metabolic rate assay. Laminin supported neuronal cells with the highest cell metabolic rate of 0.148, which was to be expected as it is a component of the extra cellular matrix. Neuronal cells on MA1 had a metabolic rate of 0.13. NG108-15 neuronal cells on AAc had a similar metabolic rate to those on laminin of 0.127, higher than neuronal cells on glass (0.12). None of the differences were significant however, so a time point longer than 72 hours may have enhanced existing differences. From reported work, NG108-15 neuronal cells under serum conditions on AAc would have encountered a surface dominated by fibrinogen, with albumin almost absent and immunoglobulin G (IgG) present in very low amounts[20]. Maleic anhydride surfaces would have covalently bound serum albumin to a greater or lesser degree depending on the coating conditions used (lower power used for MA 1 and 2 would lead to higher proportion of anhydride groups and therefore greater covalently bound albumin compared to MA 3). Conversely, another report indicated that hydrophilic surfaces have a lower albumin and IgG adsorption compared to hydrophobic surfaces[13] and that albumin is replaced quicker than IgG.

The possibilities as to why maleic anhydride supported a stronger response in the metabolic rate assay may be due to the reduced motility of BSA proteins. Although adsorbed albumin would have been replaced by larger proteins on the AAc surface, a certain amount of albumin would have been restricted from altering conformation or being replaced on the MA surfaces. XPS results showed that the MA 1 surface contained an average of 16.2% C-(O)=O groups, which would include anhydride groups. A live/dead assay alongside the metabolic rate measurement may have been a useful tool to decide whether the cells were responding positively to the maleic anhydride surface or not, as the metabolic rate could have been tied into the number of alive cells on the surface. However, the micrographs showed a positive phenotype that was not indicative of stress, with strong microfilament labelling and multiple protrusions, which indicates good adhesion.

Neuronal cells on TCPS had 94.7% neurons with neurites, slightly more compared to the other surfaces. 93.5% of neuronal cells on laminin had neurites, which was the positive control. Neuronal cells on AAc had 91.4% neurons with neurites, whilst maleic anhydride had slightly more neurons with neurites compared to glass (90.3%) with 90.5%. The results were expected as TCPS and laminin had the most neurites per neuron and the plasma polymerised surfaces also stimulated neurite outgrowth of over 90%. This agrees with studies which have compared extra cellular matrix proteins[34, 28, 32], and also with studies that have looked at neuronal cell types on AAc[3, 2, 22, 16]. Neuronal cells on glass also gave expected results compared to similar studies[22], with fewer neurites per neuron compared to the functionalised surfaces. Regarding maleic anhydride, previous reports[6, 9] have suggested that a negative charge on a given surface can have a repulsive effect on the negatively charged cell membrane. Anhydride groups that didn't react with BSA would hydrolyse to carboxylic acid and lower the local pH. The reduction in local pH could be the cause of any detrimental effects seen by the neuronal cells on maleic anhydride. However, if there was a detrimental effect on the cells, this should have been apparent from the neuronal measurements, MTS metabolic rate assays and immunolabelled micrographs.

Results from the number of neurites per neuron again showed the expected trend of neuronal cell measurements on TCPS and laminin with 3.01 and 2.8 respectively. Both values were significantly higher than glass, a result corroborated by existing studies[2, 22]. Although the surfaces are suitable for neuronal cell culture, TCPS is non degradable so would not be used for applications in peripheral nerve conduits. Laminin is expensive and derived from animal sources, so has certain

disadvantages when considering its potential in peripheral nerve conduits. Surprisingly, neurons on AAc, MA 1 and glass all had an average of 2.6 neurites each. As mentioned for previous results, a factor that may have affected results is the medium used. For the first 48 hours of experiments using NG108-15 neuronal cells 10% DMEM was used, then the medium was changed to 1:1 DMEM : Hams F12 with N2 supplement (Differentiation medium) for the last 24 hours. This medium was used as it had previously been used within the research group [14]. A study reports that in conjunction with differentiation medium, AAc can have a detrimental effect on overall cell number[6]. The medium protocol was used to increase the adhesion of the NG108-15 neuronal cells, so that labelling protocols could be used without washing off substantial numbers of cells. It was thought that the surface would then enhance any neurites that were already present due to the differentiation medium.

Neuronal cells on AAc demonstrated a significantly higher result compared to glass regarding maximum neurite length (23.9 μm), along with TCPS and laminin that had maximum neurite lengths of 24.4 μm and 24.2 μm respectively. Again, this agrees with existing literature that AAc stimulates longer neurites compared to glass but slightly less than laminin[2, 22]. Neuronal cell on MA 1 had slightly longer neurites than glass at 22.5 μm, whilst neuronal cells on glass had the shortest at 21.9 μm. These results were expected for the other neuronal measurements as well as the metabolic rate assay. The similarities between AAc and laminin regarding maximum neurite length are promising, as laminin is currently seen as the gold standard for neuronal cell culture.

In order to have a large enough sample for neuronal measurements, colonies of cells were found and measured, rather than random fields of view. Although this meant that there was a large sample of cells for the neuronal measurements, more information may have been gathered by taking random fields of view. Total cell number may have also been calculated, which would have given an indication of the adhesion of the cells on the different surfaces. If low numbers had been reported, along with the metabolic rate assay this would have been a good indication of how well the cells adhered to the surface.

It is already established that serum proteins play a major role in the attachment and proliferation of cells[33], however the relatively large size of the common proteins (bovine serum albumin is 66.5 kDa, fibronectin is around 440 kDa) contained within serum may alter the reaction of cells to the surface functionalisation. Because of this, the experiment comparing MA and AAc along with laminin and glass was repeated under serum free conditions. Random fields of view were used to identify labelled

neuronal cells, which meant that total cell count could be calculated. Overall, slight trends shown from serum conditions between surfaces were enhanced when repeated in serum free conditions and there were clear differences in neurite outgrowth across the studied surfaces under serum-free conditions. Regarding the relative metabolic rate experiment, as expected there was a lower metabolic rate across all surfaces compared with serum. As the NG108-15 neuronal cells are deprived of protein with which to proliferate with when under serum free conditions, this reduction in metabolic rate was expected. Neuronal cells on AAc had a slightly higher metabolic rate compared to those on glass. Neuronal cells on laminin showed a significantly higher metabolic rate compared to glass, whilst cells on MA 1 nearly a third higher. MA 1 stimulated a much higher comparative metabolic rate in serum free conditions compared to serum containing. With regards to glass, laminin and AAc, this agrees with past work[17, 2, 22]. Regarding total cell count, the trend from the MTS relative metabolic rate assay was continued. There were significantly more cells adhered on laminin and MA 1 compared to those on glass, whilst AAc supported 2.45 more neuronal cells / field of view compared to neuronal cells on glass.

The percentage of neurons with neurites when grown in serum free conditions showed an increase over the serum results. When neuronal cells were cultured under serum conditions there were no real differences across the groups except that glass had slightly lower values. Whilst there was a dramatic drop in the percentage of neurons with neurites on glass when in serum free conditions, similarly to the serum conditions, there were no real differences across the other groups. This was a positive result, as the plasma polymerised surfaces show very similar results compared to laminin, the positive control surface.

There were clear differences between surfaces when looking at the number of neurites per neuron in serum free conditions. Neuronal cells on glass and AAc demonstrated the lowest values of three neurites per neuron, whilst cells on TCPS, laminin and MA stimulate nearly four; significantly higher than glass. It would have been expected for AAc to stimulate more neurites compared to glass[22], however the relatively high standard error of 0.74 for AAc may be a reason for the similar results to glass.

The most surprising yet clearest result came from the maximum neurite lengths in serum free conditions. This measurement took the length of the longest neurite from each neuron that had neurites. Whilst neuronal cells on TCPS, glass, laminin and AAc all showed results between 40 and 50 μm, MA 1 stimulated an average maximum

neurite length of 69 μm. This was significantly higher than glass. This was corroborated by the micrographs, which showed long neurite extensions on MA 1. Possible explanations may include the report that amine groups in BSA covalently react with anhydride groups, which would restrict movement of other serum proteins on the plasma polymerised surface [21]. Due to the results showing the potential of MA 1 plasma polymerised surface to support neuronal cell differentiation, experiments then moved to investigating primary rat Schwann cells. As detailed in the introduction, Schwann cells play an essential role in peripheral nerve regeneration, forming Bands of Bünger, extra cellular matrix proteins and neurotrophic secretion to encourage neurite extension. Therefore it was appropriate to assess whether the surface functionalities of AAc and MA influenced the proliferation and morphology of Schwann cells.

3.1.6 Conclusion

- Plasma polymerised surfaces AAc and maleic anhydride were investigated using NG108-15 neuronal cells, versus glass, laminin and TCPS

- As maleic anhydride had not been previously investigated, three conditions were compared that had different relative percentages of anhydride groups. MA 1 demonstrated the most promising results with regards to neurite extension, so investigations then compared MA 1 with AAc

- Initial studies used serum conditions, which did not show any major differences between conditions. As the presence of serum proteins may have modulated the cellular adhesion and proliferation of neuronal cells, serum free conditions were then used to compare the plasma polymers. When NG108-15 neuronal cells were cultured on MA1 under serum free conditions they demonstrated significantly longer neurites compared to glass. Neurite lengths on MA 1 were also longer than on laminin or AAc

- As Schwann cells are the first cell type to migrate in to a nerve injury site during regeneration, they have a defined role in supporting neuronal proliferation and differentiation. It was therefore the next part of the investigations into plasma polymerised surfaces

3.1.7 References

1.   General Cell Collection: NG108-15. www.hpacultures.org.uk, Catalogue No: 88112302.
2.   Armstrong, S.J., M. Wiberg, G. Terenghi, et al., ECM molecules mediate both Schwann cell proliferation and activation to enhance neurite outgrowth. Tissue Engineering, 2007. **13**(12): p. 2863-2870.
3.   Armstrong, S.J., M. Wiberg, G. Terenghi, et al., Laminin activates NF-kappaB in Schwann cells to enhance neurite outgrowth. Neuroscience Letters, 2008. **439**(1): p. 42-46.
4.   Bell, J.H.A. and J.W. Haycock, Next Generation Nerve Guides: Materials, Fabrication, Growth Factors, and Cell Delivery. Tissue Engineering Part B-Reviews, 2012. **18**(2): p. 116-128.
5.   Boyd, J.G. and T. Gordon, Neurotrophic factors and their receptors in axonal regeneration and functional recovery after peripheral nerve injury. Molecular Neurobiology, 2003. **27**(3): p. 277-323.
6.   Buttiglione, M., F. Vitiello, E. Sardella, et al., Behaviour of SH-SY5Y neuroblastoma cell line grown in different media and on different chemically modified substrates. Biomaterials, 2007. **28**(19): p. 2932-2945.
7.   Cargill, R.S., K.C. Dee, and S. Malcolm, An assessment of the strength of NG108-15 cell adhesion to chemically modified surfaces. Biomaterials, 1999. **20**(23-24): p. 2417-2425.
8.   Colley, H.E., G. Mishra, A.M. Scutt, et al., Plasma Polymer Coatings to Support Mesenchymal Stem Cell Adhesion, Growth and Differentiation on Variable Stiffness Silicone Elastomers. Plasma Processes and Polymers, 2009. **6**(12): p. 831-839.
9.   Detomaso, L., R. Gristina, G.S. Senesi, et al., Stable plasma-deposited acrylic acid surfaces for cell culture applications. Biomaterials, 2005. **26**(18): p. 3831-3841.
10.   Edgar, D., R. Timpl, and H. Thoenen, The Heparin-Binding Domain of Laminin Is Responsible for Its Effects on Neurite Outgrowth and Neuronal Survival. Embo Journal, 1984. **3**(7): p. 1463-1468.
11.   Fine, E.G., I. Decosterd, M. Papaloizos, et al., GDNF and NGF released by synthetic guidance channels support sciatic nerve regeneration across a long gap. The European journal of neuroscience, 2002. **15**(4): p. 589-601.
12.   Gordon-Weeks, P.R., Microtubules and growth cone function. Journal of Neurobiology, 2004. **58**(1): p. 70-83.
13.   Holmberg, M., K.B. Stibius, N.B. Larsen, et al., Competitive protein adsorption to polymer surfaces from human serum. Journal of Materials Science-Materials in Medicine, 2008. **19**(5): p. 2179-2185.
14.   Kaekhaw, R., Primary Schwann and adipose-derived stem cells for peripheral nerve repair. Edition ed. Series Primary Schwann and adipose-derived stem cells for peripheral nerve repair, ed. Series Editor. Vol. Volume. 2011, Sheffield: Publisher. 150.
15.   Kaewkhaw, R., A.M. Scutt, and J.W. Haycock, Anatomical site influences the differentiation of adipose-derived stem cells for Schwann-cell phenotype and function. Glia, 2011. **59**(5): p. 734-749.
16.   Kelly, J.M., R.D. Short, and M.R. Alexander, Experimental evidence of a relationship between monomer plasma residence time and carboxyl group retention in acrylic acid plasma polymers. Polymer, 2003. **44**(11): p. 3173-3176.

17. Khung, Y.L., G. Barritt, and N.H. Voelcker, Using continuous porous silicon gradients to study the influence of surface topography on the behaviour of neuroblastoma cells. Experimental Cell Research, 2008. **314**(4): p. 789-800.

18. Kowtha, V.C., J.N. Quong, H.J. Bryant, et al., Comparative Electrophysiological Properties of Ng108-15 Cells in Serum-Containing and Serum-Free Media. Neuroscience Letters, 1993. **164**(1-2): p. 129-133.

19. Krystosek, A., Neurite Formation by Neuroblastoma-Glioma Hybrid-Cells (Ng-108-15) in Defined Medium - Stochastic Initiation with Persistence of Differentiated Functions. Journal of cellular physiology, 1985. **125**(2): p. 319-329.

20. Lassen, B. and M. Malmsten, Competitive protein adsorption at plasma polymer surfaces. Journal of Colloid and Interface Science, 1997. **186**(1): p. 9-16.

21. Liu, S., M.M.L.M. Vareiro, S. Fraser, et al., Control of attachment of bovine serum albumin to pulse plasma-polymerized maleic anhydride by variation of pulse conditions. Langmuir, 2005. **21**(19): p. 8572-8575.

22. Murray-Dunning, C., Electrospun aligned biodegradable microfibers and plasma polymerization techniques to improve peripheral nerve repair. 2010, Sheffield: 200 pages.

23. Murray-Dunning, C., S.L. McArthur, T. Sun, et al., Three-dimensional alignment of schwann cells using hydrolysable microfiber scaffolds: strategies for peripheral nerve repair. Methods in Molecular Biology, 2011. **695**: p. 155-166.

24. Patel, M.I., R. Tuckerman, and Q. Dong, A Pitfall of the 3-(4,5-dimethylthiazol-2-yl)-5(3-carboxymethonyphenol)-2-(4-sulfophenyl)-2H-tetra zolium (MTS) assay due to evaporation in wells on the edge of a 96 well plate. Biotechnology Letters, 2005. **27**(11): p. 805-808.

25. Smalheiser, N.R. and N.B. Schwartz, Kinetic-Analysis of Rapid Onset Neurite Formation in Ng108-15 Cells Reveals a Dual Role for Substratum-Bound Laminin. Developmental Brain Research, 1987. **34**(1): p. 111-121.

26. Solecki, D.J., Sticky situations: recent advances in control of cell adhesion during neuronal migration. Current opinion in neurobiology, 2012. **22**(5): p. 791-798.

27. Strasser, G.A., N.A. Rahim, K.E. VanderWaal, et al., Arp2/3 is a negative regulator of growth cone translocation. Neuron, 2004. **43**(1): p. 81-94.

28. Thompson, D.M. and H.M. Buettner, Neurite outgrowth is directed by schwann cell alignment in the absence of other guidance cues. Annals of Biomedical Engineering, 2006. **34**(1): p. 161-168.

29. Tojima, T., H. Akiyama, R. Itofusa, et al., Attractive axon guidance involves asymmetric membrane transport and exocytosis in the growth cone. Nature neuroscience, 2007. **10**(1): p. 58-66.

30. Tojima, T. and E. Ito, Signal transduction cascades underlying de novo protein synthesis required for neuronal morphogenesis in differentiating neurons. Progress in Neurobiology, 2004. **72**(3): p. 183-193.

31. Tojima, T., Y. Yamane, M. Takahashi, et al., Acquisition of neuronal proteins during differentiation of NG108-15 cells. Neuroscience Research, 2000. **37**(2): p. 153-161.

32. Wang, G.Y., K. Hirai, and H. Shimada, The role of laminin, a component of Schwann cell basal lamina, in rat sciatic nerve regeneration within antiserum-treated nerve grafts. Brain Research, 1992. **570**(1-2): p. 116-125.

33. Woo, K.M., V.J. Chen, and P.X. Ma, Nano-fibrous scaffolding architecture selectively enhances protein adsorption contributing to cell attachment. Journal of biomedical materials research. Part A, 2003. **67**(2): p. 531-537.

34. Yao, L., G. Damodaran, N. Nikolskaya, et al., The effect of laminin peptide gradient in enzymatically cross-linked collagen scaffolds on neurite growth. Journal of Biomedical Materials Research Part A, 2010. **92A**(2): p. 484-492.

4.1 The response of primary rat Schwann cells to plasma polymer surfaces

4.1.1 Primary Schwann cell culture

The above analyses have so far studied the response of NG108-15 neuronal cells to plasma-polymerised surfaces. Whilst neuronal measurements are important to assess whether surfaces are conducive for neuritogenesis and extension, it is known that Schwann cells play a major role in nerve regeneration[19]. When injury to the peripheral nervous system occurs, the nerve ends remodel during the initial phase of Wallerian degeneration[6]. Macrophages are recruited to the injury site to clear the site of myelin debris and stimulate the dedifferentiation of Schwann cells, resulting in the loss of the myelin sheath. Schwann cells then proliferate and form the bands of Büngner, laying down basement membrane proteins that include fibronectin, collagen and laminin[2]. The migration and proliferation of Schwann cells occurs for around two weeks and is essential for nerve regeneration [7]. Schwann cells also secrete a cocktail of neurotrophic factors, which includes nerve growth factor (NGF) and brain-derived neurotrophic factor (BDNF) [2]. Recent work has demonstrated that a significant number of Schwann cells can be isolated and grown from a length of adult sciatic nerve within two weeks[8], introducing the possibility of transplanting autologous Schwann cells clinically. It has been shown that the addition of Schwann cells to a nerve guide can improve neurite extension,[12] and recent work has focused on sourcing autologous Schwann cells from different anatomical locations. Mesenchymal stem cells (MSC) have received considerable interest as a potential source of Schwann cells, although it seems that the differentiation of MSCs to a glial phenotype before transplantation to a nerve injury site is required [10, 16, 17]. However, surgery to retrieve the stem cells from bone marrow is invasive and painful. Adipose-derived stem cells (ADSCs) have also been investigated as a potential source of Schwann cells[11, 18, 9], especially as the procedure is less painful and invasive. Additionally, the yield of adipose-derived stem cells is higher compared to bone marrow-derived MSCs[4]. In a comparative study, differentiated ADSCs invoked better nerve responses after injury compared to differentiated MSCs[5].

The importance of Schwann cells during nerve regeneration has been shown in numerous studies, so their investigation with plasma-polymerised surfaces is valuable. Schwann cells have been investigated on acrylic acid (AAc) coatings, with similar relative metabolic rate results to laminin [13]. Maleic anhydride has not previously been

investigated using primary Schwann cells. Because of this, AAc was again included for continuity and as a comparison to maleic anhydride 1 (MA 1). Schwann cells were isolated from white male Wistar rats, using a well-characterised technique[9]. Poly-L-lysine was used as a positive control, due to its well-established affect in supporting proliferation of Schwann cells and retaining their functional characteristics.[15]. The relative metabolic rate of the Schwann cells on various surfaces was analysed, as was the total cell count. Morphology was then quantified using Image J, measuring the length and width of each cell. This data then was used to provide aspect ratio measurements for each surface. As Schwann cells wrap around neurons in the *in vivo* environment, a longer, thinner morphology indicates the retention of functional characteristics[3]. The aspect ratio, relative metabolic rate and cell count results were used to assess the potential of the plasma polymerised surfaces to promote Schwann cell proliferation and appropriate morphology.

4.1.2 Materials and methods

Primary Schwann cell harvest and culture

Primary Schwann cell harvest and culture was performed as previously described (Kaewkhaw, 2012). 2-month-old white Wistar rats were sacrificed according to the Animals (Scientific Procedures) Act 1986 (Schedule I). Sciatic nerves were harvested, the outer epineurium was carefully stripped off with tweezers, in order to minimise any contaminating connective tissue. This was done using a stereo microscope and mounted fine needle. The nerve was then minced finely longitudinally with scalpels. Minced sciatic nerves were added to 0.05% (w/v) collagenase type I for 1 hour, with a brief agitation after 30 minutes. FCS was added and the digest filtered through a sterile strainer. The cell solution was centrifuged at 400 g for 6 minutes, then resuspended in 1 ml of selective medium, which consisted of DMEM (With D-valine, PAA) with 10% (v/v) FCS, 100 U/ml penicillin and 100 μg/ml streptomycin, 0.25 μg /ml amphotericin B, 1% (v/v) N2 supplement, 2 mM glutamine, 20 μg/ml (w/v) bovine pituitary extract, 5 μM forskolin. 500 μl of cell suspension was added to 2 ml selective medium, in a small Petri dish pre-coated with 1 mg/cm^2 laminin and 0.01 mg/cm^2 poly-L-lysine (Sigma Aldrich). 1 ml of selective medium was added on day 7, and then medium changed on day 11 and every 2 days thereafter until confluent. After isolation, Schwann cells were cultured for 21 days before trypsinising and re-plating, at which point the cultures were all free of any contaminating cell types. For all experiments, cells were seeded at 1.66x10^4 cells/well and cultured in selective medium for 9 days before fixation. Schwann cells were used for experimentation up to and including passage 8. The Schwann cell phenotype was confirmed using S100β immunohistochemistry.

Glass and Poly-L-lysine surface preparation

13 mm^2 glass slides (VWR international) were added to a 24 well plate (Costar, Corning Inc). All surfaces were sterilised by an industrial methylated spirit (IMS) rinse followed by 3xPBS rinses. No further treatment was done for glass surfaces. For poly-L-lysine surfaces, 200 μl of 0.01% poly-L-lysine (Sigma) was added to the glass slides for 10 min then taken off. Slides were left for 2 hours then rinsed twice with PBS.

Immunocytochemistry for S100β

Immunohistochemistry for S100β was used as the protein is expressed by Schwann cells located in the peripheral nervous system. After rinsing cells with warmed PBS, primary

Schwann cells were fixed in 3.7% warmed formalin for 20 min. Cells were permeabilised with 1% TritonX-100 (v/v) for 5 min in the fridge, then rinsed with PBS x3 for 10 min. Samples were then blocked with 3% (w/v) BSA in PBS for 60 min then rinsed with PBS. Primary anti-S100β antibody (Dako, 1:250) in 1% (w/v) BSA was added and the samples chilled at 4°C overnight, then washed with 3x5 min PBS. Secondary antibody fluorescein-conjugated anti rabbit IgG (Vector labs, 1:100) in 1% (w/v) BSA for 1 hour at room temperature, before 3x10 min PBS washes. Schwann cells were also then stained with DAPI (1:500 of 1mg/ml in PBS, Sigma) for 15 min then washed 3x3 min PBS.

Cell Relative Metabolic Rate Assay

To analyse cell relative metabolic rate, CellTiter 96$^{®}$ AQ$_{ueous}$ One Solution Cell Proliferation Assay (MTS) was used (Promega), with modifications to the manufacturers protocol. After washing with warmed PBS, glass slides were transferred to a fresh plate with 0.5 ml warmed MTS, then incubated for 2.5 hours. MTS was taken off and centrifuged at $1x10^4$ rpm for 5 minutes so that any cells that lifted off would be removed, then 2 x 200 µl/well was added to a 96 well plate and read with a plate reader at 490 nm.

Image Analysis and Aspect Ratio Measurement

Micrographs were taken using the ImageXpress epifluorescent microscope at x20 magnification. Random fields of view of each sample were taken in order to calculate total cell count. Nuclei were labelled using DAPI and imaged at λex = 350 nm / λem = 470 nm, whilst primary antibody S100β labelled specifically with secondary antibody fluorescein anti-rabbit IgG was imaged using λex = 490 nm / λem = 525 nm. Micrographs were then analysed for aspect ratio using Image J software. One-way analysis of variance (ANOVA) was performed with the averages and standard deviation of n=3. If the differences in mean values among treatment groups were greater than would be expected by chance, a Holm-Sidak post-hoc analysis versus the control group (glass) was used to determine if results were significant.

4.1.3 Results: Primary Schwann cell culture on plasma polymers

To assess whether Schwann cells reacted similarly to the AAc and MA 1 surfaces compared to NG108-15 neuronal cells, primary Schwann cells were cultured on coated glass slides for 9 days and then evaluated in terms of cell relative metabolic rate, total cell number and aspect ratio. S100β immunolabelling specifically identifies neural crest derived cells including Schwann cells and was used to characterise Schwann morphological features. DAPI fluorescent labelling was used for total cell count, which binds to the DNA of all cells.
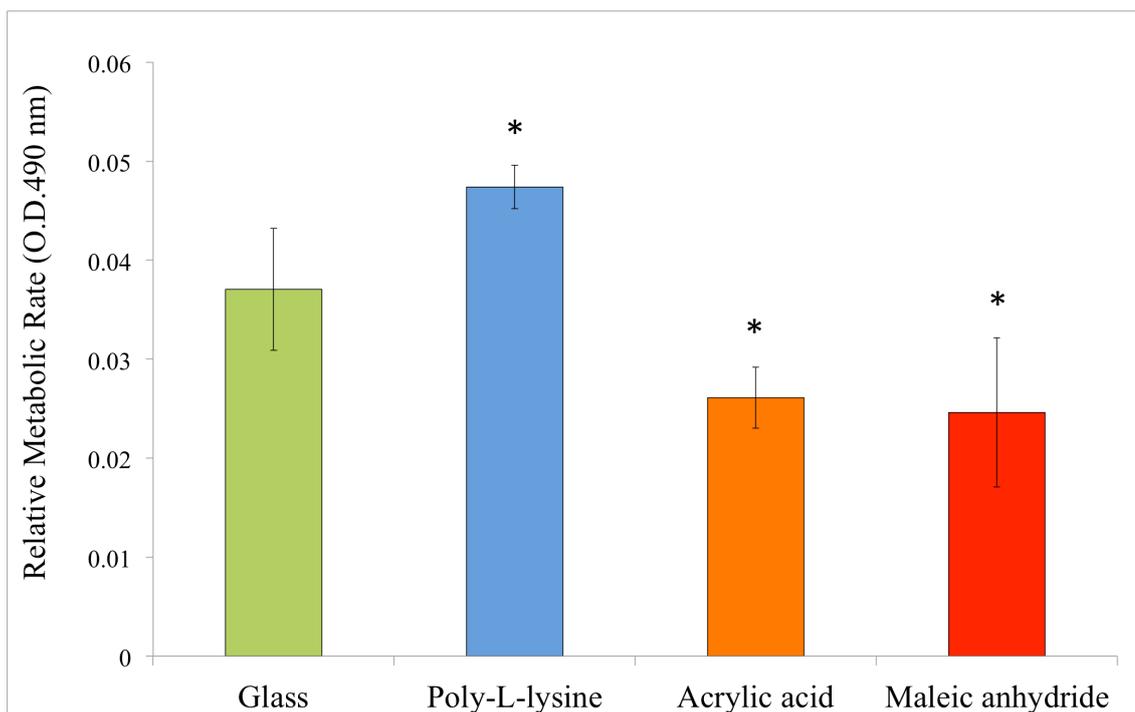

Figure 4.0: Comparison of different surfaces on the cell relative metabolic rate of primary Schwann cells. 1.6×10^4 primary Schwann cells were seeded onto 13 mm^2 coated and uncoated glass slides then cultured for 9 days. Cells were immersed in MTS solution for 2.5 hours and optical density determined. Tissue culture plastic was omitted due to the difference in culture surface area and therefore number of cells. Data points show mean ± SEM (N=3), *p<0.05 compared to glass control.

Poly-L-lysine supported Schwann cells with the highest average cell number and relative metabolic rate, with an average of 183.1 cells per field of view and a relative metabolic rate of 0.047. This was expected, as it was the positive control. Schwann cells on glass had an average cell number per field of view of 137.6 and metabolic rate of 0.037 that was interesting, considering that the surface lacked functional groups of interest and was an inferior surface with regards to neurite outgrowth of NG108-15 neuronal cells. It was clearly demonstrated that glass seemed to be a more conducive surface for Schwann cell proliferation compared to plasma polymers. Schwann cells on AAc had a slightly higher total cell count than TCPS of 83.7 and a relative metabolic

rate of 0.026, which is also interesting considering the positive results seen with NG108-15 neuronal cells. MA 1 supported the least number of Schwann cells, with a low average (0.025) relative metabolic rate and a total cell count of 39.9. This was again interesting, as the NG108-15 neuronal cells demonstrated positive results on MA 1 in the previous chapter. The overall negative charge of the AAc and MA 1 surfaces could have modulated the protein attachment, which in turn had an effect on the negatively charged cell membranes of the Schwann cells; a positively charged surface such as allylamine would have been a good comparison. However, there were limitations to the number of conditions due to the number of Schwann cells available.
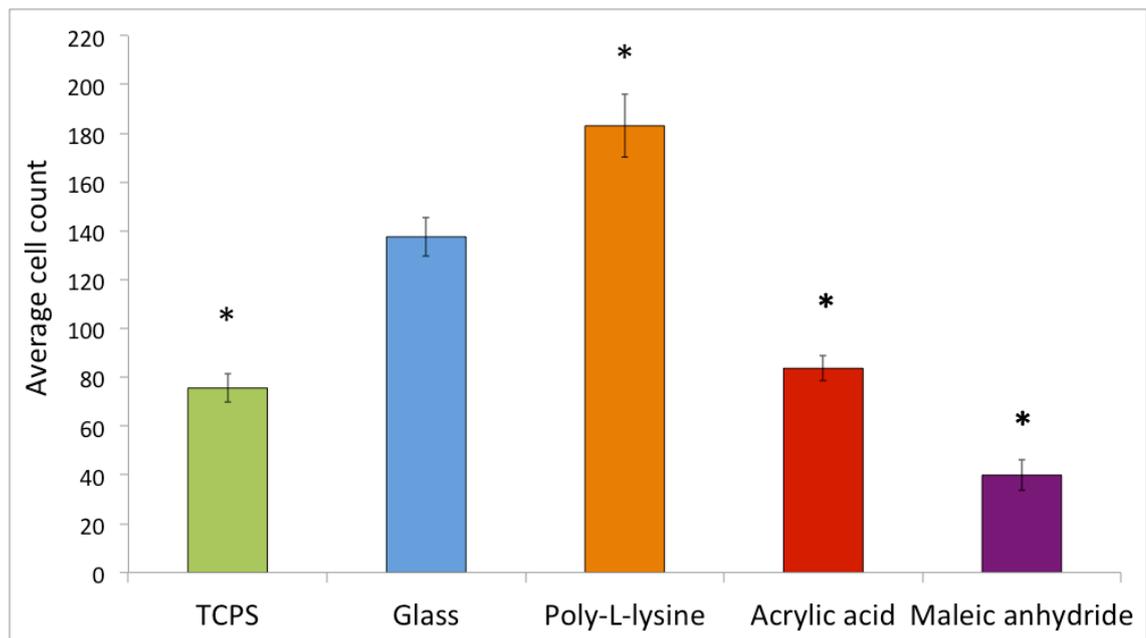

Figure 4.1: Comparison of different surfaces on the total cell count of primary Schwann cells. 1.6 x 10^4 primary Schwann cells were seeded onto 13 mm^2 coated and uncoated glass slides then cultured for 9 days. Cells were fixed and labelled with DAPI and S100β then counted using 20 fields of view per sample and analysed using Image J software. Data points show mean ± SEM (N=3), *$p < 0.001$ compared to glass control.

TCPS could not be investigated using the MTS metabolic rate assay as the surface areas between TCPS and the other conditions were different, which may have led to a difference in cell numbers due to the surface area differences rather than surface characteristics. The average cell count of labelled Schwann cells on TCPS was low at 75.6. All samples were checked at different stages during the immuno labelling process with a light microscope to check that the labelling process did not lead to obvious detachment of fixed cells and influence the cell count.
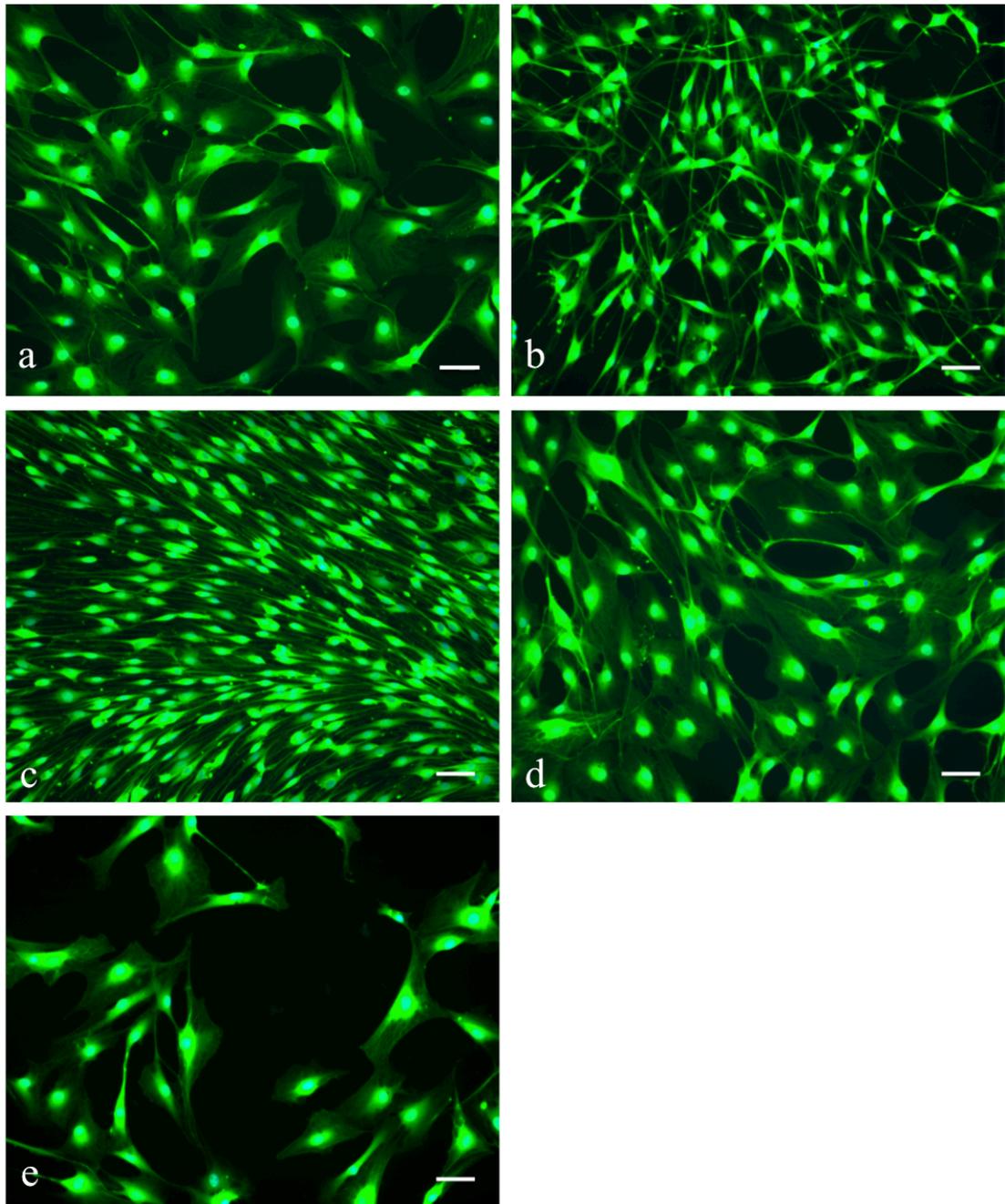
Figure 4.2: Micrographs showing Schwann cells on: a) TCPS, b) Glass, c) Poly-L-lysine, d) AAc and e) MA 1. Scale bar shows 50 μm. 1.6 x 10^4 primary Schwann cells were seeded onto 13 mm^2 coated and uncoated glass slides then cultured for 8 days. Cells were fixed and stained with S100β and DAPI. Scale bar shows 50 μm.

Schwann cells were cultured on the surfaces for nine days, after which they were fixed and immunolabelled for S100β and DAPI. Micrographs were then analysed using Image J software, and the morphology analysed. The length and width of each cell was quantified then compared against other surfaces. Schwann cells on poly-L-lysine were observed to have the longest and thinnest morphology, with an aspect ratio of 7.95. This was not significant compared to glass however, as glass also supported Schwann cells with a long and thin phenotype. As the aspect ratio of Schwann cells on glass was 6.64,

Schwann cells on TCPS, AAc and MA 1 had significantly lower aspect ratios. Schwann cells on TCPS had the most polygonal shape, with an aspect ratio of 2.93. Schwann cells on AAc had an aspect ratio of 3.44, whilst Schwann cells on MA 1 had an aspect ratio of 3.47. Although AAc and MA 1 supported Schwann cells with a slightly longer and thinner phenotype compared to TCPS overall, the Schwann cells were still mostly polygonal.
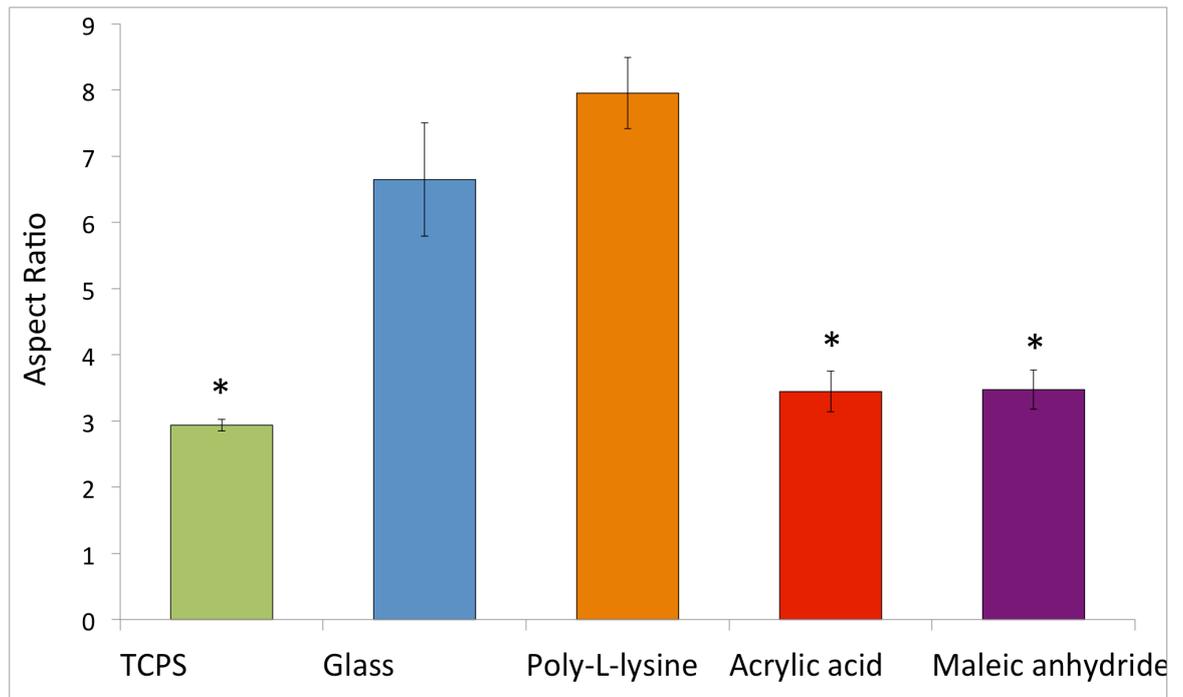

Figure 4.3: Comparison of different surfaces on the aspect ratio (length/width) of primary Schwann cells. 1.6 x 10^4 primary Schwann cells were seeded onto 13 mm^2 coated and uncoated glass slides then cultured for 8 days. Cells were fixed and stained with S100β then analysed using 5 fields of view per sample and Image J software. Data points show mean ± SEM (N=3), *p<0.001 compared to glass control.

4.1.4 Discussion

Results obtained from primary Schwann cells were unexpected, as Schwann cells when grown on AAc and MA 1 had significantly lower cell metabolic rates and total cell count than on glass. Schwann cells grown on poly-L-lysine were observed to have a relative metabolic rate of 0.047 and 183.1 average number of cells, which was the highest. Although there were no significant differences with poly-L-lysine, it supported considerably more Schwann cells than any other surface. This was expected as it was used as the positive control, and corroborates previous work reported for poly-L-lysine[9, 13]. Poly-lysine is a homopolymer of the essential amino acid L-lysine, that similarly to all amino acids contain both carboxyl and amine groups. This is compared to the acrylic acid and maleic anhydride surfaces that contain carboxyl and anhydride/carboxyl groups, the level of carboxyl groups on the maleic anhydride surface dependent on the plasma coating process parameters and level of anhydride hydrolysis at any given time. Schwann cells grown on TCPS had a relative cell count of 75.6, which was significantly lower than Schwann cells on glass (137.6) but higher than the number of cells on both plasma polymerised surfaces (83.7 on acrylic acid and 39.9 on MA 1). This was more expected, as TPCS was used as a 'universal' substrate for most cell types.

Both the metabolic rate (0.026) and cell counts (83.7) of Schwann cells on AAc were interesting, as there were some positive results with neuronal cells. Schwann cells on AAc demonstrated a higher number of cells compared to TCPS, but significantly lower than Schwann cells cultured on glass. As work with Schwann cells comparing poly-L-lysine and AAc hasn't been reported previously, there are no studies to the best of my knowledge for comparison. However, considering that Schwann cells on glass had similar metabolic rates compared to laminin[13], the relative metabolic rate and cell count values for AAc were lower than expected. Primary rat Schwann cells, when grown on MA 1, had the lowest relative metabolic rate of 0.025 and total cell count of 39.9, contrary to the NG108-15 neuronal results. This was intriguing, as the anhydride groups were capable of supporting neuronal cell attachment and neuronal cell extension when under serum free conditions, but less amenable in supporting Schwann cell proliferation.

The presence of serum proteins may have altered the reaction of the Schwann cells, especially as the effect of serum on plasma polymerised surfaces was demonstrated in the previous chapter. However, Schwann cells are generally quite senescent cells, and would not have proliferated sufficiently if cultured under serum free

conditions. Schwann cells have been cultured in serum free conditions successfully when used in conjunction with mitogenic factors[14], however the numbers would not be sufficient for the experiments carried out in this chapter. The presence of forskolin, N2 supplement and bovine pituitary extract would have also had a modulatory effect on the growth of Schwann cells on plasma polymerised surfaces, however, these factors were required for the adherence and proliferation of the Schwann cells. Overall, the primary Schwann cells showed low relative metabolic rates and total cell number on the plasma polymerised surfaces compared to glass and poly-L-lysine. This corroborates with Buttiglione et al[1], who found that AAc had a negative effect on cell number when cells were also cultured in differentiation medium[1]. It may also be that a longer culture period is necessary as the cells were fixed 8 days after seeding.

The aspect ratio results were related to and agreed with the total cell numbers and relative metabolic rate, where it seems that the more Schwann cells on a given surface, the more elongated and thinner they become. In mammals, Schwann cells wrap around neurons, displaying a specialised elongated phenotype[10]. The progression of morphological changes was therefore interesting to monitor. The Schwann cells on poly-L-lysine initially had a polygonal shape until confluent, whereupon a 'squashing' effect occurred in order to facilitate further proliferation. Eventually, Schwann cells had a highly dendritic morphology and the highest aspect ratio when cultured on poly-L-lysine, as seen in figure 4.2.

Schwann cells on glass had similar aspect ratio to poly-L-lysine, however whilst Schwann cells when grown on poly-L-lysine packed very closely in parallel alignment, there was no alignment when cultured on glass. Schwann cells cultured on TCPS, AAc and MA 1 all exhibited a polygonal morphology. The aspect ratios of the Schwann cells grown on the plasma-polymerised surfaces agreed corresponded with the data on metabolic rate and average cell counts. Whilst the morphology of the Schwann cells on TCPS, AAc and MA 1 was observed to spread well and demonstrated a well adhered morphology, the long and thin morphology of Schwann cells on poly-L-lysine is currently the *in vitro* gold standard.. The plasma polymers seem to have been relatively poor at supporting the proliferation and elongated phenotype of primary Schwann cells compared to glass or poly-L-lysine. It is interesting that the Schwann cells would react poorly to the plasma polymerised surfaces, however it may be in agreement with Buttiglione et al[1] that serum containing media can have an adverse effect. Although the paper used a neuroblastoma line, there is not a published comparison that uses Schwann cells to the best of my knowledge.

4.1.5 Conclusions

- Primary Schwann cells were cultured on TCPS, glass, poly-L-lysine, AAc and MA 1 surfaces under serum-containing conditions, with added mitogenic factors

- Poly-L-lysine supported the highest number of Schwann cells that had a dendritic and bipolar morphology

- Glass supported lower numbers of Schwann cells compared to poly-L-lysine, with lower relative metabolic rate measurements

- Aspect ratio results also showed that Schwann cells showed a more polygonal morphology when cultured on TCPS compared to glass or poly-L-lysine

- Plasma polymerised surfaces supported fewer cells than poly-L-lysine or glass, and had a comparatively polygonal morphology

- Dorsal root ganglion (DRG) were then investigated, as DRG contain both primary Schwann and neuronal cells. Given the different results found from neuronal and Schwann cells, both neuronal and Schwann cell types in a co-culture environment were investigated with plasma polymerised surfaces.

4.6 References

1.   Buttiglione, M., F. Vitiello, E. Sardella, et al., Behaviour of SH-SY5Y neuroblastoma cell line grown in different media and on different chemically modified substrates. Biomaterials, 2007. **28**(19): p. 2932-2945.
2.   Chen, Z.L., W.M. Yu, and S. Strickland, Peripheral regeneration. Annual Review of Neuroscience, 2007. **30**: p. 209-233.
3.   Chew, S.Y., R. Mi, A. Hoke, et al., The effect of the alignment of electrospun fibrous scaffolds on Schwann cell maturation. Biomaterials, 2008. **29**(6): p. 653-661.
4.   da Silva Meirelles, L., T.T. Sand, R.J. Harman, et al., MSC frequency correlates with blood vessel density in equine adipose tissue. Tissue engineering. Part A, 2009. **15**(2): p. 221-229.
5.   di Summa, P.G., D.F. Kalbermatten, E. Pralong, et al., Long-term in vivo regeneration of peripheral nerves through bioengineered nerve grafts. Neuroscience, 2011. **181**: p. 278-291.
6.   Guertin, A.D., D.P. Zhang, K.S. Mak, et al., Microanatomy of axon/glial signaling during Wallerian degeneration. The Journal of neuroscience : the official journal of the Society for Neuroscience, 2005. **25**(13): p. 3478-3487.
7.   Hall, S.M., Regeneration in Cellular and Acellular Autografts in the Peripheral Nervous-System. Neuropathology and Applied Neurobiology, 1986. **12**(1): p. 27-46.
8.   Kaewkhaw, R., Primary Schwann cell and adipose-derived stem cells for peripheral nerve repair. Edition ed. Series Primary Schwann cell and adipose-derived stem cells for peripheral nerve repair, ed. Series Editor. Vol. Volume. 2011, Sheffield: Publisher. 150.
9.   Kaewkhaw, R., A.M. Scutt, and J.W. Haycock, Anatomical site influences the differentiation of adipose-derived stem cells for Schwann-cell phenotype and function. Glia, 2011. **59**(5): p. 734-749.
10.   Keilhoff, G., A. Goihl, F. Stang, et al., Peripheral nerve tissue engineering: Autologous Schwann cells vs. transdifferentiated mesenchymal stem cells. Tissue Engineering, 2006. **12**(6): p. 1451-1465.
11.   Kingham, P.J., C. Mantovani, and G. Terenghi, Notch independent signalling mediates Schwann cell-like differentiation of adipose derived stem cells. Neurosci Lett, 2009. **467**(2): p. 164-168.
12.   Madduri, S. and B. Gander, Schwann cell delivery of neurotrophic factors for peripheral nerve regeneration. Journal of the Peripheral Nervous System, 2010. **15**(2): p. 93-103.
13.   Murray-Dunning, C., Electrospun aligned biodegradable microfibers and plasma polymerization techniques to improve peripheral nerve repair. 2010, Sheffield: 200 pages.
14.   Needham, L.K., G.I. Tennekoon, and G.M. Mckhann, Selective Growth of Rat Schwann-Cells in Neuron-Free and Serum-Free Primary Culture. Journal of Neuroscience, 1987. **7**(1): p. 1-9.
15.   Porter, S., M.B. Clark, L. Glaser, et al., Schwann-Cells Stimulated to Proliferate in the Absence of Neurons Retain Full Functional Capability. Journal of Neuroscience, 1986. **6**(10): p. 3070-3078.
16.   Scuteri, A., A. Cassetti, and G. Tredici, Adult mesenchymal stem cells rescue dorsal root ganglia neurons from dying. Brain Research, 2006. **1116**(1): p. 75-81.

17.   Tohill, M., C. Mantovani, M. Wiberg, et al., Rat bone marrow mesenchymal stem cells express glial markers and stimulate nerve regeneration. Neuroscience Letters, 2004. **362**(3): p. 200-203.

18.   Tse, K.-H., M. Sun, C. Mantovani, et al., In vitro evaluation of polyester-based scaffolds seeded with adipose derived stem cells for peripheral nerve regeneration. Journal of Biomedical Materials Research Part A, 2010. **95A**(3): p. 701-708.

19.   Webber, C. and D. Zochodne, The nerve regenerative microenvironment: early behavior and partnership of axons and Schwann cells. Experimental Neurology, 2010. **223**(1): p. 51-59.

5.1 Evaluation of Plasma Polymers using Primary Rat Dorsal Root Ganglion

5.1.1 Primary rat dorsal root ganglion culture

NG108-15 neuronal cells are a well-established cell line[18, 19], with relatively fast proliferation capabilities. However, whilst the NG108-15 cell line has been used as a neuronal model for numerous published experiments[18, 5, 2], there are limitations. As a Sendai virus fused neuroblastoma and glioma cell line, they are immortal and a hybrid of two cell types. Information gathered from the cell line as a neuronal model for peripheral nerve repair is therefore not entirely comparable to how the recovery of an animal / human would progress with a peripheral nerve injury. Primary animal cells can therefore be used to bridge the gap between immortal cell line experiments and *in vivo* experiments. Given the results obtained using the NG108-15 neuronal cell line, investigation moved onto studying primary cells; rat dorsal root ganglion (DRG).

DRGs are located on the interior of the spinal cord, and connect the central nervous system to the peripheral nervous system. During the third week of embryonic gestation, the formation and thickening of the neural plate from the ectoderm occurs. By the end of the third week, a longitudinal infolding of the ectoderm results in the neural groove, which closes to form the neural tube. At the lateral edge of the ectoderm and each side of the neural tube towards the edge of the embryo, the neural crest forms. During embryonic development, spinal ganglia originate as part of the neural crest, as well as other neuronal cell types such as Schwann cells[11]. DRGs contain both neuronal and glial cell types, along with surrounding connective tissue. The neuronal cell bodies of the peripheral nervous system are located within the DRG, whilst their neurite processes extend far out to the extremities of the limbs. Whilst Schwann cells can be extracted from both the DRG tissues and from isolating the sciatic nerve, neuronal cell bodies can only be isolated from the ganglia. Response and growth of primary neuronal cells from the spinal cord of rats, although quicker than humans, can be indicative of the clinical response[21].

There are two main methods to retrieve neuronal cells from the DRG. DRG explants are nodules of tissue that can be extracted from the inside of the spinal column, then cultured. The explants are placed on a given surface, from which various cell types grow out from after around 6 days. Whilst there can be outgrowth from connective tissue components i.e. fibroblast cells[17], it is a relatively straightforward protocol. As

fibroblasts proliferate and migrate across a peripheral nerve defect[6], this can be a positive aspect. However, depending on the medium used, the fibroblasts may also inhibit Schwann cell growth due to contact repulsion between the two cell types[15]. This method was initially used, as explants had not been used on plasma polymer surfaces previously. Another method is to dissociate the neuronal and Schwann cells from the explant tissue. The explants are enzymatically dissociated using collagenase type 4 and trypsin, then mechanically dissociated. Using this method, most of the contaminating fibroblast population can be removed from the culture[3]. Once immunolabelled, it was easier to identify the neurite outgrowths of dissociated DRG compared to explants, facilitating analysis. Once investigations were performed with the explants, further studies then moved onto dissociated DRG to try and obtain a more comprehensive study of primary cell responses on plasma polymer surfaces.

To my knowledge, original research articles have not been published regarding the capabilities of maleic anhydride (MA) to support the cell migration, attachment or proliferation of primary neuronal cells. There has also not been any published work to my knowledge of primary rat DRG cell cultures grown on acrylic acid (AAc), although it has been reported using NG108-15 neuronal and Schwann cells[14].

5.1.2 Materials and methods

Dorsal root ganglion explant isolation

1-month-old white Wistar rats were sacrificed according to the Animals (Scientific Procedures) Act 1986 (Schedule 1). The spinal column was excised and trimmed, then cut into thirds. The spinal cord was removed to expose the dorsal root ganglia and roots. DRGs were gently pulled from the spinal column along with the roots, and up to 25 DRGs per rat put into a 35mm dish containing F12 medium. Using a stereomicroscope and scalpel, DRG explants were trimmed from the roots and rinsed in F12 medium. All F12 medium used contained 100 U/ml penicillin and 100 μg/ml streptomycin and 0.25 μg / ml amphotericin B. Explants were then rinsed in PBS. For optimisation experiments, two explants were carefully placed on each laminin-coated surface within a 24 well plate, which was performed in triplicate per condition. As contact between outgrowing explants occurred, one explant was cultured per well for the plasma polymer experiment to minimise the effect of soluble factors and contact guidance / inhibition. For each experiment comparing surface chemistries, six DRG explants were used for each surface chemistry, for N=1. Each explant was cultured in a separate well. Substrates used included MA 1 (on-time of 80 μs and an off-time of 800 μs, 5W peak power for 20 minutes) and AAc (15W continuous power for 10 minutes). Any residual PBS was carefully pipetted off from the edges of all explants, so that each explant would attach to the surface. After incubating the dry explants for 15 min, 160 μl of 10% DMEM with 100 U/ml penicillin and 100 μg/ml streptomycin and 0.25 μg /ml amphotericin B was added gradually. Although it was shown previously that serum-containing medium affected the response of NG108-15 neuronal cells, preliminary experiments demonstrated that outgrowth from explants in serum free medium was sporadic and unpredictable, with a high standard deviation. Therefore, experiments with explants used serum-containing medium. This process of dry incubation was repeated until the explants attached to the surface. Medium changes occurred with fresh 160 μl medium every other day.

Dissociated dorsal root ganglion isolation

1-month-old white Wistar rats were sacrificed according to the Animals (Scientific Procedures) Act 1986 (Schedule 1). DRGs were dissected and dissociated as previously described[10]. DRGs were isolated by excising and halving the spinal cord, followed by the gentle extraction of DRG explants into F12 medium. As before, all F12 medium

used contained 100 U/ml penicillin and 100 μg/ml streptomycin (Sigma) and 0.25 μg/ml amphotericin B. Explants were then transferred to 1.25 mg/ml collagenase type 4 in F12 medium and incubated for 1 hour. Digestion medium was then replaced with fresh digestion medium for a further 45 minutes. After gently rinsing explants in F12 medium, explants were transferred to 2.5 mg/ml trypsin in F12 medium and incubated for 30 min. DRGs were rinsed in F12 with 50% FCS to arrest further digestion. To remove all FCS, explants were rinsed in fresh F12 medium 3 times. Using a glass pipette, explants were then mechanically dissociated for 4 min, the supernatant aspirated and the mechanical dissociation repeated in fresh F12 medium. This was repeated 4 times. The collected supernatant was filtered through a 70 μm filter then centrifuged at 300 g for 5 min. The medium was then carefully removed apart from the last 500 μl, which was resuspended. This concentrated cell solution was carefully pipetted down a prepared track of 10% bovine serum albumin (BSA) protein in PBS then centrifuged at 500 g for 10 min. Two layers of liquid resulted from the centrifugation, with the DRG neurons at the base and unwanted debris material suspended in the top layer. The top layer supernatant was pipetted off and discarded, leaving the cell pellet. The cell pellet was resuspended in modified Bottenstein and Sato (B&S) medium. This consisted of F12 medium (with 100 U/ml penicillin and 100 μg/ml streptomycin and 0.25 μg/ml amphotericin B) with 100 μg/ml (w/v) BSA and 10 μl/ml (v/v) N2 supplement. 400 μl of the resuspended solution was added to each coated coverslip in a 6 well plate. Substrates used were glass, laminin, AAc (15W continuous power for 10 minutes) and MA 1 (on-time of 80 μs and an off-time of 800 μs, 5W peak power for 20 minutes). One rat generated enough cells for approximately 6-9 coverslips, so experiments were performed in duplicate. Experiment was then repeated three times. Plates were incubated for 2 hours in order for neuronal, Schwann and fibroblast cells to adhere to the surfaces, then another 2 ml of B&S medium was carefully added to each well. 77 ng/ml NGF was also added to each well, from separate aliquots.

Immunolabelling for β-tubulin III and S100β

Dissociated DRG and explants were rinsed in warmed PBS, then fixed in 3.7% (v/v) formalin for 20 min. Cells were permeabilised with 1% (v/v) Triton X-100 for 5 min in the fridge, then carefully rinsed with PBS x3 for 10 min. Samples were blocked with 3% BSA (w/v) in PBS for 60 min then rinsed with PBS. Monoclonal mouse anti-β-tubulin III (1:2000; Promega) and polyclonal rabbit anti-S100β (1:250; Dako) in 1%

BSA (w/v) were added and the samples chilled at 4˚C overnight. Samples were then rinsed with 3 x 5 min PBS. Texas Red-conjugated secondary anti-mouse IgG (1:100; Vector labs, UK) and FITC-conjugated secondary anti-rabbit IgG antibody (1:100 in 1% BSA; Vector labs) in 1% BSA (w/v) was added for 1 hour at room temperature, before 3x10 min wash. Samples were also stained with 1:500 DAPI for 15 mins, then washed 3 x 3 min with PBS.

Image Analysis

All micrographs were taken using a confocal laser-scanning microscope (Carl Zeiss, LSM510-META, Germany). Micrographs of the anti-β-tubulin III label with Texas Red conjugated secondary antibody were taken (λex = 595 nm / λem = 615 nm), whilst the DAPI label for nuclei was imaged at λex = 350 nm / λem = 470 nm. The secondary antibody fluorescein anti-rabbit IgG specifically labelled primary antibody S100β and then imaging was conducted using λex = 490 nm / λem = 525 nm. Neuronal measurements were made by hand using Image J software.

Statistical analysis

One-way analysis of variance (ANOVA) statistical test was performed with the averages and standard deviation of three repeats. If the differences in mean values among treatment groups were greater than would be expected by chance, Holm-Sidak post-hoc analysis versus the control group (glass) was used to determine if results were significant.

5.1.3 Optimisation of dorsal root ganglion explant culture

DRG explant culture has not been reported previously using plasma-polymerised surfaces, so optimisation experiments were carried out initially. As laminin was a positive control surface, it was used to assess growth rate and time of culture. Explants were excised from the spinal cord, placed on freshly coated laminin surfaces, then PBS removed and the explants incubated dry for 20 min to facilitate the attachment of explants onto the surfaces. Explants were cultured for 10, 15 and 20 days, with 160 µl serum-containing medium, which was

Figure 5.0: Illustration of how migration distances from each explant were measured.

changed every 48 hours. Phase contrast micrographs were also taken every second day and outgrowth measured radially outwards, from the top and bottom of each explant.
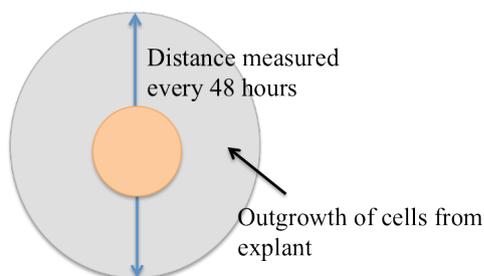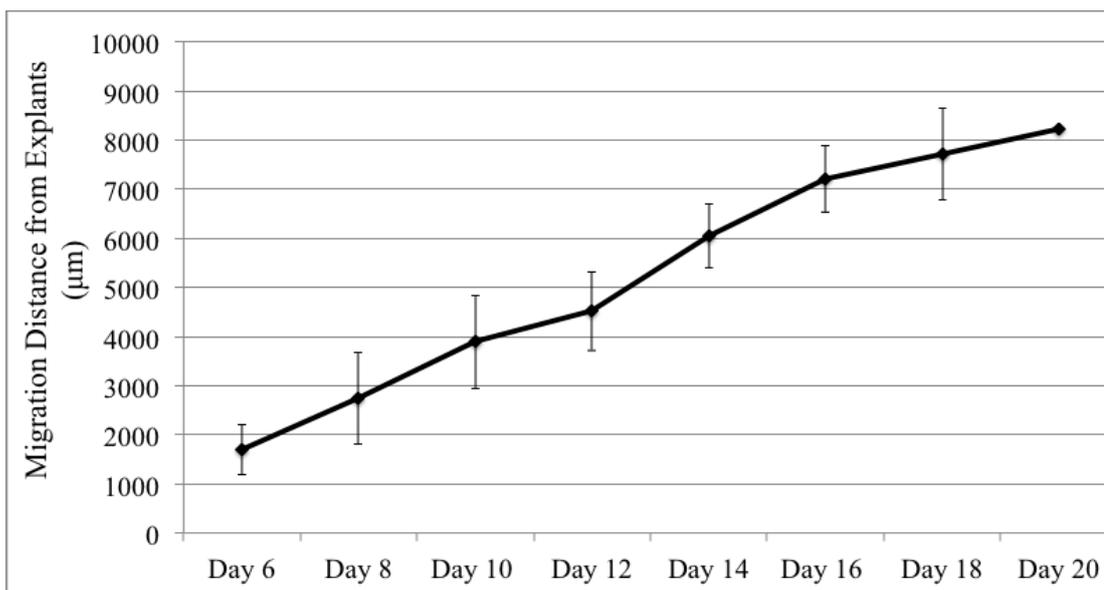

Figure 5.1: Comparison of migration distances of DRG explants, between day 6-20. Explants from the spinal cord of Wistar rats were extracted and cultured on laminin for 20 days. Distances were measured from the top and bottom of each explant using a phase contrast microscope. Measurements were stopped when DRG outgrowth reached the edge of the slide. As the explant outgrowth reached 8 mm and the substrates were 13 mm, only one explant was measured on day 20. Data points show one measurement at day 20, with standard deviation at other time points (n=6).

Phase contrast light microscope pictures were taken in series, then distances measured using Image J. Initial outgrowth was observed at day 5 or 6, so measurements were started on day 6. As seen in figure 5.1, average outgrowth was measured at 1698 µm for day 6, 2744 µm at day 8, 3890 µm at day 10, 4517 µm at day 12, 6053 µm at day 14, 7210 µm at day 16, 7716 at day 18, then 8223 µm at day 20.
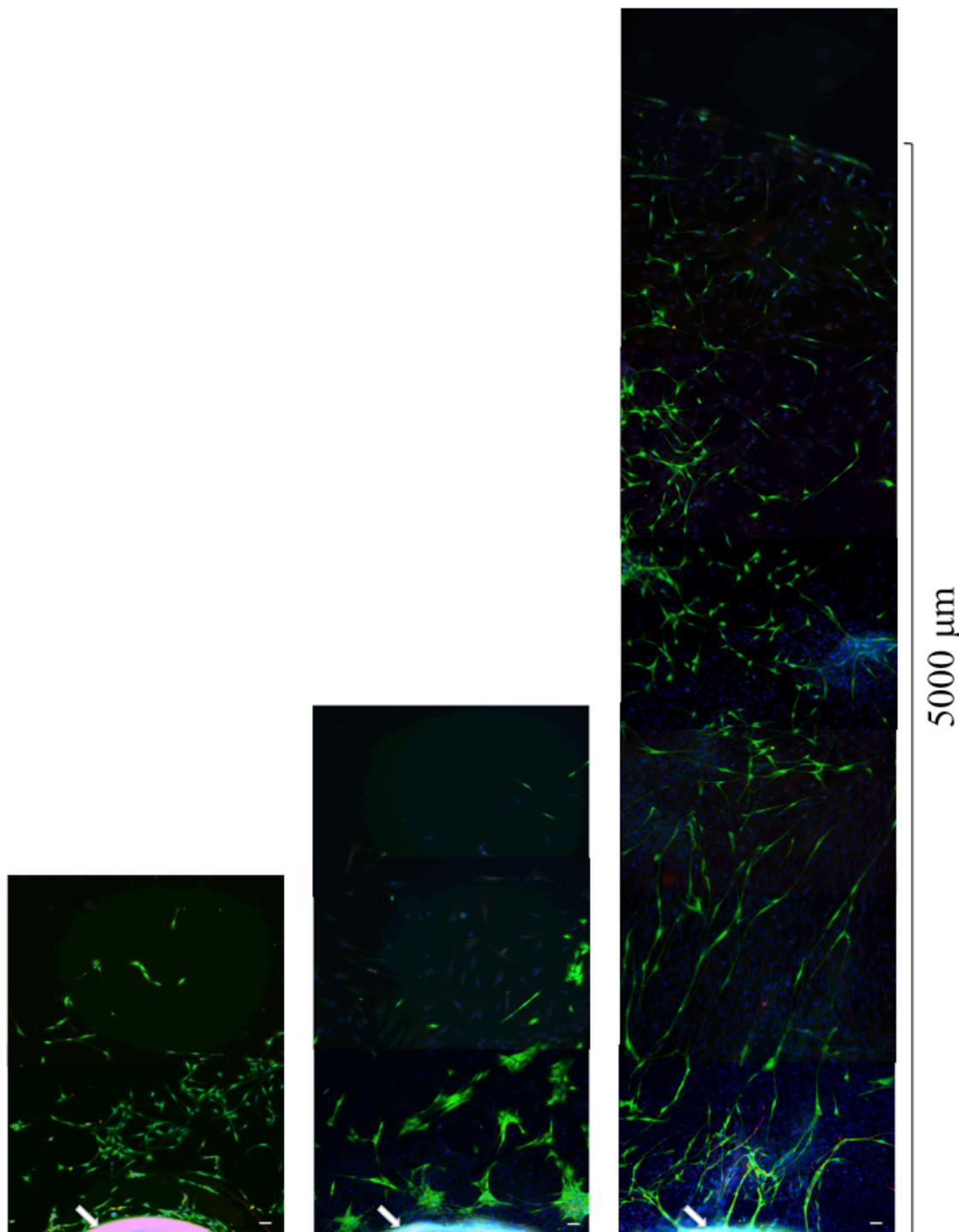
Figure 5.2: Micrographs of anti-β-tubulin III (red: neurites), anti-S100β (green: Schwann cells) and DAPI (blue: nuclei) labelled DRG explants. Comparison of migration distance of DRG explants, at day 10 (left), 15 (middle) and 20 (right). Explants from the spinal cord of wistar rats were extracted and cultured on laminin for up to 20 days. (n=6). Arrows indicate top edge of DRG explant, phase microscope measurements were taken from the top and bottom of each explant. Scale bar shows 50 μm.

It was found that the average migration rate of primary DRG was 606.55 μm / day, ± 149.5. Examining figure 5.2, it can be seen that the morphology of the Schwann cells change throughout the experiment. At day 10 Schwann cells had an elongated and

bipolar structure, with good attachment. Each Schwann cell could be distinguished individually, with very few other non-labelled cell types in the area (the non-specific DAPI stain highlighted any non-S100β positive cells). There was no neuronal staining visible. At day 15 Schwann cells were observed to clump into small colonies, where individual cells could not be distinguished and began to orientate towards the explant. Non-labelled cells were also observed and were believed to be fibroblasts emerging from the explant. These cells migrated further than the Schwann cells. As the migration distances shown in figure 5.1 were recorded using a light microscope that did not distinguish between cell type, migration distances were not comparable to the labelled micrographs. By day 20, a confluent layer of non-labelled cells was seen, interspersed with Schwann cells. A high degree of orientation and alignment was observed in cell morphology, as Schwann cells 'lined up' perpendicularly to the top of the explant. The neuronal marker β-tubulin III was observed to be faintly expressed, so the 20-day time point and serum-containing medium was used for further work.

5.1.4: Dorsal root ganglion explant culture on plasma polymers

DRG explants were cultured on glass, laminin, AAc and MA 1 for 20 days in serum-containing medium. Samples were then fixed and stained for β-tubulin III, S100 β and DAPI.
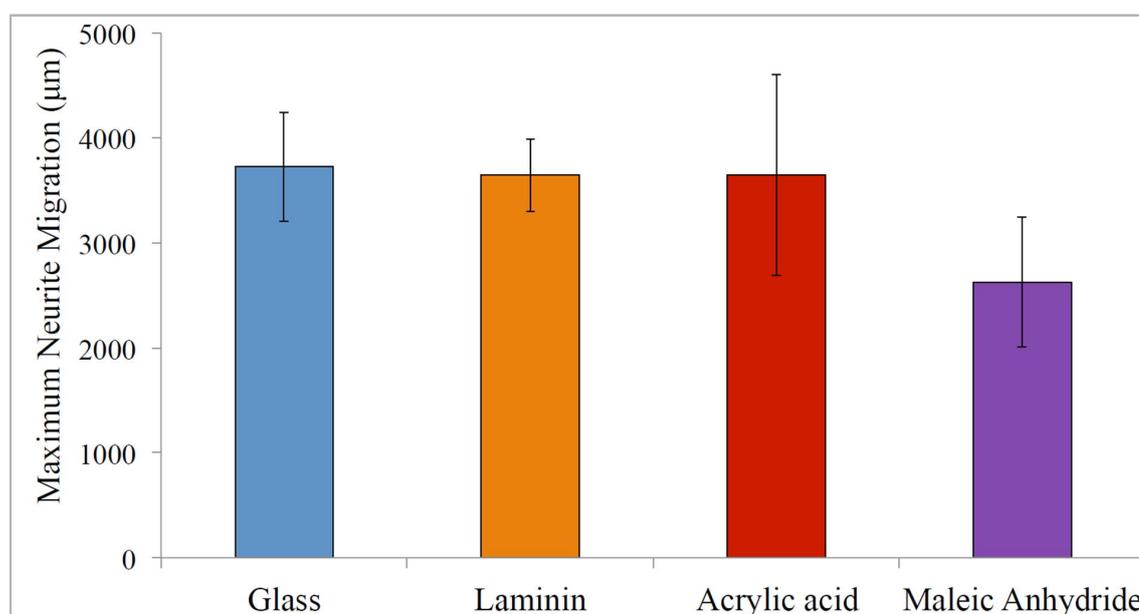

Figure 5.3: The effect of different surfaces on the maximum neurite length from DRG explants. Explants were cultured for 20 days in serum-containing medium, after which were fixed and stained for β-tubulin III, S100 β and DAPI. Confocal micrographs were taken, then analysis using Image J software measured the maximum length from explants of β-tubulin III stained neuronal outgrowth. N=3.
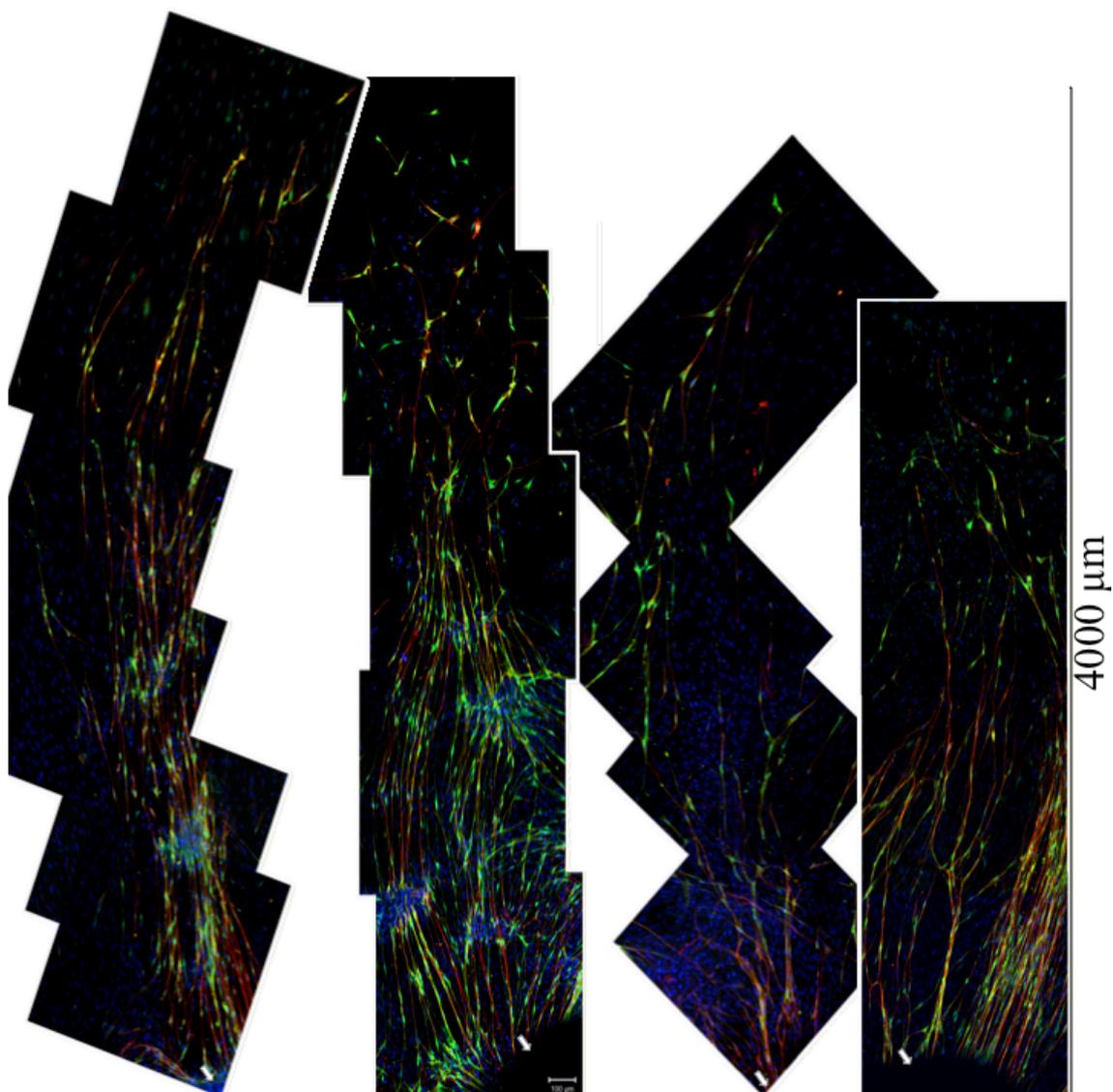
Figure 5.4: The effect of DRG explants on different surfaces after 20 days in serum containing medium. Micrographs show anti-β-tubulin III (red: neurites), anti-S100β (green: Schwann cells) and DAPI (blue: nuclei) labelled DRG explants. Arrows indicate top edge of DRG explant, the furthest migrated distance from each explant labelled for anti-β-tubulin III was taken. Scale bar shows 50 μm. From left to right: glass, laminin, AAc and MA 1. Scale bar on micrograph shows 100 μm (N=3).

Micrographs were tiled using confocal microscopy, and the maximum migration distance of anti-β-tubulin III labelled cells was measured from each explant using Image J software. Rather than measuring the radial outgrowth from the top and bottom of each explant, the furthest migrated distance per explant was taken. DRG explants on glass, laminin and AAc had similar values of 3724 μm, 3645 μm and 3646 μm for maximum neurite outgrowth after 20 days, whilst DRG explants on MA 1 demonstrated a

migration distance of 2626 μm. As the standard error of the mean values were quite large, no significant differences were identified between samples. Comparing figure 5.3 to the results from NG108-15 neuronal cells cultured on plasma polymers under similar conditions, there were some differences. Regarding maximum neurite length of NG108-15 neuronal cells cultured under serum-containing conditions, neurite lengths on glass and MA 1 were both slightly shorter compared to those measured on laminin and AAc. This is in contrast to DRG explants cultured for 20 days, where neurite outgrowth from DRG explants on MA 1 is substantially shorter. Whilst the comparisons are limited due to the differences in serum-containing medium used and length of culture, a limited appraisal of similarities between cell lines and primary neuronal cells can be made.
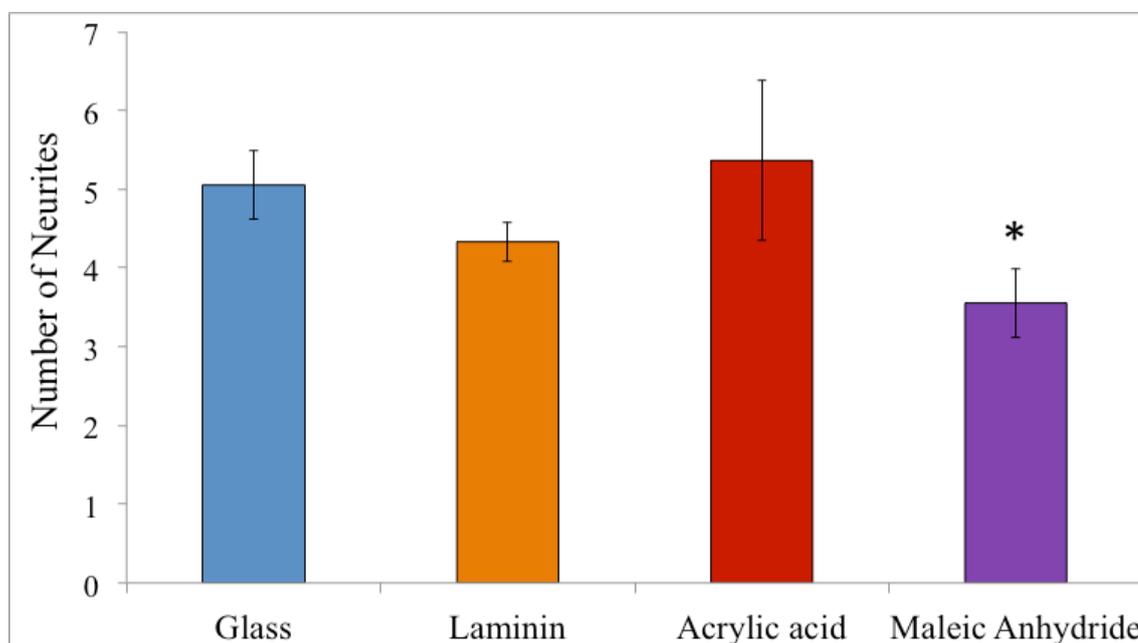

Figure 5.5: The number of neurites from DRG explants when cultured on various surfaces. Explants were cultured for 20 days in serum-containing medium, after which were fixed and stained for β-tubulin III, S100 β and DAPI. Confocal micrographs were taken, then analysis using Image J software measured the number of neurite and Schwann cell 'bunches' from explants. Data points show mean ± SEM (N=3); *$p<0.05$ compared to glass control.

The micrographs shown in figure 5.4 showed clear labelling of neuronal cells expressing β-tubulin III, Schwann cells expressing S100β and the non-specific nuclear stain DAPI. There were aligned tracks of Schwann and neuronal cells perpendicular to the explant interface, with some co-localisation. There was a confluent monolayer of DAPI-labelled cells, assumed to be fibroblasts. There was a lower abundance of fibroblasts on MA 1, which could be indicative of why the outgrowth was lower compared to other surfaces. Discrete areas shown on glass and laminin in figure 5.4 have colonies of fibroblast cells, with tracks of neuronal and Schwann cells leading into

and out of these regions. Examining the number of neurites, it was decided that each collection of neurites growing in the same direction and in close proximity was measured as a neurite. Figure 5.4 illustrates one neurite per explant on each surface. DRG explants on glass and AAc had the highest number of neurites, with 5.1 and 5.4 neurites per explant respectively. DRG explants on laminin had an average of 4.3 neurites per explant, whilst DRG explants on MA 1 had 3.6 neurites per neuron that was significantly lower compared to glass. Regarding the control surfaces, as glass was the basal control and laminin the positive control, the results were interesting. As DRG explants on AAc showed the longest neurite length (significantly longer compared to laminin and MA 1), it was shown that DRG explant proliferation and neurite extension can be supported when cultured on AAc. This can be compared to NG108-15 neuronal cells on plasma polymers under serum conditions, where little difference was observed between all groups.

It was noted during optimisation experiments that certain explants would grow outwards, whilst others would not. As it could not be confirmed whether lack of outgrowth from explants was due to surface chemistry or lack of sufficient adherence when preparing the experiment, the overall percentage of explants with neurites was not calculated.

5.1.5 Dissociated DRG on plasma polymers

A high proportion of fibroblasts were observed in explant experiments, so to study this in further depth, studies were conducted to investigate whether reducing the presence of fibroblasts would influence neuronal and Schwann cell growth on the plasma polymerised surfaces[15]. Dissociated DRGs can be obtained by mechanical and enzymatic degradation of the explant tissue. By filtering out the connective tissue components of each explant, the abundance of fibroblasts can be reduced. Dissociated DRGs were obtained using 25 explants from each rat. The supernatant was then used for up to 9 samples in 6 well plates[10]. The serum levels used for dissociated DRG were 100 μg/ml (w/v), rather than 10% (v/v) serum that was used for the explant culture.

As neuronal and Schwann cells have a very close partnership within the *in vivo* environment, the combination of primary rat neuronal and glial cell types *in vitro* is a more reliable indicator of the ability of plasma polymerised surfaces to support neuronal and Schwann proliferation and neurite extension[12, 1]. Regarding the percentage of neurons with neurites (figure 5.6), it can be observed that 83.8% of the dissociated DRG

on laminin had neurites, whilst the basal control of glass supported 23.3% neurons with neurites. Dissociated DRG on AAc and MA 1 had similar percentage of neurons with neurites of 51.9% and 49.1% respectively.
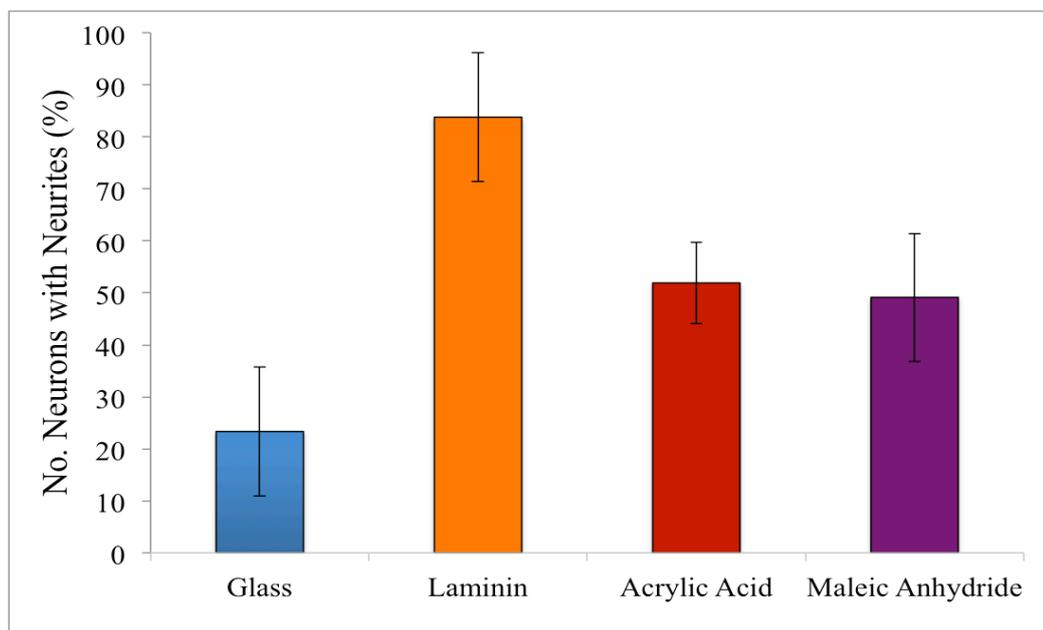

Figure 5.6: Comparison of different surfaces on the percentage of neurites from dissociated DRG. Explants from the spinal cord of Wistar rats were enzymatically and mechanically dissociated. Dissociated DRG were cultured in B&S medium with NGF for 4 days. DRG were then fixed and co-immunostained with β-tubulin III, S100β and DAPI. Data points show mean ± SEM (N=3).

The confocal micrographs (figure 5.7) illustrate the morphology of the neuronal and glial cell types. Any other cell types such as fibroblasts were shown subtractively using the DAPI nuclei label. Fewer non-labelled cells were observed by confocal microscopy compared to the micrographs of the DRG explants (figure 5.4), which was a desired outcome of the dissociation isolation procedure. Around 5 neuronal bodies per field of view were observed and neurons on glass had short neurites. Neuronal cells on laminin had long, multiple neurites that often made contact with neighbouring neurons. Neurons on AAc and MA 1 showed similar morphologies, with longer neurites compared to neurons on glass

After immunohistochemical staining the samples, it was found that Schwann cells only survived the isolation procedure for one of the experimental repeats (whilst neuronal quantitative results were included from all repeats, micrographs from the two repeats without Schwann cells are shown). Only non-labelled and neuronal cells were present after two of the repeats were immunolabelled (figure 5.7). When Schwann cells were present, close association between neuronal and Schwann cells was observed on plasma polymers, identified by co-localisation of S100β and β-tubulin-III labels.

Although Schwann cells cultured on laminin were numerous and would be present in the same area of the neuronal bodies and neurites, co-localisation did not occur as frequently. There were comparatively low numbers of Schwann cells on glass. There was also a substantial decrease regarding the percentage of neurons with neurites across all surfaces, when Schwann cells were present: 55%.
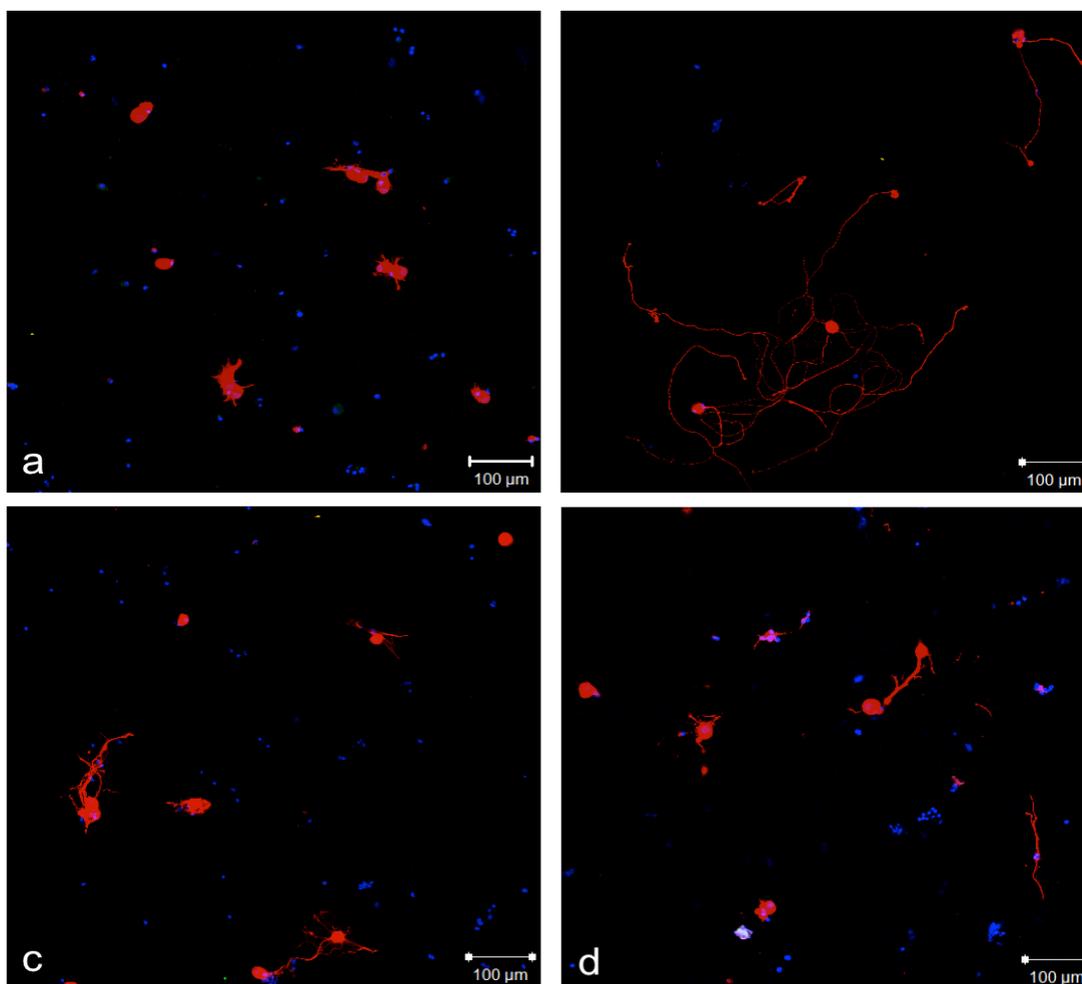

Figure 5.7: Micrographs show dissociated DRGs immunolabelled for β-tubulin III (red: neurites) and DAPI (blue: nuclei) on the following surfaces: a) Glass, b) Laminin, c) AAc and d) MA 1. Explants from the spinal cord of Wistar rats were enzymatically and mechanically dissociated, then cultured in B&S medium with NGF for 4 days. DRGs were then fixed and co-immunostained (N=3).

neurons on glass without Schwann cells present had neurites, whilst 15% neurons had neurites on glass when Schwann cells were present. Regarding laminin, 100% neurons had neurites when Schwann cells were not present compared to 63% with Schwann cells. Acrylic acid supported 67% neurons with neurites in the absence of Schwann cells, 43% with Schwann cells. 78% of neurons had neurites on MA 1 without Schwann cells compared to 40% with Schwann cells.

Dissociated DRGs had more neurites per neuron when grown on the plasma polymers compared to glass (figure 5.8). There was an average of 5.3 neurites per
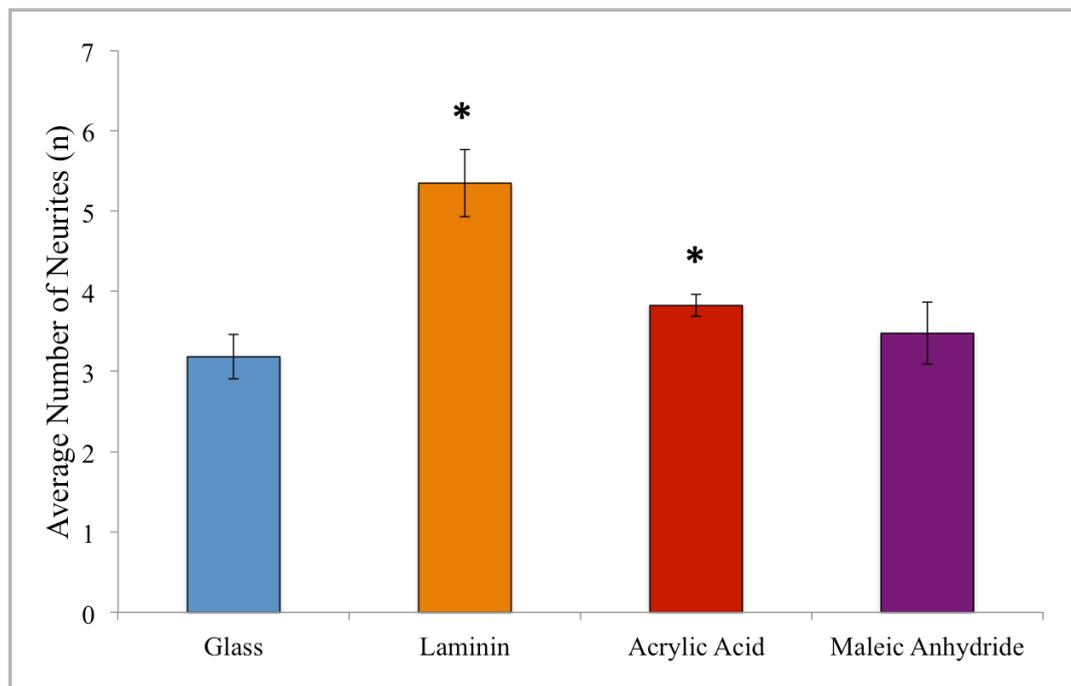
Figure 5.8: Comparison of different surfaces on the number of neurites from dissociated DRG. Explants from the spinal cord of wistar rats were enzymatically and mechanically dissociated. Dissociated DRG were cultured in B&S medium with NGF for 4 days. DRG were then fixed and co-immunostained with β-tubulin III, S100β and DAPI. Data points show mean ± SEM (N=3); *p<0.001 compared to glass control.

neuron on laminin, which was significantly higher than neuronal cells on glass, neuronal cells on which had 3.2 neurites on average. Neuronal cells on AAc had 3.8 neurites on average, which was again significantly higher than glass, whilst neuronal cells on MA 1 had 3.5 neurites. Interestingly, the number of neurites per neuron when Schwann cells were present slightly decreased from 3.45 without Schwann cells to 2.6 for glass, but slightly increased from 3.0 without Schwann cells to 4.26 with Schwann cells for MA 1. The number of neurites per neuron on laminin and AAc were not affected by the presence or absence of Schwann cells.

Looking at the maximum neurite length results, neurons on glass had an average maximum neurite length of 54.4 μm, whilst the length was 84.8 μm on AAc. MA 1 supported neurons with a maximum neurite length of 75.7, slightly shorter than AAc. Laminin stimulated significantly longer neurites per neuron compared to glass, with an average maximum of 254 μm. Laminin is often used as a positive control surface when comparing surface chemistry [20]. Interestingly, the maximum neurite length of neurons on laminin was reduced in the absence of Schwann cells, from 337 μm with Schwann cells to 87 μm without Schwann cells, which accounts for the high variance. Comparatively, neuronal cells on glass, AAc and MA 1 saw reductions in maximum neurite length of ~50 μm. Overall, glass had the lowest values compared to laminin and

the plasma polymers regarding all the neuronal measurements assessed for dissociated DRGs (percentage, number and maximum length of neurites per neuron). Plasma polymers clearly demonstrate an ability to support the attachment, neuritogenesis and neurite elongation of primary rat neuronal cells from dissociated DRG.
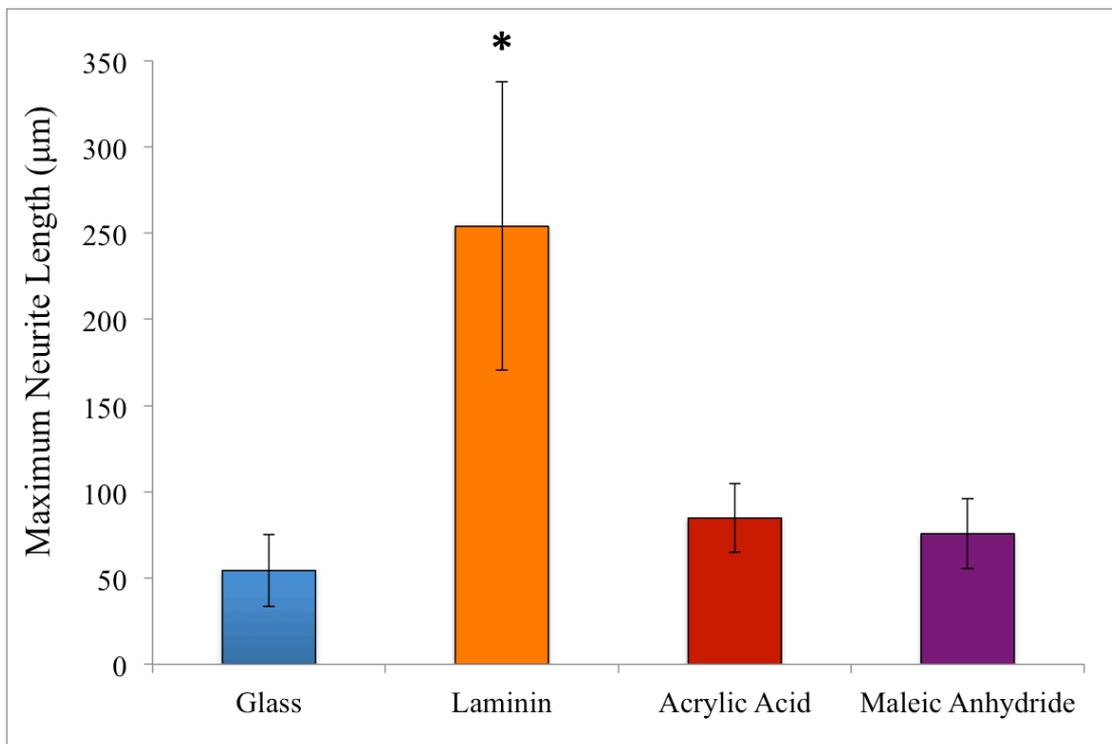

Figure 5.9: Maximum neurite length of dissociated DRG on different surfaces.. Explants from the spinal cord of Wistar rats were enzymatically and mechanically dissociated. Dissociated DRGs were cultured in B&S medium with NGF for 4 days. DRGs were then fixed and co-immunolabelled with β-tubulin III, S100β and DAPI. Data points show mean ± SD (N=3): *p<0.001 compared to glass control.

5.1.6 Discussion

As there was no previous work or protocols within the research group regarding the isolation and culture of dorsal root ganglion, optimisation of the plasma polymerised surfaces for cell culture was completed initially. Explants were used in order to become familiar with the isolation and culture procedure. As the protocol for dissociated DRG can take up to 14 hours to complete, the knowledge gained from the explant experiments was then used for the dissociated DRG culture. It became clear from preliminary experiments and studies that cells from the explants would not migrate out predictably unless cultured under serum-containing conditions[8]. As dissociated DRG could be cultured in very low serum conditions (100 μg / ml), this was seen as a useful comparison.

Initial experiments demonstrated that between day 6 and 20 of explant culture on laminin in 10% serum, the migration rate of unlabelled cells was 607 μm / day. As human *in vivo* nerve growth following injury is reported at 0.5mm / day for large nerves and rat nerve regeneration is generally quicker[16], the corresponds with published results. After 20 days, outgrowth reached 8223 μm from the explant edge. Examination of the micrographs indicated that neurite expression was present at day 20, which was then used as the time point for later studies.

Explant studies with plasma polymers were not in agreement with serum-containing NG108-15 neuronal results. Whilst maximum neurite lengths of NG108-15 neuronal cells in serum-containing conditions on laminin, AAc and MA 1 were longer compared to glass, maximum neurite lengths of explants on glass were higher by ~100 μm compared to laminin and AAc. Maximum neurite length results of DRG explants were similar on glass, laminin and AAc, whilst MA 1 supported neurons with maximum neurite length of 2626 μm, ~1000 μm shorter compared to glass, laminin and AAc. The standard error mean for all experiments was quite high, indicating variability. This could be a combination of using primary rat tissue, which has an inherent variability compared to cell lines. Explants were taken from the whole length of each spinal column, with no distinction between the cervical, thoracic, lumbar or sacral regions.

The micrographs of DRG explants on plasma polymerised surfaces showed strong neuronal and Schwann labelling on all surfaces, with co-localisation and aligned tracks leading from the explant. This was in contrast to the optimisation experiment, where after 20 days culture on laminin there was comparatively weak neuronal labelling. Regarding the number of neurites per explant, explants on glass and AAc

supported more neurites compared to laminin. MA 1 supported nearly two fewer neurites per explant (3.6) compared to AAc (5.4). DRG explants demonstrated the same trend as results from Schwann cells in that MA 1 supported the least number of cells. An obvious reason for this would be the anhydride groups, which has interesting implications. As Schwann and neuronal cells were found to respond very differently to anhydride-containing surfaces, strategies to improve Schwann cell growth may be different to that for neuronal cells. This has potentially interesting implications, especially as neuronal and Schwann cells have a very close association *in vivo*. The results regarding laminin, glass and AAc were not in agreement with existing studies that looked at NG108-15 neuronal cells on AAc or results from other cell types in earlier chapters[4, 14].

Experiments then moved onto using dissociated DRGs, as the culture conditions used low concentrations of serum proteins. As NG108-15 neuronal cells showed varying results regarding neuronal measurements in the presence and absence of serum, this was seen as an interesting avenue to investigate. As the culture conditions used for dissociated DRG were low serum (100 μg/ml), results could then be compared to serum-free conditions of NG108-15 neuronal cells in a limited way. Whilst the dissociation method also uses explants taken from all regions of the spinal column, 25 explants from each rodent were combined together. As neuronal and Schwann cells from all the spinal column regions would therefore be present on all surfaces, this may have been a factor in the lower variation seen with dissociated DRG compared to DRG explants.

The percentage of neurons with neurites showed that laminin supported 84% of the dissociated neurons to produce neurites. AAc and MA 1 plasma polymers supported 52% and 49% neurons with neurite outgrowths respectively, whilst only 23% of the neuronal population on glass developed neurites. These results were more consistent with studies reported by Murray-Dunning[14], where laminin was also the positive control and glass the basal. This trend was repeated for the number of neurites and maximum neurite length, where neurons on glass demonstrated fewer, slightly shorter neurites compared to the plasma polymers and laminin. The micrographs of dissociated DRG also agree with the quantitative results reported.

As a low concentration of 100 μg/ml FCS was used in the dissociated DRG medium, results from NG108-15 neuronal cells under serum-free conditions may be the closest comparison. When cultured under serum free conditions for four days, over 90%

NG108-15 neuronal cells on the plasma surfaces and laminin had neurites, whilst 77% neurons on glass had neurites. The differences shown with NG108-15 neuronal cells have therefore been enhanced but show similar trends to dissociated DRG, which further supports the use of NG108-15 neuronal cell culture. This can be compared to serum conditions, where all conditions stimulated 90% or more neurons with neurites.

Dissociated DRG on plasma polymers had higher numbers of neurites per neuron compared to glass, whilst neurons on laminin had the longest and most numerous neurites. Results from dissociated DRG were interesting, and agree with published scientific studies[4, 14, 7] that the plasma polymerised surfaces support higher numbers of neuronal cells compared to glass. Under serum free conditions with NG108-15 neuronal cells, MA 1 supported neurons with the same number of neurites to laminin (Chapter 3, figure 3.23), whilst the number of neurites per neuron on AAc and glass were also equal. From the results using dissociated DRG, it can be seen that there is a difference between the NG108-15 neuronal results and primary dissociated DRG [13, 9].

Due to the lower variability, dissociated DRG were shown to be a more reliable method for assessing the effect of plasma-polymerised surfaces on neuronal measurements compared to explants. Although primary Schwann cell work showed that Schwann cells cultured on glass had longer and thinner aspect ratios with higher metabolic rates compared to Schwann cells on plasma polymers, plasma polymerised surfaces were capable of supporting primary rat dissociated neuronal cells with a higher percentage of neurons with neurites , whilst acrylic acid supported primary neuronal cells with a significantly higher number of neurites compared to glass.

5.1.7 Conclusion

- Optimisation experiments confirmed that rat DRG explants should be cultured for 20 days in a serum-containing environment

- Average migration rate of DRG explants was 606.55 μm per day

- Explant results on plasma polymers, laminin and glass demonstrated that MA 1 was an inferior surface with regards to number of neurites and maximum neurite lengths per neuron, whilst neurons on AAc had neurites of a length similar to glass and laminin. However, there was a high inherent variation of explants when cultured on AAc

- Further experiments used dissociated DRG, neuronal measurements from which had a lower variability

- A clear trend was shown that laminin was the superior surface with regards to the neuronal measurements

- Plasma polymers were capable of supporting primary dissociated DRG attachment and neurite extension

- The use of laminin as a nerve guide coating would be difficult due to the high cost. However, plasma polymers would be a cheaper coating and supported primary neurons with a higher percentage of neurites compared to neurons on glass

- The results from this chapter indicate that further work into the use of plasma polymers as nerve guide coatings in the *in vivo* environment would be worth pursuing

5.1.8 References

1.   Adams, D.N., E.Y.C. Kao, C.L. Hypolite, et al., Growth cones turn and migrate up an immobilized gradient of the laminin IKVAV peptide. Journal of Neurobiology, 2005. **62**(1): p. 134-147.
2.   Armstrong, S.J., M. Wiberg, G. Terenghi, et al., Laminin activates NF-kappaB in Schwann cells to enhance neurite outgrowth. Neuroscience Letters, 2008. **439**(1): p. 42-46.
3.   Britland, S., C. Perridge, M. Denyer, et al., Morphogenetic guidance cues can interact synergistically and hierarchically in steering nerve cell growt. Experimental Biology Online, 1996. **1**(2).
4.   Buttiglione, M., F. Vitiello, E. Sardella, et al., Behaviour of SH-SY5Y neuroblastoma cell line grown in different media and on different chemically modified substrates. Biomaterials, 2007. **28**(19): p. 2932-2945.
5.   Cargill, R.S., K.C. Dee, and S. Malcolm, An assessment of the strength of NG108-15 cell adhesion to chemically modified surfaces. Biomaterials, 1999. **20**(23-24): p. 2417-2425.
6.   Clements, I.P., Y.-t. Kim, A.W. English, et al., Thin-film enhanced nerve guidance channels for peripheral nerve repair. Biomaterials, 2009. **30**(23-24): p. 3834-3846.
7.   Colley, H.E., G. Mishra, A.M. Scutt, et al., Plasma Polymer Coatings to Support Mesenchymal Stem Cell Adhesion, Growth and Differentiation on Variable Stiffness Silicone Elastomers. Plasma Processes and Polymers, 2009. **6**(12): p. 831-839.
8.   Dombrowski, A.M. and F.C. Kauffman, Growth of Adult-Rat Superior Cervical-Ganglion Explants in Serum-Free Media. Brain Research, 1981. **219**(2): p. 407-421.
9.   Frostick, S.P., Q. Yin, and G.J. Kemp, Schwann cells, neurotrophic factors, and peripheral nerve regeneration. Microsurgery, 1998. **18**(7): p. 397-405.
10.   Haycock, J.W., 3D cell culture: a review of current approaches and techniques. Methods in molecular biology, 2011. **695**: p. 1-15.
11.   Jessen, K.R. and R. Mirsky, The origin and development of glial cells in peripheral nerves. Nature reviews. Neuroscience, 2005. **6**(9): p. 671-682.
12.   Krsko, P., T.E. McCann, T.T. Thach, et al., Length-scale mediated adhesion and directed growth of neural cells by surface-patterned poly(ethylene glycol) hydrogels. Biomaterials, 2009. **30**(5): p. 721-729.
13.   Madduri, S. and B. Gander, Schwann cell delivery of neurotrophic factors for peripheral nerve regeneration. Journal of the Peripheral Nervous System, 2010. **15**(2): p. 93-103.
14.   Murray-Dunning, C., Electrospun aligned biodegradable microfibers and plasma polymerization techniques to improve peripheral nerve repair. 2010, Sheffield: 200 pages.
15.   Parrinello, S., I. Napoli, S. Ribeiro, et al., EphB signaling directs peripheral nerve regeneration through Sox2-dependent Schwann cell sorting. Cell, 2010. **143**(1): p. 145-155.
16.   Recknor, J.B. and S.K. Mallapragada, Nerve Regeneration: Tissue Engineering Strategies, in The Biomedical Engineering Handbook: Tissue Engineering and Artificial Organs,, ed. J.D. Bronzino2006, New York: Taylor and Francis.
17.   Schnell, E., K. Klinkhammer, S. Balzer, et al., Guidance of glial cell migration and axonal growth on electrospun nanofibers of poly-epsilon-caprolactone and a

collagen/poly-epsilon-caprolactone blend. Biomaterials, 2007. **28**(19): p. 3012-3025.

18.　Smalheiser, N.R. and N.B. Schwartz, Kinetic-Analysis of Rapid Onset Neurite Formation in Ng108-15 Cells Reveals a Dual Role for Substratum-Bound Laminin. Developmental Brain Research, 1987. **34**(1): p. 111-121.

19.　Tojima, T., Y. Yamane, M. Takahashi, et al., Acquisition of neuronal proteins during differentiation of NG108-15 cells. Neuroscience Research, 2000. **37**(2): p. 153-161.

20.　Wang, G.Y., K. Hirai, and H. Shimada, The role of laminin, a component of Schwann cell basal lamina, in rat sciatic nerve regeneration within antiserum-treated nerve grafts. Brain Research, 1992. **570**(1-2): p. 116-125.

21.　Weber, R.A., W.C. Breidenbach, R.E. Brown, et al., A randomized prospective study of polyglycolic acid conduits for digital nerve reconstruction in humans. Plastic and Reconstructive Surgery, 2000. **106**(5): p. 1036-1045.

6.1 Discussion and future work

Overall, this work indicated that plasma polymerisation of maleic anhydride and acrylic acid was successful and that the coatings are capable of supporting and promoting the neuritogenesis of single cultures of NG108-15 neuronal cells as well as dissociated primary neuronal and Schwann cell co-cultures to a greater degree than glass. Regarding the plasma polymerisation step, it would have been useful for the biological work to use chemical derivatisation techniques, to investigate if there was a correlation between the relative percentage of anhydride and carboxylic acid groups and the neurite outgrowths/relative metabolic rates. Another aspect that would have been interesting to improve would be the adherence of the MA coatings. Whilst the coating adherence of MA was sufficient for the biological work, extra care and time had to be taken during the immunohistochemical staining to ensure that the coating did not lift off. A pretreatment method to improve MA adherence was developed by Schiller et al.[1] that could be used for further longer term cultures or *in vivo* work; however for the initial *in vitro* investigations this was not necessary.

The differences in results of serum free conditions compared to serum conditions demonstrate the dramatic effect serum adsorption and orientation can have on a surface. Whilst slight trends were seen with serum conditions, these were exaggerated when under serum free conditions. Glass supported fewer neurons with shorter and fewer neurites when in serum free conditions compared to serum, whilst neurons on AAc gave similar neurite results for both serum-containing and serum-free media compositions. Neuronal cells on laminin generally had longer and more numerous neurites in both serum and serum free conditions when compared to TCPS, glass, AAc and MA 1, whilst MA 1 supported neuronal cells with longer and more neurites compared to glass when in serum free conditions.

The dramatic effect of MA 1 under serum-free conditions on supporting the longest neurite length of NG08-15 neuronal cells became apparent upon looking at the live cells under a light microscope, and was unexpected but certainly reproducible. It was thought that this effect may be repeated with the dissociated DRG experiments due to the low serum conditions used, however the MA 1 surface did not support primary neuronal cells with longer neurites compared to laminin. It would have been very interesting to investigate the cellular mechanisms of how the NG108-15 neuronal neurite outgrowth was so markedly enhanced when under serum free conditions and on MA 1 compared to all other surfaces investigated. Although NG08-15 neuronal cells are

a cell line and therefore limited compared to investigations of primary cells, NG108-15 neuronal cells have been characterised thoroughly in various publications and the mechanism may even prove useful with regards to the growth of neuronal carcinomas, as the NG108-15 were a Sendai-virus fused glioma and neuroblastoma.

Regarding possible mechanisms or processes that led to the significantly longer neurite outgrowths by NG108-15 neuronal cells on MA1 under a serum-free environment, the response of mammalian cells to a surface is governed by many factors, including the adsorbed protein layer. The kinetics of protein attachment is governed by the 'Vroman effect'[2], where competitive serum proteins adsorb to a surface. Smaller proteins have been shown to reach a surface first and adsorb, which are then gradually replaced by proteins that have a higher affinity[3]. Over 24 hours, proteins then rearrange their position, conformation and orientation in order to maximise protein coverage on a hydrophilic surface[4]. It has been postulated that the amine groups of BSA covalently bind with non-hydrolysed anhydride groups[5], which would then restrict rearrangement of serum proteins on the surface before cellular attachment occurs. Even though the media conditions did not contain serum, NG108-15 neuronal cells were passaged under serum conditions and it is known that cells can take up proteins and presumably use the proteins to interact with a surface even under serum-free environments[6].

The level of bovine serum albumin (BSA) attachment was also studied on plasma polymerised maleic anhydride under different conditions[5], where it was found that the low duty cycles (similar to MA 1 and 2) resulted with the highest amount of covalently bound BSA. As BSA is one of the most prevalent proteins in serum and covalently binds to the anhydride groups, this may have obstructed the rearrangement of proteins that usually occurs. As it has been shown that serum proteins have to be correctly presented in order to facilitate cell attachment[7], this could potentially explain more clearly the results observed with MA 1. Studies with AAc have shown that fibrinogen is one of the main protein within serum that attaches, whilst albumin barely attached and immunoglobulin (IgG) was present in low levels[4]. Whilst the results cannot be directly compared as only albumin was used with the maleic anhydride study, it is interesting to note the potential differences in densities of attached proteins between the plasma polymers.

Interestingly, preliminary work with explants demonstrated that serum-free culture was possible. However, as neurite outgrowth was very sporadic and

unpredictable under serum-free conditions (1 out of 3 explants would adhere to the surface and show *in vitro* cellular migration) and occurred at much slower rates, it was not used in investigations reported here. Serum-free culture with Schwann cells was not investigated due to time constraints; however it would be interesting to culture Schwann cells on the plasma polymerised surfaces under varying levels of serum to investigate any potential differences. This work has demonstrated the significance of serum-containing versus serum-free media when performing *in vitro* investigations on plasma polymerised surfaces, presumably due to the relative thinness of the surfaces compared with the size of the serum proteins.

Another area of interest would be the comparative surfaces. I recently compared allylamine, PCL, AAc, MA 1 and an allylamine/AAc mix. The allylamine/AAc mix would be intriguing to compare against poly-L-lysine, as poly-L-lysine contains both amino and carboxyl groups. Whilst preliminary results indicated that allylamine may have stimulated slightly stronger neurite outgrowth compared to AAc, experimental complications meant that immunostaining was not completed and quantitative comparisons could not be made. Comparisons of the plasma polymer coated nerve guide materials versus uncoated guides would also be very relevant for future work.

A clear direction future work could take is towards *in vivo* study. As pioneering work on fabricated nerve guides is now using 2-photon polymerisation techniques[8], it would be interesting to coat such guides with plasma polymerised AAc and investigate if nerve regeneration distance is affected. As studies have looked into a combination of stem cells and nerve guides as a method of increasing nerve regeneration[9,10], it would be useful to differentiate stem cells towards a glial lineage[11], then evaluate the effects of the plasma polymers at various points.

6.1.1 Conclusion and key findings

The aim of this report was to investigate the effect of plasma polymerisation surfaces on the metabolic rate and morphological characteristics of immortalised neuronal NG108-15 cells, primary rat Schwann cells, explanted and dissociated primary rat dorsal root ganglion (DRG). Main conclusions were:

1. Optimisation and characterisation of plasma polymerised surfaces using XPS and contact angle demonstrated retention of carboxyl groups on AAc coated surfaces. The presence of anhydride groups on maleic anhydride plasma polymerised surfaces was also confirmed using ToF-SIMS and XPS. AFM showed that the glass surfaces were not significantly altered topographically by any plasma polymerisation condition

2. MA 1 and AAc supported NG108-15 neuronal cells with similar neurite outgrowth compared to glass under serum conditions, whilst it was shown that MA 1 supported a significantly higher number of NG108-15 neuronal cells with significantly higher maximum neurite lengths and neurites per neuron compared to glass under serum free conditions. AAc and MA 1 supported neuronal cells with a higher percentage of neurites compared to glass under serum-free conditions

3. Primary rat Schwann cell cultures demonstrated higher metabolic rate and aspect ratio measurements on glass and laminin compared to the plasma polymers

4. DRG explants cultured on MA 1 demonstrated the lowest number of neurites and maximum neurite length compared to glass, AAc and laminin. However, high standard error mean across all surfaces indicated relatively unreliable results

5. Dissociated primary rat DRG cultures showed that plasma polymers supported a higher percentage of neurons with neurites compared to glass, whilst acrylic acid supported neurons with longer maximum neurite lengths and higher average number of neurites compared to glass

6.1.2 References

1. Schiller, S., J. Hu, A.T.A. Jenkins, et al., Chemical structure and properties of plasma-polymerized maleic anhydride films. Chemistry of Materials, 2002. **14**(1): p. 235-242.
2. Vroman, L., Effect of adsorbed proteins on the wettability of hydrophilic and hydrophobic solids. Nature, 1962. **196**: p. 476-477.
3. Slack, S.M. and T.A. Horbett, The Vroman effect - A critical review. Proteins at Interfaces Ii, 1995. **602**: p. 112-128.
4. Lassen, B. and M. Malmsten, Competitive protein adsorption at plasma polymer surfaces. Journal of Colloid and Interface Science, 1997. **186**(1): p. 9-16.
5. Liu, S., M.M Vareiro, S. Fraser, A.T Jenkins, Control of attachment of bovine serum albumin to pulse plasma-polymerized maleic anhydride by variation of pulse conditions. Langmuir, 2005. **21**(19): p. 8572-8575.
6. Ryser, H. J-P., Uptake of protein by mammalian cells: an underdeveloped area: the penetration of foreign proteins into mammalian cells can be measured and their functions explored. Science, 1968. **26** (159): p. 390-396.
7. Wilson, C.J., R.E. Clegg, D.I. Leavesley, et al., Mediation of biomaterial-cell interactions by adsorbed proteins: a review. Tissue Engineering, 2005. **11**(1-2): p. 1-18.
8. Koroleva, A., A.A. Gill, I. Ortega, et al., Two-photon polymerization-generated and micromolding-replicated 3D scaffolds for peripheral neural tissue engineering applications. Biofabrication, 2012. **4**(2).
9. Yim, E.K., S.W. Pang, and K.W. Leong, Synthetic nanostructures inducing differentiation of human mesenchymal stem cells into neuronal lineage. Experimental Cell Research, 2007. **313**(9): p. 1820-1829.
10. Zhang, Y., H. Luo, Z. Zhang, et al., A nerve graft constructed with xenogeneic acellular nerve matrix and autologous adipose-derived mesenchymal stem cells. Biomaterials, 2010. **31**(20): p. 5312-5324.
11. Kaewkhaw, R., A.M. Scutt, and J.W. Haycock, Anatomical site influences the differentiation of adipose-derived stem cells for Schwann-cell phenotype and function. Glia, 2011. **59**(5): p. 734-749.